Imperial College London

Bacteriophage: from Bacteria to Targeted Gene Delivery to Mammalian cells

A thesis submitted to Imperial College London for

the degree of Doctor of Philosophy

Teerapong Yata

Imperial College London

Faculty of Medicine

Division of Brain Sciences

Declaration

I, Teerapong Yata, hereby declare that the work presented in this thesis was undertaken in the Department of Medicine, Imperial College London, during the year 2010-2014. Certain experiments have been carried out with the help of students and/or scientists advised by myself and my supervisor.

Experiments and analysis depicted in Figures 3.2-3.6, 3.8-3.12 (Chapter 3) were performed with the assistance of Miss Amanda Donnelly, an MSc student, whom I trained and co-supervised.

Experiments and analysis (physical characterizations) depicted in Figure 3.7a-d (chapter 3) and Figure 4.5 (chapter 4) were performed with the assistance of Dr. Koon-yang Lee, a research associate in Department of Chemical Engineering, Imperial College London.

Experiments and analysis depicted in Figures 6.8-6.10 (Chapter 6) were performed with the assistance of Miss Llucia Inès Albertí Servera, an MSc student, whom I trained and co-supervised.

Experiments and analysis depicted in chapter 5 were performed with the assistance of Mr. Eugene Lee, a BSc student, who I trained co-supervised.

Copyright Declaration

Abstract

Bacteriophage (phage), bacterial viruses, have been improved as non-human pathogenic viral vectors for the purpose of introducing genetic materials into mammalian cells. Previously, our group generated a novel Adeno-associated virus/Phage (AAVP) hybrid vector as a valuable tool for targeted gene transfer to mammalian cells. However, the efficacy of bacteriophage-based vectors is considered relatively poor, meaning that ways of improving it are of considerable interest.

First approach to improve AAVP-mediated gene delivery is through chemical modification. We showed that the transduction efficiency of AAVP was increased by the complexation of phage vectors with cationic molecules and calcium phosphate co-precipitation. Application of the bacteriophage complex carrying a cytotoxic gene resulted in eradication of cultured brain tumour cells. The chemically modified vector showed superior gene delivery over the conventional vector and can thus be regarded as an improved version of phage-based vector that has promise in cancer gene therapy.

Next, we demonstrated that Extracellular Matrix (ECM) presents an obstacle for AAVP. Using brain cancer cell lines as a model, AAVP transduction was significantly increased by collagenase and hyaluronidase-mediated degradation of ECM, which can subsequently be translated into tumour cell eradication through AAVP-mediated gene therapy. Our findings prove that combination of AAVP

vectors with ECM depletion represents a powerful strategy to advance phage-guided gene transfer.

Finally, we engineered the prototype bacteriophage-based multifunctional vector as a proof-of-concept model that can simultaneously display three different peptides and carry a mammalian transgene cassette. Our results show that bacteriophage can be used as a scaffold for constructing multifunctional carriers that integrate multiple functions, which may have great potential for gene delivery applications. Together, the data demonstrate the potential for improved AAVP-based gene transfer to mammalian cells focusing on the use of chemical modification, manipulation of ECM, and the generation of multifunctional phage vectors.

Acknowledgements

This work was done in the Phage Group, in the Department of Medicine within the Division of Brain Sciences at Hammersmith Hospital Campus, Imperial College London. The work was performed between October 2010 and January 2014. My sincere gratitude is owed to a number of people who participated in this project.

Firstly, I would like to express my deep appreciation to Dr. Amin Hajitou, my supervisor, for his wisdom, invaluable guidance and professionalism from the initial to the final level enabled me to develop an understanding of the subject. Dr. Amin Hajitou has been an excellent mentor and has provided unfailing support throughout my PhD studies.

I would also like to thank the past and current members of the Phage Therapy groups, in particular, Paladd Asavarut, Justyna Przystal, Efi Tsafa, Charlotte Stoneham, and Azadeh Kia for their friendship, advice and encouragement over the past 4 years.

I am grateful for the Science and Technology Scholarship awarded to me by the Royal Thai Government.

I am extremely grateful to my family and my friends especially my parents who have supported me all the way and have made this possible.

Lastly, I offer my regards and blessings to all of those who supported me in any respect during the completion of the program.

Table of Contents

List of Figures

List of Tables

List of Abbreviations

AAV	Adeno-associated viruses
AAVP	Adeno-associated virus/phage
ASGRP-R	Asialoglycoprotein receptors
BBB	Blood brain barriers
BGF	Basic fibroblast growth factor
bp	Base pair
BSA	Bovine serum albumin
CAR	Coxsackievirus and adenovirus receptor
CED	Convection-enhanced delivery
CLICs	Clathrin- and dynamin-independent carriers
CMV	Cytomegalovirus
CNS	Central nervous system
DAPI	4',6-diamidino-2-phenylindole
DEAE.DEX	Diethlyamioethyl-dextran
D-MEM	Dulbecco's Modified Eagle's medium
DMSO	Dimethyl sulfoxide
DNA	Deoxyribonucleic acid
DOTAP	Dioleoyltrimethylammonium-propane
ECM	Extracellular matrix
EDTA	Ethylenediaminetetra acetic acid
EEP	Endosomal escape peptide
EGF	Epidermal growth factor
EPR	Enhanced permeability and retention
EtBr	Ethidium bromide
FACS	Fluorescence-activated cell sorting
FBS	Foetal Bovine Serum
FDA	Food and Drug Administration
GAG	Glycosaminoglycans
GALA	Glutamic-alanine-leucine-alanine
GBM	Glioblastoma multiforme
GBP	Gold-binding peptide
GCV	Ganciclovir
GEEC	Glycosyl phosphatidylinositol-anchored protein enriched early endosomal compartments
GFP	Green fluorescence protein
Grp	Glucose-regulated protein
HA	Hemaglutinin
HBS	Hepes-buffered saline solution
HSPG	Heparin sulphate proteoglycan
HSV	Herpes simplex viruses
HSVtk	Herpes simplex virus thymidine kinase

HIV	Human immunodeficiency virus
hnRNP	Heterogeneous nuclear ribonucleoprotein
IFP	Interstitial fluid pressure
IPTG	Isopropyl-beta-D-thiogalactopyranoside
ITR	Inverted terminal repeat
LB	Luria-Bertani
LTR	Long terminal repeat
Luc	Firefly Luciferase
MHC	Major histocompatibility complex
MR	Mannose receptors
miRNA	Micro-ribonucleic acid
NLS	Nuclear localization signal
NPC	Nuclear pore complex
PB	Polybrene
PBS	Phosphate buffer saline
PCR	Polymerase chain reaction
PDL	Poly-D-lysine
PEG	Polyethylene-glycol
PEI	Polyethyleminine
PFA	Paraformaldehyde
PS	Protamine sulphate
RGD	Arginine-glycine-aspatic acid
RES	Reticuloendothelial system
REV	Reverse phase evaporation method
RLU	Relative luminescence units
RNAi	RNA interference
rpm	Revolutions per minutes
SBP	Streptavidin-binding peptide
SV	Simian virus
TAE	Tris-acetate-EDTA
TAT	Transactivator of transcription
TGF	Transforming Growth Factor
TMZ	Temozolamide
TNF	Tumour necrosis factor
TSP	Thrombospondin

1. Introduction

1.1. Overview

Introduction of genetic materials into mammalian cells is a key approach in cell and molecular biology. Expression of transgenes in cell culture or animal models provides a suitable system to determine the regulation and function of a desired gene.[1] The interest in this research area has also dramatically increased with the development of other biomedical technologies such as gene therapy. Many gene transfer methods are based on viruses as a means to deliver genes into target cells. The most commonly used viral vectors for gene transfer are derived from adenoviruses, adeno-associated viruses (AAV), retroviruses, lentiviruses, and herpes simplex viruses (HSV).[2] Though viruses were evolutionarily designed to transfer their genetic material into host cells efficiently with various tissue tropisms, their use as vectors for therapeutic gene delivery is hindered by a number of limitations including deoxyribonucleic acid (DNA) packaging capacity[3], immunogenic concerns[1,4], and the potential for insertional mutagenesis, which can be oncogenic[5,6], whereby the latter two significantly restrict their clinical use. Although most recombinant viral vectors are replication-deficient and require helper virus functions for propagation, they are amenable to replication-competent virus breakthrough, raising biosafety concerns.[7] In addition, the co-infection of packaging cells with a wild type helper virus to produce infectious viral particles is required for some viruses (AAVs and HSV), resulting in a contamination with the helper virus, which often cannot be fully eliminated during preparation of the viral

stock[8] and can have cytotoxic effects[9]. Although commercial kits are available, replication-defective systems still require transfection steps or cloning of packaging cell lines which is time consuming to generate virus stocks, and subsequent purification of the virus particles. Important limitations also include a limit to the size of the DNA that can be engineered into their genome[10] and complex protein structures, effectively creating an expensive and complicated manufacturing process.[10] In order to reduce side effects and lower the amount of viral vectors required, infection must be restricted to target cells, also known as cell targeting or transductional targeting.[10] Although animal viruses have been shown to have potential for ligand-targeted gene delivery, eliminating their native tropism and re-targeting them to different receptors substantially reduce their efficacy.[11,12]

Alternatively, transgene expression can be achieved by transfection of target cells using non-viral vectors such as naked DNA, cationic liposomes, cationic polymers, and synthetic peptides.[13] The most commonly used *in vitro* gene delivery method is DNA plasmid containing a gene of interest. However, this approach requires a large quantity of plasmid DNA with expensive commercial transfection reagents.[7] Although these non-viral vectors are highly effective in gene transfer to *in vitro* cultured cells, they appear to be significantly less effective *in vivo*.[13]

The prokaryotic single-stranded DNA bacteriophage virus, which only infects bacteria, has also been proposed as a gene delivery vector.[14,15] One of the major advantages of the bacteriophage as a gene delivery vector is its simple, fast, and cost effective production. Phage vectors carrying a gene of interest can be easily

produced with high titres in the supernatant of *Escherichia coli (E.coli)* host cell cultures and can be purified on a large scale.[16] In contrast to replication-deficient animal viral vectors in which helper functions are used to produce virus, the phage-based system provides a good compromise. The phage is propagated in bacterial cells; thus any risk of breakthrough of replication-competent virion can be avoided. In addition, they are safe, having long been used for both prophylaxis and treatment of bacterial infection, both in adults and children, with no safety concerns being identified.[17] They have also been approved by the U.S. Food and Drug Administration (FDA) to be used as safe antibacterial food additives.[18] Interestingly, a recent study has found a new form of symbiosis at mucosal surface of many animal species including humans with bacteriophage, which provides non-host-derived immunity against bacterial infection.[14]   In terms of their packaging capacity, bacteriophages do not seem to have a defined packaging limit because they possess a capsid composed of the major pVlll coat protein arranged in an almost perfect α-helical array, which can be extended to accommodate larger DNA constructs.[19]

Despite their attractive advantages, phage-based vectors are still considered to be poor vectors for gene transfer which restricts their application in a broad range of disciplines. It is clear that the phage has evolved to exclusively infect bacterial cells and has no optimized strategies to transfer and express transgenes in mammalian cells. However, the phage-based vector, due to its genetic and structural simplicity,

is uniquely suited to methods that use directed evolution to improve its performance.[20]

New generations of gene delivery vectors have incorporated elements from different vectors in order to obtain the ideal vector with the desired attributes. These hybrid or chimeric vectors are expected to outperform their conventional counterparts by adding new abilities or replacing certain undesirable elements.[21] Previously, our group reported a novel adeno-associated virus/phage (AAVP) hybrid vector system by combining bacteriophage with attributes of the AAV animal virus.[22] Phage is a prokaryotic virus, which has no natural tropism for eukaryotic mammalian cells.[23] Targeting peptides genetically inserted into phage coat proteins alter its tropism and can transduce mammalian cells.[24] AAV vector genomes serve as an excellent eukaryotic expression cassette due to their long-term transgene expression without problems associated with insertional mutagenesis and has enabled a number of clinical trials using this gene delivery system.[25] Incorporating the genetic cis-elements inverted terminal repeat (ITR) from AAV2 into the phage genome resulted in altered transgene cassette and subsequently in improved gene transfer efficacy of bacteriophage.[26] The resulting AAVP can efficiently transduce target cells and has a long-term stable transgene expression. Finally, AAVP titres can reach approximately 10^{10}-10^{11} bacterial transducing unit/μl.

1.2. Background review

1.2.1. Gene delivery

Gene transfer is the introduction of nucleic acids into cells. This technology provides the ability to genetically manipulate the target cells, and has contributed to a number of applications.[2] A major approach in the field of cell biology is the transfer of genes of interest in selected cell cultures or animal models, with the aim to study the gene's function by overexpressing a gene of interest, knocking down target proteins via micro-ribonucleic acid (miRNA) or RNA interference (RNAi), or expressing mutant versions of genes.[4] Moreover, the production of biopharmaceutical proteins, such as hormones, growth factors, cytokines, and immunoglobulins that is used to treat a broad spectrum of diseases largely relies on the expression of recombinant proteins in cultivated mammalian cells.[5] The most important contribution of gene transfer innovation involves the direct use of genetic material as a therapeutic agent to treat or prevent diseases. This so-called 'gene therapy' holds the promise for curing a large number of monogenic disorders, cardiovascular diseases, infectious diseases, cancer, and many others.[7] Most importantly, it has been realized that development of gene carriers or vectors that can safely and efficiently transport the therapeutic payload selectively to disease sites is a bottleneck in clinical applications of human gene therapy.[27,28] Generally, vectors for gene delivery are classified into two categories; viral- and nonviral-based vectors. Viral vectors are derived from natural viruses, whereas

non-viral vectors generally consist of DNA (usually plasmid DNA) delivered to target cells with the aid of delivery vehicles such as cationic lipids or polymers.

1.2.2. Viral-based gene delivery vector

At present, gene transfer is achieved with modified viruses (**Figure1.1**). The characteristics of the three most commonly used viral vectors for gene transfer are summarised in **Table 1.1**. Adenoviral vectors are useful for gene transfer due to their broad infection spectrum and high levels of gene delivery compared to other available vectors. Adenoviral vectors are easily manipulated using recombinant DNA techniques.[29] Another commonly used viral vector, the non-pathogenic AAV, serves as an excellent gene delivery vector due to its long-term transgene expression without problems associated with insertional mutagenesis.[25] Other vectors of interest include retroviruses and lentiviruses, a subset of the retrovirus family. Lentiviruses (e.g., human immunodeficiency virus type 1, HIV-1) are of particular interest because they can integrate their genome into the host cell genome, allowing stable, long-term transgene expression.[30]
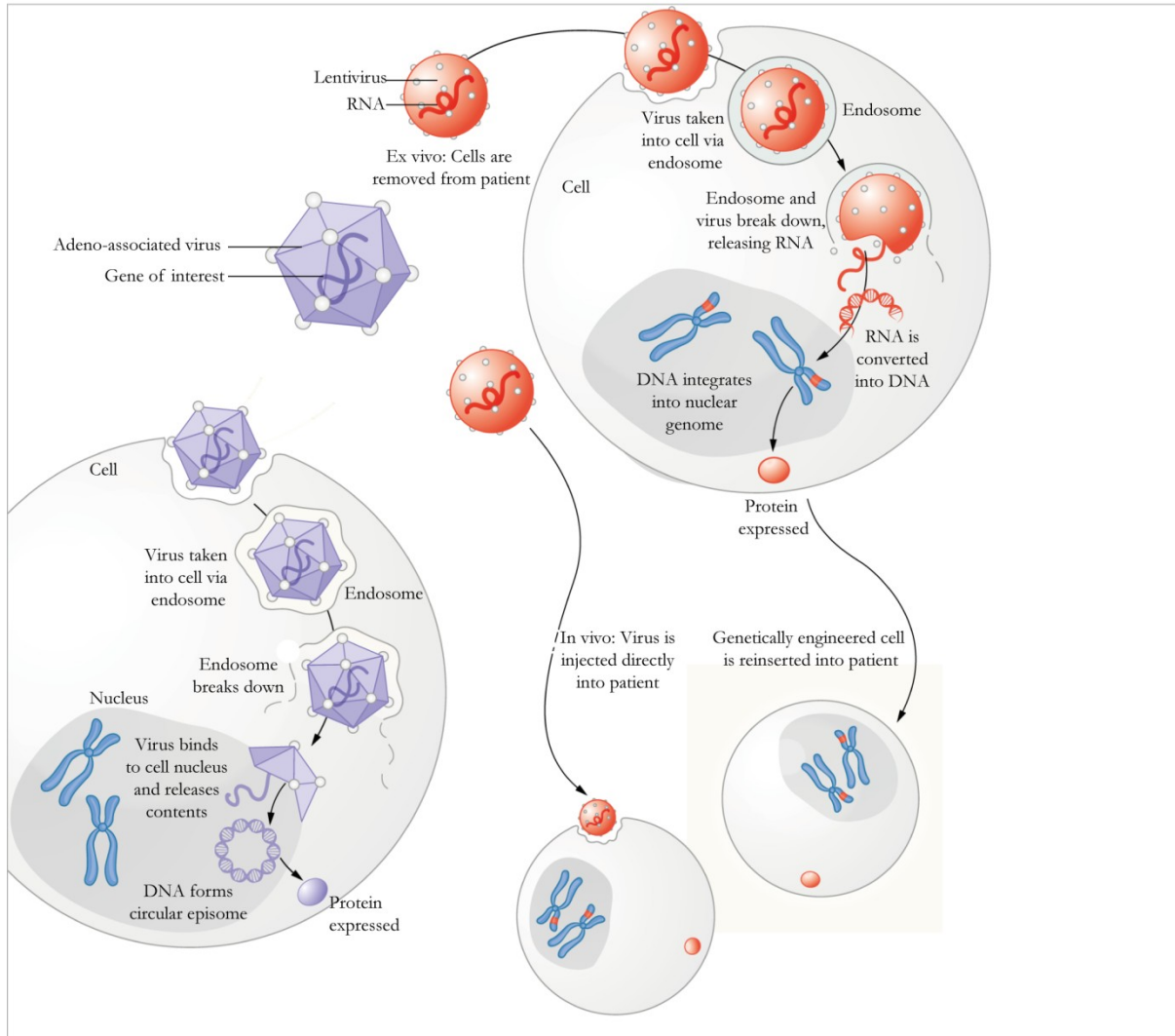
Figure 1.1: The annotated graphical representation of the viral-based gene delivery. The most commonly used viral vector is the modified AAV. The DNA makes its way to the nucleus, where it predominantly forms episomes. In contrast, integrating viruses insert their DNA into the host genome. The lentivirus, for example, delivers its payload to the cytoplasm, where a reverse transcription occurs. The DNA then enters the nucleus, where it integrates into the genome.

	Adenovirus	AAV	Retrovirus/lentivirus
Family	Adenoviridae	Parvoviridae	Retroviridae
Genome	dsDNA	ssDNA	ssRNA$^+$
Particle size	70-100 nm	20-25 nm	100 nm
Infection/tropism	Dividing and non-dividing cells	Dividing and non-dividing cells	Dividing cells
Entry mechanism	Receptor (CAR)-mediated endocytosis, endosomal escape and microtubule transport to the nucleus	Receptor-mediated endocytosis, endosomal escape and transport to the nucleus	Receptor binding, conformational change of Env, membrane fusion, internalisation, uncoating, nuclear entry of reverse-transcribed DNA
Host genome interaction	Non-integrating	Non-integrating	Integrating
Transgene expression	Transient	Potential long lasting	Long lasting
Packaging capacity	7.5 kb	4.5 kb	8 kb
Vector yield (transducing units/ml)	High (10^{12})	High (10^{12})	Moderate (10^{10})
Limitations	Triggers strong immune response against vehicle and transgene Production is time consuming and labour-intensive	Small packaging capacity Production is time consuming and labour-intensive	Insertional mutagenesis Production is time consuming and labour-intensive

dsDNA, double-stranded DNA; ssDNA, single-stranded DNA; AAV, adeno-associated virus; CAR, coxackie and adenovirus receptor; Env, viral envelope protein.

Table 1.1: Features of viral-based gene delivery systems. (Modified from Waehler, R. *et al.* 2007)[31]

Adenoviral vectors

Adenovirion consists of a ~36 kilobases (kbs) linear double stranded DNA genome encapsulated in a non-enveloped icosahedral particle of 70-100 nanometres (nm) in diameter (**Figure 1.2a**). The viral genome contains nine major complex transcription units divided into early (E1A, E1B, E2-E4) and late (L1-L5) transcripts flanked by ITR (**Figure 1.2a**). The deletion of the E1 and nonessential region of E3 allows 7-8 kb of transgene to be inserted into the vector genome.[32] Adenovirus enters cells via Coxsackievirus and adenovirus receptor (CAR)-mediated binding followed by internalisation via receptor-mediated endocytosis. After endosomal escape into the cytosol where capsid disassembly occurs, viral

DNA is transported into the nucleus through the nuclear envelope pore complex. The viral DNA is not integrated into the host genome, but is rather maintained as an episome.

Adeno-associated virus vectors (AAV)

A recombinant AAV is originally derived from a non-pathogenic parvovirus, a satellite virus of human adenovirus.[33] The small icosahedral particle is approximately 18-26 nm in diameter and contains either the sense or antisense of a single strand of DNA of 4-5 kb in size with equal efficiency (**Figure 1.2b**).[33] The AAV particle enters the cell via receptor-mediated endocytosis after which its genome is released into the nucleus where the single-stranded DNA is converted to double-stranded vector genome form. Viral genome DNA is composed of two open reading frames; the *rep* and the *cap* regions[17] both of which are replaced by the transgene sequences in order to construct AAV vectors. Each end of the viral genome has a 145-base long ITR sequence responsible for integration of AAV genome into a specific site in chromosome 19, although AAV exist primarily in episomal form (**Figure 1.3**).

To date, many strategies have been developed to improve targeting or retargeting desired cells only. This includes not only chemical engineering[34], , chimeric vectors[35] and so on, but also novel methods involve direct evolution of capsid proteins[36], direct display of random peptides on the AAV capsid[37], etc. However, it is still challenging to eliminate some AAV intrinsic restrictions, such as incomplete viral native tropism, and low packaging titre.[38]

Retroviruses

Retroviruses are enveloped viruses with nucleocapsids of 80-130 nm in diameter containing two copies of a linear, positive stranded 7-11 kb RNA genome.[39] The most commonly used retroviral vectors include the gammaretrovirus (or simple retrovirus) and lentivirus (or complex retrovirus) (**Figure 1.2c, d**). The viral genome is encapsulated within the capsid along with the viral reverse transcriptase and the integrase enzyme. Replication elements are replaced by the transgene, while retaining all the necessary RNA regions, primarily the long terminal repeat (LTR) that is associated with packaging, reverse transcription, and integration. Such vectors can accept up to 7 kb of an exogenous gene sequence (**Figure 1.2c, d**).[39,40] Following attachment and internalisation via receptor-mediated endocytosis, viral reverse transcriptase mediates the conversion of the viral genome to a double stranded DNA provirus, which is subsequently inserted into the host genome with the help of the integrase enzyme.[39,41] Due to its ability to stably integrate, allowing long-term expression, retroviral vectors have been used theoretically for single administration that could have a sustained long-term curative effect.
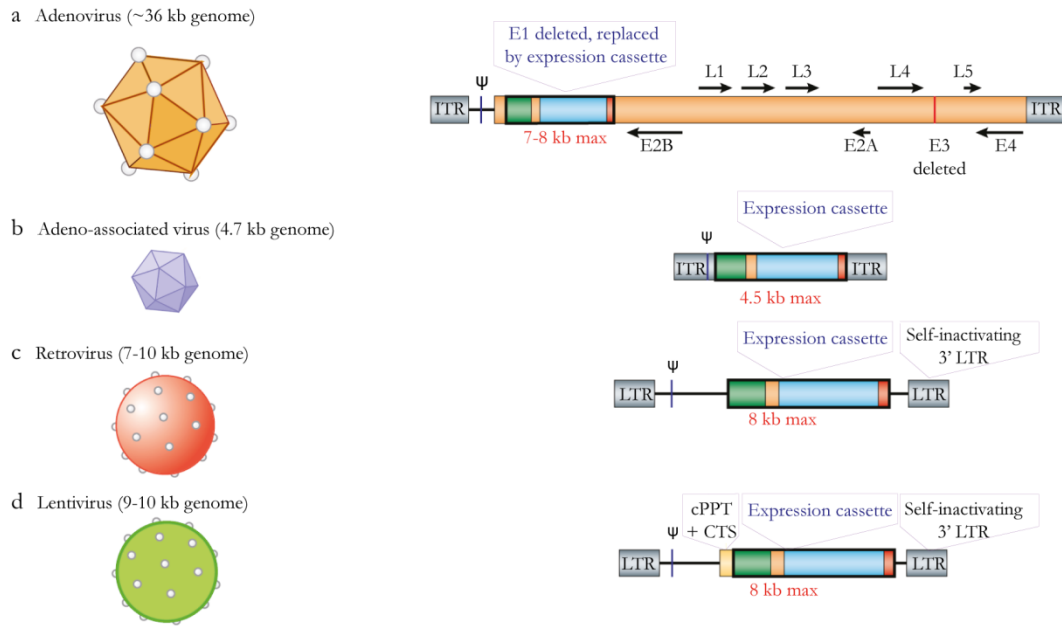
Figure 1.2: Diagram of the viral particles and organisation of the recombinant genome of the modified viral vectors. a) Adenovirus, b) AAV, c) Retrovirus, and d) Lentivirus (Modified from Sheridan, 2011)[42]

a

```
        T
    T       T
    C       G
    C       G
    A       T
    G       C
    C       G
    G       C
    G       C
    G       C
    C   GGCCTCAGT GAGCGAGCGAGCGCGC AGAGAGGGAGTGG CCAACT CCATC -3'
    T
    G   CCGGAGTCA CTCGCTCGCTCGCGCG TGTGTCCCTCACC GGTT -5'
    C       G
    G       C
    G       C
    G       C
    C       G
    C       G
    C       G
    G       C
    A       A
        A
```

                RBE   trs

-5'   -3'

4.7 kb genome   ITR

b

Host cell chromosome

ssDNA

Double stranding

Double-dtrand break

dsDNA

Vector genome integration

Vector genomes predominantly remain as episomes
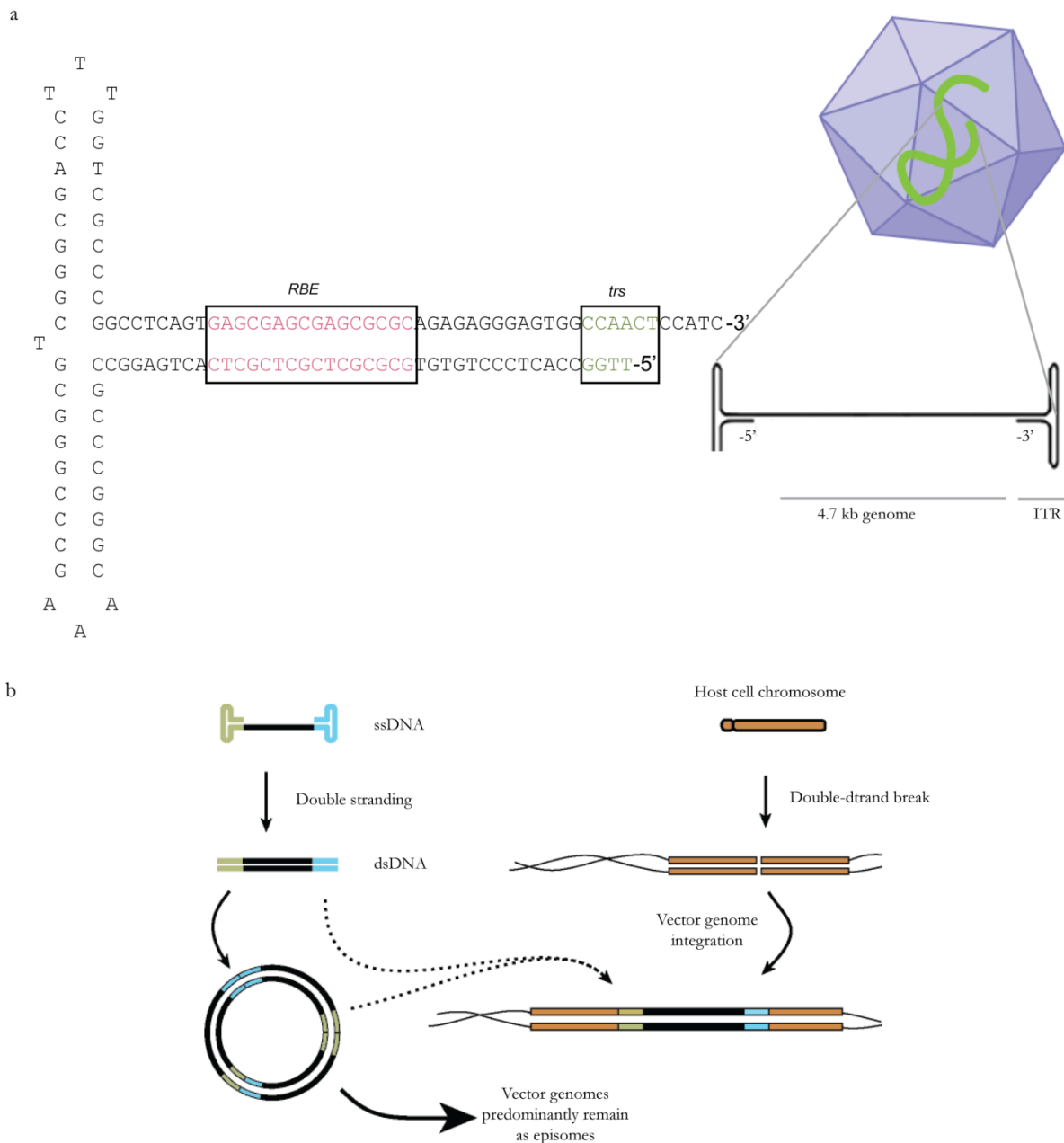
Figure 1.3: Fate of adeno-associated virus (AAV) genome. a) Structure and sequence of an inverted terminal repeat (ITR) in the single-stranded genome encapsulated in the AAV particle. **b**) The single-stranded DNA is converted into double-stranded through DNA synthesis and/or annealing. The AAV concatamer is formed by head-to-tail, head-to-head, and tail-to-tail intermolecular ligations. The AAV genome predominantly remains as episomes. Integration can occur with low frequency, most probably at chromosomal double-stranded breaks. (Modified from Schultz, B.R. and Chamberlian, J.S. 2008)[43]

1.2.3. Nonviral-based gene delivery vector

While viruses have been used successfully for gene transfer, the use of non-viral vectors has been explored as an alternative method to deliver transgenes into cells. The process of introducing nucleic acids into cells by non-viral methods (also defined as transfection) can be achieved by neutralizing or obviating the issue of introducing negatively charged nucleic acid into cells with negatively charged surface membrane. Cationic polymers and lipid-based reagents as well as calcium phosphate, which neutralize or even create an overall positive charge in the complex, facilitate efficient binding of complexes to cell surfaces and make it easier to cross the cell membranes. In this chapter, we will discuss some of the most commonly used non-viral gene delivery vectors which are included in **Figure 1.4**.

Calcium phosphate (CaPi) precipitation

Calcium phosphate (CaPi) co-precipitation was the first non-viral technique widely used to transfect foreign DNA into cells mainly due to its simplicity and inexpensiveness.[44] This technique is based upon DNA precipitation on the cell surface. The protocol involves mixing DNA, calcium chloride ($CaCl_2$), and a buffered saline/phosphate solution in a controlled manner. The CaPi-DNA precipitates are dispersed onto cultured cells and are taken up by cells via endocytosis or phagocytosis. However, CaPi co-precipitation is not suited for *in vivo* gene delivery. Moreover, the transfection efficacy of CaPi method can be compromised by small pH changes (±0.1).[45]

Cationic polymers

Another category of non-viral gene delivery vectors is cationic polymers. One of the first cationic polymers used to deliver nucleic acids into mammalian cells *in vitro* was diethlyamioethyl-dextran (DEAE.DEX). This method is based upon the complex formation (referred to as polyplex) between the negatively charged DNA and the positively charged polymer (**Figure 1.5**). An excess of positive charge contributed by the polymer content in the DNA:polymer complex leads to adherence of the complex to the negatively charged cell surface and subsequent endocytosis. Other synthetic cationic polymers have been used to transfect DNA into cells, including polylysine.[46] Polylysine has been shown to form complexes with DNA as a result of an electrostatic bridge between the negative charge of DNA and the positive charge of amino groups of the lysine residues.[47] However, *in vivo* application of polylysine, leads to non-specific interactions between the positively charged complex and blood components, resulting in failure of safe and efficient gene delivery.[48,49] Among the most widely used cationic polymers as gene carriers are polyethyleminines (PEIs). Linear or branched PEIs have been efficiently used for *in vitro* gene transfer. Similar to that of polylysine, these complexes have been shown to suffer from high degree of cytotoxicity, rapid clearance and self-aggregation.[50] This technique is widely used because the components are easily available and inexpensive in addition to protocol being simple, rapid and reproducible. Other synthetic cationic polymers have been employed to transfect DNA into cells, including polybrene (PB)[51] and dendrimers

[52,53]. Cationic polymers serving as DNA carriers can be conjugated with receptor-recognizing molecules capable of directing DNA into eukaryotic cells via receptor-mediated pathways. Conjugates of corresponding ligands with cationic polymers are taken up by various cells and exhibit high transfection activity. Both the uptake and transfection efficiency correlate with the level of receptors.[54] Transferrin and insulin receptors have been used for receptor-mediated transfection.[55]

Although these polyplexes are favourable for *in vitro* gene delivery efficiency, their *in vivo* application is hampered by their relatively low efficiency when compared to viruses, and by the necessity of an overall net positive charge. This results in potentially low bioavailability and lack of cell specificity.[48] Upon systemic delivery, the charged polyplexes interact with the blood components and non-target tissues, reducing targeting ability and triggering toxic effects.[48,56-58] To improve properties of this class of gene delivery vectors, various surface modified derivatives of caitionic polymers have emerged. Surface conjugation of cationic polymers with polyethylene glycol has been shown to prevent their aggregation, lower toxicity, increase circulation time, and improve systemic gene delivery.[56,59-64] Unfortunately, masking the surface charge of polyplexes by PEGylation appears to reduce their transfection efficiency due to reduced interactions with cell surfaces.[63,65,66] Such *in vivo* problems of gene delivery can also be overcome by targeted transfection. It is a complementary approach where the target cells can be selected based on specific interactions, e.g. ligand receptor, with the transfecting complex. Conjugates of sugar moieties (e.g., lactose or galactose) with poly-lysine allow polyplexes to target

asialoglycoprotein, unique receptors of hepatocytes.[67,68] In addition, folate receptors overexpressed on cancer cells can also be used as targets for folate-grafted gene delivery vectors.[69] There have also been efforts to conjugate antibodies (e.g., anti-JL1 antibody) to polylysine polyplexes allowing efficient leukemia-specific cell internalisation and specificity.[70]

Liposome-based gene delivery systems

The most effective nonviral gene delivery vectors developed so far are made of liposomes. The term "liposome" refers to an artificially-prepared spherical vesicle with bilayer membrane structure composed of natural or synthetic amphiphilic lipid molecules.[71] Nucleic acids are encapsulated within liposomes by the reverse phase evaporation method (REV).[72] However, the production of liposomes containing the DNA molecules inside requires multiple challenging steps. Another possible problem associated with liposomes is that small-sized liposomes may be incapable of encapsulating large amounts of DNA. Therefore, stable cationic liposomes spontaneously interacting with nucleic acids and therefore forming liposome/nucleic acid complexes (referred to as lipoplexes) have been developed to overcome some of the mentioned shortcomings of liposomes. It is believed that the negatively charged DNA interacts with the positively charged groups of the liposomes. The most widely used cationic lipid is dioleoyltrimethylammonium-propane (DOTAP).[73] Lipoplexes can be easily prepared by the addition of DNA to liposomes dispersed in solution.[74] The lipid to DNA ratio and overall lipid concentrations are important factors for efficient transfection and vary with

applications.[75] To date, a number of cationic liposome formulations are commercially available, such as Fugene, Lipofectin, Lipofectamine, and many others are under development.[76,77]
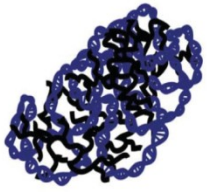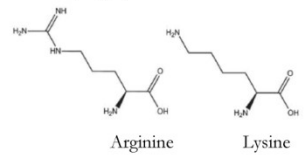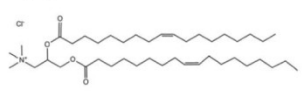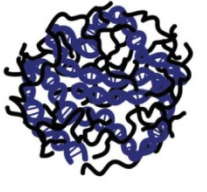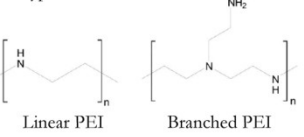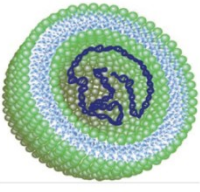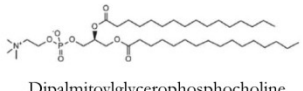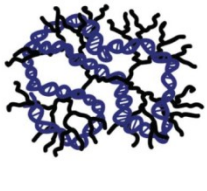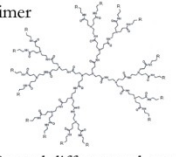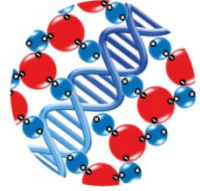
Figure 1.4: Structures of non-viral vectors for gene delivery.
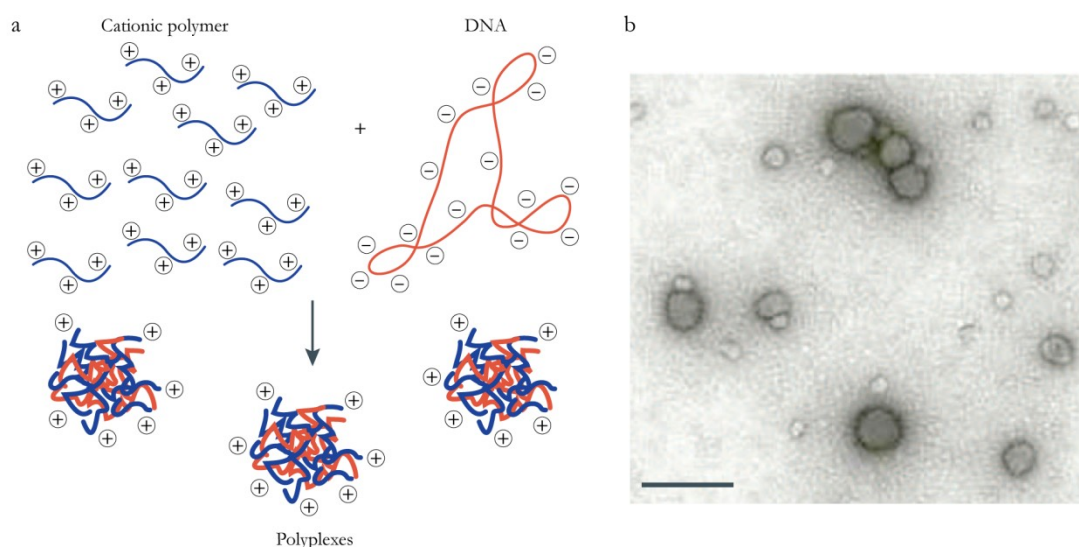
Figure 1.5: Formation of polymer-plasmid DNA polyplexes. a) Polyplexes are formed by electrostatic interactions between cationic polymers and negatively charged DNA. For gene delivery, an excess of positively charged polymers generates particles with a positive surface charge which favours cellular uptake and transfection. **b**) Transmission electron micrograph of polyplexes (Modified from Pack, D.W. *et al.* 2005)[78]

1.2.4. Extracellular Barriers to gene delivery vectors

Successful gene delivery to target cells is not a simple task because there are many barriers encountered by both viral and nonviral-based gene delivery vectors. Vectors must first overcome the extracellular barriers, such as rapid clearance and/or degradation of vector before it reaches its target cells. Extracellular barriers faced by gene delivery vectors after systemic administration are schematically depicted in **Figure 1.6**.

Packaging of nucleic acids

Naked nucleic acids as macromolecules are generally difficult to deliver, primarily due to their sensitivity to environmental conditions such as pH or enzymes (e.g., nucleases) that can degrade and destroy them. DNA condensation provides size reduction and protection against degradation. Viral vectors are natural systems capable of condensing nucleic acids into their capsid efficiently as they have highly evolved machinery for protecting and delivering their genomes to host cells. Cationic polymers or lipids are widely used to condense negatively charged nucleic acids by electrostatic interaction into small particles (i.e., polyplexes, lipoplexes), for protecting nucleic acids from degradation. However, the synthesis procedure for polyplexes or lipoplexes is less controllable compared to viral vectors which relies on precise mechanism of biosynthesis. The presence of excessive amounts of nitrogen residues compared to phosphate groups on DNA yields positive charges on the complexes, facilitating their binding to the negatively charged cell surface.

This electrostatic interaction promotes endocytosis and subsequently, high levels of gene expression.

Opsonisation and phagocytosis

Opsonisation is the process of coating a foreign organism or particle with phagocytosis-enhancing molecules called opsonins. The blood plasma proteins involved in opsonisation are primarily albumins, fibronectins, fibrinogens, complement proteins, immunoglobulins and apolipoproteins.[67,70,79,80] This process makes the opsonin-coated particles or microbes more immunologically 'visible' and susceptible to phagocytic cells (e.g. monocytes, macrophages, neutrophils, and dendritic cells). Following opsonisation, phagocytosis can efficiently occur, leading to destruction or removal of foreign materials from circulation by the mononuclear and polymorphonuclear phagocyte systems.[68] Particles can be opsonized within minutes upon exposure to blood, depending on their intrinsic surface characteristics, such as charge and hydrophobicity. Typically, phagocytes are unable to recognize foreign particles without adsorbed opsonin proteins. Adsorption of opsonin proteins on particles results in conformational changes from an inactive to activated form of protein structure that can be subsequently recognized by phagocytes.[81] In addition to facilitating particle recognition by the immune cells, opsonisation alters the effective size of the particle diameter referred to as the *in vivo* hydrodynamic diameter, which may be larger than the *in vitro* particle diameter.

Renal clearance

In order to avoid the possible side effects resulting from catabolism or breakdown, renal excretion is a desirable pathway for the removal of particles from the vascular compartment of the human body. In general, intravascular molecules with a final hydrodynamic diameter smaller than 5 nm are filtered by glomerular filtration resulting in rapid and efficient urinary excretion, while increased hydrodynamic diameter by over 8 nm prevents renal excretion. Glomerular filtration of molecules with the intermediate hydrodynamic diameter of 6-8 nm depends upon both size and charge of the particle. The effect of surface charge on glomerular filtration is due to at least 2 factors: (i) adsorption of serum proteins resulting in increased hydrodynamic diameter[82], and (ii) direct interaction between charged particles and fixed charge within the glomerular capillary wall.[83] The increase in size significantly reduces glomerular filtration and likely shifts the route of renal excretion to the liver. Macromolecules that are too large to be filtered through the glomerular pores tend to accumulate in the liver due to its loose structure and high blood perfusion.[84]
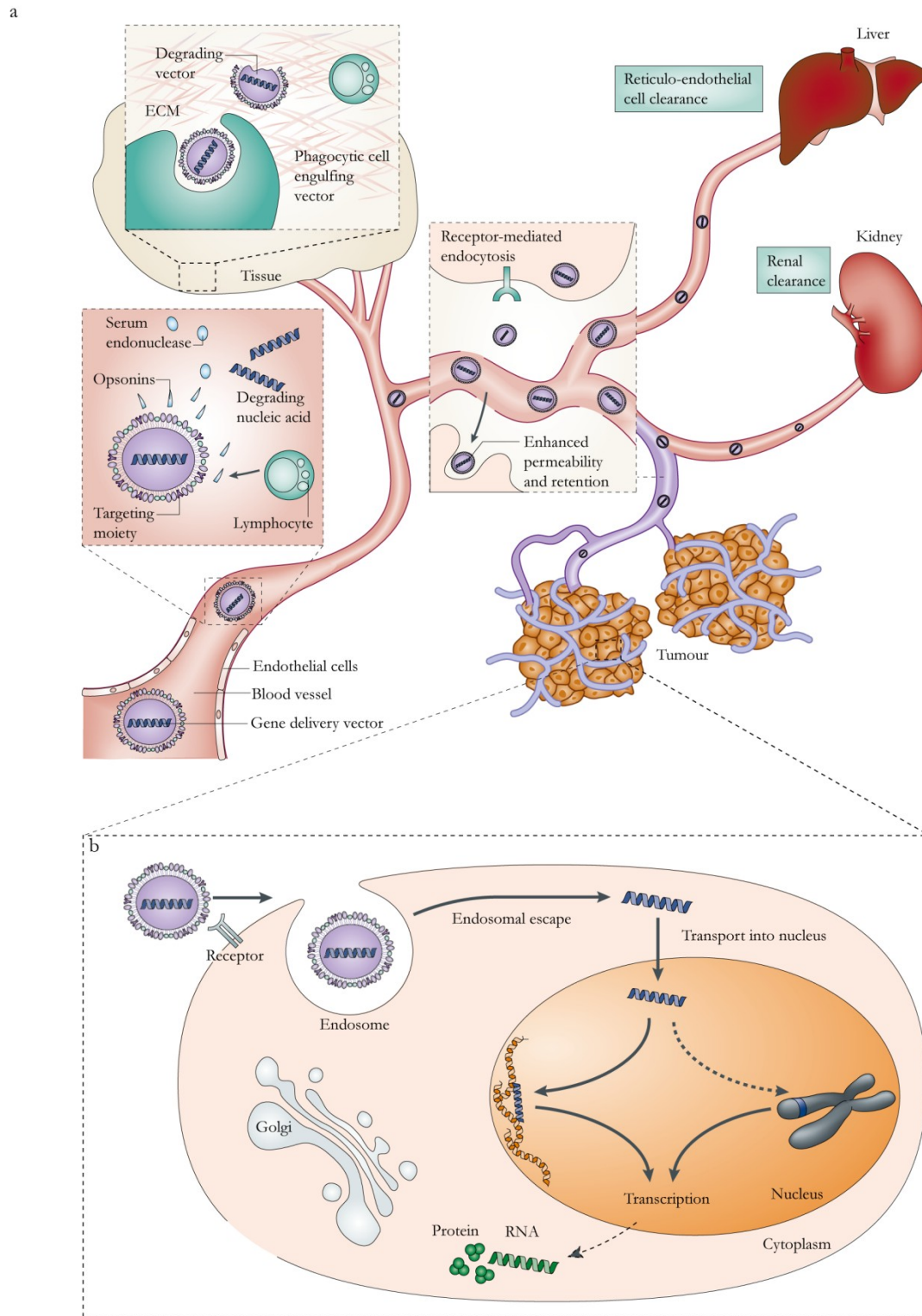
Figure 1.6: Summary of the extra-and intracellular barriers faced by gene delivery vectors following systemic administration. Gene transfer efficacy of gene delivery vectors has been hindered by numerous obstacles. **a**) After systemic administration, vectors must overcome rapid clearance and/or degradation of the vector before it reaches its target tissue. **b**) Intracellular barriers include plasma membrane and endocytosis, endosome escape, and nuclear translocation. (Modified from Pecot, C.V. *et al.* 2011)[85]

Reticuloendothelial system organ uptake and retention

The reticuloendothelial system (RES) is a part of the immune system, comprised of phagocytic cells such as monocytes and macrophages located in different organs of the body. Specialized macrophages located in the liver, termed Kupffer cells, and in the spleen rapidly take up opsonin-coated materials as these cells possess receptors for endocytosis of complement proteins and for the Fc fragment of IgG.[86] These particles are taken up by the liver, spleen, or other parts of RES depending on their physical characteristics such as size and charge. This function of RES involves the efficient capture and elimination of particles on the scale of 10-20 nm including virus particles.[82]

To achieve adequate circulation time, surface modifications of particles may be required to prevent or lessen opsonisation. Particles with more hydrophilic surfaces (> 35 nm diameter) show much less uptake by the liver and spleen than hydrophobic particles.[87] One widely used approach is molecular modification via the attachment of polyethylene glycol (PEG) polymer to particles referred to as PEGylation. Although reduction of particle size and stabilization of particles with a layer of amphiphilic polymers are promising, a complete avoidance of the RES system has not been possible.[88] Another promising approach to prevent serum protein adsorption is zwitterionic coating. Creating particles with zwitterionic surface charges provides the highest solubility and smallest hydrodynamic diameter and is therefore a useful strategy to obtain more favourable clearance properties of particles intended for clinical applications.

Extravasation

Endothelial cells, which form the inner cellular lining of blood vessels, act as a semi-selective barrier that regulates exchange of fluid and molecules between the vascular compartment and the extravascular space.[89] The leakage of intravascular agents into extracellular space of surrounding tissues, referred to as extravasation, is a result of intercellular openings between endothelial cells. Particles with hydrodynamic diameter less than 5 nm are rapidly removed from the circulation through the 5 nm-sized pore in normal intact endothelium.[90] In contrast, larger particles have limited diffusion across the endothelium resulting in prolonged circulation times.

Although endothelial pores have sizes that vary substantially by tissue throughout the body (from 10 to 1,000 nm)[91,92], each microvasculature has a characteristic pore-size distribution.[93] These pore sizes provide each microvessel with a particular restriction of permeation of macromolecules across a capillary wall. More particularly, the abnormal tumour vasculature is more permeable to larger particles.[94,95] However, the vasculature of each tumour type has its own range of endothelial pores.[96] For example, the pore size for a brain tumour may be ~7 nm versus less than 1 nm for normal brain tissues[96], whereas in breast or pancreatic tumours they might be ~50-60 nm versus ~5 nm for normal breast or pancreatic tissues.[97-99] Therefore, the pore-size heterogeneity of the vasculature in a specific tissue and its tumour is a critical consideration for the design and development of nano-sized objects for biomedical applications.

Blood brain barriers (BBB)

Another major challenge is the BBB, which is formed by the endothelial cells that line cerebral microvessels if the target site is located in the central nervous system (CNS) (**Figure 1.7a**). Unlike capillaries elsewhere in the body, the structure of the BBB is characterized by the tight-junctions that are tightly resistant to ion or small molecule exchange. In addition to the interendothelial tight junctions, the altered expression of trans-endothelial transporter contributes to the barrier properties. Moreover, a large number of pericytes and perivascular antigen-presenting cells around the endothelial cells play an important role in regulating the barrier functions of BBB. Therefore, the BBB represents the main determinant of effective delivery of therapeutic agents to the CNS.

The BBB in brain tumours is compromised due to a loss of tight intercellular junctions and poorly developed astrocytic pericapillary sheath, all of which contribute to its increased permeability. However, this disrupted BBB still acts as an obstacle for many therapeutic agents.[100] Therefore, the capacity of compounds to penetrate the BBB is a crucial factor for drug choice in the treatment of brain tumours (**Figure 1.7b**). Small and lipophilic molecule drugs (e.g., temozolamide, TMZ and carmustine) can cross the BBB by transmembrane diffusion.[101] Certain endogenous large molecules (i.e., insulin, transferrin) cross the BBB via a specific receptor-mediated transcytosis.[102] Alternatively, molecules that not cross the BBB are coupled to molecules that can be used to improve pharmacokinetic profile of a substance. Therefore, the so-called trojan-horse strategy can enable BBB transport

of large molecule drugs or plasmid DNA.[103] Another pathway that provides a means for brain delivery of therapeutic agents across the BBB is adsorptive-mediated transcytosis. This mechanism enables binding and uptake of positively charged molecules to the luminal surface of endothelial cells, followed by exocytosis at the abluminal surface.[102] The conversion of the protein carboxyl groups to primary amino groups (referred to as cationization), or the attachment of cationic import peptides to proteins using either chemical conjugation or genetic fusion is therefore a promising strategy to trigger transport across the BBB via this pathway.[104]
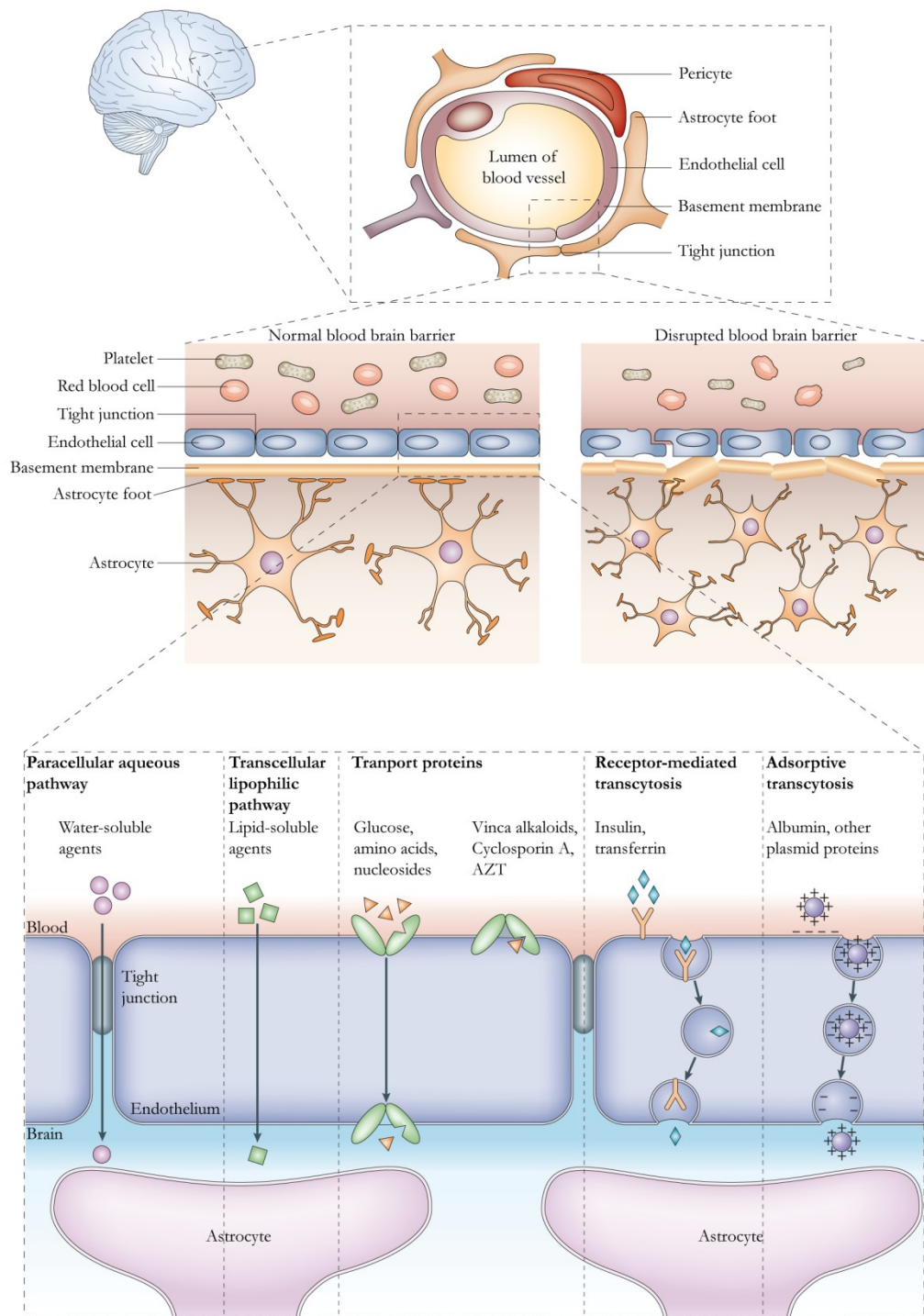
Figure 1.7: The blood brain barrier. a) A schematic diagram of the blood brain barrier (BBB) formed by endothelial cells and their associations with the perivascular endfeet of astrocytes. However, the BBB is disrupted in the setting of a brain tumour, allowing enhanced permeability of molecules. **b**) The main routes for molecular traffic across the BBB. (Modified from Abbott, N.J. 2006)[102]

Extracellular matrix (ECM)

In most tissues, cells are surrounded by the ECM, which is a dense network mainly composed of fibrous proteins (i.e., collagen, laminin, fibronectin) and polysaccharides. The ECM plays an important role in regulating a number of cell functions. For example, ECM proteins bind to integrins and other cell surface receptors, triggering signal transduction that regulates cellular morphology, adhesion, migration, proliferation, and apoptosis.

After a vector leaves the blood stream, it must diffuse through the ECM, which is the most immediate physical barrier that can create resistance to the transport of macromolecules.[105] Diffusion through the ECM is hindered by steric, hydronynamic, and electrostatic interactions between particles and components of the ECM.[106] In addition to the physiochemical properties of the ECM, the movement of particles in the tissue depends on their intrinsic characteristics (i.e., size, charge, and configuration).[107] Several investigations have demonstrated that the transport of therapeutic agents through the ECM could be improved by degradation of ECM proteins.[108] More particularly in tumours, increased amounts of matrix molecules such as collagen and hyarulonic acid can form a barrier that limits the distribution of therapeutic agents through the interstitial space (**Figure 1.8**). These ECM molecules create pores of approximately 10-100 nm and can sterically block particles through hydrodynamic and electrostatic interactions.[109]
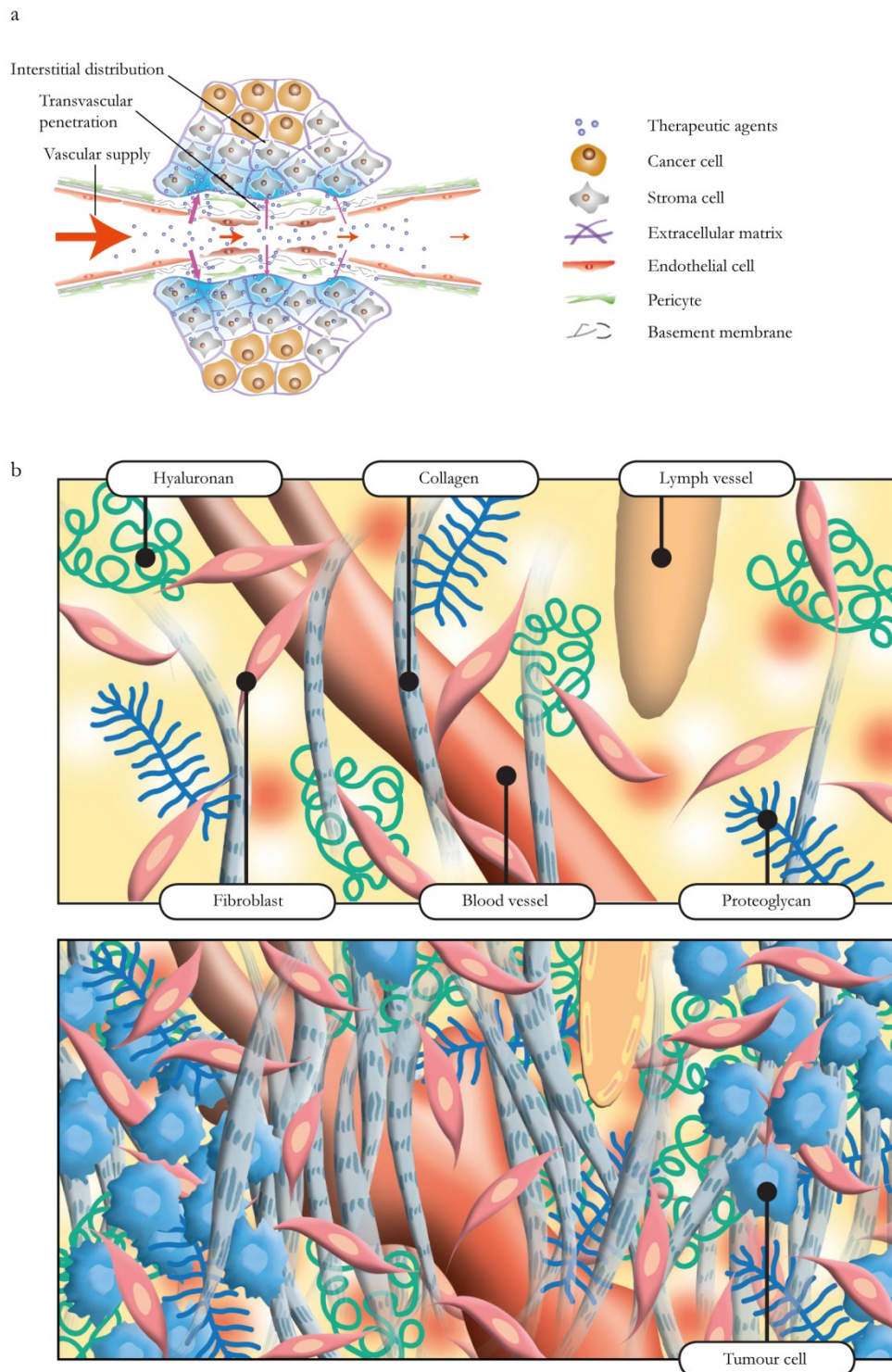
Figure 1.8: The transport barriers to delivery in tumours. a) Therapeutic agents enter a tumour through its blood supply. These particles must cross the blood vessel walls (extravasate) to penetrate into tissues and then diffuse through the interstitial space to reach their target cancer cells.. **b**) The interstitial space in normal tissue and tumours. The interstitium in tumours (bottom) is more disorganized and dense than in normal tissue (top)

1.2.5. Intracellular Barriers to gene delivery vectors

Once the vector can avoid extracellular barriers and has reached its particular target, it must traverse the cell membrane, escape the endosome, and enter the nucleus in order for gene expression to occur. Intracellular barriers faced by gene delivery vectors are depicted schematically in **Figure 1.6**.

Uptake mechanism

The first interaction between a vector and a cell is crucial to promote internalisation. Viral vectors are known for their high efficiency in attachment and entry into host cells. The virus binds to a cell surface receptor and in some cases multiple receptors, triggering its subsequent endocytosis. Adenovirus binds to its cellular CAR through its globular knob of the C-terminal segment of the viral fiber protein. Subsequently, arginine-glycine-aspatic acid (RGD) peptide motif on the viral penton base (the capsid protein at the base of the fibre) interacts with the cellular integrins and facilitates cell entry by endocytosis (**Figure 1.9a**).[110] The first interaction between the cell and AAV2 as shown in **Figure 1.9b** occurs between basic residues of capsid protein VP3 (positions R_{585} and R_{588}) and heparin sulphate proteoglycan (HSPG).[49] The second interaction is between the RGD motif on the viral penton base and the cellular co-receptor, which can either be an integrin (shown here), human fibroblast growth factor receptor or a hepatocyte growth factor receptor.[58] In contrast, membrane fusion is the main mechanism of enveloped viruses such as retrovirus (lentivirus). Following initial non-specific attachment of the virus and cell surface[64], envelope glycoproteins, which

determines the host range of retroviral vectors, binds specifically to their cognate receptors **Figure 1.9c**, resulting in fusion between the lipid membranes of the virus and the host cell after which the viral nucleocapsid is released into the cytoplasm.[60,63] In some cases, membrane fusion is triggered by conformational changes in the viral proteins after receptor binding. In others, a conformational rearrangement of the viral fusion machinery is triggered by a reduction in pH in an endosomal compartment.

For cellular uptake to occur, non-viral vectors must associate with the cell surface, either through nonspecific (for example, electrostatic attraction) or specific (ligand-receptor) binding (**Figure 1.9d**).[111] Nonspecific binding forces that promote cellular contact and particle uptake primarily result from intrinsic characteristics of vectors. For example, surface charge affects particles' interactions with charged phospholipid head groups or protein domains on cell membranes.[112] Other characteristics of particle surface (for example, size, shape, radius of curvature) also play an important role in their cellular uptake.[113-115] In contrast, the specific binding results from interactions between certain ligands and complementary molecules or receptors on the cell membrane, leading to receptor-mediated endocytosis of vectors.[115] Ligands can be either of biological origin (i.e., protein, peptide, and antibody) or abiotic ligands such as chemical moieties or surface functionalities (for example, polymeric substances such as polycationic PEI and polyamidoamine[116]), all of which promote binding affinity and subsequent internalisation. By exploiting the diversity of cell surface receptors, internalisation

and transfection efficiency can be enhanced by attachment of complementary ligands to gene delivery vectors. Incorporation of targeting ligands is expected to decrease the vector amount required to achieve an efficient transfection. Several studies have demonstrated that the use of targeting ligands functions to increase receptor-mediated internalization which is faster than non-specific uptake, and therefore improves intracellular accumulation.[48,117-122] The most popular ligands are transferrin, RGD peptide recognized by integrins of tumour vasculature, lactose by the asialoglycoprotein receptors (ASGRP-R) of the hepatocytes, mannose by mannose receptors (MR) of macrophages and dendritic cells, and folic acid by folate receptors on certain tumour cells.[123]
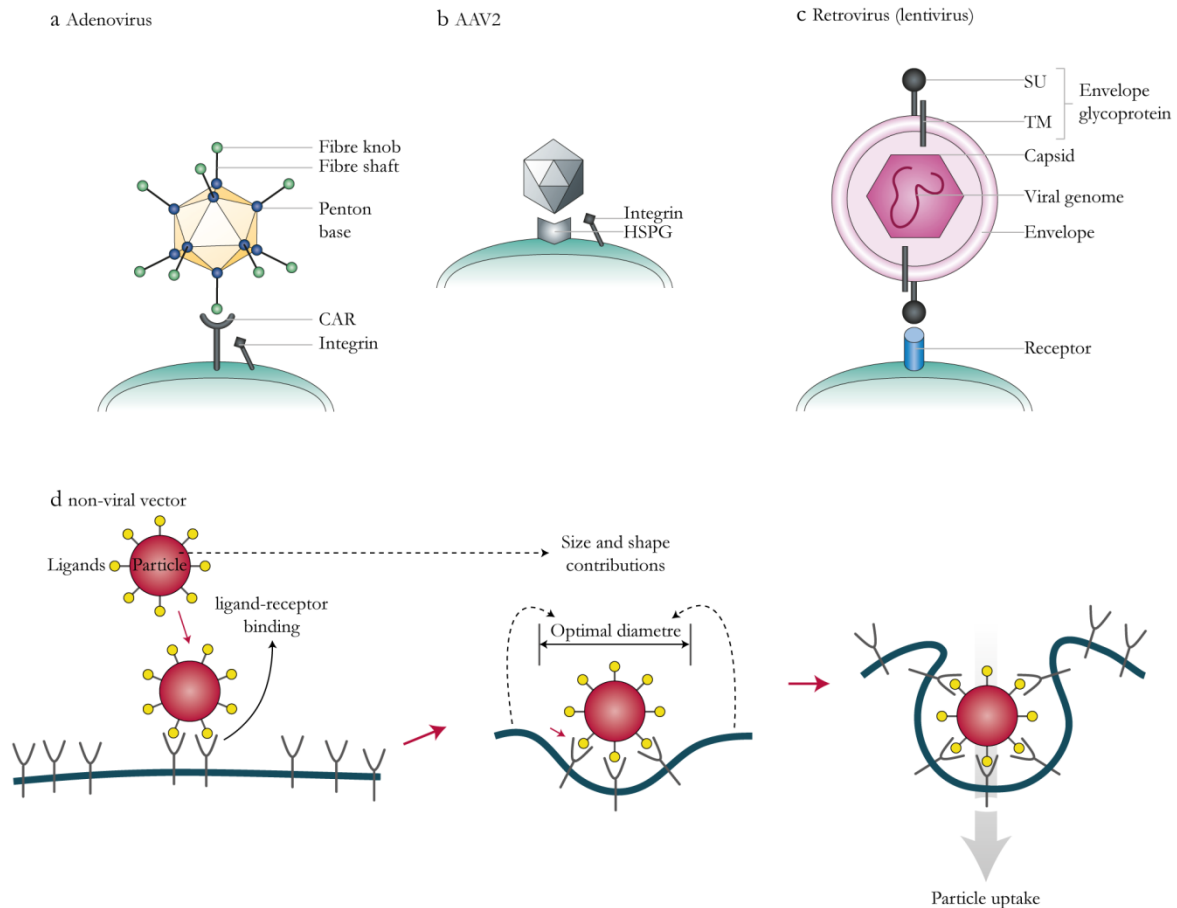
Figure 1.9: Entry mechanisms of viral and non-viral vectors. a) Adenovirus virions bind to the coxsackie adenovirus receptor (CAR) and integrins on the plasma membrane through its fibre knob, and enter the cell by receptor-mediated endocytosis. **b**) AAV binds to heparin sulphate proteoglycan (HSPG) and the co-receptor (integrins, human fibroblast growth factor receptor, or hepatocyte growth factor receptor), and is internalised by endocytosis. **c**) Retrovirus (lentivirus) utilises the membrane fusion mechanism to enter the cells and deliver its genome into the host genome. Following initial nonspecific binding of the virus particle to the cell membrane, viral glycoproteins bind specifically to their cognate receptors. **d**) Specific binding of non-viral vectors on cell membrane via ligand-receptor interactions, resulting in receptor-mediated endocytosis. This process is affected by factors (vector's size and shape, cell membrane's elasticity).

Many endocytosis pathways have been identified and their simple models are schematically shown in **Figure 1.10**. Large particles can be taken up by phagocytosis. This pathway is primarily found in specialised immune cells such as macrophages, dendritic cells, neutrophils, and monocytes. In contrast to phagocytosis, that is limited to a few cell types, most cells are capable of macropinocytosis.[66] Activation of this pathway results in intense actin and microfilaments remodelling and membrane ruffling. The other well characterized mechanism is clathrin-mediated and caveolae-mediated endocytosis. Receptor-mediated endocytosis is the most common route for both viral and non-viral gene delivery vectors and encompasses a variety of entry pathways using clathrin- or caveolin-coated vesicles in order to uptake vectors into the cell from the surface. These pathways are so-called clathrin- or caveolin-mediated endocytosis, respectively. Caveolin-coated vesicles are first transported to intermediate compartments called caveosomes, whereas clathrin-coated vesicles directly traffic to early endosomes. Cargos are also endocytosed via a clathrin/caveolin independent entry pathway using clathrin- and dynamin-independent carriers (CLICs) derived from the plasma membrane, which subsequently traffic to glycosyl phosphatidylinositol-anchored protein enriched early endosomal compartments (GEEC), *en route* to the early endosome.

Many viruses are known to use multiple endocytic pathways to enter cells. For example, AAV2 enters cells via one or more of the following pathways: CLIC/GEEC endocytosis, clathrin-mediated endocytosis or caveolar

endocytosis.[55] Members of the same family may use different pathways. Moreover, viruses may have adapted to *in vitro* cells and may use other pathways *in vivo*. In some cases, sequential binding of viruses to the cell surface triggers different signalling pathways within the cell, recruiting components normally observed to drive different endocytosis pathways. It is therefore difficult to determine whether they use multiple entry pathways or different components of one complex pathway. Similarly, the endocytic pathway of previously reported non-viral vectors greatly varies with the cell types and molecular component of the cell surface in addition to their intrinsic characteristics (e.g., charge and size, etc.), generating conflicting data regarding the internalisation mechanism used.[124-126]
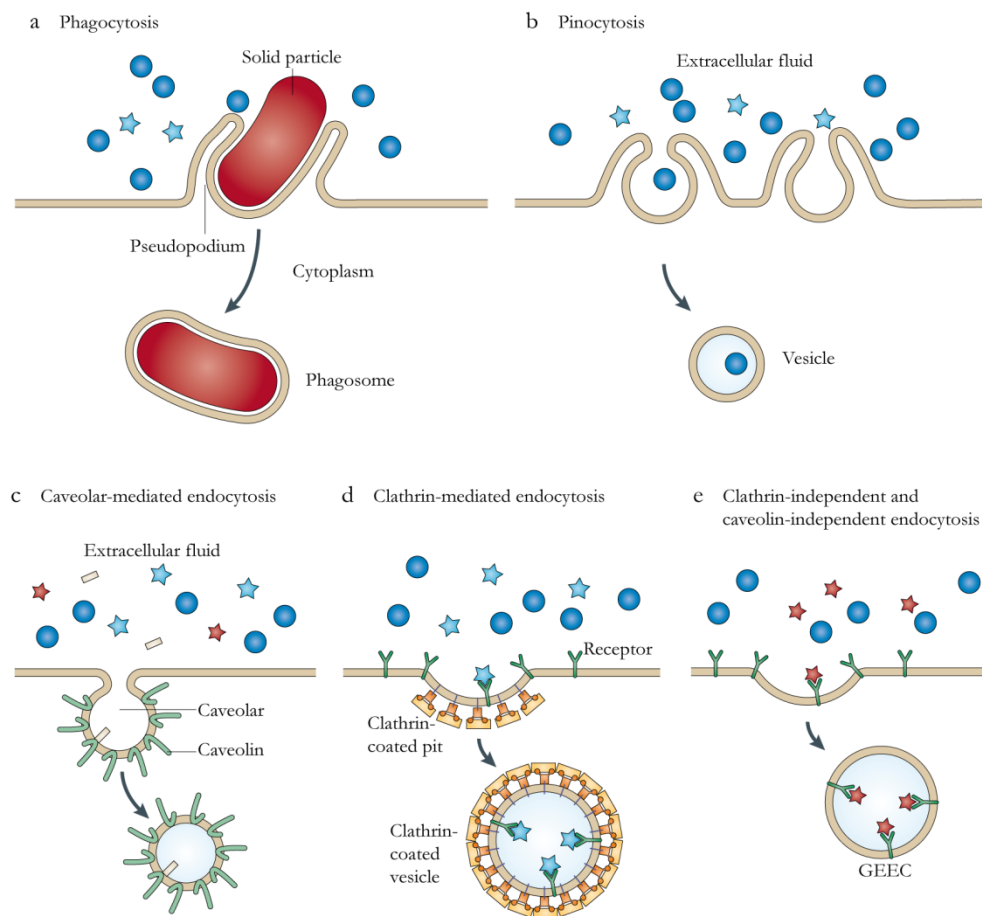
Figure 1.10: Pathways of endocytosis. Internalisation of large particles is facilitated by phagocytosis (**a**), whereas fluid uptake occurs through pinocytosis (**b**). Different cargos can be also internalised through several pathways, including caveolar-mediated endocytosis (**c**), clathrin-mediated endocytosis (**d**) and clathrin-independent and caveolin-independent endocytosis (**e**)(Modified from Petros, R.A. and DeSimone, J.M.2010)[127]

Endosomal escape

Regardless of cell entry pathways, virtually all particles will be localized within endocytic vesicles and fuse or at least interact with the early endosomes which is eventually trafficked to a late endosome. Transition from early to late endosome is marked by the rapid decrease in pH (pH 5-6) due to the action of the ATPase proton-pump enzyme located on endosomal membranes. Subsequent trafficking to lysosomal compartments leads to further acidification (pH 4) and the activation of various hydrolytic enzymes, which represent a hostile environment known to facilitate vector degradation.

Various strategies are employed by different viruses to gain access to the cytosol. Endosomal escape of non-enveloped viruses requires a mechanism of membrane disruption via carper-like mechanism (for example, in adenovirus) or transmembrane pore formation via a barrel-stave mechanism (for example, parvovirus), whereas enveloped viruses use membrane fusion between the viral envelope and endosomal membrane.[128] (**Figure 1.11**) This fusion is mediated by fusion proteins which undergo conformational changes in the acidic environment of endosome, and subsequently interact with the membrane bilayer, enabling cytosolic translocation of the viral genome.[129]

In contrast to viral vectors, which have highly evolved endosomal escape mechanisms[130], the endosomal entrapment and subsequent lysosomal degradation are still regarded as a major limitation for non-viral vectors. Design of gene delivery vectors with capability of endosomal escape is therefore critical for high

transfection efficiency. Integrating the viral mechanism into non-viral gene delivery system are main strategies being employed to facilitate endosomal escape. Influenza viruses escape the endosome with help from a short chain of N-terminal amphiphilic anionic peptide residues (termed hemaglutinin A2 HA2) (**Figure 1.11b**).[130] Modification of non-viral vectors with HA2 peptide facilitating endosomal escape resulted in significant augmentation of the delivery efficiency.[69] Synthetic peptides mimicking virus's fusogenic peptides have also been designed for gene delivery system, leading to the enhanced transfection efficiency of non-viral vectors. For example, the synthetic GALA peptide with a repeated amino acid sequence (i.e., glutamic-alanine-leucine-alanine) was designed to interact with lipid bilayers following a conformational change to give a helical structure at low pH.[131] Similarly, INF7 and H5WYG improved endosomal escape of non-viral vectors.[132]

The endosomal escape of some non-viral vectors is dependent on the complexing material used. In case of polyplexes, cationic polymers provide high transfection efficiency due to their intrinsic endosomolytic activity. Escape of polyplexes into the cytosol is mediated by the proton sponge mechanism (**Figure 1.12**), which has been observed in certain cationic polymers with a high buffer capacity over a wide pH range. These polymers, which usually contain protonable secondary and/or tertiary amine groups with pKa close to endosomal pH, behaves as a sponge that absorbs protons, after which an influx of counter chloride ion against the proton accumulation leads to increased osmotic pressure, followed by flow of water and subsequent endosome swelling and rupture. However, recent studies suggested an

alternative mechanism where endosomal escape relies on time-dependent protonation-induced membrane permeabilization by tight binding of polyplex and the lumen side of the endosomal membranes.

For cationic lipid-based delivery systems, the lipid mixing mechanism was proposed to be their endosomal escape mechanism (**Figure 1.13**). Following the electrostatic interaction between carrier lipids and the endosomal membranes, negatively charged lipids (mainly found in the cytoplasmic-facing leaflet) of the endosomal membrane laterally diffuse into cationic lipoplexes. This leads to the formation of charge-neutral ion pairs with the lipoplex, thereby destabilizing the endosomal membrane organization and causing release of nucleic acids into the cytosol. The other proposed lipid mixing mechanism involves lipoplex degradation, followed by dissociation of lipid molecules that allows the passive release of nucleic acids. Subsequently, integration of free lipids results in transient pore formation and cytoplasmic transport of nucleic acids.
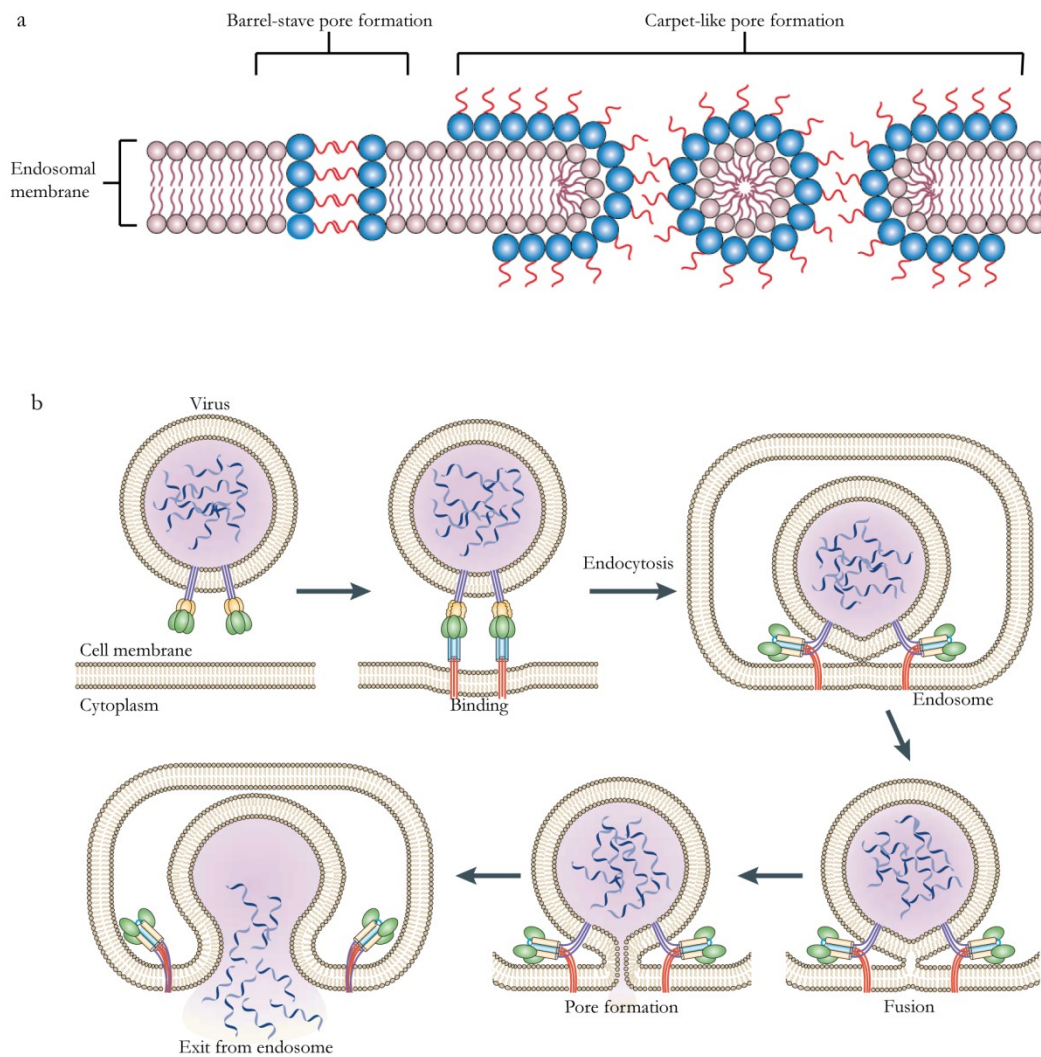
Figure 1.11: Endosomal escape mechanism of non-enveloped and enveloped viruses. a) Two proposed mechanisms for endosomal escape of non-enveloped viruses; carpet-like or a barrel-stave mechanism. In the carpet mechanism, the peptides interact with the lipid head group and do not insert into the hydrophobic region of the membrane. With a barrel-stave mechanism, the peptides insert into the hydrophobic core of the membrane, resulting in the formation of transmembrane pores. **b**) Influenza virus, which is endocytosed into an endosome, is shown as an example. In the acidic endosomes, HA mediates the fusion of the viral and endosomal membranes. (Modified from Dimitrov, D.S. 2004 and Hurdle, J.G. *et al.* 2011)[128,133]
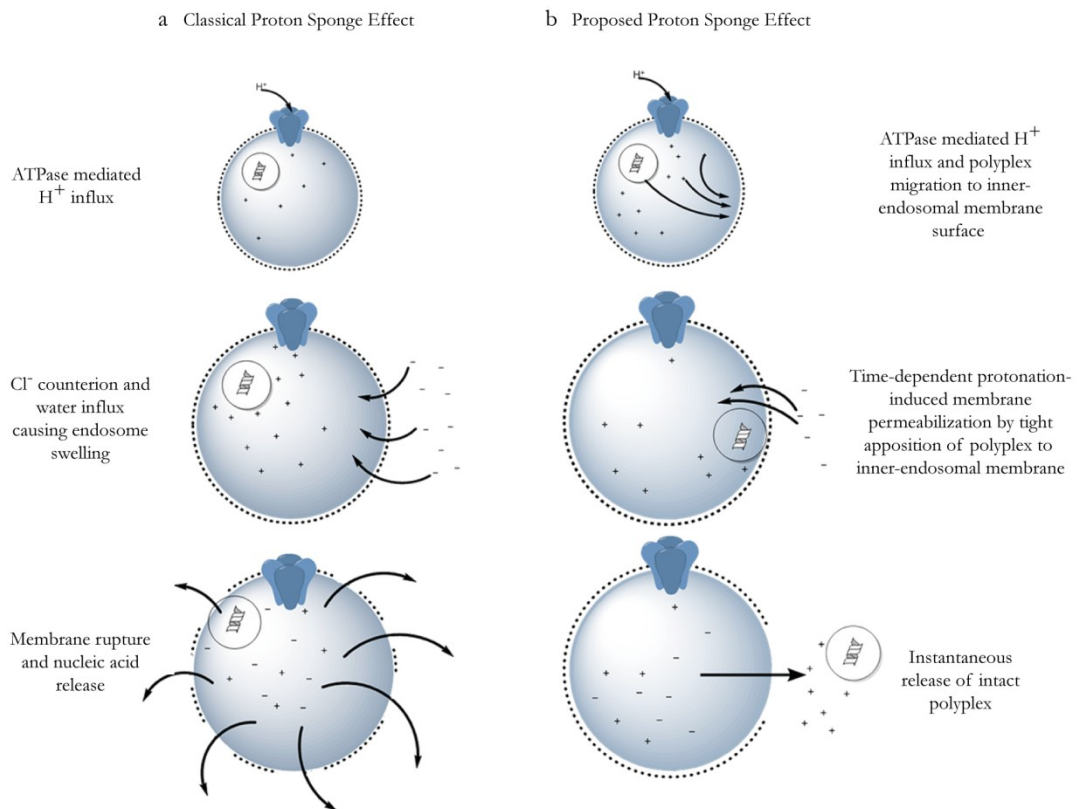
Figure 1.12: Schematic representation of classical and proposed proton sponge mechanisms. a) Classical mechanism **b**) proposed mechanism.
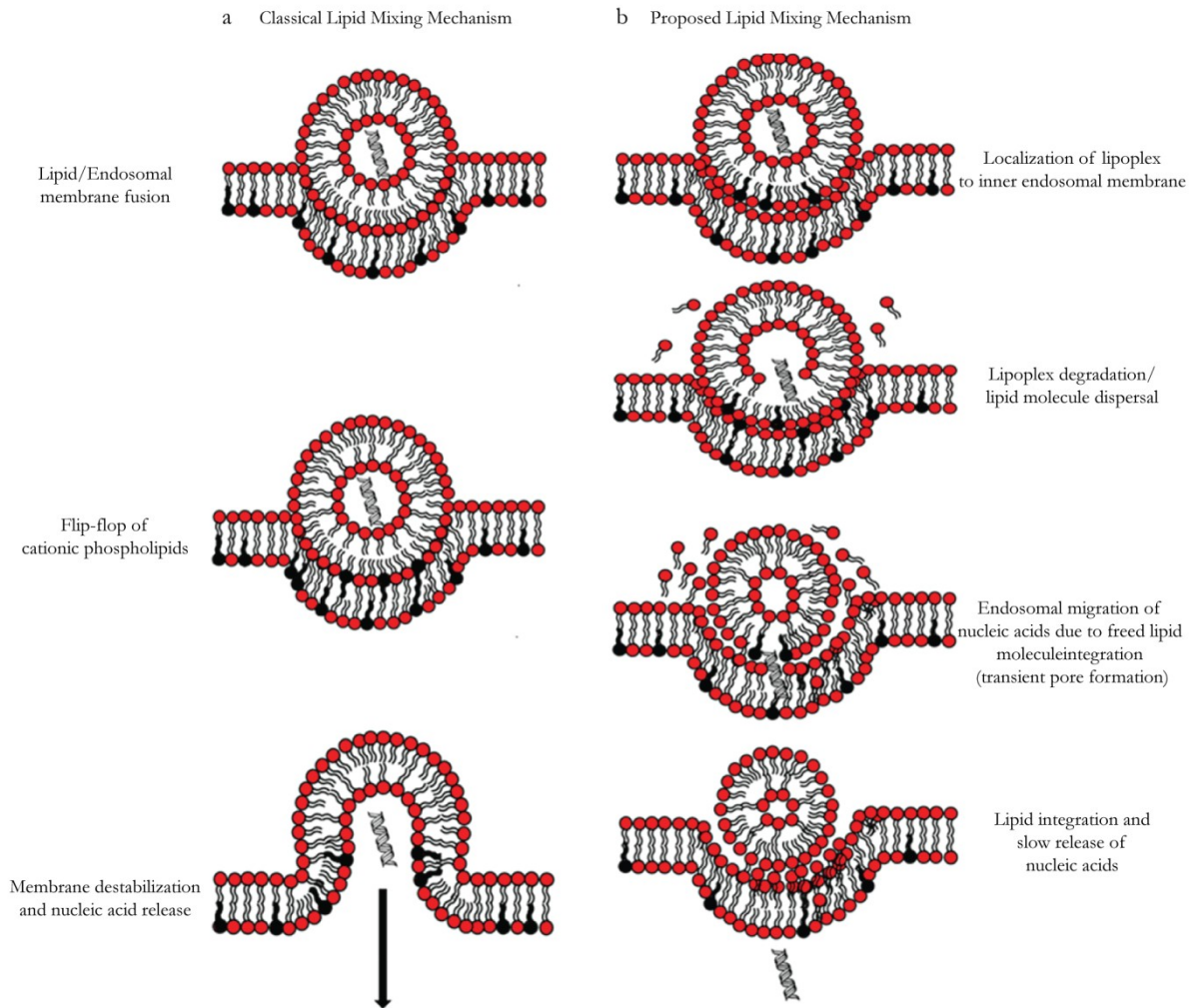
Figure 1.13: Schematic representation of classical and proposed lipid mixing mechanisms. a) Classical mechanism **b**) proposed mechanism.

Nuclear import

The cell's genetic material is separated from the surrounding cytoplasm by the nuclear envelope, which functions as a physical barrier for nuclear import of macromolecules. The nuclear pore complex (NPCs) that fuses the inner and outer membranes to form aqueous translocation channels tightly regulates nucleocytoplasmic trafficking and limits passive diffusion of molecules with sizes >30 kDa.[134] The process is energy dependent and requires the nuclear localization signal (NLS) to allow nuclear translocation of macromolecules. Many NLS peptides have been used to increase nuclear import of DNA, showing improvements in gene expression. The well-characterized NLS in the field of gene delivery include a classical NLS peptide (PKKKRKV) derived from the large tumour antigen of the simian virus 40 (SV40)[135] and the M9 sequence of the heterogeneous nuclear ribonucleoprotein (hnRNP) A1.[136]

1.2.6. Gene therapy

Gene therapy is considered to be the treatment of gene-associated diseases by transferring exogenous nucleic acids into the appropriate cells of patients.[137] Advances in molecular biology and biotechnology as well as the completion of Human Genome Project have led to the identification and characterization of numerous genes associated with diseases.[27] A mutation in any gene can result in a disease, physical disability, or shortened life span. Therefore, the direct use of nucleic acid as a therapeutic agent to treat or prevent genetically-related diseases (so-called gene therapy) has attracted great interest over the past few decades.

Gene therapy holds the promise of cures for genetic defects such as cystic fibrosis, haemophilia, muscular dystrophy and sickle cell anaemia, complex acquired diseases such as cancers, cardiovascular diseases, sensory deficits such as blindness and hearing loss, infectious diseases such as anti-HIV gene therapy and DNA vaccine.

On the website of the Journal of Gene Medicine, the number of gene therapy clinical trials having commenced worldwide for the past 20 years are shown (for updated information see http://www.wiley.co.uk/genmed/clinical/). In 2013, the total number of protocols reached 1,972 and the numbers per year have been stable. In the analysis of indication (**Figure 1.14a**), most of the trials have been developed against cancer, followed by monogenic diseases (those caused by inherited single gene defects). In the analysis of clinical phases (**Figure 1.14b**), 78.5 % of clinical trials are Phase I or I/II, suggesting that a vast majority of the trials are early stage. However, 4.7 % of clinical trials are now at the late stages of clinical trial phase II/III or III and 0.1 % of all clinical trials have succeed in entering phase IV, which has been marketed and designed to assess any adverse effects associated with widespread use. These data suggest that clinical gene therapy is becoming more mature year by year. In the analysis of gene types (**Figure 1.14c**), the top gene type used is 'antigen', indicating that the DNA vaccine has recently been often investigated in clinical trials because vaccination is now a common therapy for infectious diseases and cancer.
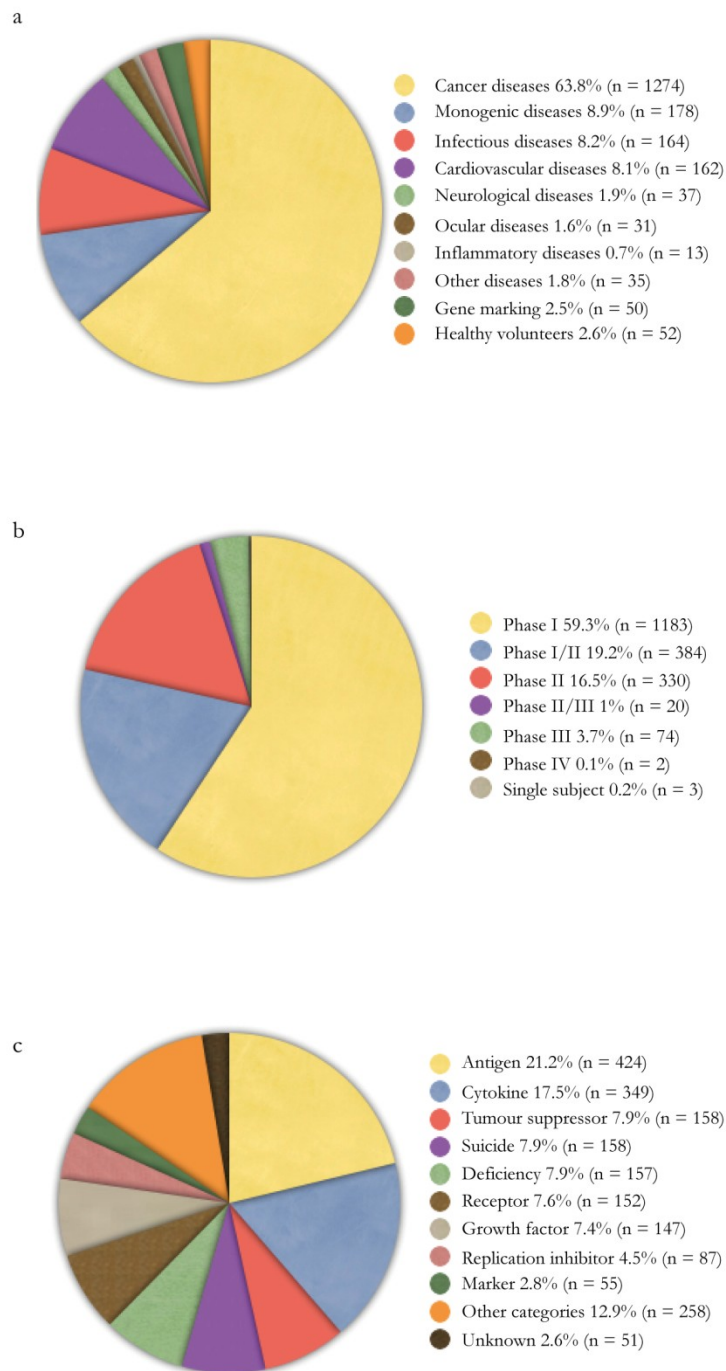
Figure 1.14: Clinical gene therapy worldwide. a) Indications addressed by gene therapy clinical trials. **b**) Phases of gene therapy clinical trials. **c**) Gene types transferred in gene therapy clinical trials.

1.2.7. Strategies for Gene therapy of cancer

Cancer development requires multiple altered genetic events, some of which include mutations of the tumour suppressor genes resulting in the loss of cell growth and apoptosis regulation.[18] The restoration of the functional tumour suppressor gene through gene therapy is therefore a possible treatment. For example, a cell cycle regulatory protein p53 is frequently mutated in human cancers. The successful replacement of p53 gene in ovary cancer patients has caused upregulation of this gene and other enzymes downstream from p53. Other well-characterized tumour-suppressor genes that have been used for cancer treatment include p16, p27, and PTEN.[138-141] Another common cancer genetic event involves a mutation that causes the upregulation of oncogenes, which enables uncontrolled cell proliferation and survival, promotes angiogenesis, invasion and metastasis. One such oncogene frequenty mutated in cancers, K-Ras, has been targeted for suppression of tumour growth using siRNA.[142] RNA interference can also be used to target other oncogenes such as the anti-apoptosis gene livin and cyclin-E.[143] Another potential cancer gene therapy application is prodrug activation (**Figure 1.15a**). This strategy involves the expression of an exogenous enzyme within cancer cells that can convert a systemically administered non-toxic prodrug into a potent anti-cancer drug. An example of a commonly used enzyme-prodrug pair is the herpes simplex virus thymidine kinase (HSVtk) and phosphorylated ganciclovir (GCV). If GCV is delivered to a HSVtk-expressing cell, the thymidine kinase will phosphorylate the GCV converting it to a DNA synthesis

inhibitor.[144] Some other enzyme-prodrug combinations that have been investigated for therapeutic efficacy include the DNA synthesis inhibitors cytosine deaminase and 5-fluorouracil, the DNA cross-linking reagents nitroreductase and CB1954, and hepatic cytochrome P450 and cyclophosphamide.[144,145] Alternatively, the delivery of cytokine genes, such as Granulocyte-macrophage colony-stimulating factor (GM-CSF), interleukins or interferons, to activate or attract immune cells against the tumour, also hold potential for tumour therapy (**Figure 1.15b**).[146-148]

a
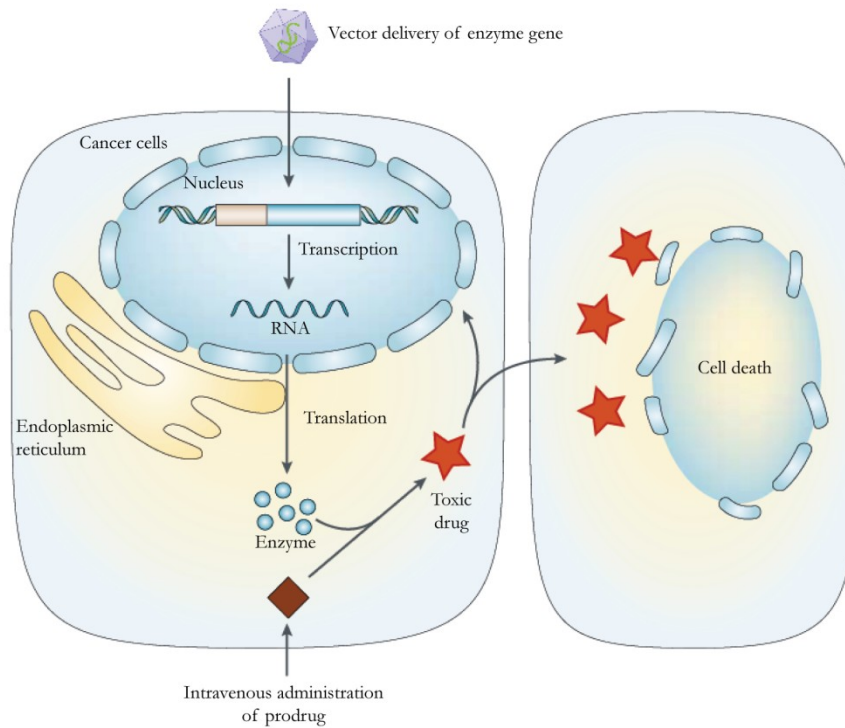
b
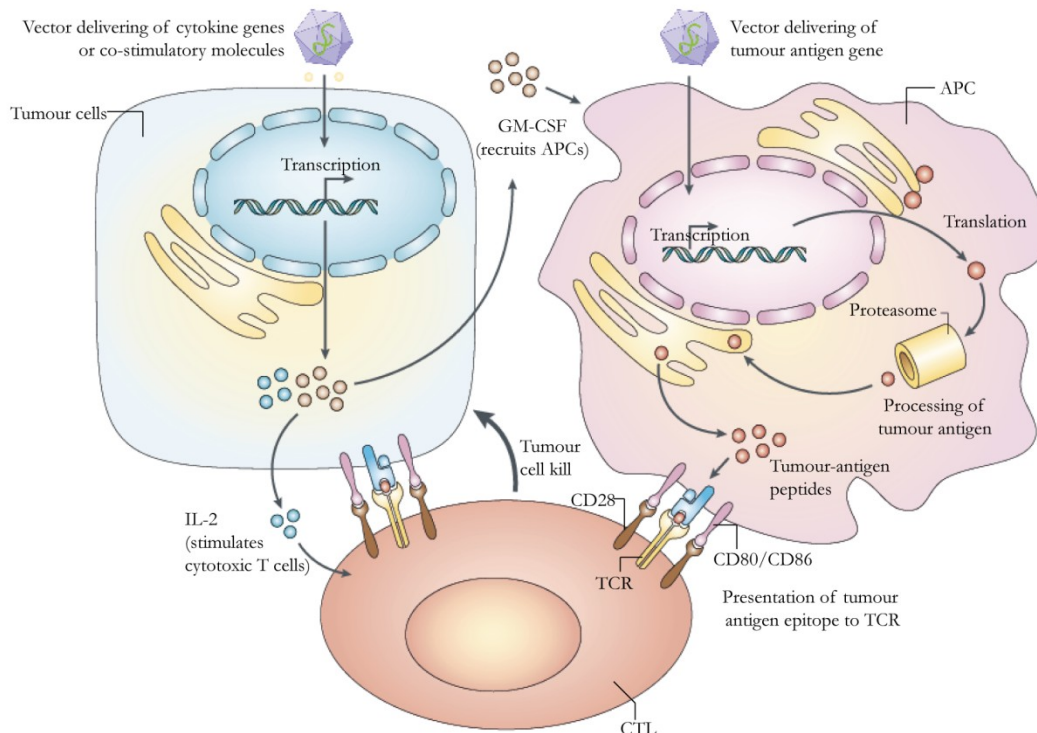
Figure 1.15: Major approaches employed for gene therapy of cancer. a) Delivery of a suicide gene to convert the prodrug into toxic compound capable of killing tumour cells. **b**) Delivery of cytokine or tumour antigen genes to activate or attract immune cells against the tumour.

1.2.8. Ligand-directed vector for targeted gene therapy of cancer

The ability to target the delivery of nucleic acids or any therapeutic agents can minimize side effects, maximize treatment to the target site and allow for more flexibility in dosing limits. Integrating high affinity, high specificity peptide ligands into gene delivery vectors that target tumours and avoid healthy tissues has the potential to make gene therapy a reality for cancer.[149] Targeting peptides for a specific receptor can be obtained using knowledge of the naturally existing ligand's binding site, sequence, and secondary structure to create a biomimic peptide, or by the screening of phage display peptide libraries. The latter technique has enabled the rapid selection of a bacteriophage expressing the appropriate peptide sequences as fusions to the coat proteins with a high affinity for any substrate of interest. To date, the screening of phage display peptide libraries is one of extensively used high-throughput technologies for the identification of tumour-specific markers. In most cases, the method involves *in vitro* selection by immobilizing the target molecules such as proteins or other macromolecules onto plastic or direct biopanning on cultured cells.[150] On the other hand, *in vivo* phage selection involves the intravenous administration of the phage library into an animal and isolating phages that home preferentially to the target tissue or organs due to their binding to tissue-specific receptors (**Figure 1.16**).

Anti-angiogenic gene therapy has emerged as a new modality to treat human cancers and has received much widespread attention.[151] Endothelial cells associated with the tumour vasculature are particular suitable for anti-angiogenic therapy

because they are easily accessible to intravenously delivered agents and are less likely to accumulate mutations that render them resistant to therapy due to their more stable genetics than cancer cells.[152]

Enzyme/prodrug-based gene therapy has been frequently used to target the tumour vasculature in order to deconstruct the tumour mass. Generally, solid tumours cannot grow beyond a few millimetres in a diameter without the support of blood vessels to provide essential elements as well as to facilitate the removal of metabolic wastes.[153,154] Unique epitopes expressed on the tumour-associated endothelial cells, which allow the tumour vasculature to be distinguished from the normal vasculature, could serve as targets for tumour-specific binding of targeting agents.[155] In contrast to most cancer-associated epitopes expressed on malignant cells inside the tumour compartment, these epitopes are readily accessible to the lumen of blood vessels, which mediate efficient targeting of therapeutic agents.
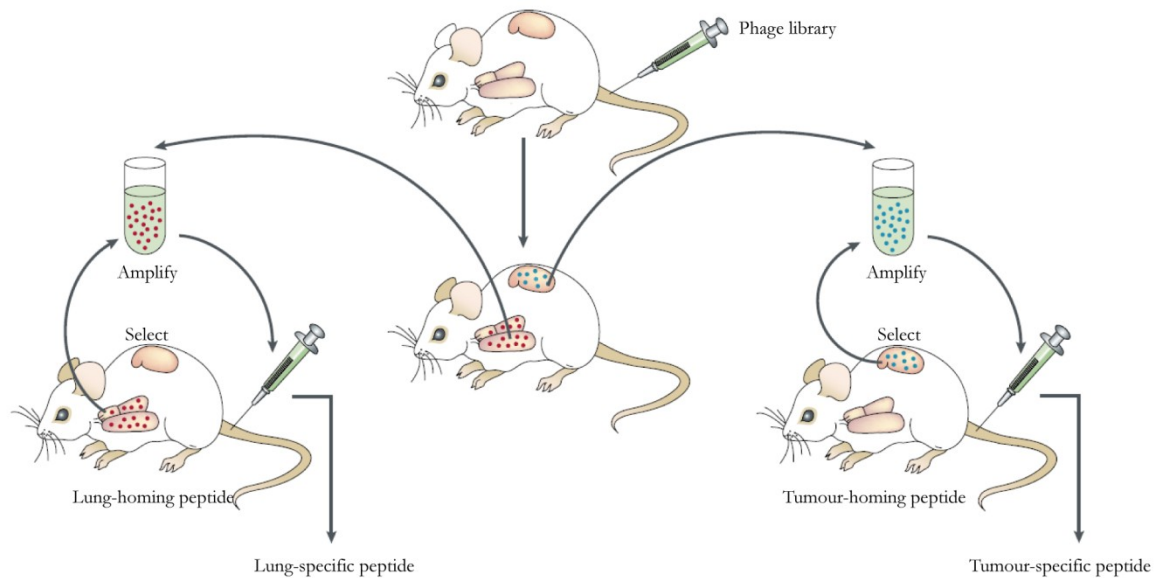
Figure 1.16: The workflow of in vivo phage display screening. The process starts with intravenous injection of the phage library, after which the target organ is isolated and homoginized. The homogenate is used for phage amplification for subsequent rounds of selection. The DNA encoding the expressed peptide is then sequenced.

1.2.9. Gene delivery with peptides targeting integrins

One approach to targeted gene delivery for cancer treatment takes advantage of elevated levels of receptor expression in tumours. For example, the $\alpha_v\beta_3$ and $\alpha_v\beta_5$ integrins which serve as receptors for RGD-containing protein have been found to be overexpressed on most tumour cells as well as tumour-associated endothelial cells during the formation of new capillary blood vessels (angiogenesis) (**Figure 1.17**).[156] The RGD motif is found in extracellular matrix components including fibronectin, vitronectin, laminin, and collagen. The motif is also found in the penton base of adenovirus capsid which is known to bind the $\alpha_v\beta_3$ integrin.[157] In this context, targeting the tumour vasculature or tumour cells by RGD-based strategies is a promising approach for delivering therapeutic agents for cancer treatment. It has been shown that the integrin $\alpha_v\beta_3$ is overexpressed not only on the tumour-associated endothelium but also on cancer cells.[158,159] On the contrary, other largely described ligands such as folate or transferrin receptors are only expressed on cancer cells. The targeting mechanism of RGD-grafted therapeutic agents is schematically shown in **Figure 1.18**. Moreover, $\alpha_v\beta_3$ integrins are known to be absent or barely detectable in non-angiogenesis endothelial cells, whereas transferrin is upregulated on cancer cells as well as on brain capillaries, endocrine pancreas, or hepatic kupffer cells.[160] In addition, some ligands, such as folate which is supplied by food, show naturally high concentrations in the human body, resulting in the competition for binding of the drug-conjugated ligand to the target receptor, and therefore reducing the effective intracellular accumulation of the

delivered drug.[161] The RGD4C peptide (ACDCRGDCFC), in which the RGD sequence is flanked by cysteines on either end and can therefore form two disulphide bonds, was originally identified via phage display of a random peptide library.[162] In order to suppress tumour angiogenesis and growth, a great effort has been made to use RGD peptides as antagonists for several integrins, such as $\alpha_v\beta_3$ and $\alpha_v\beta_5$. Unfortunately, a cyclic RGD pentapeptide (cilengitide) did not meet its primary endpoint of significantly increasing overall survival when combined with the current conventional chemoradiotherapy regimen, ie temozolomide and radiotherapy in a Phase III clinical trial, indicating how challenging glioblastoma remains. However, the $\alpha_v\beta_3$ and $\alpha_v\beta_5$ integrins are still the ideal target for specific delivery of cancer therapeutics. In addition to their direct use as therapeutic targets, integrin-targeted nanoparticles with a broad spectrum of anti-cancer payloads also represent a particularly promising area for cancer treatment.[158] The RGD peptides have been extensively used to functionalize a broad range number of nanoparticles, such as, polymers, gold nanoparticles, magnetic nanoparticles for molecular imaging and many other vectors such as liposomes for their efficient accumulation in tumour sites.[149] These RGD-targeted nanoparticles have recently proven advantageous in delivering biopharmaceutical drugs (i.e., peptides, proteins, nucleic acids) and chemotherapeutic drugs. Several advantages are attributable to these RGD-targeted nanoparticles: (i) they may specifically address therapeutic agents to angiogenic endothelial cells and/or cancer cells by interaction between the RGD motif and $\alpha_v\beta_3$ overexpressed on these cells, allowing active targeting of the

tumours;[163] (ii) RGD-targeted nanoparticles can be endocytosed via receptor-mediated mechanism, which cannot be found with single peptide constructs or with nontargeted nanoparticles; this is particularly interesting for the intracellular delivery of therapeutic agents to cancer cells.[164] (iii) the size of these nanoparticles (20-400 nm) leads to the passive targeting of tumour via the so-called enhanced permeability and retention (EPR) effect;[165] (iv) the avoidance of renal filtration due to the size of these systems leads to prolonged circulation times and longer ligand exposure to receptors within the target tissues.[166]
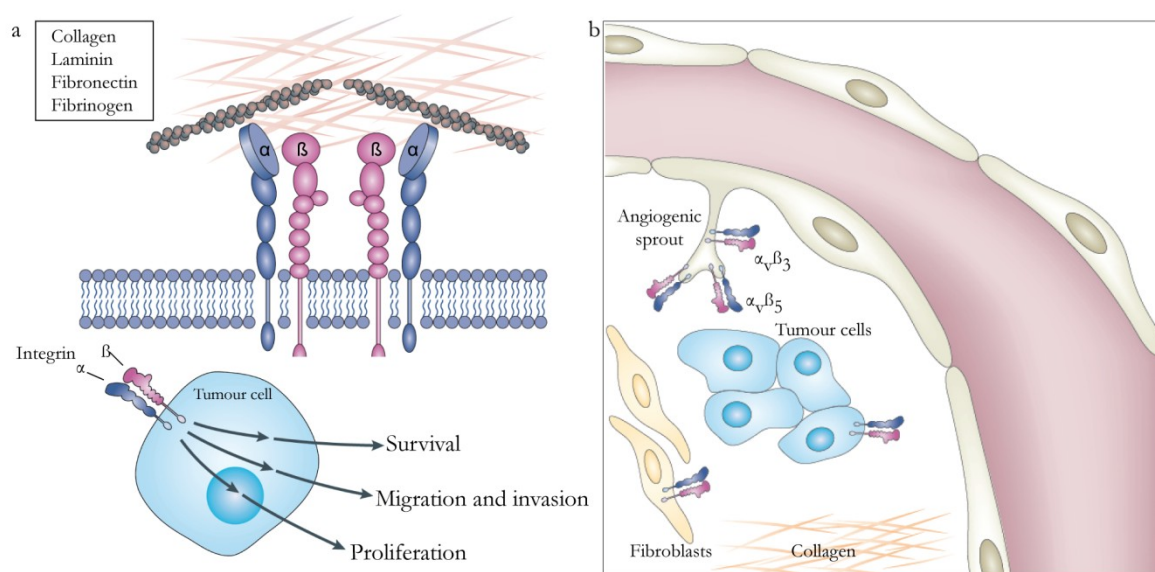
Figure 1.17: Integrins in tumour cells and tumour-associated cells. **a**) Integrins, heterodimeric cell surface receptors, are formed by the combination of α- and β-subunits. Certain integrins directly bind to the ECM components and regulate cell motility and invasion. In tumour cells, integrin signalling regulates a number of cellular functions including survival, proliferation, migration and invasion. **b**) In addition to tumour cells, integrins are also expressed on tumour-associated cells, such as the vascular endothelium and fibroblasts. In endothelial cells, integrins are responsible for the migration, proliferation and survival necessary for the new formation of blood vessels (angiogenesis). The tumour-associated fibroblasts produce large amounts of collagen that may contribute to resistance to therapy in some tumours.(Modified from Danhier, F. *et al.* 2012)[149]
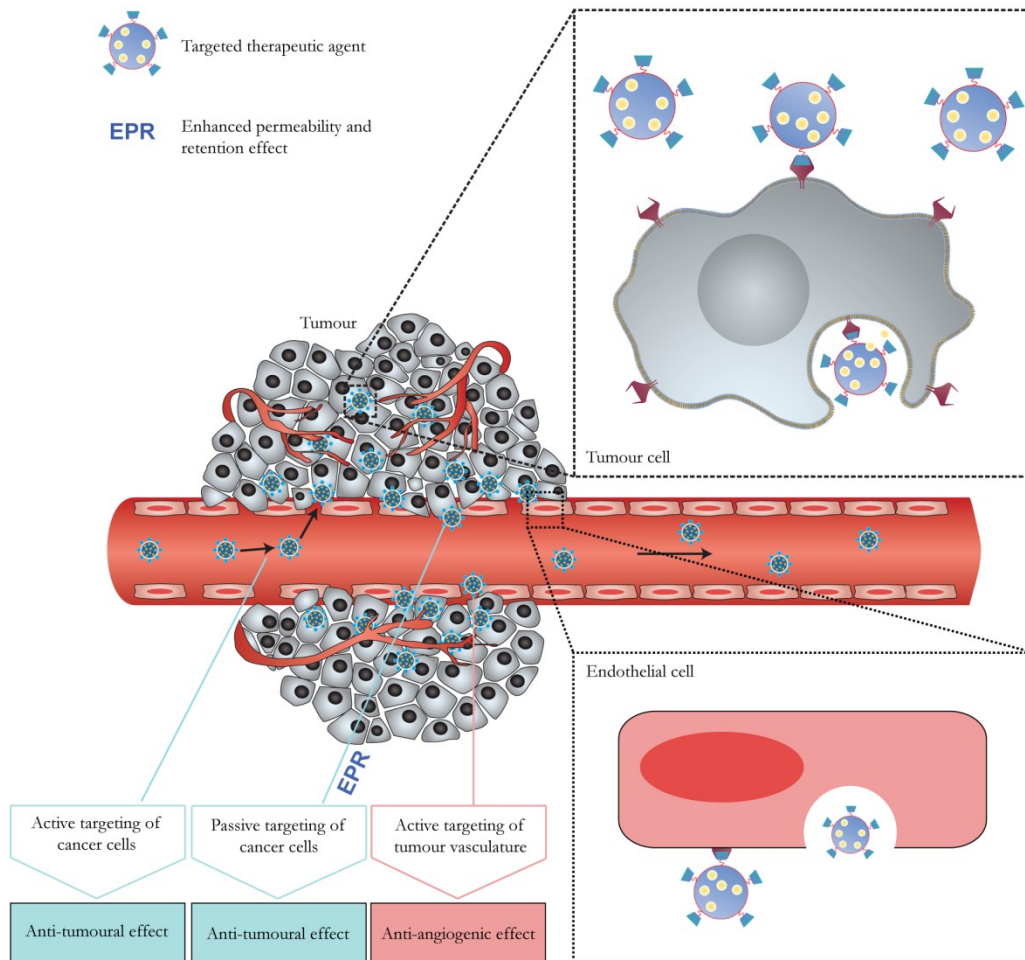
Figure 1.18: Schematic representation of targeting mechanisms of RGD-grafted vectors. Circulating RGD vectors can bind to integrins overexpressed on tumour-associated endothelial cells, followed by internalisation via receptor-mediated endocytosis. The release of therapeutic agents then leads to cancer cell killing. The tumour destruction is resulted from the antiangiogenic effect in which the death of tumour is induced by the lack of oxygen and nutrients. RGD vectors also enter the tumour via the EPR effect. The EPR effect combined with the active targeting of cancer cells leads to the anticancer effect of therapeutic agent-loaded RGD vector.

1.2.10. Bacteriophage vectors

Bacteriophages, also abbreviated as phages, are the most abundant biological entities in the biosphere and exist in various environments as part of a microbial ecosystem.[167] They can be found even in the human or animal bodies.[139] These particles consist of a protein coat containing a DNA or RNA genome. The routinely used and well characterized phages as gene delivery vectors are the filamentous M13 and lambda. However, filamentous bacteriophages have been used as gene delivery vectors in this study. Accordingly, this thesis will focus on filamentous phages despite fundamental difference from lambda phages and its relatives such as T4 and tailed.

The virion of filamentous phages has a cylindrical shape with a length of 800 nm and a diameter of 6 nm and is composed of a circular single stranded DNA genome encapsulated by a tube made of five coat proteins, namely pIII, pVI, pVII, pVIII, and pIX. At one end, there are five copies of pIX and pVII and 5 copies of pVI and pIII at the other end (**Figure 1.19**). The body of the phage is composed of thousands of helically arrayed major coat protein pVIII subunits and represents 98% of the phage mass. The M13 filamentous bacteriophage virus of the Ff family infects *E. coli* which is a vital component of the intestinal flora and uses host cells to assemble progeny phage without lysing and killing the host; instead, they are secreted into the environment. The life cycle of filamentous bacteriophages is shown in **Figure1.20**.

Peptides and proteins of interest can be fused to the phage coat protein and thereby displayed on the outer surface of the phage particles. This review will cover the display of foreign proteins on the most commonly used pIII and pVIII. Modes of displaying peptides can be classified into three systems. The first is based on the original filamentous phage genome. The sequence encoding the foreign peptide is inserted between the coding sequences for the signal peptide and the mature coat protein, without disturbing the protein reading frame. Peptides can be fused to all five copies of the pIII (type 3 display) or to all copies of pVIII (type 8 display). Second, a hybrid system, in which the phage genome contains a recombinant gene in addition to a wild type gene, can be employed.[168] In this system peptides or proteins can be displayed on one copy of pIII or on approximately 150 copies of pVIII, while the remaining pIII and pVIII subunits are wild type (type 33 or 88 display). The first two systems are shown in **Figure 1.21**. The third system is the use of plasmid vectors (also known as phagemids), in which the wild-type and recombinant genes are carried on separate genomes present in the same cell.[169,170] This system has been extensively used to display antibody and antibody fragment (i.e., Fv, scFv or Fab).[169] The use of the phagemid system to display guest peptides will not be covered here.
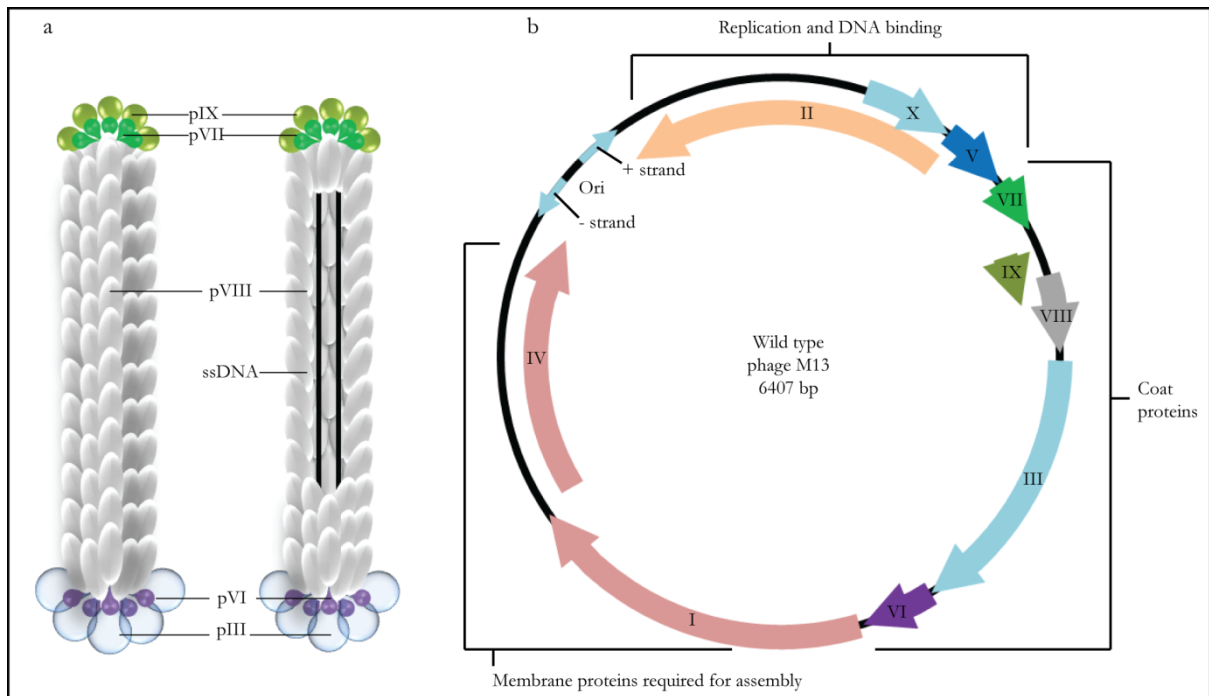
Figure 1.19: Schematic representation of the structure and genome organization of filamentous bacteriophage. a) The localisation of filamentous bacteriophage coat proteins. **b**) Genetic map of the Ff phage. The gene products are grouped based on their known functions.
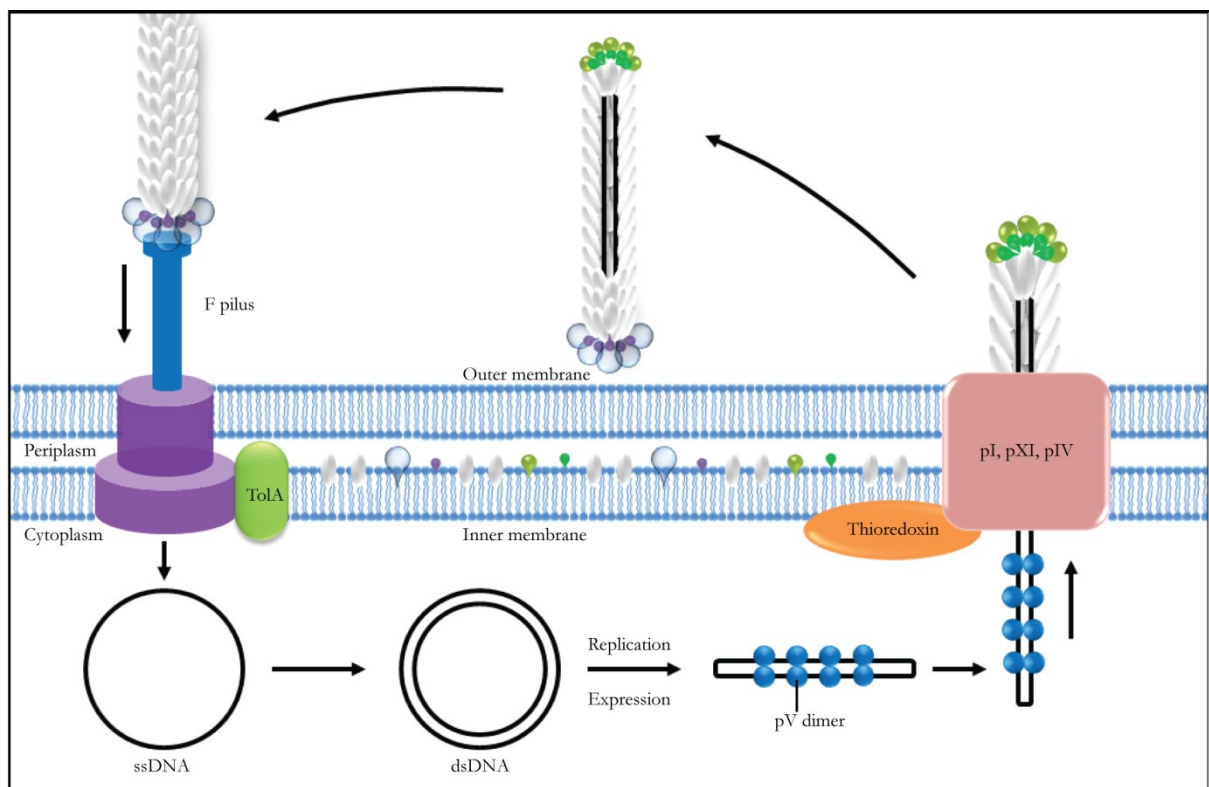
Figure 1.20: Life cycle of filamentous bacteriophage. Following the binding of phage to the F-pilus of bacteria via pIII, the introduced ssDNA is converted to dsDNA. Gene expression is then initiated after which the assembly and release of the phage particles occurs at the bacterial membrane.
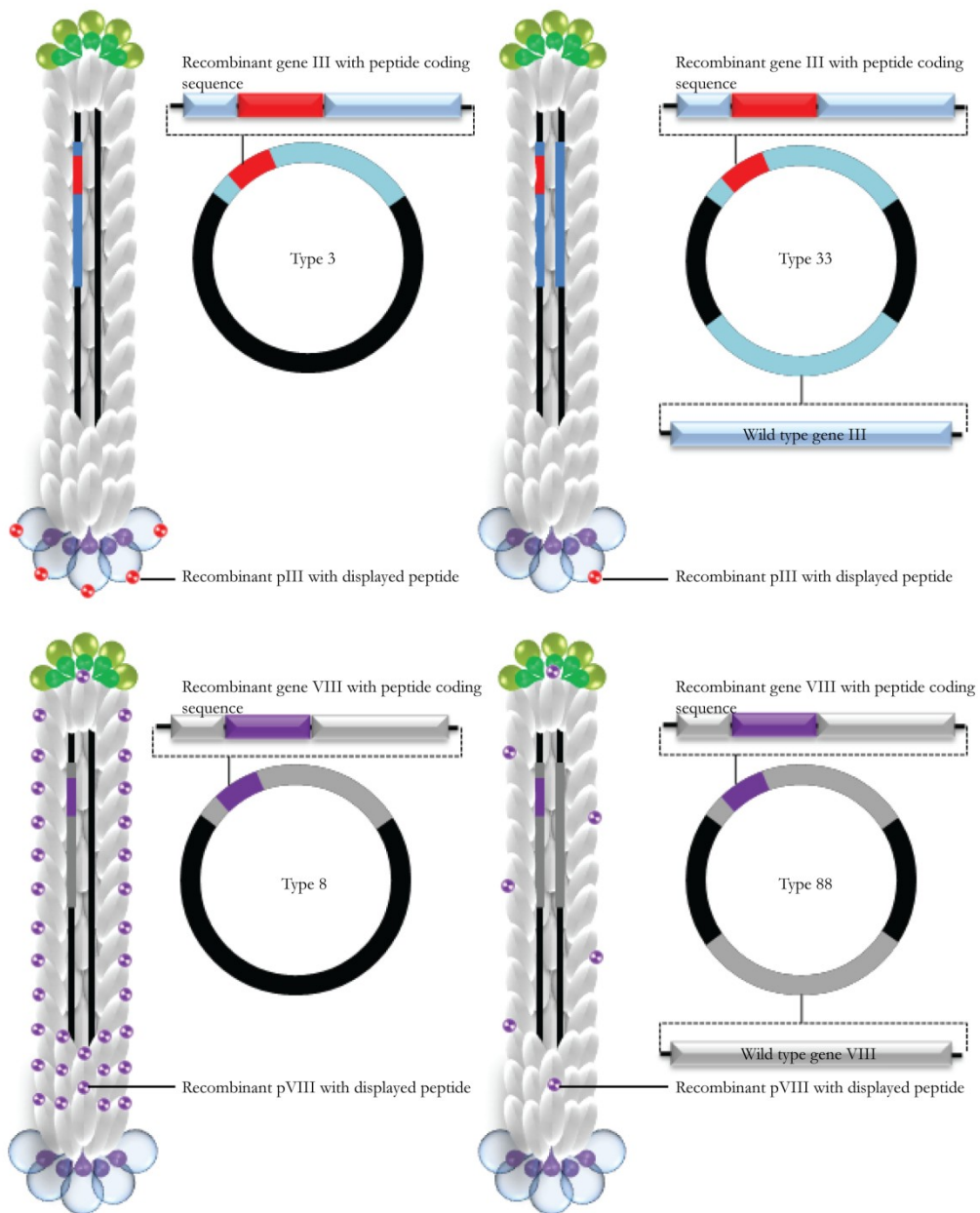
Figure 1.21: Modes of displaying foreign peptides fused to pIII or pVIII coat proteins. Recombinant genes carrying sequences encoding the guest peptides and their corresponding recombinant proteins displaying the guest peptide are coloured red and purple for pIII and pVI, respectively.

1.2.11. Hybrid AAVP

Despite several advantages, the efficiency of transgene delivery by phage-based vectors has been considered poor compared to that of animal viral vectors because bacteriophage species have evolved to infect bacteria exclusively and have no optimised mechanisms for gene transfer to eukaryotic cells. Previously, our group has developed a hybrid vector that combined the advantageous features of bacteriophage with those of the AAV vectors.[171] This was achieved by flanking a transgene cassette in the phage genome by ITR sequences from AAV2, resulting in a prokaryotic-eukaryotic hybrid vector termed AAVP.[22] This is depicted schematically in **Figure 1.22**. In this vector, the phage particle serves as a vehicle displaying targeting peptides genetically incorporated into the capsid. The AAV vector has the potential for replication and integration of transgenes flanked by ITRs. Previous studies from our group have confirmed that the presence of AAV ITR in phage genome can mediate the concatamerization of AAV circular genomes and thereby confers sustained transgene expression in mammalian cells. In the reported studies, the efficiency of a hybrid vector was assessed by using the well-established double cyclic RGD4C motif genetically displayed on the pIII minor coat protein to facilitate active targeting of cancer cells as well as the associated endothelium via specific interaction between the RGD4C motif and the overexpressed $\alpha_v\beta_3$ integrin. As a proof of concept, transgene delivery and specificity of the so-called targeted RGD4C.AAVP vectors was confirmed using several animal models of cancer as well as in pet dogs with natural cancers.[171-174]

This hybrid vector showed superior gene delivery compared to the parental phage vectors with long-term transgene expression *in vivo*.

To assess therapeutic efficacy of tumour-targeted RGD4C.AAVP vector, a number of preclinical experimentations have been performed on models of cancer in immunocompromised mice carrying xenograft tumours by using vector carrying a widely used suicide gene HSVtk and subsequent GCV treatment. Tumour growth in immunodeficient mice bearing human Karposi's sarcoma (KS1767) as well as in immunocompetent BALB/c mice bearing subcutaneous EF43-FGF4 mammary tumours was remarkably suppressed by a single intravenous administration of the RGD4C.AAVP.[171] Similarly, the inhibition of tumour growth was observed in nude mice bearing UC3-derived bladder carcinomas and DU145-derived prostate carcinomas.[171] RGD4C.AAVP-HSVtk vector was also assessed in a model of human soft-tissue sarcoma in athymic rats (large rodents) and resulted in tumour growth suppression.[172]

An additional experiment was carried out by researchers at the National Cancer Institute (NCI) to assess the cancer-targeting properties of RGD4C.AAVP in mice bearing melanoma xenograft. In this study, systemic administration of the vector carrying the gene encoding the antitumour agent tumour necrosis factor-α (TNF-α) resulted in significant reductions in the tumour volumes without any evidence of systemic toxicity to normal organs. Another investigation carried out under the direction of the NCI have proven that targeted RGD4C.AAVP-TNF-α provided

safe and effective treatment in domestic dogs, resulting in a reduction of tumour volumes with no notable cytotoxicity.
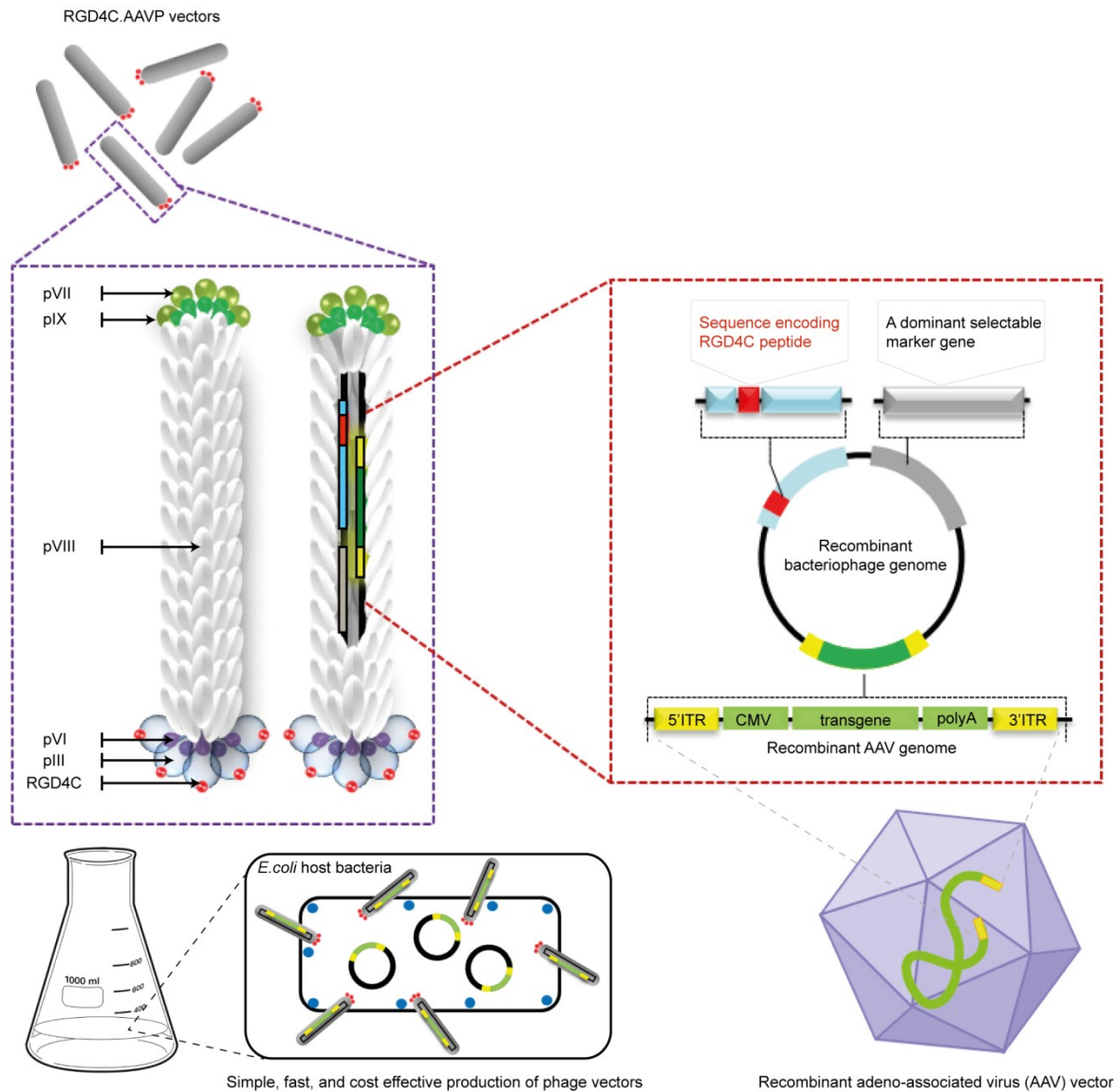
Figure 1.22: Schematic representation of the AAVP hybrid vector. The vector displays the α_v integrin-targeting RGD4C ligand on the pIII minor coat protein and a rAAV transgene cassette inserted in the phage genome. The AAVP vector can be easily produced and purified from the E.coli host cells.

1.3. Hypothesis

Hypothesis 1: Chemical modification of the bacteriophage capsid could be applied to improve the capability of AAVP vectors to attach to cells and escape from endosomes, which are barriers for the effective gene delivery by bacteriophage.

Hypothesis 2: Bacteriophage could be used as a multifunctional platform that integrates multiple ligands and peptides to escape a series of significant barriers in order to mediate the delivery of therapeutic/imaging genes into target cells.

Hypothesis 3: The effectiveness of AAVP vectors is hindered by ECM through blocking diffusion and/or physical masking of target receptors on malignant cells and therefore ECM depletion could improve the transduction efficiency, with respect of two specific ECM molecules (i.e. collagen and hyaluronic acid).

1.4. Aims of thesis

The main overall goal of this thesis is to investigate the application of modified bacteriophage as potential vectors for gene delivery to mammalian cells.

Specific aims

To achieve this goal, three specific aims were defined:

Aim 1: This aim screened the effect of genetic modification and/or different chemical treatment of bacteriophage capsid, in AAVP-mediated gene transfer to mammalian cells. This aim also examined the role of chemical modification in AAVP attachment, internalisation, and intracellular trafficking in mediating efficient gene transfer.

Aim 2: This aim designed and constructed a novel multifunctional bacteriophage through a series of genetic modifications of the capsid and evaluates these for improved gene delivery *in vitro*.

Aim 3. This aim determined the role of ECM in bacteriophage-mediated gene delivery to tumour cells and evaluated the potential use of ECM modulation as a strategy to enhance phage-mediated gene delivery in tumours.

2. Materials and Methods

2.1. Materials

2.1.1. Chemical reagents

Name	Source
DEAE-Dextran hydrochloride (DEAE.DEX, MW 500,000)	Sigma
Poly-D-lysine hydrobromide (PDL, MW 30,000-70,000)	Sigma
Polyethylenimine, Linear (PEI, MW 25,000)	Polysciences
Hexadimethrine bromide (polybrene; PB)	Sigma
Protamine sulfate salt from salmon (PS)	Sigma
Dioleoyltrimethylammonium-propane (DOTAP)	Sigma
Fugene™	Promega
Lipofectamine®	Invitrogen
Bafilomycin A1 from *Streptomyces griseus*	Sigma
Collagenase from *Clostridium histolyticum*	Sigma
Hyaluronidase from bovine testes	Sigma
ECM Gel from Engelbreth-Holm-Swarm murine sarcoma	Sigma

Table 2.1: Chemical reagents used during the investigation

2.1.2. Kits

Name	Source
ProFection® Mammalian *Transfection* System (Calcium phosphate)	Promega
Phusion Site-Directed Mutagenesis Kit	ThermoScientific
Sirius Red Total Collagen Detection Kit	Chondrex
Steady-*Glo® Luciferase Assay* System	Promega
CellTiter-Glo® Luminescent Cell Viability Assay	Promega
QIAprep Spin *Miniprep* Kit	Qiagen
HiSpeed Plasmid Midi Kit	Qiagen
QIAquick *Gel Extraction* Kit	Qiagen

Table 2.2: Kits used during the investigation

2.1.3. Antibodies

Primary Antibodies				
Name	Conjugation	Species raised	Application	Source
Anti-fd phage	-	Rabbit	IFM, FC, EM	Sigma
Anti-α_V integrin	-	Rabbit	IFM	Sigma
Secondary Antibodies				
Name	Conjugation	Species raised	Application	Source
Anti-rabbit	AlexaFluor-488	Goat	IFM	Invitrogen
Anti-rabbit	AlexaFluor-594	Goat	IFM	Invitrogen
Anti-rabbit	AlexaFluor-647	Goat	IFM, FC	Invitrogen

Table 2.3: Antibodies used during the investigation
IFM = Immunofluorescence Microscopy, FC=Flow cytometry, EM=Electron Microscopy

2.1.4. Cell lines

Name	Tissue Origin	Source
HEK293	Human Embryonic Kidney	American Type Culture Collection (ATCC)
MCF-7	Human Breast adenocarcinoma	Michigan Cancer Foundation
M21	Human Melanoma	Dr David Cheresh (University of California, La Jolla)
9L	Rat Glioma	Dr Hrvoje Miletic (University of Bergen, Norway)
C6	Rat Glioma	
LN229	Human Glioblastoma	Dr Nelofer Syed (Imperial College London)
SNB19	Human Glioblastoma	Dr Nelofer Syed (Imperial College London)
C_2C_{12}	Mouse Myoblast	Dr Francesco Muntoni (University College London, UK)

Table 2.4: Cell lines used during the investigation

2.1.5. Oligonucleotides

Oligonucleotides (oligos) for peptide display on the recombinant pVIII coat protein.	
Primers	**Sequence**
Sense oligo	5'-AGCTTTGCCAACGTCXXXXXXXXXXXXXXXXXXXXXXXXCCTGCA-3'
Antisense oligo	5'-GGXXXXXXXXXXXXXXXXXXXXXXXXXXXGACGTTGGCAA-3'

Table 2.5: Oligonucleotides used during the investigation. The sense and anti-sense oligos are 5'phosphorylated and the nucleotides X correspond to the sequence encoding for the peptide ligand of interest.

Oligonucleotides (oligos) of peptides display on the wild type pVIII coat protein	
Primers	**Sequence**
Forward	5'XXXXXXXXXGATCCCGCAAAAGCGGCCTTTG-3'
Reverse	5'-AGCAGCGAAAGACAGCATCG-3'

Table 2.6: Primer sequences used in site-directed mutagenesis. Both primers are 5'phosphorylated to avoid a spontaneous recircularization of the vector. Nucleotides in red (X) correspond to the peptide of interest.

2.2. Methods

2.2.1. AAVP preparation

AAVP production (see **figure 2.1** for procedure summarization)

A loopfull of K91 from fresh Luria-Bertani (LB) plate containing 50 μg/ml kanamycin was used to inoculate 5 ml of LB broth without antibiotic, which was then grown at 37°C with shaking at 250 rpm until optical density reaches mid-log phase (A_{600} is between 1.6 – 2.0). An aliquot of 1 ml starter culture was incubated with AAVPs for 1 hour at room temperature after which the mixture was used to inoculate 450 ml LB broth containing 1mM Isopropyl-beta-D-

thiogalactopyranoside (IPTG), 50 µg/ml kanamycin and 40 µg/ml tetracycline.

This culture was then grown overnight at 37°C with continuous shaking.
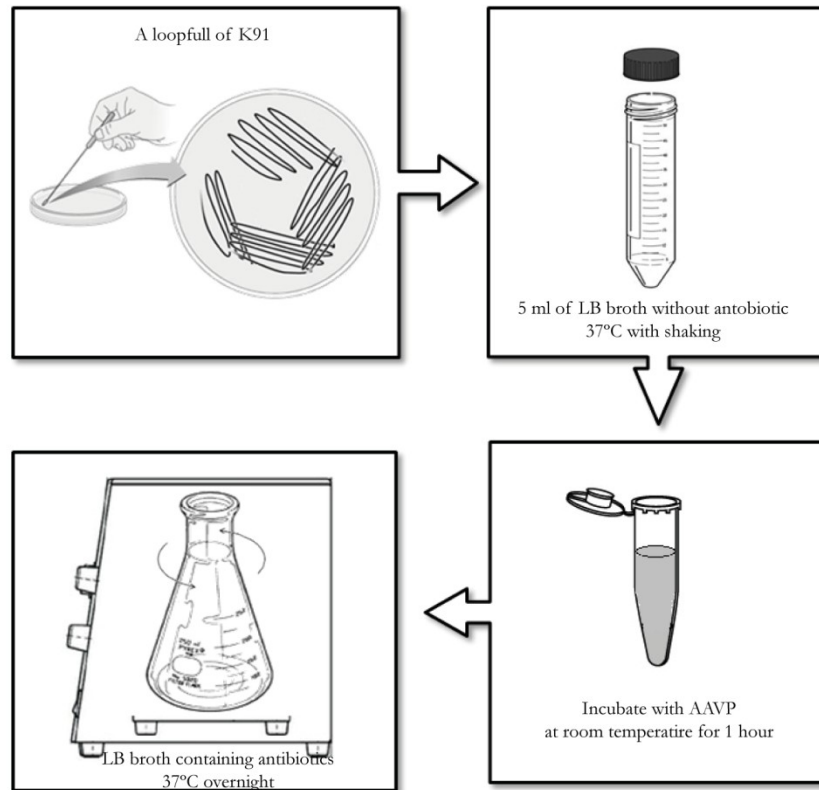
Figure 2.1: Production of AAVP viral particles
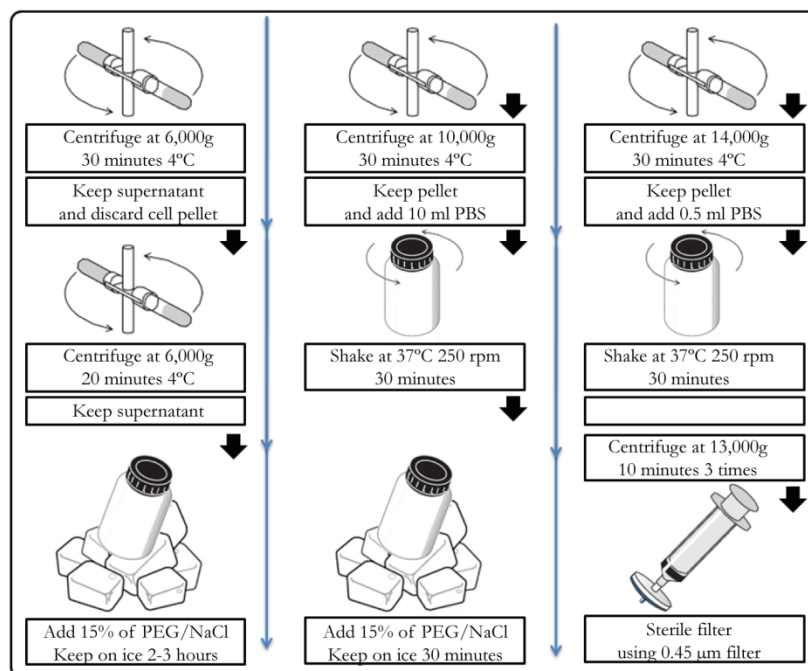
Figure 2.2: Purification of AAVP viral particles

AAVP purification (see **figure 2.2** for procedure summarization)

The overnight cultures were centrifuged at 6,000g for 30 minutes at 4°C. The pellet of bacteria was discarded and the supernatant was collected and centrifuged again to remove the residual bacterial debris. Cold Polyethylene-glycol/Sodium chloride (PEG/NaCl) was added to the supernatant (15% of supernatant volume) and incubated on ice to precipitate the AAVP particles. Following 2-3 hours incubation on ice, the mixture was centrifuged for 30 minutes at 10,000g and the supernatant was then discarded. The pellet was re-suspended in 10 ml Phosphate buffer saline (PBS) by shaking for 30 minutes in a 37°C shaker incubator 250 rpm. After the pellet was dissolved, PEG/NaCl (15% of solution) was added to the resulting solution and incubated on ice. After 1 hour incubation, the mixture was centrifuged at 14,000g for 30 minutes at 4°C and aspirated off the supernatant. The pellet was re-suspended in 1 ml PBS by shaking for 30 minutes in 37°C shaker incubator 250 rpm. To remove most of the remaining bacterial debris, the AAVP solution was centrifuged at 13,000g for 10 minutes at room temperature and the supernatant containing AAVP particles was then filtered through a 0.45 μm-filter prior to titration of the resulting phage solution. AAVP stock solution was diluted in PBS to a final concentration of 5mg/ml as measured by a spectrophotometry method, which corresponds to 6×10^{10} AAVP particles/μl.

2.2.2. Chemical modification of AAVP vectors

The AAVP particles were mixed with chemical reagents at various ratios. Solutions were incubated for 15 minutes before cell transduction to allow the formation of complexes or precipitates.

CaPi

CaPi is an inorganic based reagent. For optimisation studies, 0-0.5M $CaCl_2$ was added to 25 µg of AAVP prepared in double distilled H_2O. An equal volume of 2X Hepes-buffered saline solution (HBS) was then added to the AAVP/$CaCl_2$ solution to allow the formation of precipitates.

Cationic polymers

For optimisation studies, 25 µg of AAVP was complexed with 0-110 µl of either 100 µg/ml DEAE.DEX or 100 µg/ml polybrene reagents, [reagents/AAVP ratio 0-440 ng/1µg] in complete Dulbecco's Modified Eagle's medium (D-MEM). For PDL and PEI, 25 µg of AAVP was complexed with 0-90 µl of either 100 µg/ml PDL or 100 µg/ml PEI reagents, [reagents/AAVP ratio 0-360 ng/1µg] in complete D-MEM.

Cationic peptide

Protamine sulphate (PS) is a peptide based reagent. For optimisation studies, 25µg of AAVP was complexed with 0-90µl of 100µg/ml PS [reagent/AAVP ratio 0-360ng/1] in complete D-MEM.

Cationic lipids

For optimisation studies, 25 μg of AAVP was mixed with 0-25 μl of Fugene or Lipofectamine, [reagents/AAVP ratio 0.0-1.0μl/1μg] in complete D-MEM. For DOTAP, 25 μg of AAVP was complexed with 0-110 μl of DOTAP reagents, [reagents/AAVP ratio 0-4,200 ng/1μg] in complete D-MEM.

2.2.3. Size and charge measurement

Cationic polymers at a desired concentration were added to AAVP vector preparations, mixed gently and incubated for 15 minutes at room temperature to allow complex formation. ζ-potential charge measurements were conducted using ZetaPALS (Brookhaven Instruments Corporation, NY, USA) based on electrophoresis in 1 mM potassium chloride (KCl) electrolyte solution. The pH dependency of ζ-potential was measured by changing the pH of the electrolyte solution through the titration of 0.1N hydrochloric acid (HCl) or sodium hydroxide (NaOH).

2.2.4. *In vitro* depletion assay

HEK293 cells were seeded at a density of 5×10^4 cells/well in 48-well plates and allowed to grow until 70-80% confluent followed by treatment with AAVP prepared to optimal ratios. The plates were placed on ice for 1hr to prevent AAVP internalisation. Supernatants were extracted and serially diluted in 1X PBS. The number of AAVP particles was quantified using the K91 Kan bacterial infection method and counting transducing units, as previously reported.[168]

2.2.5. Internalisation assay

After 2 hour treatment with AAVP vectors at 37°C, cells were placed on ice to stop endocytosis and washed by PBS 3 times to remove unbound AAVPs. Surface bound AAVPs were removed by trypsinization after which cells were pelleted by centrifugation at 2000 rpm for 5 minutes and fixed in 4% paraformaldehyde (PFA) for 10 minutes at room temperature. Untreated cells were used as a negative control. To detect internalised AAVP, cells were blocked with 0.1% saponin in 2% bovine serum albumin in PBS (BSA-PBS) for 30 minutes followed by staining with rabbit anti-fd-phage antibody (diluted 1:1000) in 0.1% saponin in 1% BSA-PBS for 1hr at room temperature. Cells were pelleted and re-suspended three times in 0.1% saponin in 1% BSA-PBS and then incubated with goat anti-rabbit AlexaFluor-647 (diluted 1:500) in darkness for 1hr at room temperature. Finally, cells were washed twice with 0.1% saponin-PBS and re-suspended in PBS before analysis.

Fluorescence-activated cell sorting (FACS) analysis was carried out using a BD FACscalibur Flow cytometer (BD Biosciences) equipped with an argon-ion laser (488nm) and red-diode laser (635nm. The mean fluorescence intensity was measured for at least 10,000 gated cells per triplicate well. Results were analysed using Flojo (TreeStar) software.

2.2.6. Endosome buffering capacity measurements

The acid-base titration method was used to determine the endosome buffering capacities of the AAVP-PEI prepared to their optimised ratios in sterile water to a

total of 20ml and the pH adjusted to pH10 by NaOH. Subsequent additions of HCl were used to titrate the solution to pH3 while changes in pH were recorded using a pH meter. Titrations of sodium chloride solution (NaCl), polymer solution and AAVP solutions were used as controls. The natural endosome pH range 7.4-5.1, was used to calculate the endosome buffering capacity of the AAVP/polymer complexes.

2.2.7. Immunofluorescence staining

Cells were seeded on 18 mm^2 coverslips in 12-well plates and allowed to proliferate until 70-80% confluent. Cells were incubated with AAVP vectors for 4 hours, washed with PBS, and fixed in 4% PFA in PBS for 10 mins at room temperature. Cells were treated with 50 mm Ammonium Chloride (NH_4Cl) to quench free aldehyde groups from fixation followed by permeabilisation with 0.2% triton X-100. Cells were washed and blocked with PBS containing 2% BSA for 30 mins. Cells were then incubated for 1hr at room temperature with rabbit anti-fd bacteriophage (diluted 1:1000). For secondary staining, cells were incubated with goat anti-rabbit AlexaFluor-conjugated secondary antibodies (diluted 1:750 in 1% BSA-PBS) and with 4',6-diamidino-2-phenylindole (DAPI) (diluted 1:2000 in 1% BSA-PBS) for 1hr in darkness at room temperature. Finally, cells were mounted in Mowiol mounting medium (Invitrogen) and images were obtained with a fluorescent microscope. In addition confocal images were acquired using a Leica SP5 confocal microscope or a Zeiss Pascal confocal microscope fitted with Argon,

UV and HeNe lasers, using 63x oil objectives. Images were processed using ImageJ and Adobe Photoshop (Adobe Systems).

2.2.8. Cell culture

Maintenance of cell stocks

The cell lines used in this study are listed in **Table 2.1**. The HEK293, MCF-7, 9L, C6, LN229, and SNB-19 cell were cultured in D-MEM supplemented with 10% Foetal Bovine Serum (FBS) (Gibco), Penicillin (100 units/ml), Streptomycin (100 μg/ml) and L-glutamine (2 mM). The FBS was heat-inactivated for one hour at 56°C to destroy complement before use. Cells were cultured as monolayers on 175 cm^2 tissue culture flasks at 37°C in a humid atmosphere of 5% CO_2. Cells were passaged twice a week or when they reached 80-90% confluence. The medium was removed and cells were washed in sterile 1X PBS before addition of 2 ml of 2 ml of trypsin-ethylenediaminetetra acetic acid (Trypsin-EDTA) and incubated at 37°C for 1 – 2 minutes until the cells detached. Following the addition of 4 ml D-MEM to neutralise the trypsin, a 2 ml aliquot was transferred to a new flask containing 10 ml complete D-MEM. Cells were tested for *Mycoplasma* contamination regularly by using the MycoAlert® Mycoplasma detection kit (Lonza).

Storage of cell stocks

Following trypsinizing of sub-confluent monolayer cultures grown in 175 cm^3, the cell suspension was transferred to a 10 ml tube and centrifuged at 1000 revolutions per minute (rpm) for 5 minutes. The pellet was re-suspended in 10 ml of freezing medium containing 95% (v/v) FBS and 5% (v/v) dimethyl sulfoxide (DMSO).

Aliquots of 1 ml cell suspension were added to cryotubes. The vials were promptly placed in cryofreezing containers lined with isopropanol placed at -80°C overnight and subsequently transferred to liquid nitrogen for long term storage. Cells were recovered from liquid nitrogen by thawing cells at 37°C. These were pelleted by centrifugation at 1000rpm and DMSO containing media was removed. The cell pellet was then re-suspended in 5 ml pre-warmed growth medium before transfer to a 75 cm^3 flask for culture at 37°C in the CO_2 incubator.

2.2.9. Mammalian cell transduction by AAVP

Monolayer cell cultures

The HEK293, MCF-7, 9L, C6, LN229, and SNB-19 cell cultures were trypsinized, counted by a haemocytometer. For monolayer cell culture, a suspension of 30,000 cells in a total volume of 500 μl of complete D-MEM were seeded into 48-well flat-based plates (corning) and grown in CO_2 incubator at 37°C for 24-48 hours until the cells were 70-80% confluent. Different AAVP vector formulations were prepared as described above. Targeted (RGD4C) or non-targeted (NT) AAVP vectors without chemical treatments were used as negative controls. The medium was removed from tissue culture plate and replaced with 250 μl of chemically treated AAVP preparations. The plate was then incubated at 37°C in the CO_2 incubator for 4 hours and manually rotated every half an hour during incubation. Following 4 hour incubation, 250 μl of complete medium was added to each well. The plate was then incubated in the CO_2 incubator at 37°C. The medium was renewed every two days. Depending on the experiment, transduction efficiency as

determined by the expression of reporter transgenes was assessed at various indicated time points.

Multicellular spheroids (MCS)

For spheroid generation, a suspension of 5,000 cells in a total volume of 200 μl of complete D-MEM was seeded into 93-well ultra-low attachment (ULA) surface plates. After 48 hour incubation, a multicellular spheroid spontaneously formed in each well. 100 μl media was removed from each well after which 100 μl of AAVP formulations prepared in complete D-MEM was added. Targeted (RGD4C) and non-targeted (NT) AAVP without chemical treatment were used as negative controls. The plates were incubated at 37°C in the CO_2 incubator with 50% medium replenishment every two days. Depending on the experiment, transduction efficiency as determined by the expression of reporter transgenes was assessed at various indicated time points.

2.2.10. Generation of cells stably expressing the green fluorescence protein (GFP) gene

Sub-confluent monolayer cells cultured in 12-well flat-based plates were transduced with 50 μg AAVP vectors carrying GFP gene and puromycin-resistant gene (*puro*^{R}) or chemically treated vectors. At day 3 post transduction, cells were trypsinized and suspended in medium containing an appropriate dose of puromycin (7 μg/ml for 9L cells and 1 μg/ml for MCF-7 and HEK293 cells). Parental non-transduced cells were used as controls. The medium containing puromycin was renewed every 2-3 days. All the control cells were killed and the puromycin-resistant single cell clones

were visible after approximately 2 weeks. The puromycin-resistant cell clones were pooled to produce a population of stably transduced cells. All stable selected cells were monitored under a fluorescent microscope.

2.2.11. Examination of reporter gene expression

Luciferase assay

The Promega Steady-Glo® luciferase assay kit was used to evaluate expression of the luciferase Luc reporter transgene in transduced cells. 72 hours post transduction, medium was removed, cells were then washed with 1x PBS followed by the addition of 110 μl of 1X Glo lysis buffer and incubation for 10 minutes to allow for complete cell lysis. 50 μl cell lysate was transferred to 96-well white opaque microplates followed by the addition of 50μl Steady-Glo® luciferase substrate and incubation at room temperature for 10 minutes. Luciferase activity was quantified using a Promega plate reader.

GFP analysis

The cells were transduced as described with AAVP vectors carrying the GFP reporter gene and GFP expression was analysed using a Nikon Eclipse TE2000-U fluorescence microscope. Photographic images were obtained by using 2X magnification and fluorescent setting. Brightfield photographs were also obtained.

2.2.12.   Cell viability

The Promega CellTiter-Glo® assay kit was used to evaluate the cell viability. After 48 hour vector treatment, medium was removed. Cells were then washed with PBS followed by the addition of 110 μl of 1X Glo lysis buffer and subsequently

incubation for 10 minutes to allow for complete cell lysis. A 50 µl aliquot of cell lysate was transferred to 96-well white opaque microplates after which 50µl Steady-Glo® luciferase substrate was added and allowed to incubate for 10 minutes at room temperature. Luminescence signal was quantified using a Promega plate reader.

2.2.13. Determination of tumour cell killing *In Vitro*

Cells were seeded in a 48-well plate and incubated for 48 hr, to reach 60%-80% confluence. Next, cells were transduced with AAVP vectors carrying the HSVtk gene. GCV was added to cells (10 µM) at day 3 post vector transduction and renewed daily. Viable cells were monitored under microscope and cell viability was measured at day 5 post GCV treatment by using the CellTiter-Glo® cell viability assay kit as described above.

2.2.14. Design and construction of multifunctional phage

Multifunctional phage particles were made through a series of genetic modifications of the capsid. The RGD4C.fUSE5 vector, in which the nucleotide encoding RGD4C peptide was fused in frame with the pIII gene as previously described in the detailed protocol[22], was used as a targeted backbone phage vector for mammalian cell binding and internalisation through RGD4C binding to $\alpha_V\beta_3$ integrin receptor. Next, a f88 vector-derived DNA fragment containing a recombinant gene VIII was inserted in the RGD4C.fUSE5 backbone vector, followed by insertion of oligonucleotide encoding the peptide of interest. Subsequently, nucleotide sequence encoding a peptide of interest was introduced

into the wild-type pVIII gene by site-directed mutagenesis. Finally, a mammalian transgene cassette was inserted in an intergenic region of the resultant vector.

Construction of the RGD4C phage vector containing two major coat proteins

Two existing phage vectors RGD4C.fUSE5 and f88-4, both of which have unique restriction sites present at similar locations in their DNA, were digested with the BamHI and XbaI restriction enzymes. Next, two fragments with the corresponding sequences; 1) a 3,925 bp fragment containing gene III fused in framed with RGD4C and the wild-type gene VIII from RGD4C.fUSE5 plasmid, 2) a 5,630 bp flagment containing recombinant VIII gene, were ligated to create a chimeric RGD4C.fUSE5/f88-4.

Insert preparation and cloning of peptides in the recombinant pVIII of RGD4C.fUSE5/f88-4

The corresponding nucleotide sequence and its complementary sequence were designed. The sense and anti-sense oligonucleotides are 5'phosphorylated. The phosphorylated oligos were mixed (20 pmol/primer), heated to 95°C for 5 min and gradually cooled at room temperature to allow annealing. Annealing of sense and anti-sense oligonucleotides generates the *Hind*III and *Pst*I sticky ends, ready to be cloned in the digested RGD4C.fUSE5/f88-4 phage plasmids. An aliquot of ligation reaction was transformed into *E.coli* competent cells strain DH5α and inoculated on LB agar plate containing 50 μg/ml tetracycline. Single colonies were picked and their plasmids were isolated by using a QIAprep Spin Miniprep kit (QIAGEN). The positive clones were selected by sequencing analysis.

Display of peptides on the wildtype pVIII major coat protein

Oligonucleotide sequences encoding a peptide of short length (up to 10 amino acid residues) were introduced into the wild-type VIII gene by using the Phusion Site-Directed Mutagenesis Kit. Briefly, the 50 µl polymerase chain reaction (PCR) reaction was performed with 10 pg DNA templates, 0.5 µM 5'phosphorylated primer pairs, 200 µM dNTP and 0.02 U Phusion Hot Start II DNA polymerase. The reaction was initiated by pre-heating the reaction mixture to 98°C for 30 s; 25 cycles of 98°C for 15 s, 61°C for 30 s and 72°C for 5 mins (30 s/500 bp). The PCR products were evaluated by agarose gel electrophoresis. The linear PCR product was circularized by ligation using the T4 Quick ligase. The positive clones were selected with the same procedure as described above.

2.2.15. Standard protocol for molecular cloning

DNA agarose gel electrophoresis

1% agarose gels were prepared by dissolving 0.5g Agarose in 50 ml of fresh 1X Tris-acetate-EDTA (TAE) buffer and heating the suspension in a microwave oven until boiling. When hot agarose was completely melted and cooled to about 50 – 55°C, 7 µl of Ethidium bromide (EtBr) was added, and poured into casting tray and then let stand for 30 minutes until it is solid. The gel was placed into the electrophoresis chamber of assembled electrophoresis apparatus with enough 1X TAE Buffer (about 2-3 mm of buffer over the gel). The sample was prepared by mixing 5 µl of each sample with 1 µl of 6X Sample Loading Buffer. Each sample/sample loading buffer and 10 µl of the DNA ladder standard were pipetted

into a separate well in the gel. Electrophoresis was carried out at 100V for approximately 45 minutes. DNA was visualised by illumination on a long wave UV light box and photographed. The size of the DNA fragments was estimated by comparing their relative mobility to that of the DNA ladder.

Gel extraction and purification (QIAquick)

Plasmid DNA or DNA fragments were extracted and purified by using the Qiaquick gel extraction kit. The DNA fragment of interest was excised from agarose gel with a clean and sharp scalpel. The slice of agarose gel was transferred to an eppendorf tube and weighted. Next, 3 volumes of buffer QG were added to 1 volume of the agarose gel in order to dissolve the gel by incubating at 50°C for 10 minutes. Subsequently, 1 gel volume of isopropanol was added to sample. A QIAquick spun column was placed in a provided 2 ml collection tube after which the sample was applied to the column, followed by centrifuging for 1 minute to discard the flow-through. The QIAquick column was washed to remove all traces of agarose by adding 0.5 ml Buffer QG and centrifuged for 30–60 seconds, followed by adding 750 µl of Buffer PE and centrifuging for 30–60 seconds. QIAquick column was then placed into a clean 1.5 ml eppendorf tube and 50 µl of Buffer EB (10 mM Tris-Cl, pH 8.5) was added to the centre of membrane and centrifuged for 1 minute to elute the DNA.

Ligation

Ligations were carried with 30-50 ng of vector DNA and typically 1:5 molar ratio of vector to insert DNA was used (either a purified DNA fragment, or a pair of annealed oligonucleotides). All ligation reactions were performed in a final volume of 10 µl containing 1x Quick T4 DNA ligase buffer and 1µl Quick T4 DNA ligase (Fermentas). All reactions were incubated for 5 minutes at room temperature.

Transformation of competent bacteria by heat shock method

The tube of frozen NEB 5-alpha competent *E.coli* (BioLabs) were removed from -80°C freezer and thawed on ice. The plasmid DNA was added to 50 µl of thawed competent cells. After 30 minute incubation on ice, cells were heat shocked at exactly 42°C for 30 seconds then immediately placed on ice for 2 minutes. Next, 250 µl of super optimal broth (SOC) medium (Invitrogen) was added to the reaction and cells incubated in a shaking incubator at 37°C 250 rpm for 1 hr. Finally the cells were spread on LB-agar plates containing 40 µg/ml tetracyclin, and incubated at 37°C overnight.

Restriction endonuclease digestions

Restriction enzyme digests were performed in the recommended buffers and supplied by the manufacturer's instruction. A 50 µl reaction included 1 µg DNA, 5 µl of 10X NEB buffer, and 10 units of each restriction enzyme. The reaction was incubated at recommended temperature for 1 hour. For analysis of digestion products, reactions were terminated by inactivating enzymes at denaturing temperature, followed by gel electrophoresis to check the digestion products.

2.2.16. Infectivity assay (see figure 2.2 for procedure summarization)

A loopfull of *E.coli* K91 was used for inoculating 7 ml culture, which was then grown at 37°C with shaking (250 rpm) for approximately 1.5 – 2 hours or until mid-log phase of bacterial growth (A_{600} is between 1.5 – 2.0). Phage stock was serially diluted in PBS and the 5 µl of diluted phage preparation was added 1 ml of K91. Then, the mixture was incubated at room temperature for 20 minutes without shaking to allow infection, and 200 µl of the mixture was plated out on LB agar plates containing 100 µg/ml kanamycin and 40 µg/ml tetracycline. The plate was then incubated at 37°C overnight. The resulting bacterial colonies formed on LB agar plates were counted to determine their infectivity.
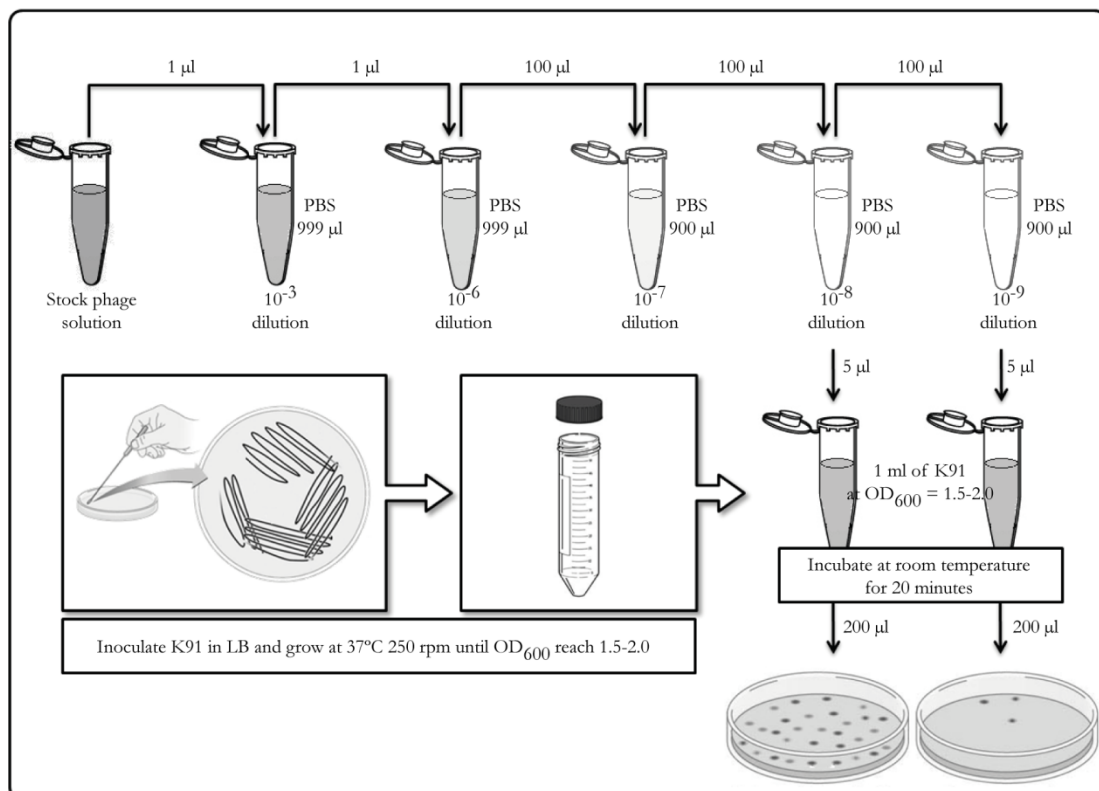
Figure 2.3: Infectivity assay

2.2.17. Collagen depletion assay

9L, M21, and MCF-7 cells were grown in 12-well plates at a density of 120,000 cells/well for 72 hours until they were confluent. After washing cells with PBS, 500µl of 0.2 mg/ml collagenase in serum free media was added to the cells and incubated at 37°C for 1 hr. Next, both cells and supernatant were processed as separate samples in a collagen I detection assay. The assay was performed based on the use of the Sirius Red dye according to the manufacturer's instructions of a Sirius Red Total Collagen Detection Kit with final measurements by using a Promega plate reader.

2.2.18.   AAVP diffusion assay

200 µl of ECM Gel from Engelbreth-Holm-Swarm murine sarcoma at 2.5 mg/ml or 5.0 mg/ml were added to a 48-well plate and allowed to set at 37°C. In the meantime fluorescently-tagged RGD4C.AAVP was prepared at a concentration of 5µg/ml. Next, 50µl of the RGD4C.AAVP solution were taken up in a pipette tip, which was inserted at a fixed position into the ECM-gel matrix and left to diffuse through the material for 1 hour. Measurements were obtained at 1 hour post diffusion and at 30 minutes intervals thereafter.

2.2.19.   Statistical analysis

GraphPad Prism software (version 5.0) was used to perform statistical analyses. Data were presented as mean±standard error of the mean (s.e.m). P values were generated by one-way or two-way ANOVA, considered significant when <0.05 and denoted as follows: $*p < 0.05$, $**p < 0.01$ and $***p < 0.001$.

3. Optimizing a hybrid Adeno-associated virus/phage (AAVP) vector system for efficient gene delivery to mammalian cells

3.1. Introduction

Protein expression from a gene of interest introduced into cultured cells not only serves as a powerful tool to study protein function, but also has major impacts on the practice of medicine. *Ex vivo* gene therapy is a prime example whereby appropriate cells are genetically modified *in vitro* and placed back into the affected area of the patients. The expression of transferred transgenes can be transient or stable. Transient gene expression is commonly used to investigate the short-term (24-72 hours post-transduction) impact of alternations in gene expression, while the stable gene transfer generate long term gene expression in cell lines. Stable expression is one of the key factors in *ex vivo* gene therapy. For example, genetic modification of human Embryonic Stem Cells (hESCs) requires stable integration of a therapeutic gene into the cell genome or maintenance as episomal forms in the nucleus.[175] Delivering transgenes into mammalian cells requires a gene carrier or vector. Viral vectors derived from animal viruses such as retrovirus, adenovirus, AAV, and HSV have emerged as vectors of choice for many applications today. However, they suffer several limitations including packaging capacity[10] and complexity of production due to the need for costly manufacturing processes.[11]

Bacteriophage (or phage), a simple bacterial virus, has made contributions in the field of gene delivery.[15] Because of their inherent simplicity, the use of bacteriophage as a gene delivery vector is an attractive concept. They are uniquely suited to modifications that use directed evolution to produce genetically optimized vectors for gene transfer.[176] The high tolerance of phage coat protein mutations allows the insertion and display of foreign peptides.[177] Phage-based vectors, among all other choices for *in vitro* gene transfer to cultured cells, is the simplest and least expensive technique since it does not require any specialized and sophisticated equipment.[16] Recently, Hajitou *et al* introduced an improved version of a M13 phage-derived vector, which combined a mammalian gene cassette flanked by ITRs from AAV2 into the bacteriophage genome at a compatible site, named AAVP. They demonstrated gene transfer and expression in mammalian cells mediated by AAVP vector carrying mammalian transgene expression cassettes.[26,171] The incorporation of ITRs from AAV2 is associated with improved fate of the delivered transgenes, maintenance of the entire mammalian transgene cassette, better persistence of episomal DNA and formation of concatamers of the transgene cassettes. All these mechanisms resulted in increased transduction efficiency over conventional phage-based vectors.[171] However, all subsequent improvement of AAVP has been exclusively done at the genome level, which is the last of many steps involved in the gene delivery process.

Indeed, it is well-established that gene delivery efficacy depends on the ability of the vector to overcome a number of extra/intracellular barriers. Firstly, the vector

needs to access its receptor on the cell surface. Secondly, following internalization, the vector has to escape from the endosomes and be released into the cytosol. Thirdly, the vector must then be transported to the nucleus where gene expression occurs. Unfortunately, current AAVP vectors are unable to efficiently circumvent these obstacles to achieve transgene expression.

In this study, we used an AAVP vector carrying a mammalian DNA cassette comprising a GFP or Luc gene with a cytomegalovirus (CMV) promoter to direct gene expression in mammalian cell lines. The aim of this study was to establish the optimal transduction conditions of the AAVP vector system and to investigate cell-AAVP interactions which form a key parameter in vector attachment to cells and subsequently determine the vector tropism. We evaluated 1) the effect of genetic modification by displaying targeting ligands on the AAVP capsid and 2) chemical modification of AAVP capsid using transduction enhancing agents such as lipid agents (DOTAP, lipofectamine, Fugene), polycationic polymers (PEI, polylysine, DEAE.DEX, PB, PS), and CaPi. Finally, we assessed the combination of both genetic and chemical modification.

3.2. Results

3.2.1. Acquisition of AAVP mammalian cell tropism by genetic modification is limited by saturation of transduction

To create a mammalian cell tropism for the AAVP vector, we previously reported the genetically modified RGD4C.AAVP displaying the α_v integrin-targeting peptides on the phage capsid.[171] Herein, we sought to investigate the effect of increasing dose of RGD4C.AAVP on transduction efficiency. Therefore, RGD4C.AAVP-mediated transduction was conducted at concentration of 0 to 500 µg of RGD4C.AAVP carrying Luc gene. NT.AAVP (unmodified capsid) was also included in this experiment as a negative control of transduction. Vectors were added to cells 3 days before measurement of the luciferase activity. The results showed a linear increase in transduction efficiency at AAVP doses of 0-50 µg for HEK293 cells and 0-200 µg for 9L and M21cells(**Figure 3.1a, b, and c**), reflecting unsaturated transduction efficiency. However, the results yielded dose-independence at higher AAVP amounts. Indeed, the transduction efficiency no longer increased above the indicated doses, suggesting transduction saturation. For example, saturation of gene expression was observed in HEK293 cells at 50 µg RGD4C.AAVP (approximately 1.5 x 10^5 RLU or 300-fold over AAVP vector) (**Figure 3.1a**). However, the optimal concentration for HEK293 was determined to be 25 µg AAVP because one ideal factor for gene delivery is to use the least amount of vector possible to achieve efficient gene delivery. No luciferase expression was observed in unmodified NT.AAVP-treated cells at any

concentration tested. These data suggest that improvement of AAVP-mediated

gene transfer is limited by the saturation effect.
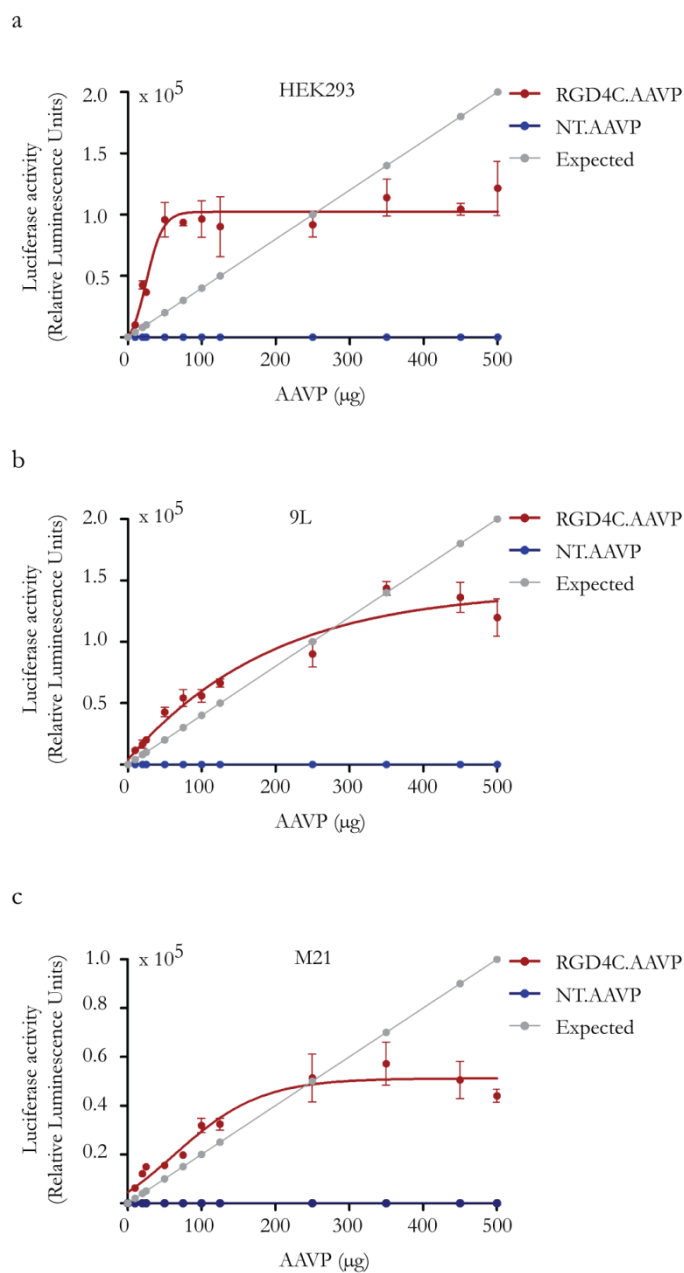
Figure 3.1: Transduction with RGD4C.AAVP resulted in saturation of transgene expression in 3 different cell lines as determined by the luciferase activity. Cells **a**) HEK293 **b**) 9L or **c**) M21 were cultured in 48-well plates and transduced with increasing doses (µg/well) of RGD4C.AAVP carrying a Luc reporter gene to determine lowest concentration required to achieve transduction saturation. The results show the mean relative luminescence units of triplicate wells ±SEM, from one representative of three independent experiments.

3.2.2. Addition of cationic lipids slightly increased AAVP-mediated gene expression in mammalian cells

Having shown that RGD4C.AAVP-mediated gene delivery efficacy is limited by saturation of transduction, we sought to investigate the mammalian cell tropism of AAVP by chemical modification of the capsid. To test whether cationic lipids had an effect on AAVP-mediated gene expression in mammalian cells, we analysed Luc gene expression in the HEK293 cells. Cells were transduced with NT.AAVP at a concentration of 25 μg/well with or without cationic lipids at different AAVP/cationic lipids ratios. Three different reagent formulations were tested: Fugene, Lipofectamine, and DOTAP. Levels of luciferase activity at 72 h post transduction were determined using a luciferase assay (**Figure 3.2**). The addition of cationic lipids increased AAVP-mediated gene expression in HEK293 cells. No cytotoxicity was observed in the concentration ranges of cationic lipids tested (Data not shown). The maximal ratios for enhancing transgene expression for Fugene, Lipofectamine, and DOTAP were 1.0 μl/μg, 1 μl/μg and 4200 ng/μl with overall increases of 70- , 80-, and 20-fold, respectively compared with unmodified AAVP (**Figure 3.2a, b, c**). However, these cationic lipid-enhanced transduction levels are considered poor, as saturation transduction by RGD4C.AAVP was determined at 300-fold over unmodified AAVP for HEK293. Therefore, cationic lipids were not chosen for further studies.
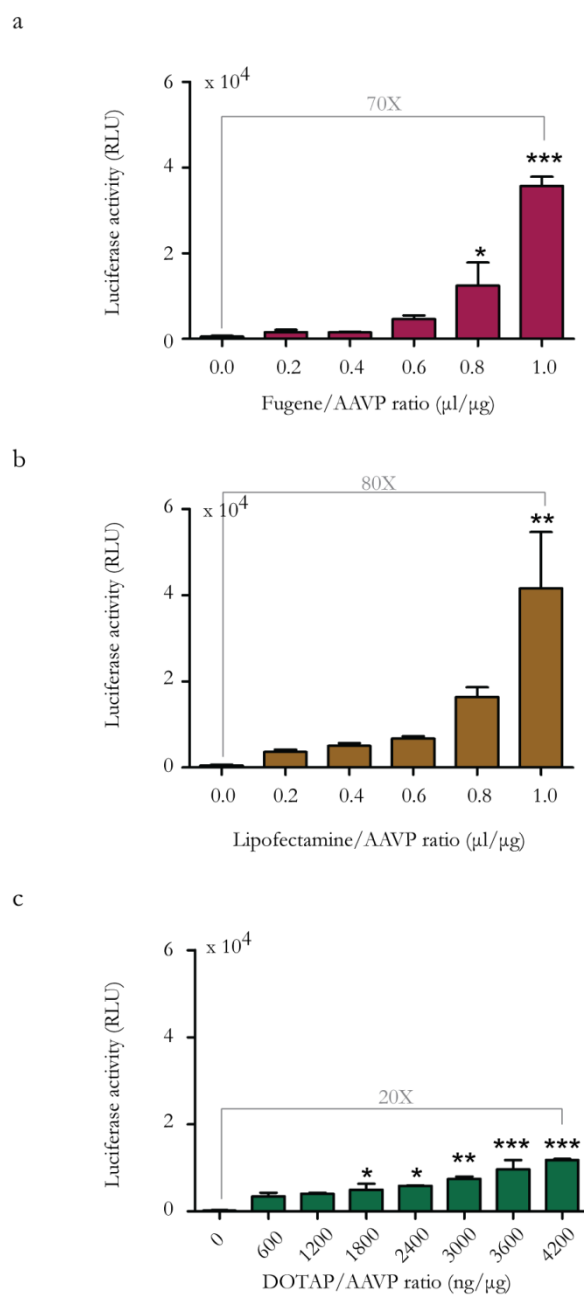
Figure 3.2: Effects of cationic lipids on AAVP-mediated gene expression *in vitro*. HEK293 cells were harvested 72 h after treatment with AAVP carrying the Luc gene at a concentration of 25 μg/well mixed with **a**) Fugene, **b**) Lipofectamine, and **c**) DOTAP at various ratios. The results show the mean relative luminescence units (RLU) of triplicate wells + SEM, from one representative of three independent experiments, significant difference; n.s.-not significant, * $p<0.05$, ** $p<0.01$, ***$p<0.001$ (one way ANOVA with tukey's post hoc test).

3.2.3. Incorporation of AAVP in a calcium phosphate coprecipitate improved gene transfer to mammalian cells

We hypothesized that delivery of AAVP in a CaPi coprecipitate would increase gene transfer to mammalian cells. We first optimized three critical parameters affecting AAVP-CaPi precipitate formation and transduction efficiency as well. We tested; i) the effect of $CaCl_2$ concentration, ii) the presence of essential reagents to form the complex, and iii) the duration of the coprecipitate complex formation. AAVP-CaPi coprecipitate was prepared by adding HBS buffer containing phosphate ions to the AAVP/$CaCl_2$ mixture prior to cell treatment. The cells were then incubated for 72 h and subsequently analyzed for luciferase activity. The data in **Figure 3.3a** show the effects of various concentrations of $CaCl_2$ on the transduction efficacy. AAVP vectors coprecipitated with 250-300 mM $CaCl_2$ showed the highest transduction efficiency. AAVP-CaPi coprecipitate-mediated transduction at optimal ratio dramatically increased luciferase reporter gene expression up to 1,300-fold compared with AAVP alone. The data in **Figure 3.3b** show the duration of coprecipitate complex formation before its addition to cells. Immediate addition to cells after AAVP-CaPi preparation showed an optimal effect on transduction of HEK293 cells. Transduction efficacy significantly decreased with increasing incubation period of complex formation. **Figure 3.3c** confirms the formation and the cell surface attachment of insoluble AAVP-CaPi precipitates when AAVP were incubated with two essential reagents: HBS, and $CaCl_2$. The precipitation could not be observed in the absence of either one or

both of them. The presence of both reagents required for the complex formation was confirmed by the successful transduction after day 3 post treatment (**Figure 3.3d**).
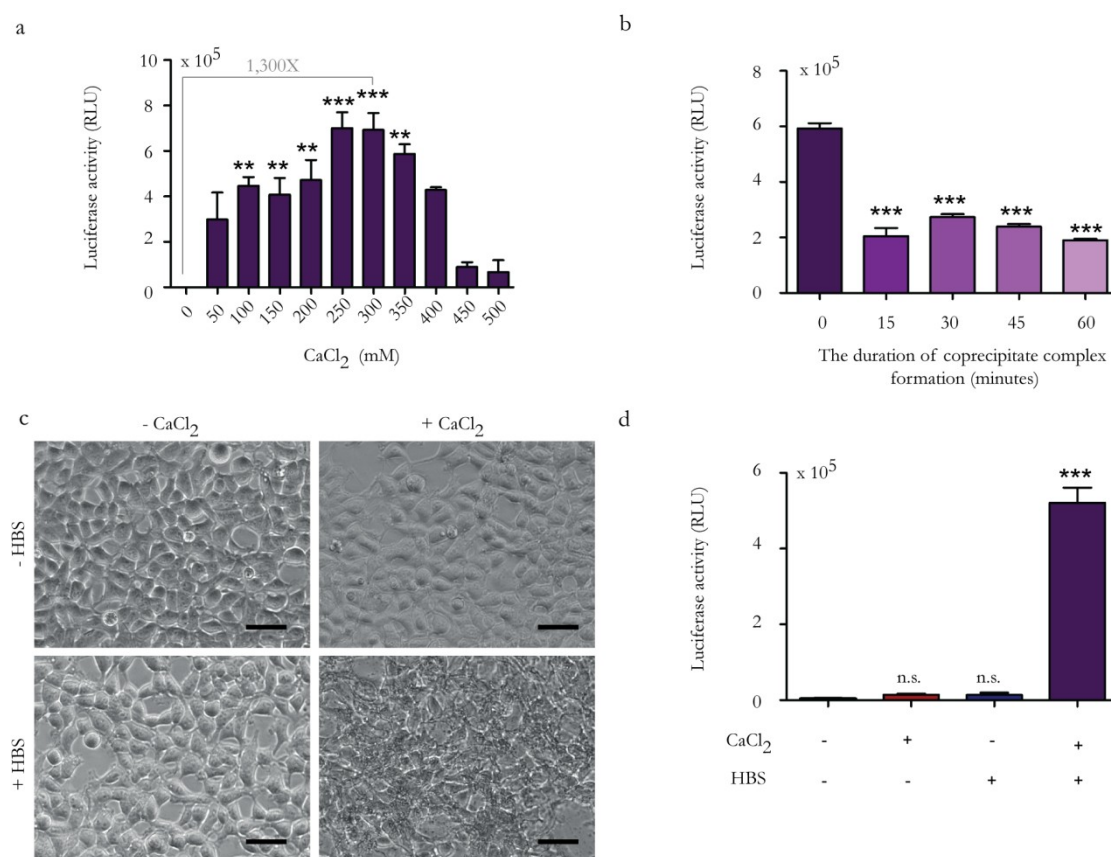
Figure 3.3: CaPi coprecipitation enhances AAVP-mediated gene transfer to HEK293 cells. a) Effect on $CaCl_2$ concentrations. AAVP vectors were mixed with increasing concentrations of $CaCl_2$ before adding HBS to form the complex. The mixtures were then added to cells and Luciferase analysis was subsequently performed 3 days post transduction. **b**) Effect of complex formation time before addition to cells. AAVP-CaPi complexes were incubated for various times before they were applied to cells. **c**) Effect of HBS and $CaCl_2$ on the formation and the cell surface attachment of AAVP-CaPi precipitates. Scale bars = 100 μm. **d**) Effect of HBS and $CaCl_2$ on AAVP-mediated transduction. (300 mM $CaCl_2$, 1X HBS buffer) Data represent the mean + SEM of triplicate samples from one representative experiments of three, significant difference; n.s.-not significant, * $p<0.05$, ** $p<0.01$, ***$p<0.001$ (one way ANOVA with tukey's post hoc test).

3.2.4. Mechanism by which calcium phosphate coprecipitation enhances AAVP-mediated gene transfer

Following the hypothesis that the mechanism of enhanced efficacy of gene transfer by AAVP-CaPi complex is associated with higher affinity to the cell surface than the NT.AAVP vector alone, we carried out experiments to demonstrate the efficacy of AAVP particle adsorption to target cell membranes. HEK293 cells were treated with AAVP alone or an AAVP-CaPi coprecipitate. RGD4C.AAVP-treated cells served as a positive control as previous reports have shown an essential role of the RGD4C ligand, displayed on AAVP coat protein, in mammalian cell attachment and internalization.[178] We performed immunofluorescence-staining assays with antibodies against the phage coat proteins (**Figure 3.4a**). The red colour represents fluorescence related to AAVP particles, and the blue shows fluorescence of DAPI-stained cell nuclei. Immunofluorescence images revealed great cell surface binding in cells treated with the AAVP-CaPi precipitate. No AAVP was observed on cells incubated with AAVP alone. We also carried out a supernatant-depletion assay by incubating the different AAVP preparations with cells, after which the supernatant containing the AAVP particles that did not attach to cells was collected and quantified by infection of host bacteria followed by colony counting. The surface-bound, non-internalized condition was achieved by incubating the cells at 4°C instead of 37°C. AAVP recovery was determined as percentage of input. As shown in **Figure 3.4b**, a large amount of AAVP (100% of AAVP input) was recovered while the AAVP-CaPi was almost completely

sequestered by cultured cells. Large amounts of the control RGD4C.AAVP were recovered when compared to the AAVP-CaPi complex. These data clearly show that the AAVP coprecipitation with CaPi results in increased binding to mammalian cells.

Next, we set out to determine if there was increased cellular uptake of AAVP coprecipitated with CaPi. Flow cytometry was carried out to quantify internalised AAVP (**Figure 3.4c**). The coprecipitaion of AAVP with CaPi led to an increase in AAVP internalisation, as indicted by higher intracellular signals compared to cells incubated with AAVP alone. The data strongly suggest that coprecipitation of AAVP with CaPi indeed alters AAVP tropism for mammalian cells by mediating efficient AAVP binding to the cell surface and subsequent internalization. Interestingly, internalisation of AAVP-CaPi complex was not significantly different from those of RGD4C.AAVP despite higher efficiency in binding to cells, suggesting an additional mechanism that assists gene transfer to mammalian cells (See discussion).
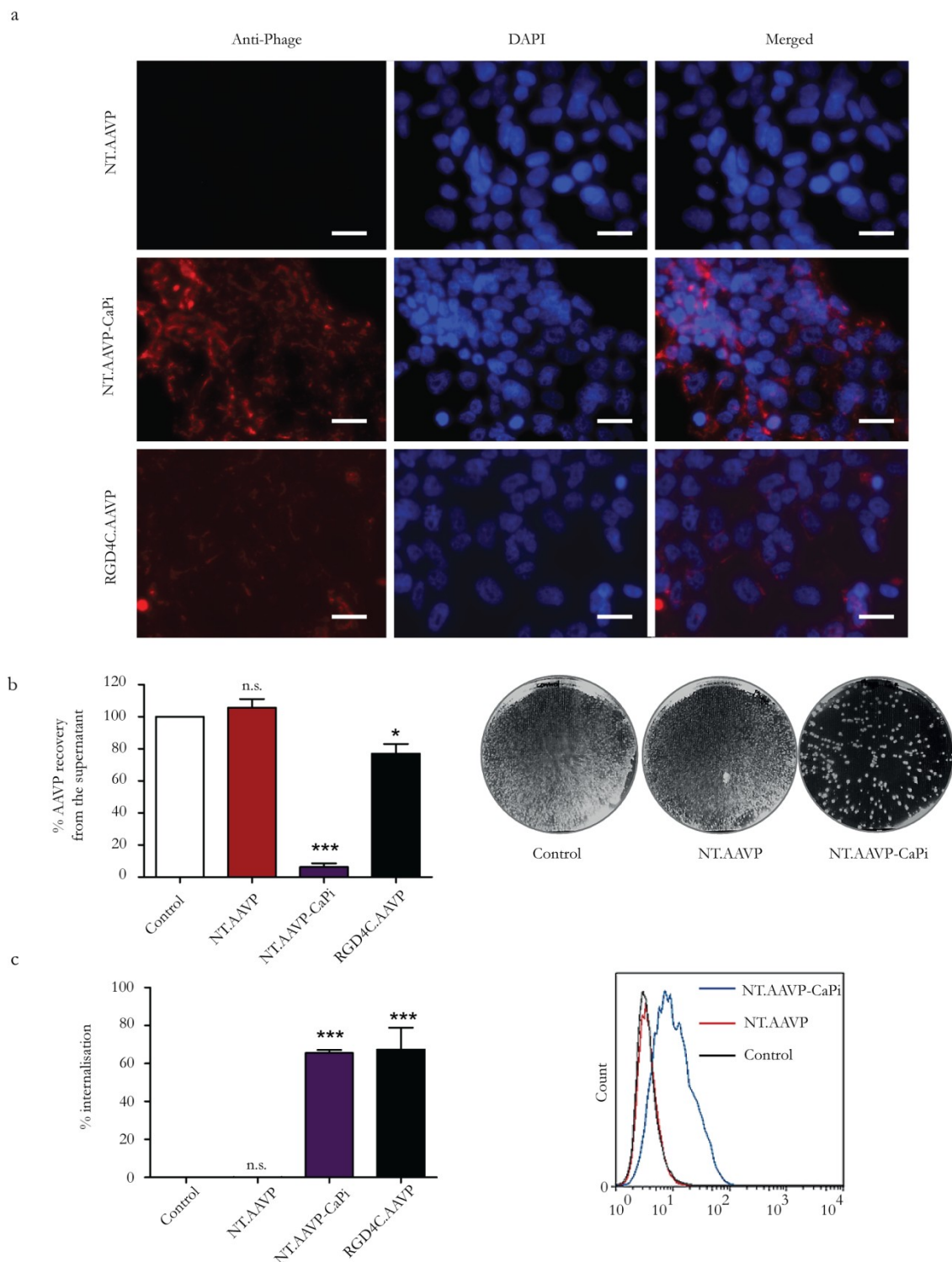
Figure 3.4: CaPi facilitates interaction between AAVP and cell membranes. a) Immunofluorescence-based AAVP binding and internalization assay with cultured HEK293 cells. Phage particles were detected by polyclonal rabbit anti-phage IgG followed by incubation with Alexa conjugated goat anti-rabbit IgG (red fluorescence). Scale bars = 100 μm. **b**) Supernatant-depletion assay. The number of free-unbound AAVP in the supernatant above the adherent cell layer was quantified by infection of host bacteria followed by colony counting and expressed as percentage of AAVP input. **c**) Evaluation of AAVP internalization. HEK293 cells were treated with different AAVP preparations for 1 h. Cells were then collected and internalization efficiency was measured using flow cytometry. Untreated cells were used as

controls. Data represent the mean + SEM of triplicate samples from one representative experiments of three, significant difference; n.s.-not significant, * p<0.05, ** p<0.01, ***p<0.001 (one way ANOVA with tukey's post hoc test).

3.2.5. Enhancing AAVP-mediated gene transfer by addition of cationic polymers

Next, optimal ratios of the complexes of AAVP with cationic polymers by gene transfer to mammalian cells were determined. We tested five cationic polymers: DEAE.DEX, PEI, PDL, PB, and PS. Results showed that incorporation of 240-440 ng of DEAE.DEX per 1 μg of AAVP greatly increased luciferase transgene expression, with maximal increase (2500-fold) at 350 ng/μg (**Figure 3.5a**). Transgene expression was also significantly increased by 80-360 ng of PEI per 1 μg of AAVP with maximal increase (1,500-fold) at 160 ng/μg (**Figure 3.5b**), and at 80-320 ng of PDL per 1 μg of AAVP, with maximal increase (800-fold) at 200 ng/μg (**Figure 3.5c**). However, not all cationic polymers tested were effective. PB, at optimal ratio 40 ng/μg, slightly increased transgene expression by 30-fold (**Figure 3.5d**). PS failed to enhance expression over a broad range of polymer/AAVP ratios (**Figure 3.5e**). Thus, complexes of AAVP with particular cationic polymers augmented gene transfer to mammalian cells.
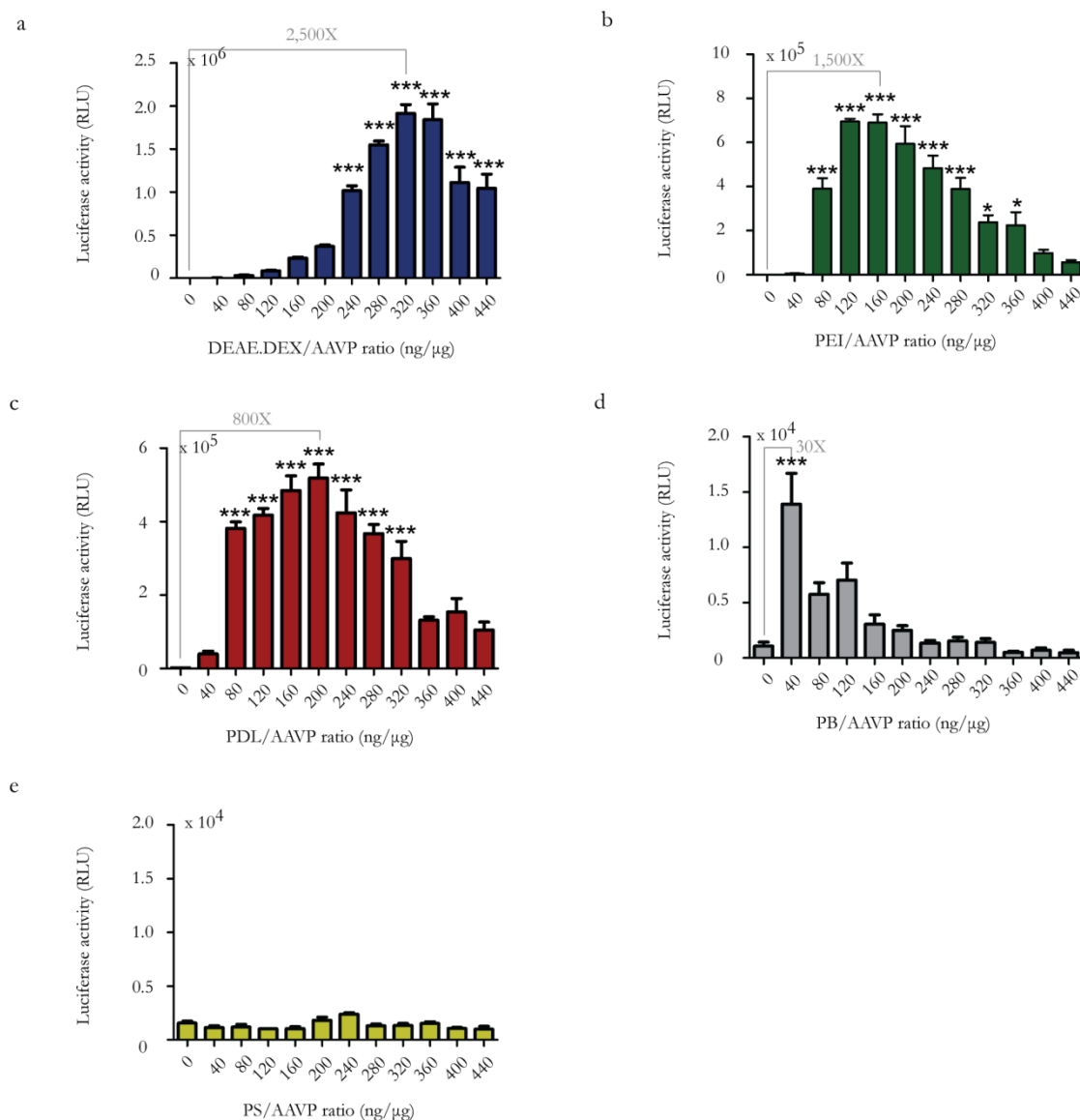
Figure 3.5: Optimisation of AAVP/cationic polymer complexes. HEK293 cells were cultured in 48-well plates and treated with AAVP carrying the Luc gene, premixed with increasing ratios of cationic polymer per AAVP. Luciferase activity was analysed at day 3 post transduction. **a**) DEAE.DEX. **b**) PEI. **c**) PDL. **d**) PB. **e**) PS. The results show the mean relative luminescence units (RLU) of triplicate wells + SEM, from one representative of three independent experiments, significant difference; n.s.-not significant, * $p<0.05$, ** $p<0.01$, ***$p<0.001$ (one way ANOVA with tukey's post hoc test).

3.2.6.   Evaluation of cytotoxicity by the AAVP/polymer complex

We sought to investigate whether the AAVP/polymer complex was toxic for the cells and whether the observed decrease in transgene expression at higher polymer content in the complex was due to cytotoxicity of the polymer at these higher concentrations. Therefore, cell viability assays were performed by using the same polymer/AAVP ratios range of 0-440 ng/µg. Cell viability was normalised as percentage of the control cells treated with AAVP alone without polymer (0 ng/µg of polymer/AAVP). At day 2 post treatment, cell viability assays (**Figure 3.6a**) revealed a significant decrease in cell survival in cells treated with AAVP complexed with high concentrations of PEI or PDL (**Figure 3.6a, top and bottom)**, but no cytotoxicity was detected at lower polymer/AAVP ratios including the optimal ratios. However, the proportion of viable cells did not change significantly after treatment with increasing DEAE.DEX concentrations (**Figure 3.6a, middle**). Morphological characteristics of HEK293 cells were visualized by brightfield microscopy. **Figure 3.6b** shows normal morphology of confluent cells in treatments with AAVP alone and in cells treated with AAVP-PEI complexes at optimal PEI/AAVP ratio. There was a dramatic increase in the number of cells detaching from the substrate by the AAVP-PEI complex, at higher PEI/AAVP ratios.
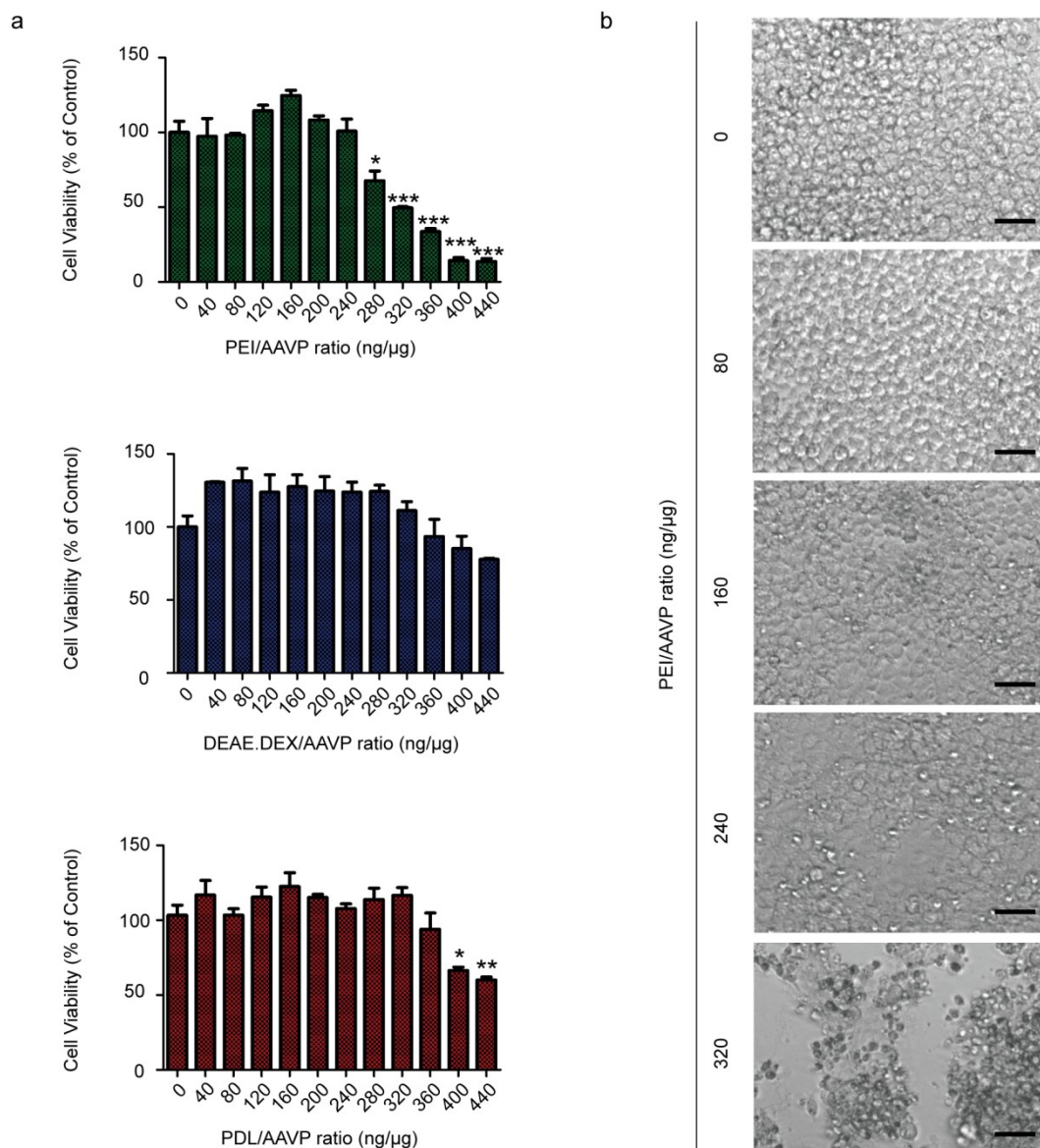
Figure 3.6: Cell viability of HEK293 cells 48 h after being exposed to various ratio of polymer/AAVP. a) The toxicity of AAVP-PEI (top), AAVP-DEAE.DEX (middle), and AAVP-PDL (bottom) was determined using the CellTiter-Glo® cell viability assay. HEK293 cells were treated with AAVP, premixed with increasing ratios of cationic polymer per AAVP. At day 2 post treatment, cell viability was determined. Mean cell viability was normalised to non-treated controls, with the mean of n=3 independent experiments shown (+ SEM), significant difference; n.s.-not significant, * p<0.05, ** p<0.01, ***p<0.001 (one way ANOVA with tukey's post hoc test). **b**) Morphological characteristics of HEK293 cells following transduction with AAVP complexed with PEI, as visualized by using bright field microscopy. Scale bars = 100 μm.

3.2.7. Physiochemical properties of AAVP/polymer complex

To gain an insight into the mechanism of the enhanced gene delivery efficacy by AAVP/polymer complexes, we explored the surface chemistry of the AAVP capsid. We first investigated the charge characteristics of AAVP particles by measuring their ζ-potential. The results show the negative charge of AAVP at physiological pH (**Figure 3.7a**). The data indicate that the AAVP vector possesses an acidic surface, with an isoelectric point of pH=3 as determined by zeta potential = f(pH). In order to characterize AAVP-polymer complex, the surface charge and the average sizes of AAVP complexed with cationic polymer were assessed (**Figure 3.7a, b**). As shown in **Figure 3.7c**, the addition of increasing cationic polymers concentrations led to a corresponding increase in the ζ-potential from a negative value to a positive value and thereafter the ζ-potential decreased significantly. For example, incorporation of PDL resulted in an increase in ζ-potential from -5 mV to +15 mV with 25 ng of PDL added per 1 µg AAVP in the solution, after which the ζ-potential decreased to reach near zero. As shown in **Figure 3.7d**, the increasing polymer concentrations resulted in an increase of the average size of complexes. No stable measurements could be taken with higher concentrations of polymer content in the complex (>40 ng/µg) either due to visible precipitation of the complex solution or formation of large particle aggregates at a ratio of 40 ng polymer per 1 µg AAVP. Taken together, these results indicate that negatively charged AAVP particles are incoporated physically with cationic polymers to form larger complexes. Under confocal microscopy

(**Figure 3.7e**), it was observed that the morphology of AAVP alone appeared as single particles. However, the addition of cationic polymers resulted in considerable aggregation of AAVP particles.
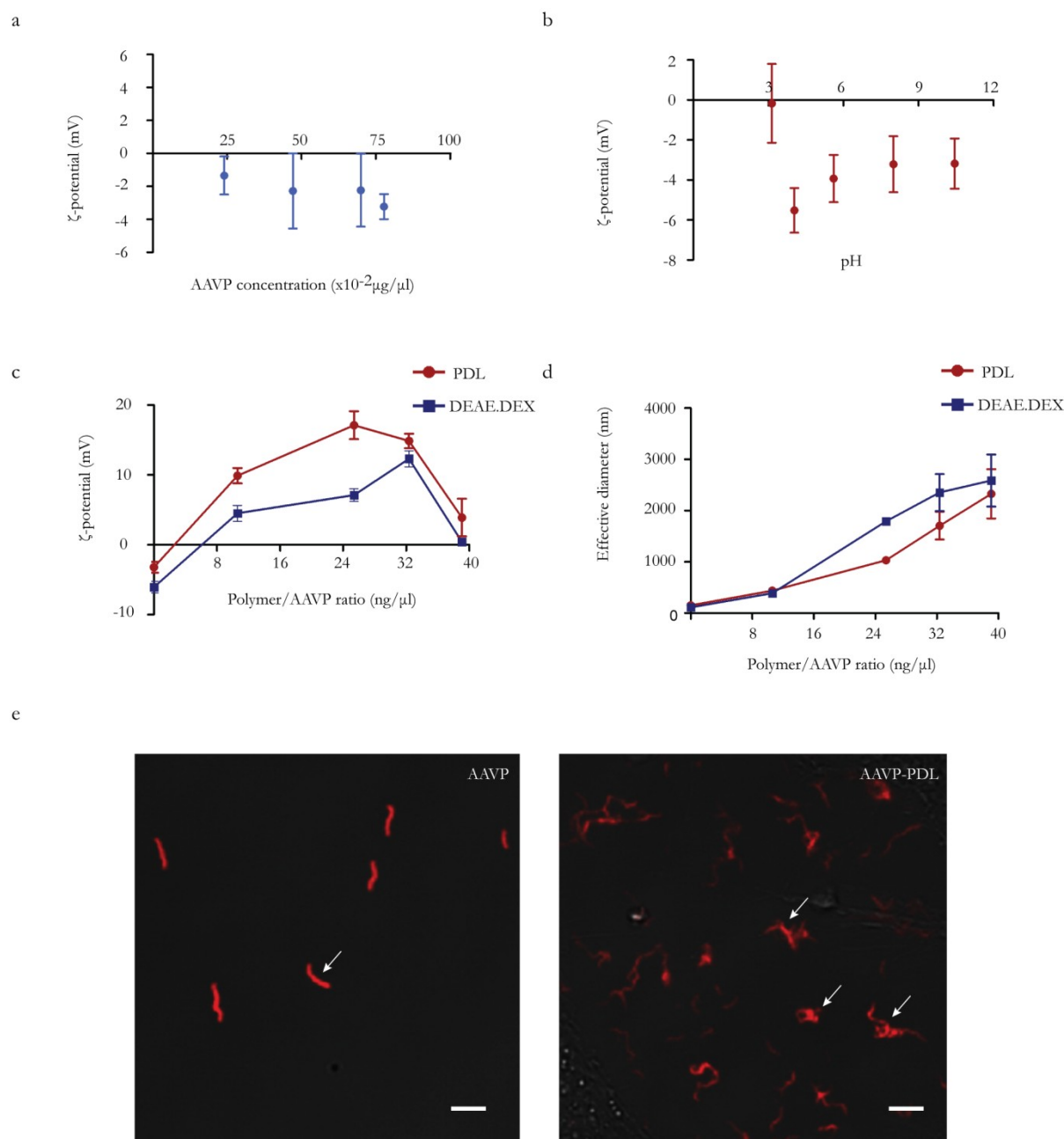
Figure 3.7: Physical characterization of AAVP/polymer complex. a) The ζ-potential of AAVP was measured by Zetasizer when varying phage titer. **b**) ζ-potential of AAVP as a function of pH. The isoelectric point of AAVP particles were determined at the cross point when the ζ -potential becomes zero. **c**) Investigation of cationic polymer (DEAE.DEX or PDL) and AAVP interaction by ζ -potential analysis. **d**) Average size distribution of AAVP or AAVP coated with polymers (DEAE.DEX or PDL) at various ratios as indicated. **e**) The appearance of AAVP/polymer complexes. Morphology of hybrid complexes and phage vectors alone were analyzed using confocal microscopy. AAVP particles were stained for immunofluorescence using anti-fd phage primary and goat anti-rabbit AlexaFluor-647 secondary antibodies. Scale bars = 1 μm.

3.2.8. Incorporation of cationic polymers into AAVP facilitates vector interaction with cells

It is well known that positive charges of gene delivery vectors can enhance their adhesion to negatively charged cell membrane, which increases the chances of cell internalization. We have determined that the AAVP/polymer complex possesses a positive charge. We therefore carried out supernatant-depletion assays and flow cytometry-based experiment to demonstrate that cationic polymers mediate efficient AAVP binding to the cell surface and internalization. Additionally, this may provide an explanation of why some polymers increased transduction efficiency while others did not. Significant depletion of AAVP in the external fluid phase above the adherent cell layer was observed in cells treated with AAVP premixed with DEAE.DEX, PDL, PEI, and PB (**Figure 3.8a**). Nearly 100% of the free cell-unbound AAVP was recovered from the supernatant of cells treated with AAVP alone as well as AAVP premixed with PS polymers. The addition of PS was unable to promote cell attachment, which is consistent with the previous luciferase study showing that PS failed to enhance luciferase gene expression. Internalisation assays revealed that incorporation of AAVP with particular polymers i.e. DEAE.DEX, PEI, PDL and PB (except for PS) allowed cell entry, as indicted by higher intracellular signal than cell incubated with AAVP alone (**Figure 3.8b**). The data indicate that these polymers enable cellular internalization of AAVP. The results also suggest that the failure in internalization of AAVP premixed with PS was due to its inability to promote cell attachment.

To visualize AAVP/polymer complex binding, fluorescence immunostaining was performed on HEK293 cells, which were treated with AAVP uncomplexed or premixed with optimal concentrations of cationic polymer; DEAE.DEX, PEI, PDL, PB, and PS. Uncomplexed AAVP acted as a control to confirm that they are unable to bind to the cell surface in the absence of these cationic polymers. Anti-Phage staining (red) revealed that AAVP premixed with DEAE.DEX, PDL, PEI, and PB co-localised with the HEK293 cell surface (**Figure 3.8c**). These results also suggest that low internalization of AAVP premixed with PB (**Figure 3.8b**) could be caused by the formation of relatively large aggregates (**Figure 3.8c**) that might inhibit the efficiency of cellular internalization, despite efficient binding to cells as determined by supernatant-depletion assay (**Figure 3.8a**). Fluorescence microscopy also revealed that no phage was observed on cells incubated with AAVP premixed with PS (**Figure 3.8c**). This is consistent with previous experiments demonstrating that the addition of PS cannot enable cell attachment (**Figure 3.8a**), internalization (**Figure 3.8b**) and therefore failed to increase transduction efficiency (**Figure 3.5e**).
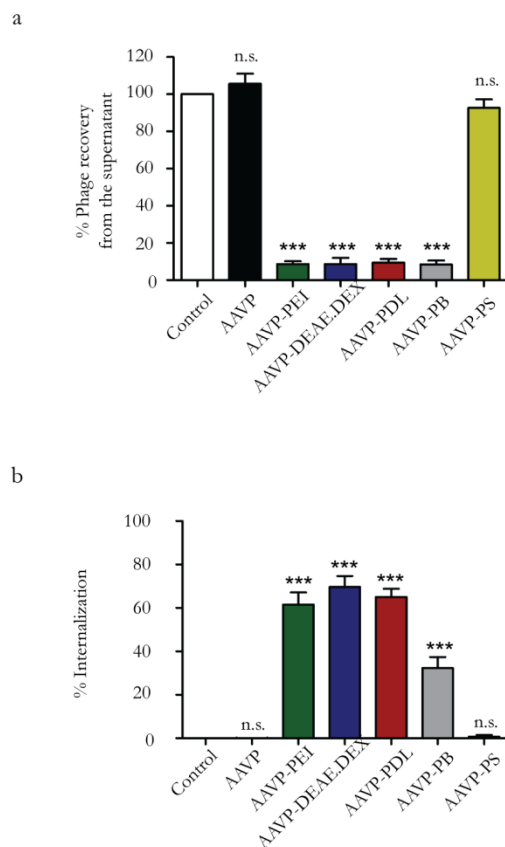
Figure 3.8: Study of cell attachment and internalization by AAVP complexed with cationic polymers. a) Supernatant-depletion assay. **b**) Evaluation of AAVP internalization. Data represent the mean + SEM of triplicate samples from one representative experiments of three, significant difference; n.s.-not significant, * $p < 0.05$, ** $p < 0.01$, ***$p < 0.001$ (one way ANOVA with tukey's post hoc test). **c**) Visualization of AAVP colocalization with cell surface membrane in HEK293 cells 4 hour post transduction using immunofluorescence staining. Scale bars = 100 μm.

c

	DAPI	Anti-Phage	Merged
AAVP			
AAVP-DEAE.DEX			
AAVP-PDL			
AAVP-PEI			
AAVP-PB			
AAVP-PS			
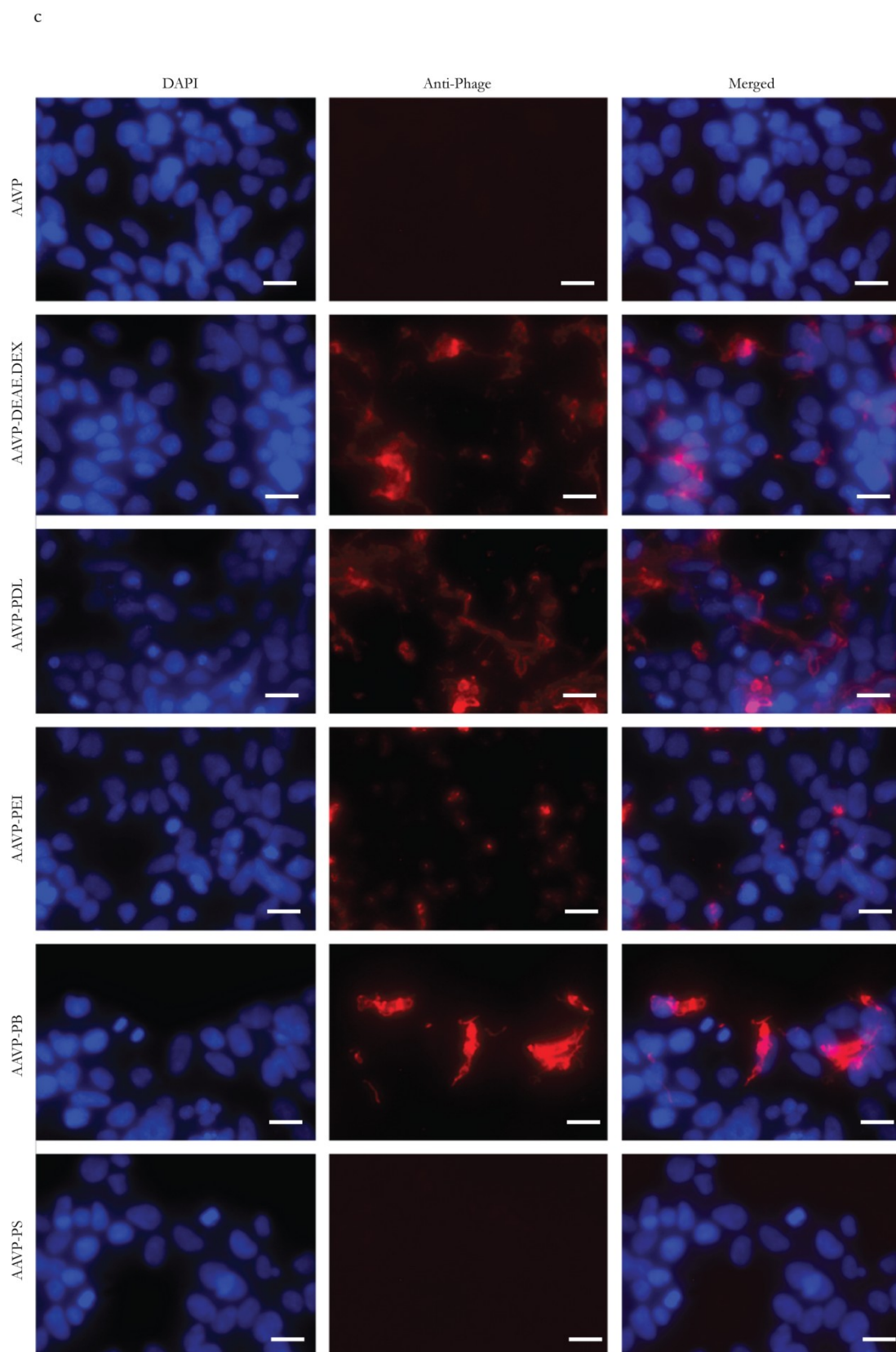
Figure 3.8 (cont): Study of cell attachment and internalization by AAVP complexed with cationic polymers

3.2.9. The proton buffer capacity of AAVP/polymer complex

Polycations with strong proton buffering capacity can induce osmotic swelling and subsequent disruption of endosomal membrane *via* a mechanism termed the 'Proton sponge effect'.[111] We performed an acid-base titration of AAVP/polymer complexes to evaluate their buffering capacity (**Figure 3.9**). The results of this study showed that AAVP alone displayed a titration curve similar to control NaCl and therefore has no buffering capacity without the presence of the polymer. DEAE.DEX or PEI alone, as well as AAVP complexed with DEAE.DEX or PEI elicited higher buffering capacity than AAVP alone. For example, approximately 0.2 ml extra HCl was required to lower the pH of the solution containing AAVP-PEI from 7.4 to 5.1 compared to control NaCl. Another important finding was that PDL combinations showed curves similar to the control NaCl solution indicating no buffering capacity compared with AAVP-DEAE.DEX and AAVP-PEI. This result was consistent with the previous luciferase analysis that demonstrated higher transduction efficacies of AAVP-DEAE.DEX and AAVP-PEI than AAVP-PDL.

Transductions were also performed in the presence of bafilomycin A1 in order to investigate the proton sponge hypothesis. Bafilomycin A, a specific inhibitor of the vascuolar ATPase proton pump was used to inhibit the acidification of early endosomes and therefore prevent endosomal escape.[179,180] The data displayed in **Figure 3.9b** indicate that there was a decrease in transduction efficiencies of RGD4C.AAVP-PEI and RGD4C.AAVP-DEAE.DEX in the presence of

bafilomycin A1. However, there was no significant difference in cell treated with RGD4C.AAVP-PDL with/without bafilomycin A1. The fact that the transduction efficiencies of RGD4C.AAVP-PEI and RGD4C.AAVP-DEAE.DEX transfections in the presence of bafilomycin A1 suffered more than RGD4C.AAVP-PDL suggested the involvement of the proton sponge effect for PEI and DEAE.DEX. This result was consistent with the proton buffer capacity as determined by the acid-base titration (**Figure 3.9a**) that demonstrated higher buffering capacity of AAVP-DEAE.DEX and AAVP-PEI than AAVP-PDL.
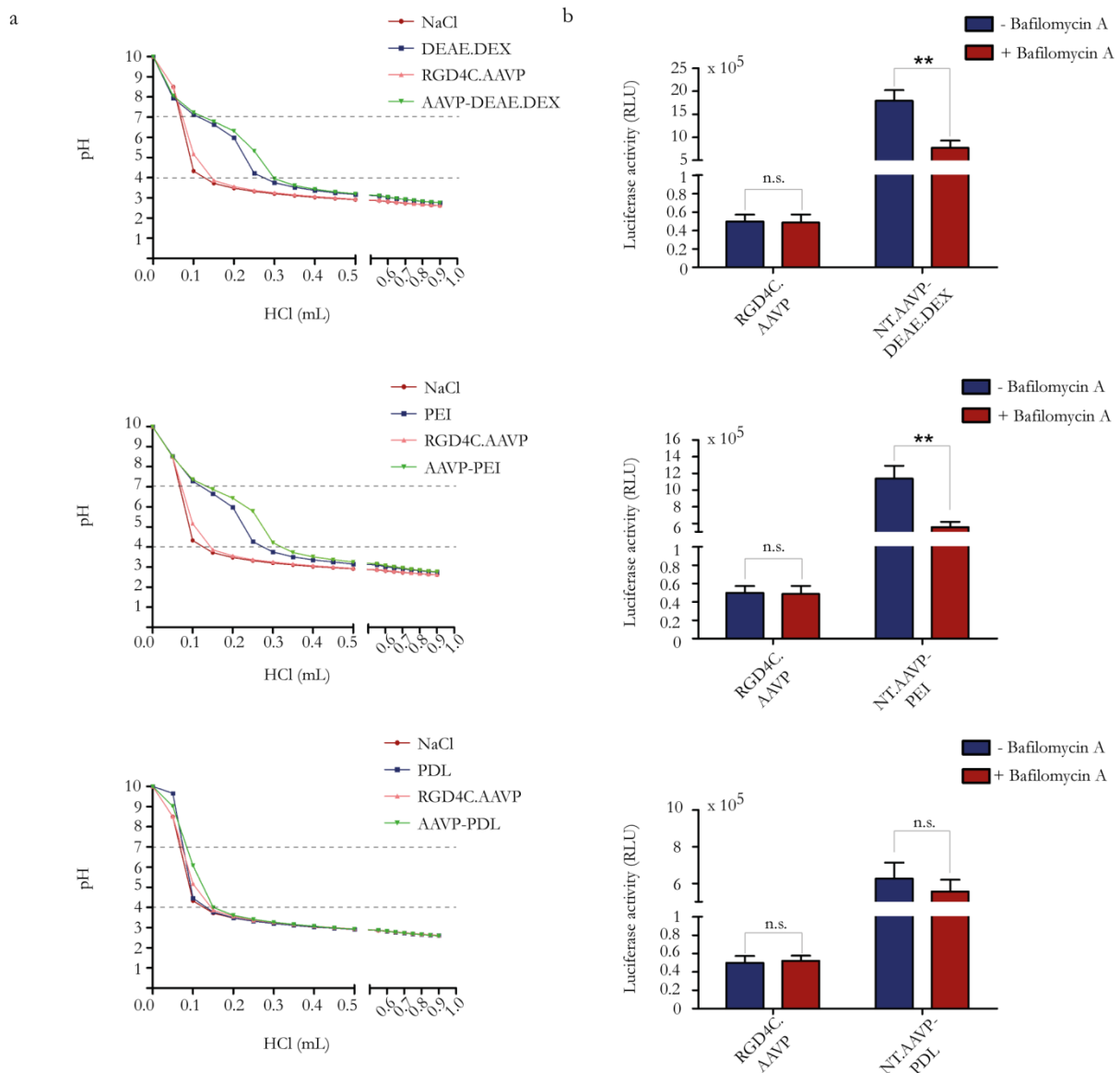
Figure 3.9: Endosome buffering capacity of AAVP/polymer complexes. a) Acid-base titration curve of AAVP/polymer complexes. To assess the proton buffering capacity of AAVP complexed with DEAE.DEX, PDL or PEI, each polymer alone, AAVP alone and AAVP/polymer complexes were dissolved to their optimised ratios in water and adjusted to pH10. HCl was used to titrate the solutions to pH 3. The pH was measured by the pH metre. Tritation curve of NaCl was used as a control. Dashed lines represent the typical pH range in endosome (pH 7.0 – 4.0). **b**) The effect of bafilomycin A1 on transduction efficiency of AAVP/polymer complexes. HEK293 cell transductions were performed in the presence of bafilomycin A1. After 1 hour incubation with 25 μM bafilomycin A1, cells were transduced with AAVP/polymer complexes or the control RGD4C.AAVP. After 3 days cells were analysed for luciferase expression. Data represent the mean + SEM of triplicate samples from one representative experiments of three, significant difference; n.s.-not significant, * p<0.05, ** p<0.01, ***p<0.001 (one way ANOVA with tukey's post hoc test).

3.2.10. Combined genetic and chemical modifications further enhances gene transfer by AAVP

Having shown that chemical modification with cationic lipids, CaPi and cationic polymers enhances AAVP-mediated gene delivery efficiency, we next sought to determine whether incorporation of genetic targeting into vector complexes can lead to further increase in transduction. We investigated the RGD4C-AAVP vector, which was genetically modified to display α_v integrin-targeting RGD4C peptide on the pIII minor coat protein. The α_v integrin receptor-expressing HEK293 cell line was chosen as it has previously been used for investigation of targeted RGD4C-AAVP.[26,171] Firstly, optimal ratios of the complexes of non-targeted NT.AAVP and targeted RGD4C.AAVP with cationic polymers by gene transfer to mammalian cells were determined (**Appendix A**). Results showed the superiority of the AAVP/polymer complexes for transduction of HEK293 cells compared to non-targeted NT.AAVP complexed with polymers and uncomplexed targeted/non-targeted AAVP. For example, incorporation of RGD4C.AAVP with optimal concentration of PEI greatly increased luciferase transgene expression, with maximal 5,500-fold increase compared to the control NT.AAVP as shown in **Figure 3.10a**, which was significantly higher than NT.AAVP-PEI and RGD4C.AAVP (1,500- and 100-fold, respectively). Maximal transduction efficiencies of RGD4C.AAVP-DEAE.DEX, and RGD4C.AAVP-PB resulted in 4500-, 120-fold greater than NT.AAVP, respectively (**Figure 3.10b, d**). However, there were no significant differences in transduction efficacy between cells

transduced with non-targeted NT.AAVP and targeted RGD4C.AAVP, both of which were premixed with PDL (**Figure 3.10c**). In addition, the results of this study did not show any significant increase in transduction by the targeted RGD4C.AAVP that was coprecipitated with CaPi (**Figure 3.10f**), or premixed with cationic lipids at various ratios (**Appendix A**).

Next, to further explore the superiority of the targeted RGD4C.AAVP, we treated HEK293 cells with RGD4C.AAVP vectors carrying a GFP reporter gene, which were complexed with various DEAE.DEX ratios. This was compared to control non-targeted NT.AAVP and transduction efficacy was subsequently assessed. The RGD4C.AAVP-DEAE.DEX complexes resulted in much higher transduction efficacy than the non-targeted AAVP-DEAE.DEX complexes. A dose response of GFP expression at increasing concentrations of polymer is shown in **Figure 3.11.** Levels of GFP expression increase with increasing DEAE.DEX/AAVP ratios. At similar ratios, the transduction efficacy of the targeted AAVP was clearly higher than those of the non-targeted AAVP.
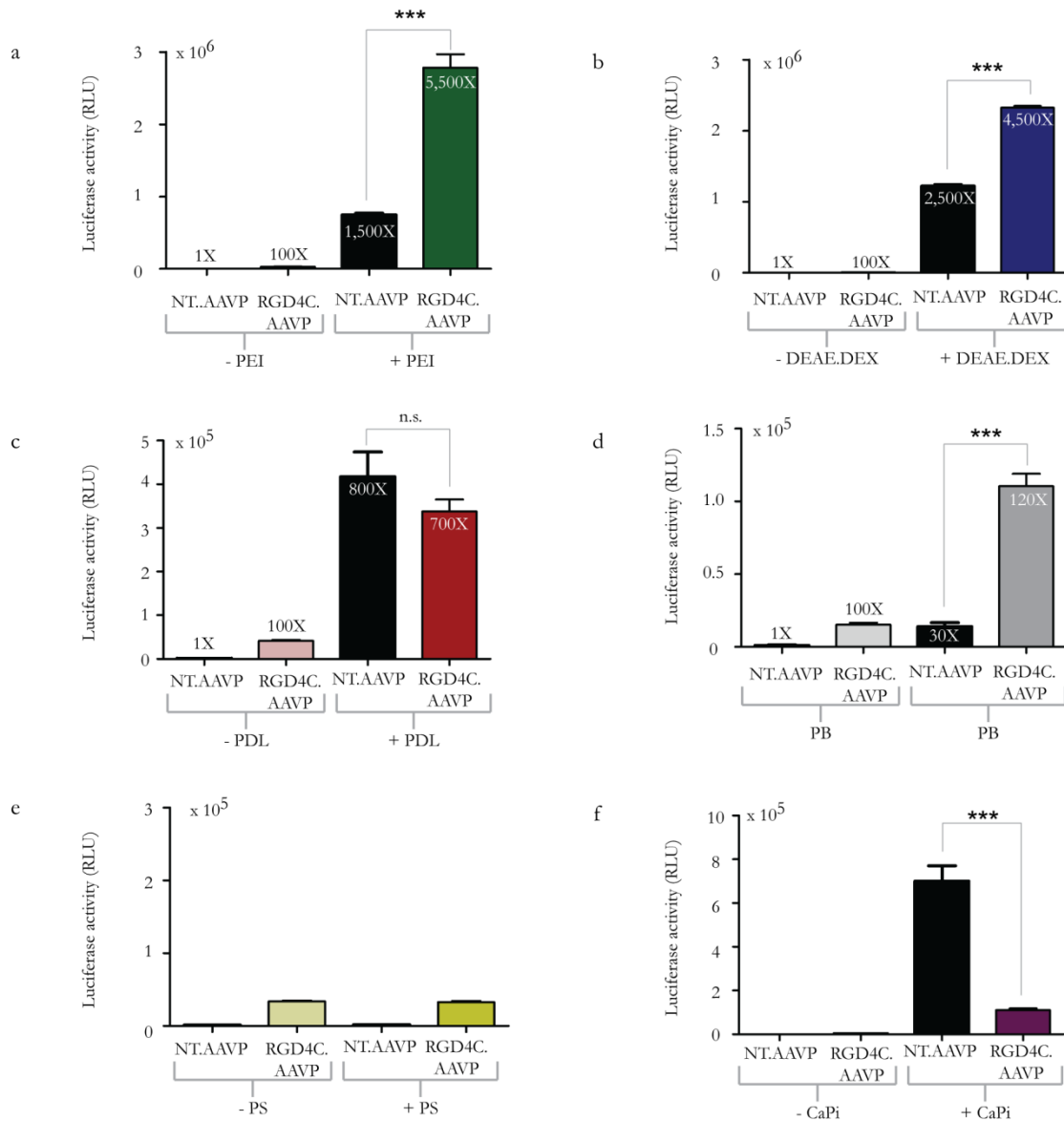
Figure 3.10: The superiority of the optimised RGD4C.AAVP/polymer complexes for transduction of HEK293. Cells were transduced with RGD4C.AAVP, carrying Luc gene, complexed with **a**) PEI, **b**) DEAE.DEX, **c**) PDL, **d**) PB, **e**) PS, and **f**) CaPi at optimal ratios and compared to control non-targeted AAVP. Analysis of luciferase activity was performed 3 days post transduction. The results show the mean relative luminescence units of triplicate wells ±SEM, from one representative of three independent experiments, significant difference; n.s.- not significant, * $p < 0.05$, ** $p < 0.01$, ***$p < 0.001$ (two way ANOVA with tukey's post hoc test).
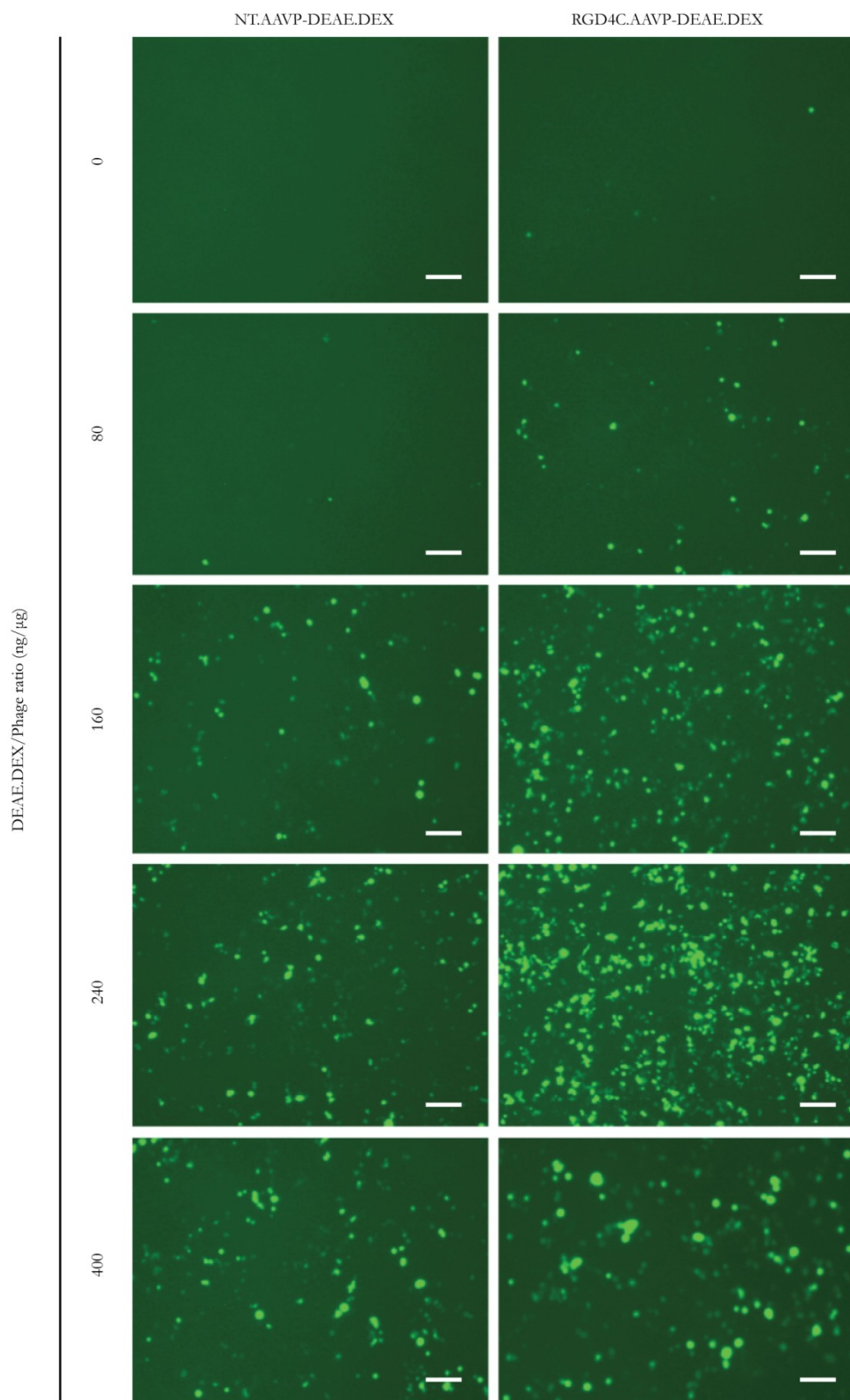
Figure 3.11: GFP expression observed after the targeted RGD4C.AAVP-DEAE.DEX complex treatment of HEK293 cells. Cells were treated with RGD4C.AAVP, carrying *GFP*, complexed with DEAE.DEX at various DEAE.DEX/AAVP ratios and compared to control non-targeted AAVP. Scale bars = 100 μm.

3.2.11. Evaluation of efficacy in a 3D multicellular spheroid

It has been reported that multicellular spheroids better mimic the microenvironment of tissues because they exhibit different characteristics compared to monolayer cultures. These three dimensional (3D) cultures serve as more relevant model systems for a better investigation of gene delivery vectors [181]. We therefore evaluated the efficacy of AAVP/polymer complexes in a 3D multicellular spheroid in addition to traditional monolayer cultures. HEK293 spheroids were first transduced with the non-targeted or targeted AAVP vectors carrying Luc gene premixed with various DEAE.DEX/AAVP ratios to determine the optimised ratio of the complexes. Luciferase activity was analyzed at day 10 post transduction and revealed that DEAE.DEX significantly increased gene expression by the targeted RGD4C.AAVP when compared to the non-targeted AAVP (**Figure 3.12a**). Next, spheroids were incubated with GFP carrying vectors integrated with optimized DEAE.DEX/AAVP ratios and compared to controls RGD4C.AAVP and non-targeted AAVP without polymers (**Figure 3.12b**). GFP expression was examined at day 10 post transduction. While, non-targeted AAVP/polymer complexes and RGD4C.AAVP or non-targeted AAVP alone showed minimal GFP expression, analysis of the targeted RGD4C.AAVP/DEAE.DEX complexes revealed a dramatic increase of GFP expression. The data are consistent with our findings from luciferase activity assays. Overall, the targeted RGD4C.AAVP/polymer complexes showed better transduction efficacy than the non-targeted AAVP/polymer complexes in a 3D

multicellular spheroid, in agreement with results obtained with monolayer culture. The data also prove that the cationic polymer is should be used in AAVP-guided gene transfer to spheroids.
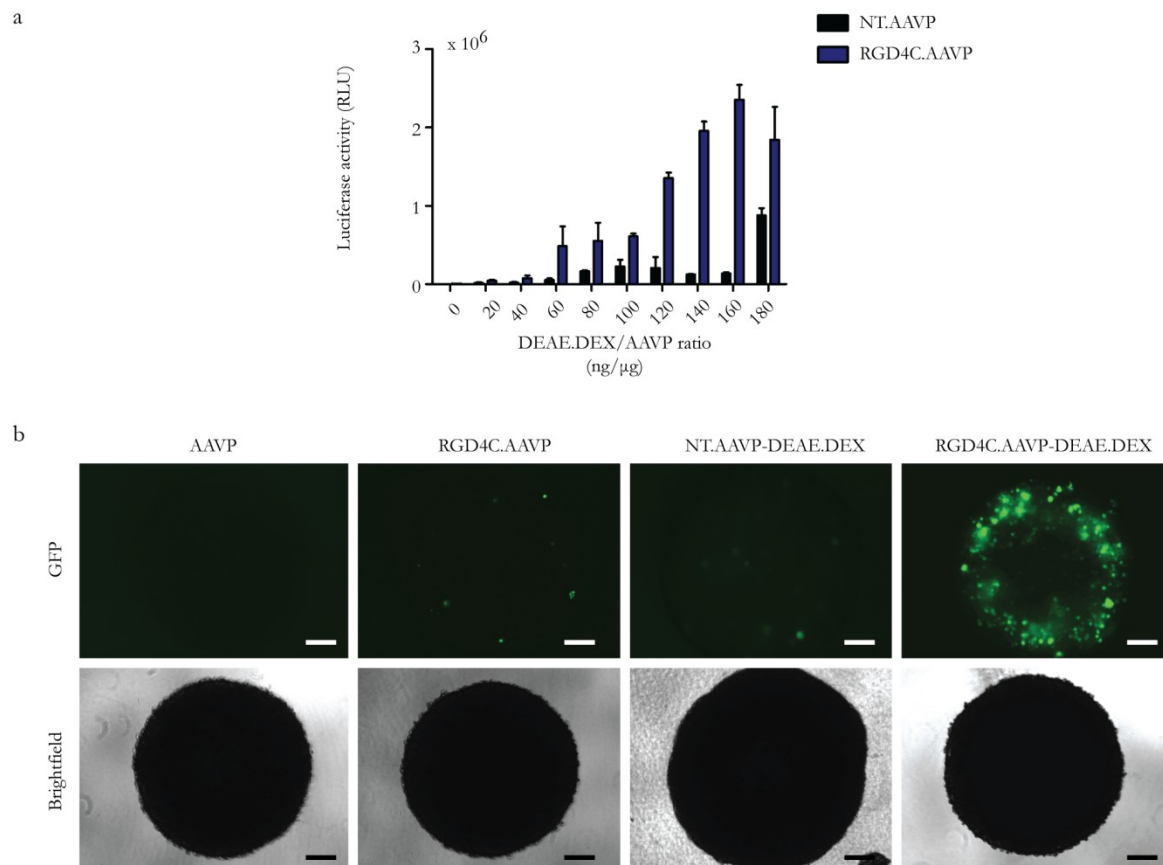
Figure 3.12: Transduction study using multicellular spheroids to evaluate AAVP/polymer complexes. a) Analysis of luciferase activity in multicellular spheroids. HEK293 cells were cultured in 96-well plate and incubated until single spheroids were formed. Spheroids were transduced with the non-targeted or targeted AAVP vectors carrying the Luciferase reporter gene premixed with various DEAE.DEX ratios. Luciferase expression was assessed at day 10 post transduction. **b**) GFP expression observed after AAVP/polymer complex treatment of multicellular spheroids. HEK293 were cultured in 96-well ULA plate in order to form spontaneous singular spheroids. Spheroids were treated with the optimised DEAE.DEX/AAVP complexes carrying GFP reporter gene and compared to controls, uncomplexed RGD4C.AAVP and non-targeted AAVP. GFP expression was analyzed at day 10 post-transduction using a fluorescent microscope. Scale bars = 0.5 mm.

3.2.12. Stable expression derived from cells transduced with AAVP/polymer complexes

Finally, we investigated whether transgene expression could be sustained if AAVP/polymer complex-transduced mammalian cells were maintained under selective pressure. Previous investigations demonstrated that including an expression cassette encoding a dominant-selectable marker in the AAVP vector allowed the selection of stably transduced cells.[182,183] Results shown above demonstrated that the combination of both chemical and genetic modifications of AAVP vectors greatly enhanced gene delivery to mammalian cells. We therefore attempted to establish the utilization of our novel targeted AAVP/polymer system as a gene delivery vector for scientific research. We aimed to determine the efficacy of transgene expression mediated by RGD4C.AAVP/polymer complex by using it for stable cell line production. The RGD4C.AAVP/polymer complex contains an expression cassette that allows selection of cells in the presence of the antibiotic puromycin. To rule out the possibility that our novel vector system is specific to a particular cell line we used MCF-7 and 9L cells in addition to HEK293 cells. Following determination of transient transduction efficiency, HEK293, MCF-7, and 9L cells were treated with the targeted RGD4C.AAVP carrying GFP premixed with optimized ratios of polymers and incubated in media supplemented with puromycin at 500 µg/ml for 14 days. Stably transduced cells were grown in colonies and the expression of GFP protein was visualised by a fluorescence microscope. Nearly all colonies were positive for GFP activity. As

shown in **Figure 3.13**, representative images of puromycin-resistant colonies of HEK293, MCF-7, and 9L cells expressing GFP arise from cultures transduced with the RGD4C.AAVP/polymer complexes. GFP-positive and negative colonies were counted.
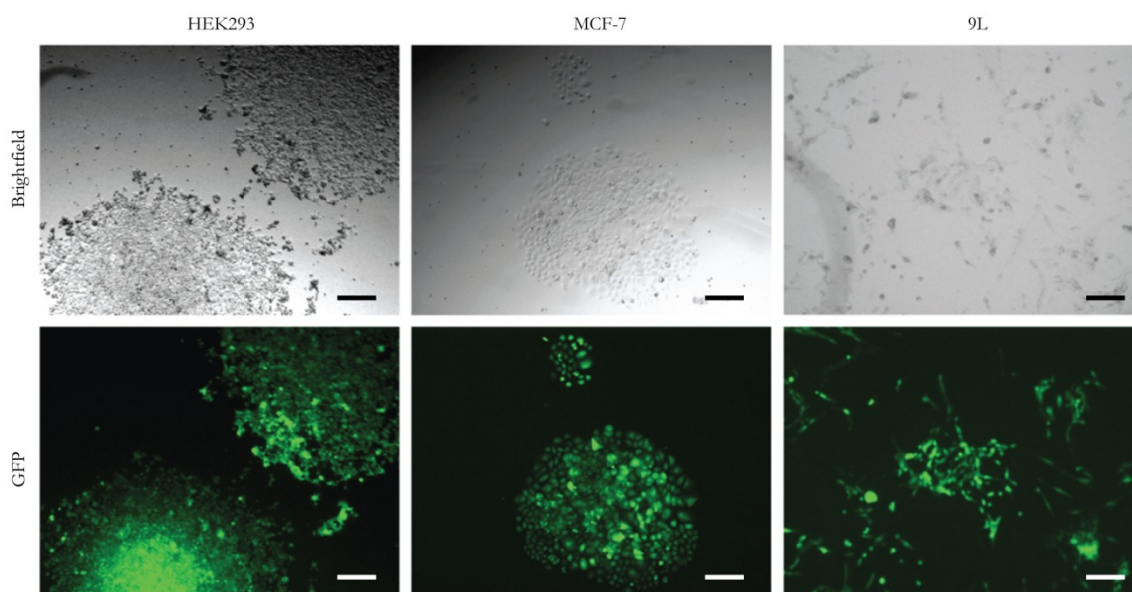
Figure 3.13: Formation of stable clones derived from the AAVP/polymer complex-transduced cells. HEK293, MCF7 and 9L cells were treated with RGD4C.AAVP vectors, carrying the *puro^r* gene and GFP reporter gene, premixed with optimised polymers. Stably transduced cells were selected using puromycin resistance and grown in colonies. Scale bars = 100 μm.

3.2.13. Stability of stable cell line formation

Following cell transduction with the RGD4C.AAVP complexed with cationic polymers in the presence of puromycin for 14 days, GFP-expressing colonies were counted under the microscope with and without a GFP filter. The results obtained from three different cell lines indicated that the nature of the cells itself is a critical factor that determines the number of resistant clones obtained. 9L cells produced the highest number of puromycin-resistant colonies followed by HEK293 and

MCF-7, respectively (**Figure 3.14**). Out of five polymers tested, PDL, PEI, and DEAE.DEX resulted in the increased number of puromycin-resistant colonies in HEK293 cells (32±5,18±1, and 15±3 clones/well, respectively) compared to cells transduced with the RGD4C.AAVP alone that yielded a low number of resistant clones (3±1 clones/well), suggesting that transduction with particular polymers achieved higher efficiency than without a polymer. Unexpectedly, the addition of PB and PS inhibited the formation of resistant clones.

To investigate the stability of GFP expression, resistant colonies were pooled and placed in media without antibiotics. All three pooled cell lines maintained GFP expression after culture for at least 20 passages in the absence of puromycin (**Figure 3.15**). These results demonstrate the effectiveness of the AAVP/polymer vector system in the creation of functional stable cell lines. Taken together, these studies indicate that the AAVP/polymer vector system provides a powerful tool for efficient production of stable mammalian cell lines over currently established systems.
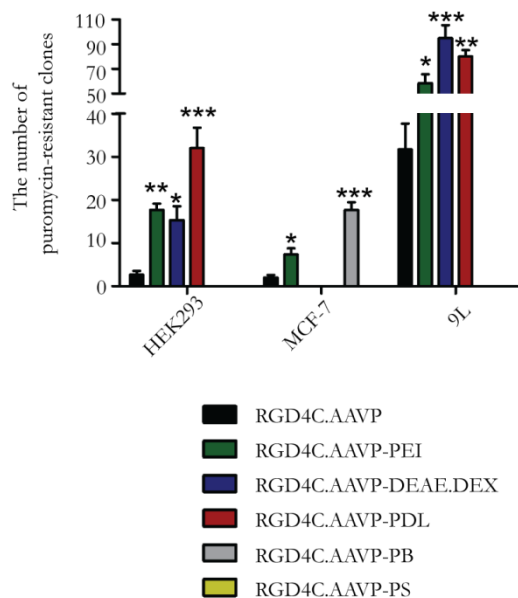
Figure 3.14: The effect of cationic polymers on the yield of puromycin-resistant colonies. Three different cell lines: HEK293, MCF-7, and 9L cells were transduced with the targeted RGD4C.AAVP alone or complexed with five different cationic polymers. Resistant colonies were counted after 14 days of selection with puromycin. Data represent the mean + SEM of triplicate samples from one representative experiments of three, significant difference; n.s.-not significant, * $p<0.05$, ** $p<0.01$, ***$p<0.001$ (one way ANOVA with tukey's post hoc test).
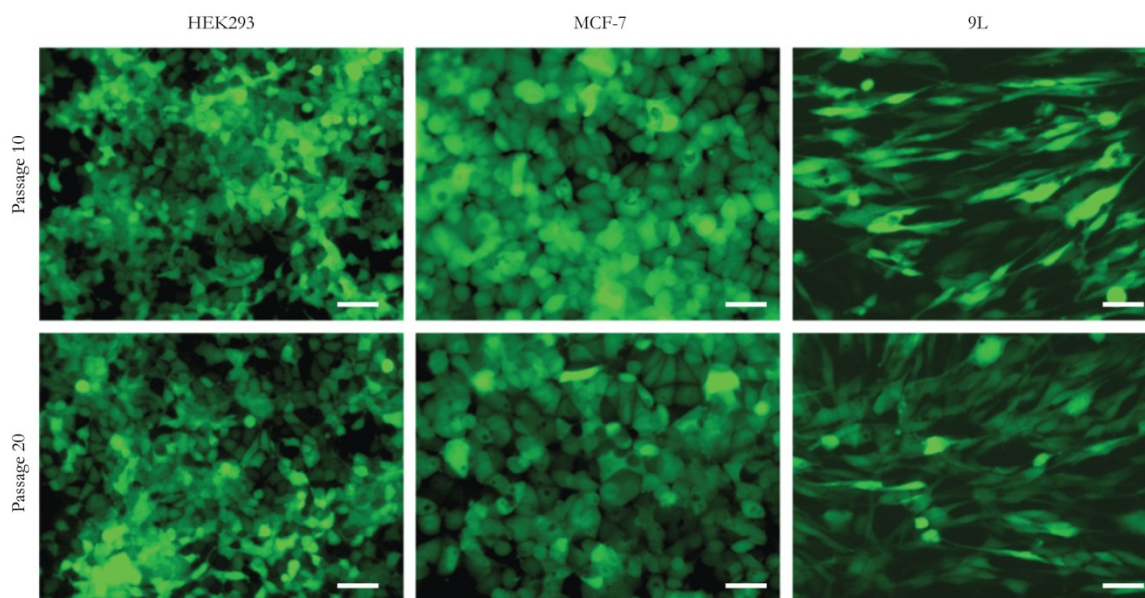
Figure 3.15: Fluorescent images of GFP positive stable cell lines. After selection with puromycin for 14 days, resistant colonies were pooled and placed in media without antibiotics. All three stable cell lines maintained GFP expression after culture for at least 20 passages in the absence of puromycin.

3.3. Discussion

Binding to the cell surface is the first element that determines viral tropism.[184] This process is necessary for the internalisation of vectors since the transgene must be transported from the cell surface to the nucleus. The effectiveness of phage-derived vectors for gene delivery to mammalian cells is limited partly due to the lack of binding to cells that do not express a receptor recognized by bacteriophages. In fact, phages have no intrinsic tropism for eukaryotic cells as they have evolved to infect bacteria only.[185] In order to develop a phage-based vector, it is therefore necessary to introduce novel tropism. Previous investigations demonstrated that tropism for mammalian cells can be conferred on bacteriophage by fusing their coat proteins to a cell-targeting ligand, such as basic fibroblast growth factor (BGF2), transferrin, or epidermal growth factor (EGF). In this respect, phage-based vectors have been successfully adapted for targeted gene delivery to mammalian cells.[178] Our group has also established an essential role of the RGD4C ligand, displayed on AAVP coat protein, for mammalian cell attachment and internalization.[26,171] However, we found transduction saturation as a limitation of RGD4C.AAVP-mediated gene delivery to mammalian cells. The saturated transduction by these vectors could result, at least in part, from the limited number of available cell surface receptors that are targeted by the RGD4C.AAVP. It has also been suggested that higher amounts of the targeting compounds has to be administered than can be accommodated by the receptors to drive the binding interaction.[186] This theory was supported by our results

demonstrating the low affinity of RGD4C.AAVP to cell surfaces as determined by a supernatant-depletion assay and fluorescence staining. A relatively high amount of RGD4C-AAVP is thus required to overcome the relative repulsion between cells and AAVP in order to achieve transduction. The weak and reversible interaction between RGD ligands and integrin receptors[187] is weakened due to inherent properties of the bacteriophage. The negatively-charged amino acid residues (Glu2, Asp4, and Asp5) of the major coat protein pVIII are responsible for an overall large negative charge on uncomplexed phage viral particles.[188] Consequently, phage particles are repelled to some extent by the negatively charged cell membranes of mammalian cells. Therefore, the ideal condition (infinite binding affinity) in which RGD4C.AAVP particles can bind the target cell equals the number of available integrin receptors is virtually impossible to achieve.

The first aim of this study was to examine if tropism for mammalian cells can be conferred to AAVP by chemical modification in addition to genetic modification. By delivering AAVP vector in a CaPi coprecipitate or including cationic polymers in the complex, we were able to alter tropism for mammalian cell. We demonstrated the higher affinity of these chemically modified AAVP compared to conventional RGD4C.AAVP for the cell surface as determined by the cell binding assays, resulting in higher transduction efficacy according to reporter gene expression. This study produced results that are consistent with the findings of a number of previous reports in this field. It has been reported that combinations of adenovirus, retrovirus and AAV with cationic molecules improved transduction

efficiency due to enhanced cell attachment in some cell types that are recalcitrant to infection due to the lack of virus receptors.[189-192] Moreover, transduction efficiency of these viral vectors was improved by coprecipitation with CaPi. These studies demonstrated that the virus-CaPi complex was efficaciously bound to cells.[193-197]

Surface charge plays an important role in particles' interactions with charged phospholipid head groups or protein domains on cell membranes.[198] In this study, we showed that the complexation of AAVP with cationic polymers generates positively charged AAVP complexes allowing better adsorption on cell-membrane surfaces. It is well known that cationic particles bind to negatively charged molecules on the cell membranes, in contrast to neutral and negatively charged particles that display low affinity of interactions.[199]

Another important aspect of cationic polymers is their ability to increase cell membrane permeability. PDL, PEI, and DEAE.DEX induced the formation of transient, nanoscale holes in living cells allowing a greatly enhanced exchange of materials across the plasma membrane.[200] Other groups also confirmed the pore formation in membranes by cationic particles.[201,202] However, the size of AAVP/polymer complexes seemed to be relatively larger than the reported pore size which should not be able to assist the AAVP entry to cells. However, we believe that this phenomenon is associated with cytotoxicity observed at high concentrations of cationic polymers. It was suggested that uncontrolled cationic

density may compromise the plasma membrane's integrity, leading to pore formation, membrane thinning and/or erosion and, subsequently, cytotoxicity.[116]

The first interaction between a gene delivery vector and a cell is crucial to promote subsequent endocytosis. In general, endocytosis can be subcategorized into macropinocytosis and receptor-mediated endocytosis.[203,204] The former is a major non-specific endocytotic process (also called adsorptive-mediated endocytosis) observed in macrophages, tumour and other growth factor or phorbol ester-stimulated cells that engulf solute macromolecules.[205] Receptor-mediated endocytosis is thought to be the major route for engulfment of targeted gene delivery vectors.[203,206] This process can be characterized into two categories: caveolae-mediated and clathrin-mediated endocytosis, both of which are triggered by a specific interaction between ligands and receptors on the plasma membranes.[204,206] Endocytosis occurs either by clathrin or caveolae depending on the cell type and/or type of molecules that are being engulfed.[207] Previously, our group demonstrated that endocytosis of targeted RGD4C.AAVP is clathrin-dependent via specific interaction between RGD4C ligands and α_v integrin receptors. In contrast, positively charged AAVP/polymer complexes are thought to be endocytosed via adsorptive endocytosis. Previous reports have demonstrated that non-specific engulfment is induced by electrostatic interactions between positively charged molecules and negatively charged plasma membrane.[104,208] Another interesting finding in this study was despite higher binding affinity of the chemically modified AAVP than the RGD4C.AAVP, there was no significant

difference in internalization. This suggests that additional benefits of chemical modification can possibly promote subsequent steps for AAVP-mediated gene delivery beyond internalisation.

Although it is generally believed that the cell tropism for virus largely relies on the presence of their cell surface receptors and/or coreceptors, multiple-step intracellular events appear to be another potential factor for determining the transduction efficiency of virus.[209] After delivery vectors are endocytosed, they are immediately transported into endocytic vesicles. Regardless of endocytosis pathways, all vesicles formed during internalization will fuse or at least interact with early endosomes.[210] Delivery vectors trapped in endosomal compartments which become continuously acidified from neutral to pH6 are then trafficked to late endosomes where the pH drops to 5-6 through the action of ATP-dependent proton-pumps.[206] Subsequently, late endosomes fuse with lysosomes, resulting in further pH reduction to 4 and exposure to digestive enzymes. Vectors that fail to escape these acidic compartments will be eventually degraded.[206,207,211] Mammalian viruses are known for their efficacious ability to deliver nucleic acid into host cells, as they have evolved sophisticated endosomal escape mechanisms that take advantage of the acidic environment. Bacteriophages, however, have no such strategy because they have evolved to infect bacteria only.

Our findings that higher transduction efficacies of AAVP coprecipitated with CaPi than RGD4C.AAVP (despite insignificant difference in cell internalization of AAVP particle) suggests an additional strategy that promotes gene transfer. A

possible mechanism for this may be explained by the increase of osmotic pressure through vector-CaPi complexes that promote endosomal escape. It is hypothesized that the degradation of CaPi by hydrolytic enzymes in an acidic environment results in release of Ca^{2+} and PO_4^{3-}, which increases osmotic pressure via water uptake. Eventually, the endosome is disrupted, releasing vectors into the cytosol.[212] Furthermore, we observed higher transduction efficacy of AAVP complexed with cationic polymers than RGD4C.AAVP, although there was no difference in cell entry, suggesting an additional mechanism. The proton sponge phenomenon has been observed in certain cationic polymers with a high pH buffering capacity over a wide range of pH and proposed as a mechanism for endosomal escape of cationic molecules with proton sponge properties.[213] During the maturation and acidification of endosomal compartments, cationic molecules will become protonated and continuously sequester protons supplied by the v-ATPase (proton pump). The proton pumping action leads to the retention of chloride ions, increasing osmotic pressure and hence water influx. Subsequent endosomal swelling and rupture cause the release of particles and their contents into the cytosol.[111]

We tested this hypothesis by studying the acid-base titration curve of AAVP complexed with cationic polymers. High buffering capacity was observed in AAVP complexed with PEI and DEAE.DEX but not with PDL. We also carried out transductions in the presence of bafilomycin A1 which inhibit vector endosome eacape via proton sponge mechanism[179,180] and observed a decreased transduction

efficiency of RGD4C complexed with PEI or DEAE.DEX but not with PDL. This also accords with earlier observations, which showed that strongly charged amino group-containing polymers, including PEI, achieved high transfection efficiency. In contrast, PDL failed to display desirable transfection efficiency as it does not possess buffering capacity.[27,52,214] A previous study showed significant chloride ion accumulation, volume expansion and membrane lysis in the strongly buffering polyamines in PEI-containing endosomes, but not the ones with non-buffering polylysine.[215] These findings provide direct support for the proton sponge hypothesis and rationale for the design of AAVP/polymer complex as a gene delivery vector. However, over-controlled administration of cationic polymers results in cytotoxicity. Lysosomal swelling and rupture not only releases the cargo to the cytosol, but also causes spillage of lysosomal content, triggering intracellular Ca^{2+} release. This enhances the permeability transition pores in mitochondria, leading to decreased ATP production and cellular apoptosis.[216]

The most interesting finding was that a combined genetic and chemical modification of AAVP capsid further enhances gene transfer. The interaction of a virus with cell surface initiates a chain of dynamic events that enable virus entry into the cells. In simplest forms, the mammalian virus binds to a cell surface receptor and directly induces the subsequent endocytosis. For example, the SV40, a polyomavirus, binds the cell surface via major histocompatibility complex 1 (MHC-1) that directly triggers endocytosis via caveolae pathway.[217] However, several viruses have multiple attachments. For example, adenovirus utilizes the first

high-affinity interaction between the globular knob of the C-terminal domain of the viral fibre protein and the cellular CAR, followed by the second low-affinity interaction between the RGD motif on the viral penton base and integrin receptors. Together they form a strong connection between the cell and the virus, leading to endocytosis.[110] In this regard, the AAVP was genetically and chemically modified to exploit multiple attachments for mammalian cell tropism. The RGD4C.AAVP/polymer complex uses its positively charged capsid (higher affinity than the parental AAVP displaying RGD4C is hampered by electrostatic repulsion force) for attachment to negative charged cell surfaces, followed by internalization by α_v integrins.

In this study we expanded the utility of AAVP/polymer complex as gene transfer vectors for selection of cell lines that stably maintain expression of the reporter gene. The generation of stable cell lines has been exploited for a broad spectrum of applications, such as gene function study[218], drug discovery assays or the production of recombinant proteins.[219] In contrast to transient gene expression, stable expression usually depends on integration of gene of interest into the target cells genome or episomal maintenance in the nucleus, allowing long term, defined and reproducible expression of the gene of interest. Previous studies established the utilization of RGD4C.AAVP as gene delivery vector for the selection of stably-transduced cells.[182,183] The persistent transgene expression is associated with the presence of genetic cis-elements ITR from the animal virus AAV2, allowing the formation of monomeric or concatemeric extrachromosomes and a rare event of

chromosomal integration of the gene of interest.[171,220] Two culture systems used for generating a stable cell lines include batch culture and limiting dilution. In a batch culture system, a mixed population of drug resistant cells is selected and directly used for experimental analysis with the advantage of generating fast results. To generate clonal cells, the resistant cells are diluted to isolate single clones. The so-called limiting dilution allows for conduction for the study that requires a defined and homogeneous cell system. In this study we generated stable cell lines using the batch culture system as proof-of-concept. The RGD4C.AAVP/polymer vector system allows us to use pools of cells surviving selection, typically following 14 days of culture. The high number of resistant clones with high percentage of positive clones saves considerable time and eliminates the need for screening a large number of colonies to identify positive clones. Taken together, these studies indicate that the RGD4C.AAVP/polymer complex is a powerful tool for efficient production and selection of stable transformants in mammalian cells.

3.4. Conclusion

Bacteriophage-based vectors suffer from low transduction efficiencies for mammalian cells, due to low viral binding to the cell surface or subsequent gene transfer steps. Integrating phage-based gene delivery with biomaterials is a promising strategy to overcome a number of these challenges associated with AAVP mediated gene delivery. Chemical modification of AAVP capsid can be employed to modulate the tropism of viruses or promote endosomal escape, both of which benefit transduction. Two efficient methods include CaPi coprecipitation

and complexation with cationic polymers. In the former method, AAVP particles, $CaCl_2$, and a phosphate buffer are mixed; the AAVP-CaPi complexes, precipitate on the cells, then enter cells through endocytosis. The latter protocol is based upon the negative charge of AAVP particles and positively charged polymers leading to the formation of a complex that adheres to the cell surface, followed by endocytosis. This technique benefits from advantages such as simple and rapid preparation steps, low cost and reproducibility. Next, we demonstrated that combined genetic and chemical modification of AAVP further enhance gene delivery efficacy. In this system, polymer complexed-RGD4C.AAVP was most effective in gene delivery. However, cells show different sensitivities to the toxicity of these compounds. Therefore, proper ratios of transduction enhancing reagents: AAVP must be determined for each cell line. We also reported transient and stable transduction of mammalian cells via AAVP-mediated gene delivery. Our results represent an important step forward in the development of bacteriophages as gene delivery vehicles.

4. A bacteriophage-based gene therapy vector for malignant glioma

4.1. Introduction

Over 20,000 malignant tumours of the CNS are diagnosed every year in the United States[221] and 9000 in the United Kingdom.[222] Of these cases, glioblastoma multiforme (GBM) is the most aggressive brain tumour with a dismal prognosis and extremely low percentage of survivors.[223] Although the number of reported glioblastoma cases is small compared to other solid tumours, the survival rate remains low due to their aggressive nature. Despite advances in diagnosis and treatments consisting of surgical resection followed by radiotherapy and chemotherapy, the prognosis has been largely unchanged over the last 30 years.[224] The median survival time for patients is approximately 12 months after initial diagnosis. Only a small proportion of patients survive more than 36 months.[225] For example, approximately 13,000 new patients are diagnosed with glioblastoma in the United States every year. Half of patients die within one year and 90% within 3 years of diagnosis.[221] These statistics highlight the urgency of developing effective therapeutic strategies against this devastating disease. Impact of surgery is often compromised due to the lack of a defined tumour edge in the brain tissue and the tendency for local invasion of the surrounding normal brain by infiltrating tumour cells, making complete eradication of the tumour by surgery virtually impossible. Additionally, it may also cause recurrence of glioblastoma either at original site or at distant satellite regions in the brain or CNS.[226] Another major factor that

contributes to the dismal prognosis for patients with glioblastoma is the ineffective delivery of therapeutic agents to tumours.

An additional problem is the tight junctions between ECs of CNS vessels, the so-called blood brain barrier (BBB), which is considered a major impediment to systemic treatment of glioblastoma.[227] To overcome this problem, researchers from the US National Institutes of Health (NIH) introduced a new delivery method, which relies on continuous infusion of molecules via intracranial catheters, known as convection-enhanced delivery (CED).[228] This technique has emerged as a leading investigational delivery method for the treatment of brain tumours, allowing for delivery of high concentrations of therapeutic agents directly into brain tumours.[229], Recently, Ksendzovsky *et al* demonstrated that this method can be exploited successfully and safely to distribute bacteriophage in the brain.[230] However, such injection protocols can be technically demanding, requiring extreme precision and accuracy to deliver therapeutic compounds as parenchyma-invading tumour cells can be released even when using small-diameter catheters.[231] Moreover, local administration by direct injection of vector to a disease site can sometimes lead to undesired widespread distribution to normal tissues.[34] The accuracy and targeting capacity of therapeutic payloads themselves or their delivery protocols can be significantly improved. It is therefore necessary to develop efficient and safe vectors capable of discriminating malignant from healthy cells.

Due to the resistance of glioblastoma to conventional therapeutic approaches, it is important to investigate other options. Gene therapy is an alternative approach for

glioma treatment, and has been in development for the past two decades with a strong record of success in pre-clinical studies and an increasing number of models in clinical investigations.[232] Several clinical behaviours and histopathological features of GBM make them particularly amenable to local gene therapy [233], defined as the direct transfer of therapeutic genes into tumour cells.[234] In most cases, GBM are single, localized lesions of rapidly proliferating cells in a background of non-proliferating cells. Metastasis of glioblastoma outside the CNS is very rare, and if recurrence occurs, it happens in the close vicinity of the original lesion.[233]

The experiments carried out in this chapter serves as an investigation of smart bacteriophage vector-mediated gene delivery to glioblastoma in two dimensional (2D) and three dimensional (3D) cell culture systems. The latter of more closely resembles *in vivo* tumour microenvironments and serves as a more *clinically relevant* model. 3D cell culture systems are currently used for earlier stages of drug screening to reduce the need for *in vivo* studies.[235,236] Luc and GFP reporter genes were used for quantitative analysis and optical monitoring of gene expression. To assess therapeutic efficacy, the enzyme-prodrug suicide gene therapy system, HSVtk, was used to kill malignant cells.
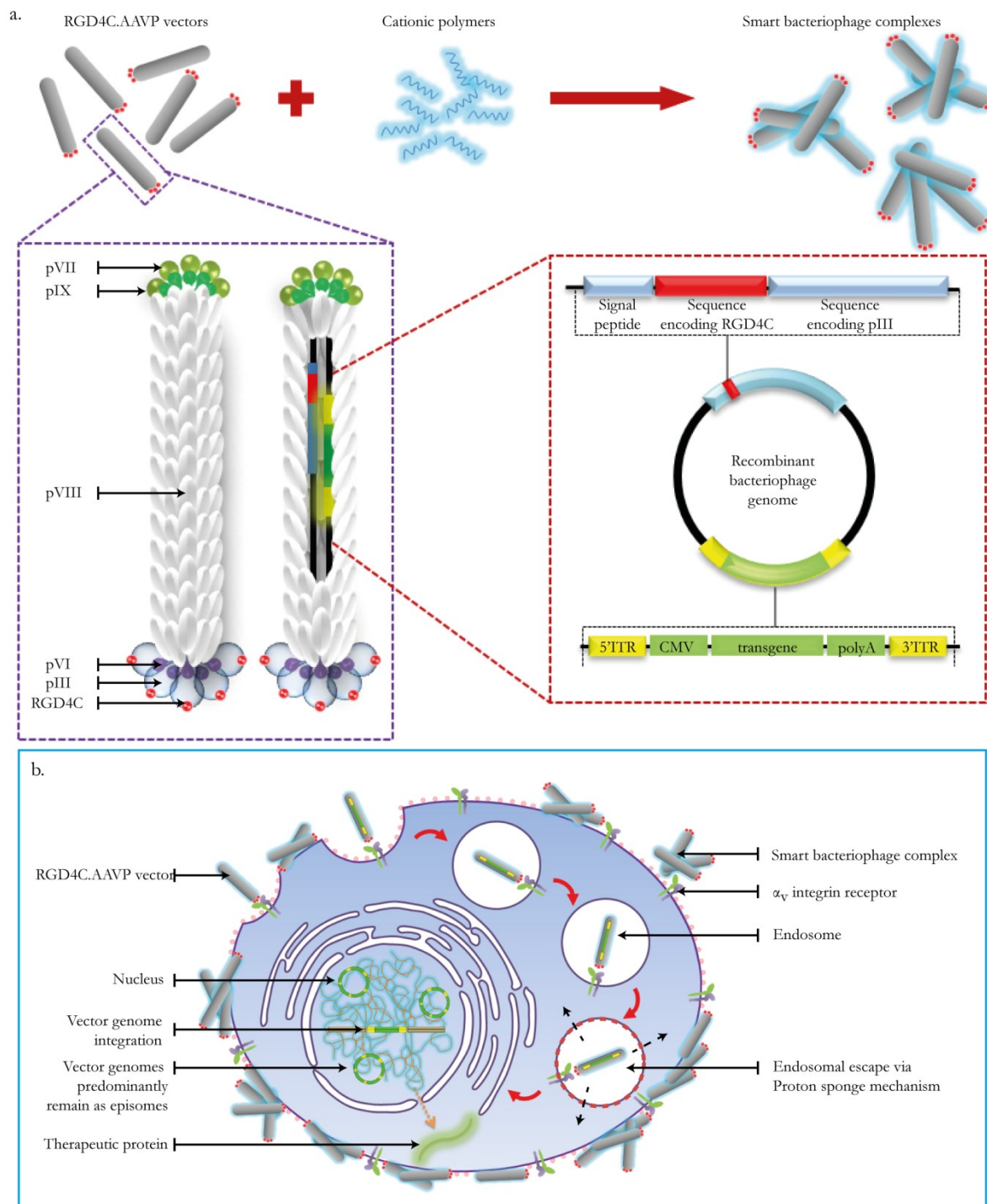
Figure 4.1: Schematic diagram of the smart bacteriophage complex. We reported a novel hybrid multi-component vector designated as a smart bacteriophage complex that combines the advantages of three gene delivery vectors: the filamentous M13 bacteriophage, the genome of rAAV and cationic polymers. (**a**) Negatively charged RGD4C.AAVP vectors were electrostatically assembled with cationic polymers to form smart bacteriophage complexes. A diagram presents recombinant filamentous bacteriophage with genetically modified genome. (**b**) A proposed mechanism of the smart bacteriophage complex trafficking. Positively charged complexes bind to negatively charged cell membrane surfaces. Vectors are then internalized into cells following vector attachment and escape from endosome via a proton sponge effect mechanism.

4.2. Results

4.2.1. Analysis of transgene expression mediated by the smart bacteriophage complex in glioblastoma cell lines

We assessed the transduction efficiency of the smart bacteriophage complex and compared it to the well-characterised RGD4C.AAVP. A schematic diagram of the smart bacteriophage complex and its proposed mechanism of trafficking were shown in **Figure 4.1**. Non-targeted NT.AAVP vector was included in these experiments as controls. We performed these studies by transducing the 9L and C6 cells, both of which are rat glioma cell lines known to express high levels of the α_v integrin receptors.[237,238] To rule out the possibility that the results are a cell type-specific or species-specific, we further assessed efficacy on SNB-19 and LN229, which are human glioblastoma cell lines.[239] We first sought to determine the optimal ratio of the cationic polymer to RGD4C.AAVP by keeping the latter fixed at 25 μg per well and adding increasing concentrations of cationic polymers using the RGD4C.AAVP vector carrying Luc reporter gene (**See appendix A**). Moreover, we assessed the suitability of different cationic polymers, namely PDL, DEAE.DEX, and PEI, which have previously been shown to dramatically enhance AAVP-mediated transduction in Chapter 3. Quantification of luciferase activity in 4 different glioblastoma cell lines at 72 hr post transduction showed that maximum gene transfer levels were achieved with the DEAE.DEX polymer in 9L, C6, SNB-19, and LN229 cells at polymer concentrations of 60, 120, 100, and 40 ng/μg, respectively. As shown in **Figure 4.2a**, treatment with optimal ratios of smart

bacteriophage RGD4C.AAVP-DEAE.DEX complexes resulted in ~10.3-, ~9.2-, ~19.8-, and ~5.1-fold increase of Luc gene expression compared to RGD4C.AAVP alone in 9L, C6, SNB-19, and LN229 cells, respectively. Addition of PDL resulted in ~8.04-, ~2.7-, and ~2.5-fold increase of transduction efficacy in 9L, SNB-19, and LN229 at optimal ratio of 40, 80, and 20 ng/μg, respectively, but failed to enhance expression in C6 cells (**Figure 4.2b**). At optimal ratios of 60 and 20 ng/μg (PEI/AAVP) showed a ~9.13- and ~4.0-fold increase of Luc expression compared to non-complexed RGD4C.AAVP in SNB-19 and LN229 cells, but failed to improve transgene expression in 9L and C6 (**Figure 4.2c**). Polybrene and protamine sulfate failed to enhance expression in all cell lines tested despite a broad range of polymer concentrations (**Data not shown**). The polymer-complexed RGD4C.AAVP (i.e. RGD4C.AAVP-PDL and RGD4C.AAVP-DEAE.DEX) was later designated as the smart bacteriophage complex.

To further explore the superiority of the smart bacteriophage (RGD4C.AAVP-PDL and RGD4C.AAVP-DEAE.DEX) complexes, we used RGD4C.AAVP vector carrying the GFP reporter gene. At day 5 post transduction, representative microscopic imaging of 9L and LN229 cells, as shown in **Figures 4.3a** and **4.3b**, respectively, revealed a dramatic increase in GFP expression in cells transduced with the smart bacteriophage complex compared with the original RGD4C.AAVP. No GFP expression was observed in cells treated with the control NT.AAVP. These data confirm that integration of cationic polymers with the RGD4C.AAVP

vector resulted in a smart bacteriophage complex that significantly boosted gene delivery to glioblastoma cells.
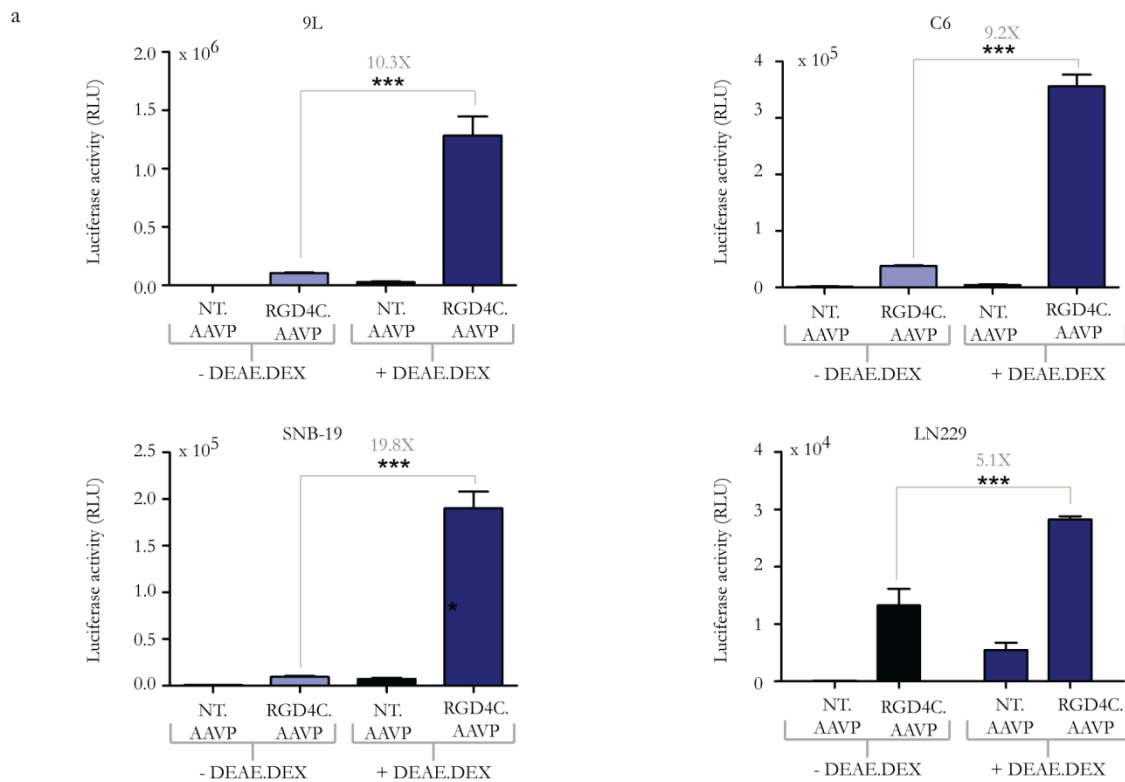
Figure 4.2: Characterization of glioblastoma cell transduction by the polymer-complexed AAVP. Luciferase activity was analysed in 9L, C6, SNB19, and LN229 glioblastoma cells 3 days after treatment with NT.AAVP (uncomplexed or polymer-complexed) and RGD4C.AAVP (uncomplexed or polymer-complexed). **a**) DEAE.DEX/AAVP ratios of 60, 120, 100, and 40 ng/μg for 9L, C6, SNB-19, and LN229, respectively. **b**) PDL/AAVP ratios of 40, 60, 60, and 20 ng/μg for 9L, C6, SNB-19, and LN229, respectively. **c**) PEI/AAVP ratios of 60, 60, 60, and 20 ng/μg for 9L, C6, SNB-19, and LN229, respectively.. The results show the mean relative luminescence units of triplicate wells ±SEM, from one representative of three independent experiments, significant difference; n.s.-not significant, * $p<0.05$, ** $p<0.01$, ***$p<0.001$ (tne way ANOVA with tukey's post hoc test).
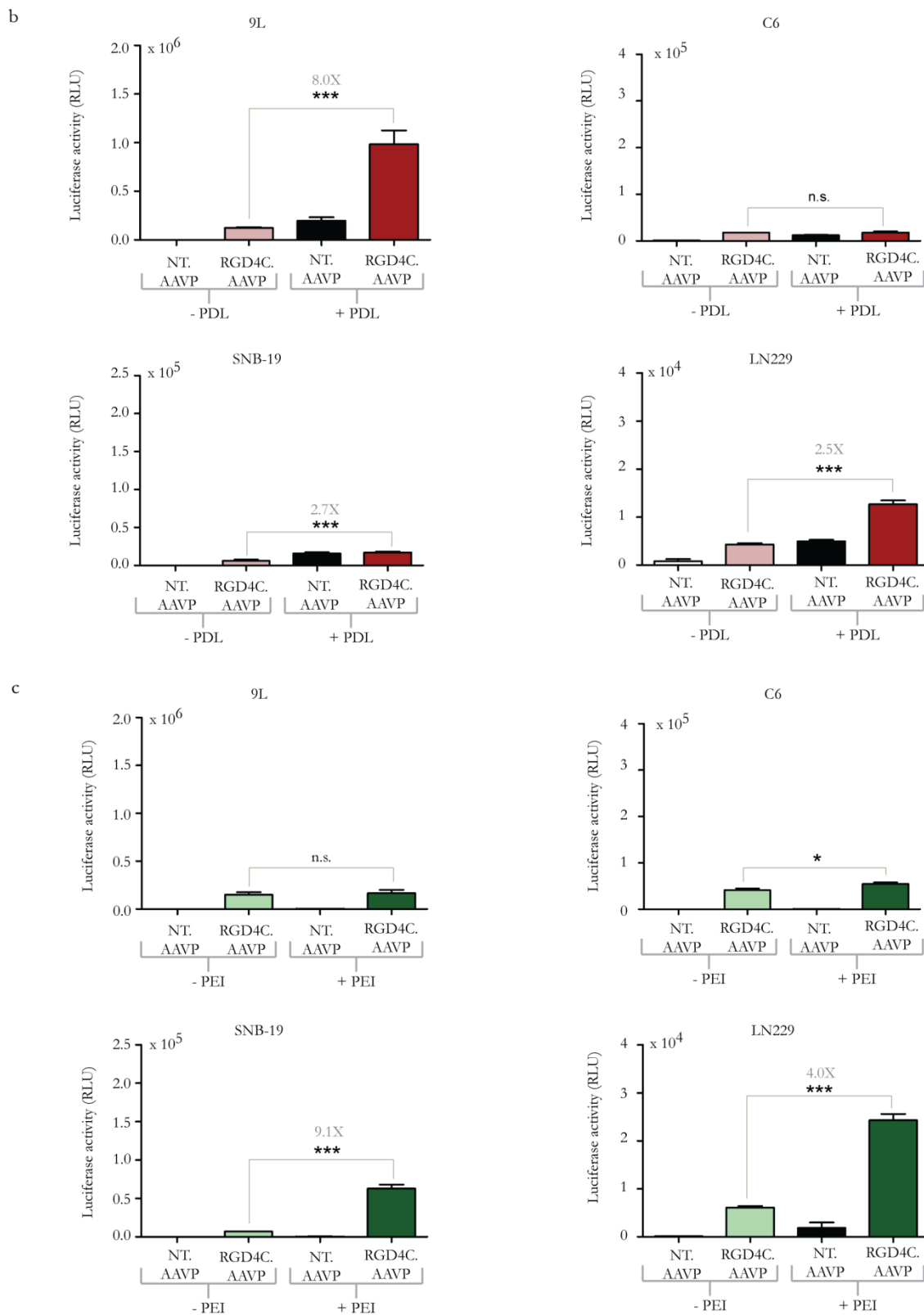
Figure 4.2 (cont.): Characterization of glioblastoma cell transduction by the polymer-complexed AAVP
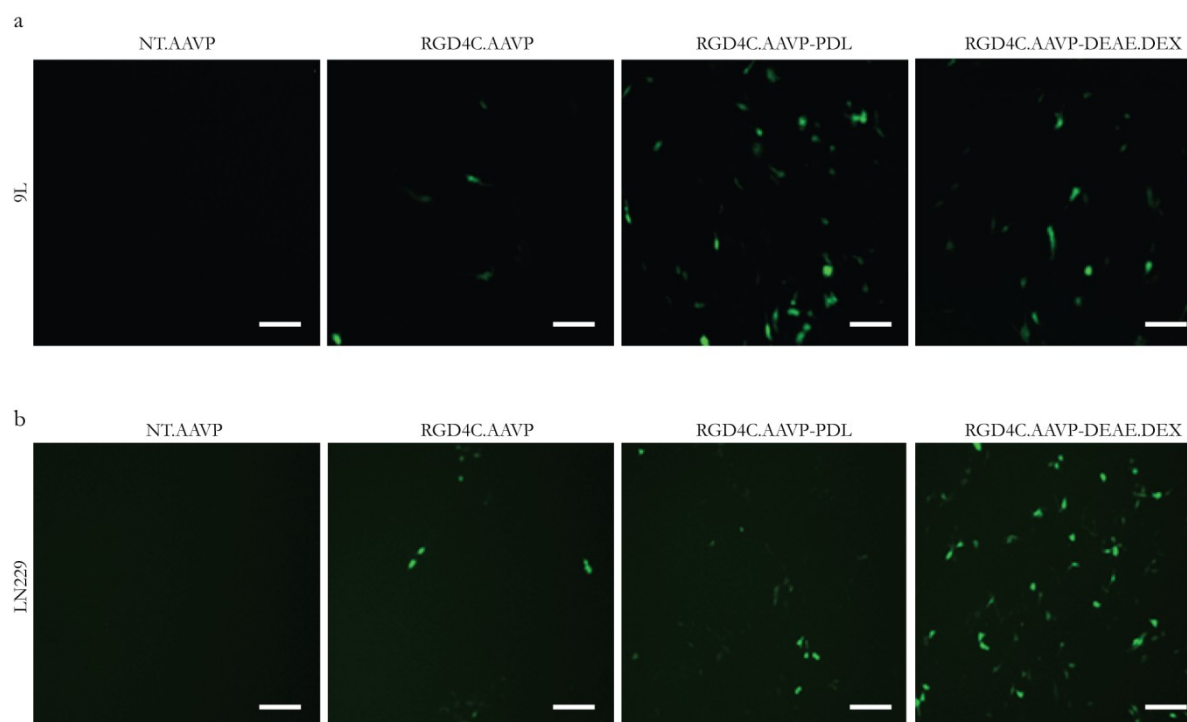
Figure 4.3: GFP expression observed after complex treatment of glioblastoma cell lines with the smart bacteriophage. 9L (**a**) and LN229 (**b**) cells were cultured as monolayers and transduced with the smart bacteriophage complex; RGD4C.AAVP complexed with the optimised polymer/AAVP ratios (40 ng PDL/µg AAVP and 60 ng DEAE.DEX/µg AAVP). Uncomplexed RGD4C.AAVP and non-targeted AAVP (NT.AAVP) were used as controls. GFP expression was assessed using a fluorescent microscope at day5 post transduction. Scale bar = 100 µm.

4.2.2. Kinetics of Luc gene expression following transduction of

glioblastoma cells by a smart bacteriophage complex

Having shown that PDL and DEAE.DEX boost gene expression by AAVP in glioblastoma cells, we sought to assess the effect of various concentrations of AAVP. Therefore, the RGD4C.AAVP vector was mixed with the two polymer formulations in optimal ratios previously identified and used to transduce 9L cells (**Figure 4.4a**). Quantification of luciferase gene expression indicated that smart bacteriophage complexes allowed higher levels of transduction at all RGD4C.AAVP doses tested. Thus, complexation of AAVP with cationic polymers requires lower AAVP concentration to achieve transduction levels similar to uncomplexed RGD4C.AAVP. For example, the level of transduction obtained with uncomplexed RGD4C.AAVP at a concentration of 350 μg/well, (i.e. $1x10^5$ RLU), can be achieved with a concentration of only 25 μg/well, if the RGD4C.AAVP is complexed with DEAE.DEX. Finally, the levels of transduction increased as the concentrations of smart bacteriophage augmented to reach plateau.

Next we carried out a time course analysis the transduction efficacies of smart bacteriophage complexes in 9L cells over a period of 5 days. A considerable increase in expression of the Luc transgene was detected in 9L cells transduced with the smart bacteriophage complex i.e. RGD4C.AAVP-PDL and RGD4C.AAVP-DEAE.DEX., as shown in **Figure 4.4b**. Luc gene expression increased dramatically over time, while it remained low in cells transduced by

uncomplexed RGD4C.AAVP, and no Luc gene expression was detected in control

NT.AAVP-transduced cells.
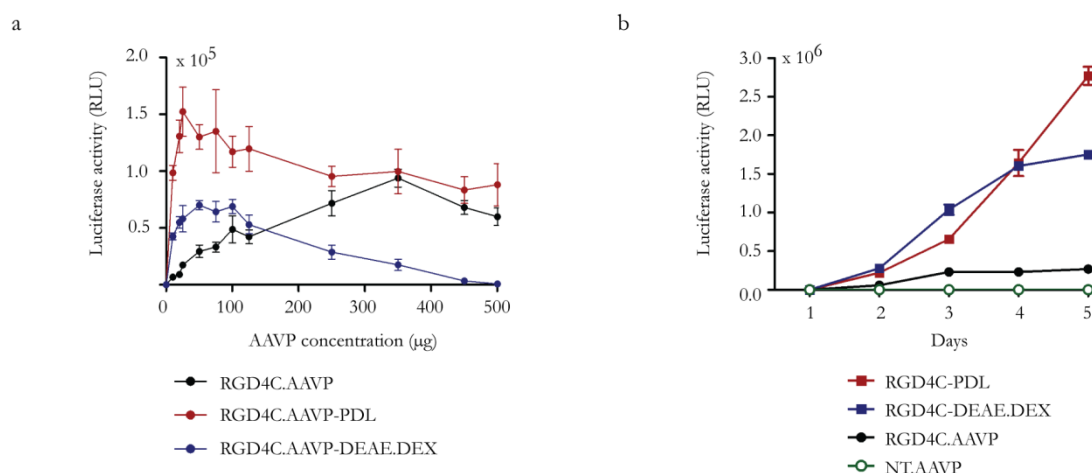
Figure 4.4: Kinetics of *Luc* gene expression following transduction of glioblastoma cells. a) Effect of various RGD4C.AAVP vector concentrations used to form the complex while keeping the optimal ratio. Transductions were performed at fixed cationic polymers/AAVP ratios with RGD4C.AAVP complexed with PDL (40 ng polymer/μg AAVP) and DEAE.DEX (60 ng polymer/μg AAVP) and compared with side by side with uncomplex RGD4C.AAVP. At day 3, *Luc* expressions were quantified. **b**) Time course of *Luc* expression in smart bacteriophage complex-transduced cells. 9L cells were treated with the RGD4C.AAVP premixed with PDL or DEAE.DEX (RGD4C.AAVP-PDL and RGD4C.AAVP-DEAE.DEX, respectively), RGD4C.AAVP alone (RGD4C.AAVP), and non-targeted AAVP (NT.AAVP). The luciferase expression was monitored daily over a time course of 5 days following vector transduction. The results show the mean relative luminescence units of triplicate wells ±SEM, from one representative of three independent experiments.

4.2.3. Physical Characterization of the smart bacteriophage complex

Having defined the optimal ratio that produced the maximal level of gene expression in 9L cells, we analyzed the zeta potential, size, and the appearance of the smart bacteriophage complex. The aim was to confirm that the positively charged smart bacteriophage complex increased gene transfer to glioblastoma mainly by aggregation and efficient binding of phage to the negatively charged cell membranes. We observed the zeta potential shifts from a negative value for uncomplexed RGD4C.AAVP, to a positive value for the smart bacteriophage complex following hybridization with PDL and DEAE.DEX (**Figure 4.5a**). These data proved the positive charge of the smart bacteriophage complex in contrast to the negatively charged surface of the uncomplex RGD4C.AAVP.

Formation of the smart bacteriophage complexes was confirmed by the measurement of particle size. Size measurement of the smart bacteriophage complex in **Figure 4.5a** revealed that RGD4C.AAVP-PDL at optimal ratio of 40 ng/μg (PDL/RGD4C.AAVP), has an average diameter of 7-fold greater than the uncomplexed RGD4C.AAVP. As shown in **Figure 4.5b,** size distributions of the smart bacteriophage complexes; RGD4C.AAVP-PDL and RGD4C.AAVP-DEAE.DEX were in the range of 750-1125 and 750-2000 nm respectively. These data also suggest the self-assembly of the AAVP and the cationic polymers yields a monodisperse product.
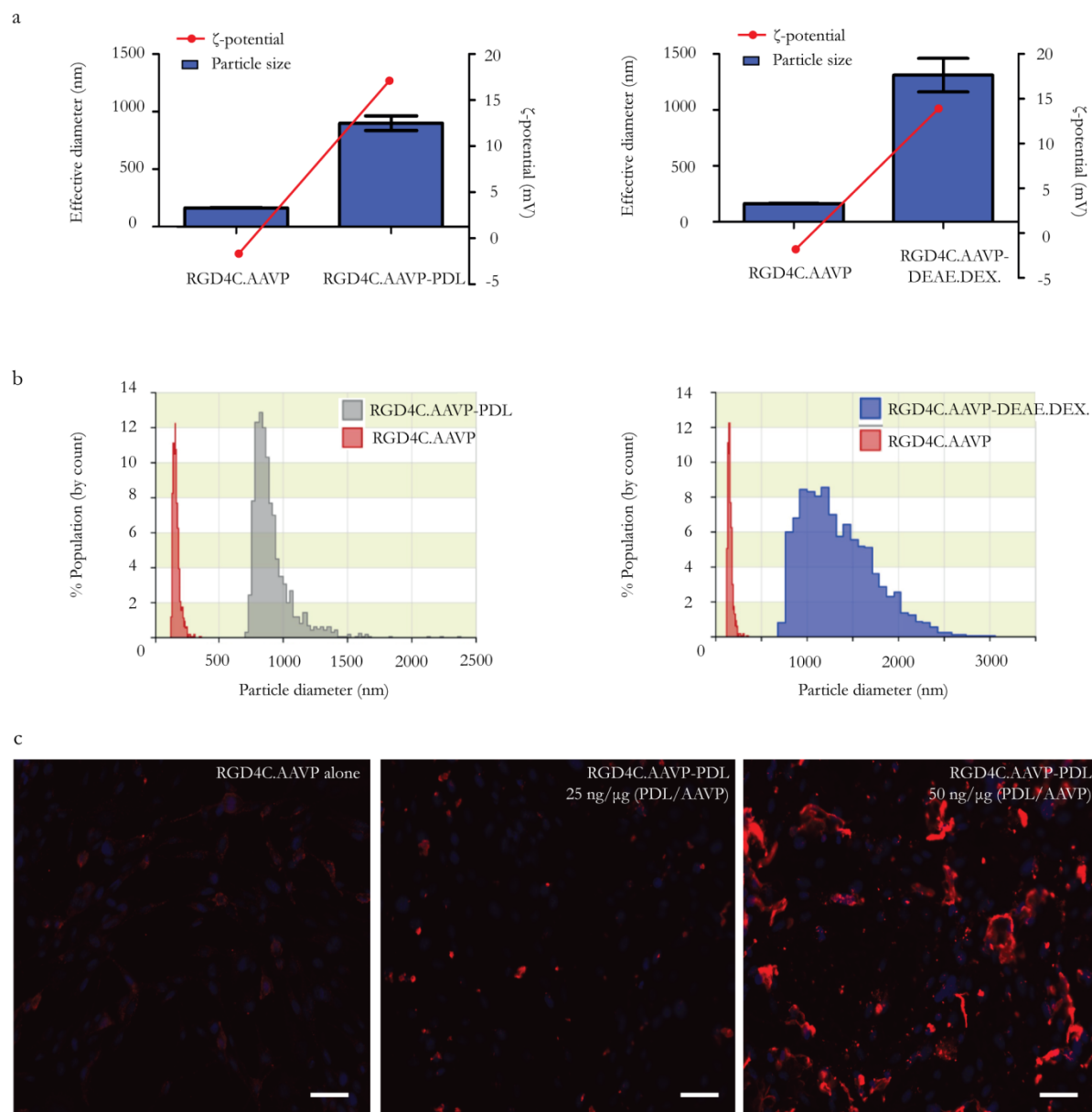
Figure 4.5 Physical characterization of the smart bacteriophage complex. a) Effect of cationic polymer on RGD4C.AAVP particle size and ζ-potential. Average diameter and zeta potential of RGD4C.AAVP vector alone or complexed with PDL (left) or DEAE.DEX (right) at optimal ratio of polymer/AAVP (40 or 60 ng/µg, respectively). All values are reported as mean ± standard error, **b**) Size distribution of RGD4C.AAVP, RGD4C.AAVP-PDL (left) and RGD4C.AAVP-DEAE.DEX (right), **c**) Effect of polymer concentration on size of the smart bacteriophage complex. Immunofluorescence images of cells treated with RGD4C.AAVP alone (left) or RGD4C.AAVP-PDL formed at a PDL/AAVP ratio of 25 ng/µg (middle) and 50 ng/µg (right). Fixation was performed 4 hours post-transduction and immunofluorescence performed using anti-phage primary and goat anti-rabbit AlexaFluor-594 secondary antibodies. Scale bar = 100 µm.

Subsequent experiments were performed to determine whether the complex is dependent on the amount of polymer incorporated into the complex at several polymer/AAVP ratios. Fluorescence images support the size results obtained by a qNano analyser. RGD4C.AAVP alone (**Figure 4.5c**) was noticeably smaller than smart bacteriophage complexes (RGD4C.AAVP-PDL) formed at an PDL/AAVP ratio of 25 ng/µg and 50 ng/µg. Similar results were also obtained for DEAE.DEX (data not shown)

4.2.4. Investigation of smart bacteriophage complex cell accessibility and entry

Next cell membrane-phage vector interactions were characterized by a supernatant-depletion assay. As shown in **Figure 4.6a,** there was a significant depletion of AAVP in the supernatant (up to 94%) when cells were incubated with the smart bacteriophage complex i.e. RGD4C.AAVP-PDL and RGD4C.AAVP-DEAE.DEX. In contrast, cells incubated with RGD4C.AAVP vectors had only 10% depletion, showing that only a small fraction of uncomplexed vectors could reach the cell surface. No depletion was observed with the control NT.AAVP due to it's the lack of targeting ligands. Recovered AAVP vectors from the supernatant were detected and counted as the formation of infected *E.coli* colonies on plates as shown in **Figure 4.6b.** The smart bacteriophage complex yielded much smaller number of colonies than the parental RGD4C.AAVP and the NT. AAVP.
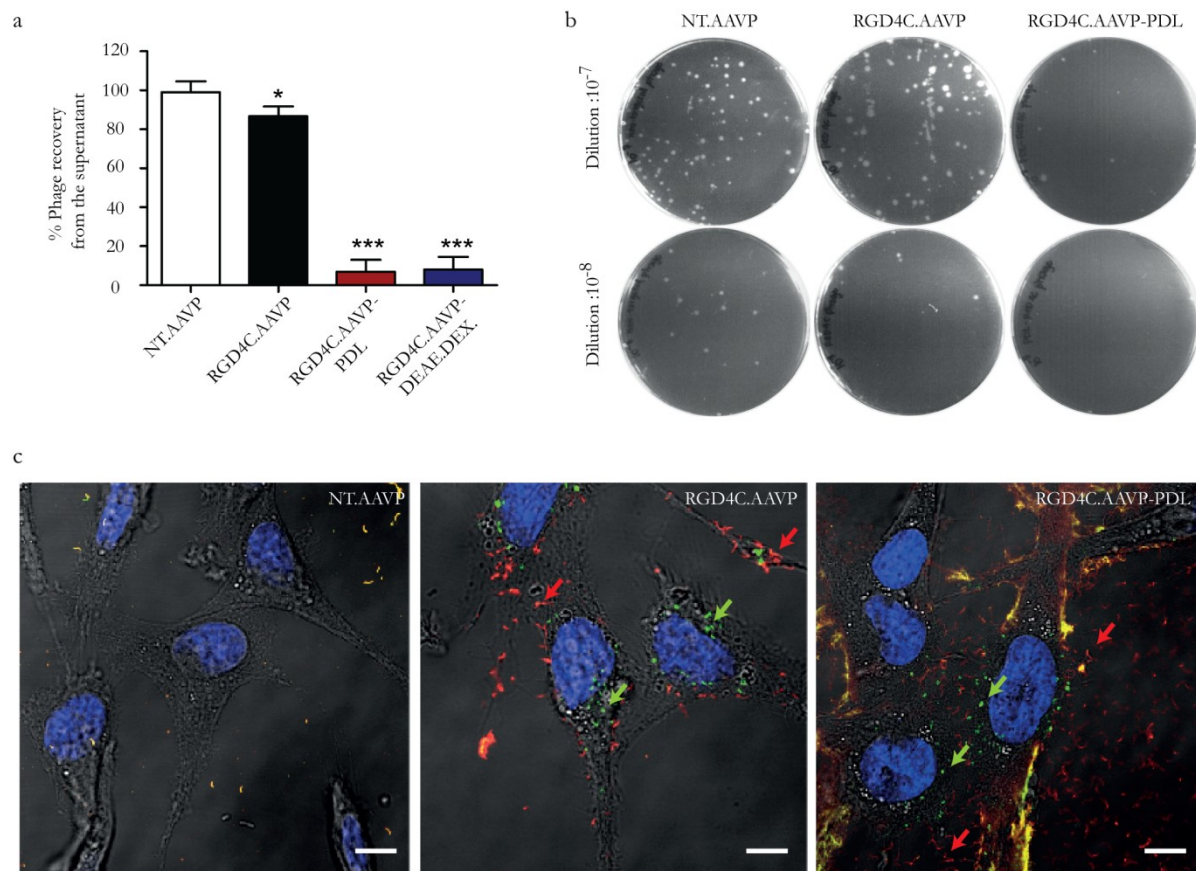
Figure 4.6: Investigation of the smart bacteriophage complex extra/intracellular processing. a) The cell membrane-phage vector interaction was characterized using a supernatant-depletion assay. Unbound AAVP in the medium above an adherent cell layer were quantified by infection of host bacteria followed by colony counting. Data represent the mean + SEM of triplicate samples from one representative experiments of three, significant difference; n.s.-not significant, * $p<0.05$, ** $p<0.01$, ***$p<0.001$ (one way ANOVA with tukey's post hoc test). **b**) Representative images of recovered AAVP vectors detected by the formation of infected *E.coli* colonies on plates. **c**) Confocal fluorescent microscopy of 9L cells after treated with different vectors. Cells were first immunofluorescently stained for extracellular phages using anti-fd phage primary and goat anti-rabbit AlexaFluor-594 (red arrows) secondary antibodies prior to permeablization and staining for intracellular particles using the same primary and goat anti-rabbit AlexaFluor-647 secondary antibodies (green arrows). Scale bar = 10 μm.

Confocal microscopy also revealed that a large number of smart bacteriophage complexes can bind to cell surfaces, whereas a few AAVP particles were observed on cell surfaces incubated with RGD4C.AAVP. There were no phage on cells incubated with the NT.AAVP (**Figure 4.6c**), suggesting AAVP accumulation on the cell membranes, and its subsequent depletion from the supernatant. Altogether, these results suggest that in contrast to the low affinity of RGD4C.AAVP, smart bacteriophage complexes can efficiently bind to cell surfaces. Confocal analysis also revealed that complexes adsorbed on cellular membranes are taken into the cell as single particles, presumably by endocytosis (**Figure 4.6c**).

4.2.5. Formation of a smart bacteriophage complex and its resistance to antibody neutralization

To rule out the possibility that addition of cationic polymers simply reflects neutralization of negative charges on target cell surfaces, we pretreated 9L cells with cationic polymers before addition of RGD4C.AAVP. The resultant transduction efficacies were compared with those obtained from transduction with the preformed smart bacteriophage complex. As shown in **Figure 4.7a**, exposure of cells to cationic polymers before addition of RGD4C.AAVP resulted in significantly lower transduction efficiency compared to transduction with the preformed complex. Improved levels of transduction were achieved when RGD4C.AAVP was complexed directly with cationic polymers, before addition to the culture medium. The requirement for this preincubation step with cationic

polymers led us to speculate that active complex formation or aggregation events has to occur to produce smart bacteriophage complexes.

To assess if the smart bacteriophage complex was protected to any extent from neutralising antibodies, antiserum raised against filamentous bacteriophage was added to the uncomplexed RGD4C.AAVP and the smart bacteriophage complex preparation before transduction. The effect on resultant transduction efficacies were noted. RGD4C.AAVP alone and the smart bacteriophage complex were preincubated with neutralizing anti-fd phage antiserum in a range of concentrations and used to transduce to 9L cells. At the same concentration of anti-phage antiserum, transduction efficiencies of smart bacteriophage complexes were clearly higher than those of the uncomplexed RGD4C.AAVP as shown in **Figure 4.7b**. This result provides evidence that the addition of cationic polymers to the surface of the AAVP renders it less susceptible to antibody neutralization *in vitro*.
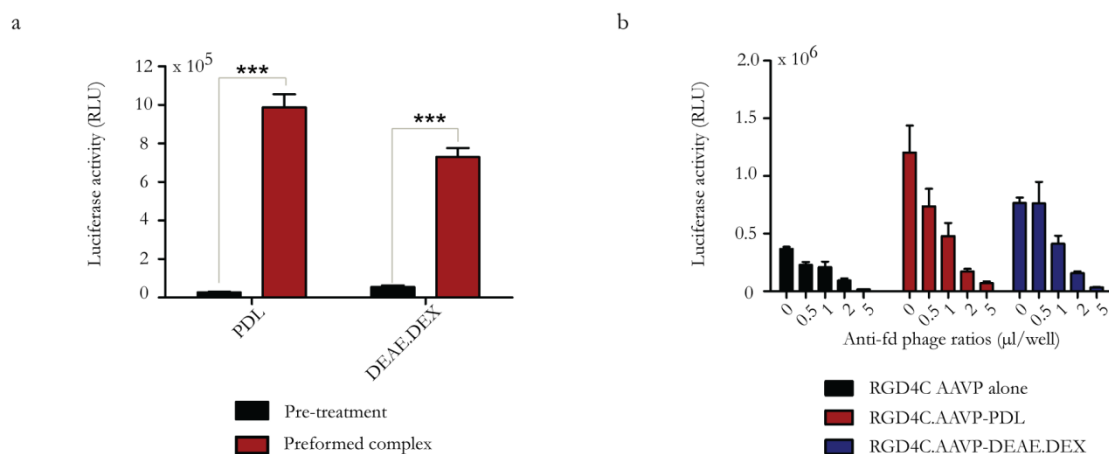
Figure 4.7: Effect of polymer complex formation on AAVP-mediated gene delivery to glioblastoma cells. a) Effect of preincubating target cells with cationic polymers on transduction with RGD4C-AAVP. The vector (25 µg/well) was used to transduce 9L cultures that had received a 30-min pre-exposure with PDL or DEAE.DEX (black column). Transductions with RGD4C.AAVP complexed directly with PDL or DEAE.DEX at optimal ratios before addition to cells were also performed (red column). At day 3 Luc expressions were quantified. **b**) Effect of anti-phage neutralising serum on the enhancement of transduction seen with the smart bacteriophage complex. 9L cells were treated with uncomplexed RGD4C.AAVP or the smart bacteriophage complex in the presence of a range of dilutions. At 72 h cultures were analysed for Luc expression. Serum dilutions are shown below the columns. Data represent the mean + SEM of triplicate samples from one representative experiments of three, significant difference; n.s.-not significant, * $p<0.05$, ** $p<0.01$, ***$p<0.001$ (two way ANOVA with tukey's post hoc test).

4.2.6. The smart bacteriophage complex retains targeting and specificity of gene delivery to glioblastoma cells

We sought to explore the targeting properties of the smart bacteriophage complex to confirm that transduction and cell internalization are specific and mediated by interaction between the RGD4C ligand and α_v integrin receptors. Targeted gene delivery to 9L cells by smart bacteriophage complexes was compared to complexes which had been used as negative controls for targeting and contained either non-targeted NT.AAVP or a mutant version of RGD4C (RGE4C, D---E). As shown in **Figure 4.8a**, cell transduction efficiency by the polymer-complexed RGE4C.AAVP and polymer-complexed non-targeted.AAVP were not significant compared to that of the polymer-complexed RGD4C.AAVP.

Next, we compared the transduction efficacy between the 9L tumour cells and the normal C_2C_{12} myoblast mouse cell line using smart bacteriophage complexes prepared with increasing concentrations of either PDL or DEAE.DEX. The expected patterns of Luciferase gene expression were reproduced in 9L transduced with the smart bacteriophage complex (**Figure 4.8b**). Neither RGD4C.AAVP-PDL nor RGD4C.AAVP-DEAE.DEX could transduce C_2C_{12} cells despite numerous attempts using a wide range of polymer concentrations (**Figure 4.8b**). Finally, we confirmed that inability to transduce C_2C_{12} cells is due to the lack of α_v integrin receptors for the RGD4C ligand. In contrast to 9L cells, the C_2C_{12} myoblast cells lack expression of this integrin (**Figure 4.8c**). Taken together, these

findings confirm that gene delivery by the smart bacteriophage complex is targeted, specific and dependent on α_v integrin receptors.
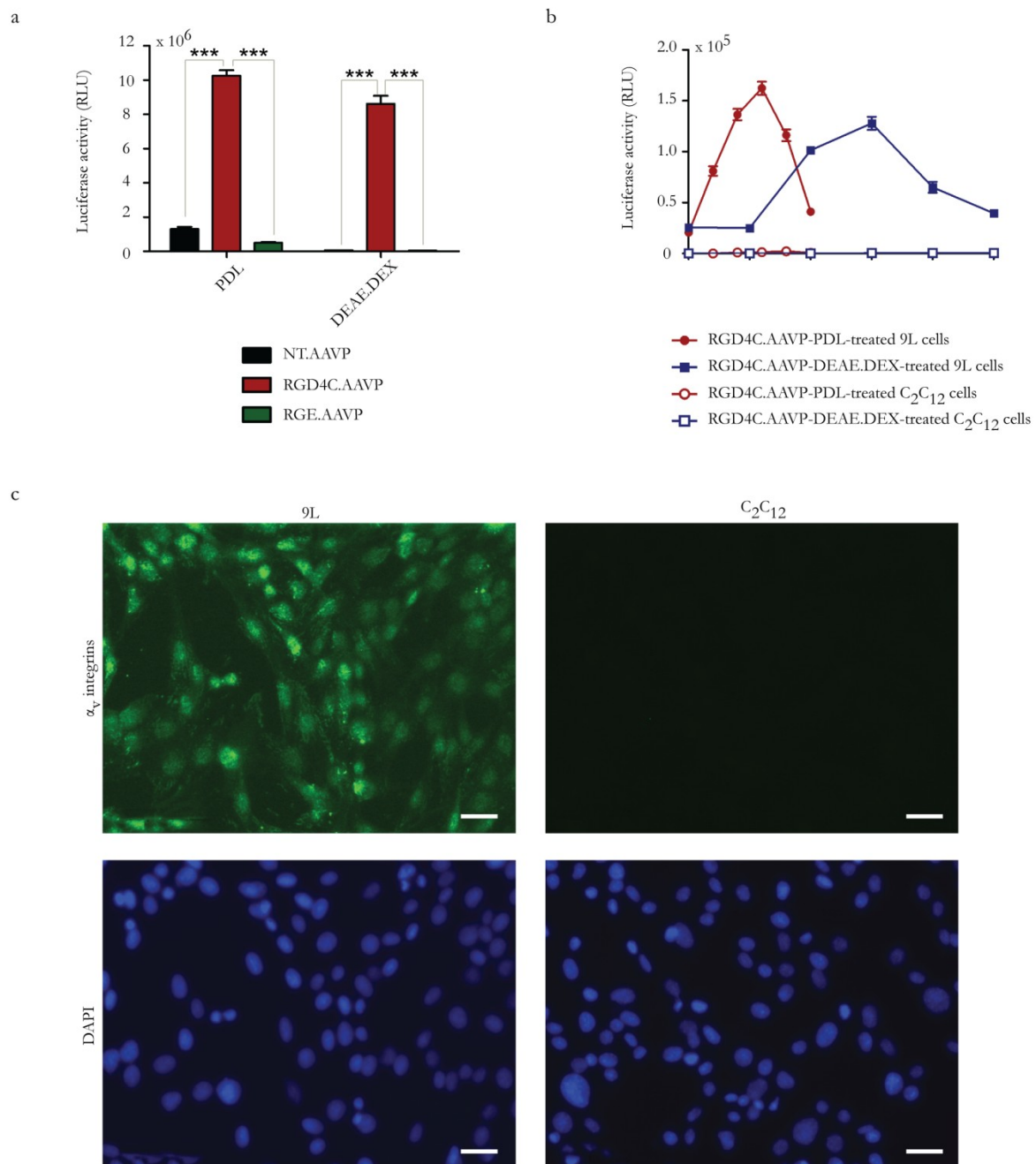
Figure 4.8: Evaluation of the specificity of glioblastoma transduction by smart bacteriophage complexs. a) Comparison of transduction efficacies of complexes containing non-targeted AAVP, mutant RGE4C.AAVP or RGD4C.AAVP in 9L cells. Data represent the mean + SEM of triplicate samples from one representative experiments of three, significant difference; n.s.-not significant, * p<0.05, ** p<0.01, ***p<0.001 (one way ANOVA with tukey's post hoc test). **b**) Assessment of targeted gene transfer by smart bacteriophage complexes in the normal C_2C_{12} myoblast cell line using a range of polymer concentrations **c**) Immunofluorescence staining of α_v integrin receptors in 9L and C_2C_{12} cells with anti-α_v integrin primary and AlexasFluor488 secondary antibodies. Scale bar = 100 μm.

4.2.7. Enhancement of the HSVtk/GCV - mediated cell death by the smart bacteriophage complex

To assess the tumour-killing efficacy of smart bacteriophage complexes, we used an RGD4C.AAVP vector carrying the HSVtk gene. We compared the uncomplexed RGD4C.AAVP vector with the smart bacteriophage complex. HSVtk suicide gene therapy was induced at day 3 post-transduction by treatment with GCV for 5 days. After 3 days post GCV treatment, morphological characteristics of 9L cells were visualized with a bright field microscope. Ethidium homodimer-1 was used to stain dead cells visualized by a fluorescence microscope. Nucleic acids of membrane-compromised cells were labelled with ethidium homodimer-1 yielding red fluorescence. **Figure 4.9a** shows normal morphology of confluent cells with a small number of dead cells in cells treated with non-targeted NT.AAVP in the presence of GCV. There was a dramatic increase in the number of dead cells by the smart bacteriophage complex compared to the uncomplexed RGD4C.AAVP. At day 5, cell viability was determined as shown in **Figure 4.9b**. GCV induced 70% cell death in cells transduced with the uncomplexed RGD4C.AAVP, and completely eradicated cells transduced with the smart bacteriophage complexes. No cell death was observed in NT.AAVP-transduced cells in the presence of GCV or in any treatment in the absence of GCV. These results demonstrate that smart bacteriophage complex has acquired an enhanced anti-tumour effect.
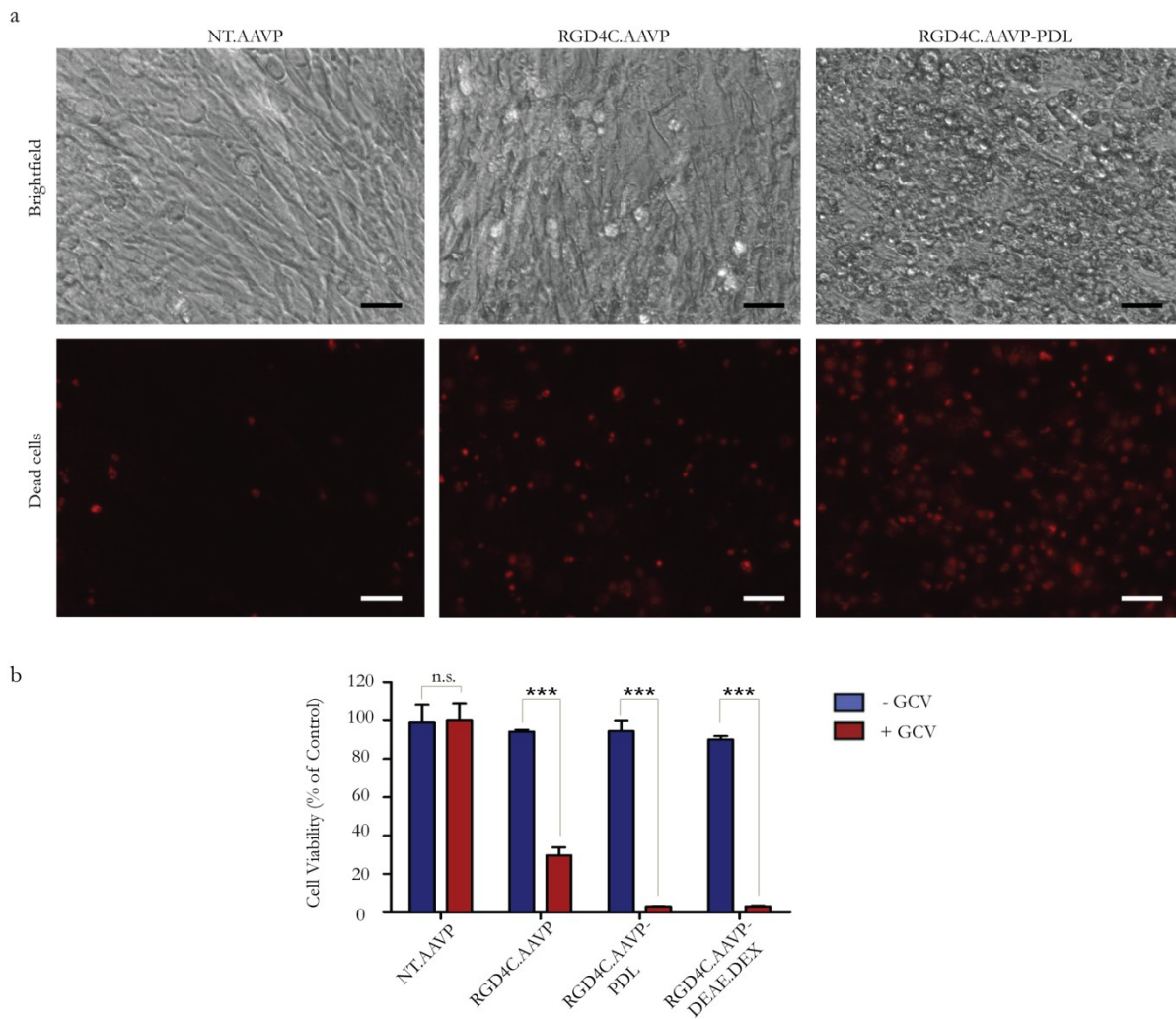
Figure 4.9: HSVtk/ganciclovir (GCV)-mediated cell death by smart bacteriophage complex. a) Following HSVtk/GCV therapy, morphological characteristics of 9L cells were visualized under the microscope. Cells were also stained with the reagents in the LIVE/DEAD® Cell Viability/Cytotoxicity Assay Kit and visualized under the fluorescence microscope. Dead cells fluoresce red-orange. Scale bar = 100 μm. **b**) Evaluation of tumor cell killing by the smart bacteriophage complex, RGD4C.AAVP, and the non-targeted AAVP in 9L cells in the absence or presence of GCV. Cell viability was determined by the CellTiter-Glo® cell viability assay. Mean cell viability was normalised to non-treated controls, with the mean of n=3 independent experiments shown (+ SEM). Statistical analysis was performed using two way ANOVA with tukey's post hoc test, n.s.-not significant, * p<0.05, ** p<0.01, ***p<0.001.

4.2.8. Efficacy of smart bacteriophage complexes in a 3D multicellular glioblastoma tumour spheroids

In vitro tissue spheroids were employed to simulate 3D tumours. 3D spheroids are considered valid models to mimic features of *in vivo* tumour environments including avascular, hypoxic regions, and micrometastases.[240,241] Many tumours are solid and inhibit the ability of therapeutic agents to penetrate central regions.[242,243] The *in vitro* 3D tumour spheroid model was therefore established in this study to imitate the avascular regions and to evaluate and confirm the efficacy of gene transfer by smart bacteriophage complexes. We first assessed transduction efficacies by using AAVP carrying the GFP reporter gene and monitored GFP expression within the spheroids. Spheroids were incubated with the smart bacteriophage complex and compared to uncomplexed RGD4C.AAVP and NT.AAVP. While the original RGD4C.AAVP and non-targeted AAVP showed minimal or no GFP expression, respectively in the spheroids at day 15 post transduction, treatment with smart bacteriophage complexes yielded dramatic increase of GFP expression (**Figure 4.10**). In 9L spheroids (**Figure 4.10a**), PDL polymer was the most efficient polymer, whereas in LN229 spheroids (**Figure 4.10b**), DEAE.DEX showed greater GFP expression. These data also show that the 3D spheroid models can overcome the limitation of cell confluency in 2D monolayers and allow monitoring of gene expression over a longer time period post vector transduction.

Next, application of HSVtk/GCV suicide gene therapy in the 3D model of 9L tumour cells resulted in pronounced regression of the 9L spheroid volumes by smart bacteriophage complexes, upon GCV treatment, compared to the uncomplexed RGD4C.AAVP (**Figure 4.11a**). Subsequently, measurement of cell viability in the spheroids showed that smart bacteriophage complexes achieved higher tumour killing, 98% for RGD4C.AAVP-PDL and 91% RGD4C.AAVP-DEAE.DEX, than the uncomplexed RGD4C.AAVP that induced 67% cancer cell killing (**Figure 4.11b, c**). These findings clearly confirm that gene delivery efficacies of smart bacteriophage complexes are superior to the established RGD4C.AAVP.
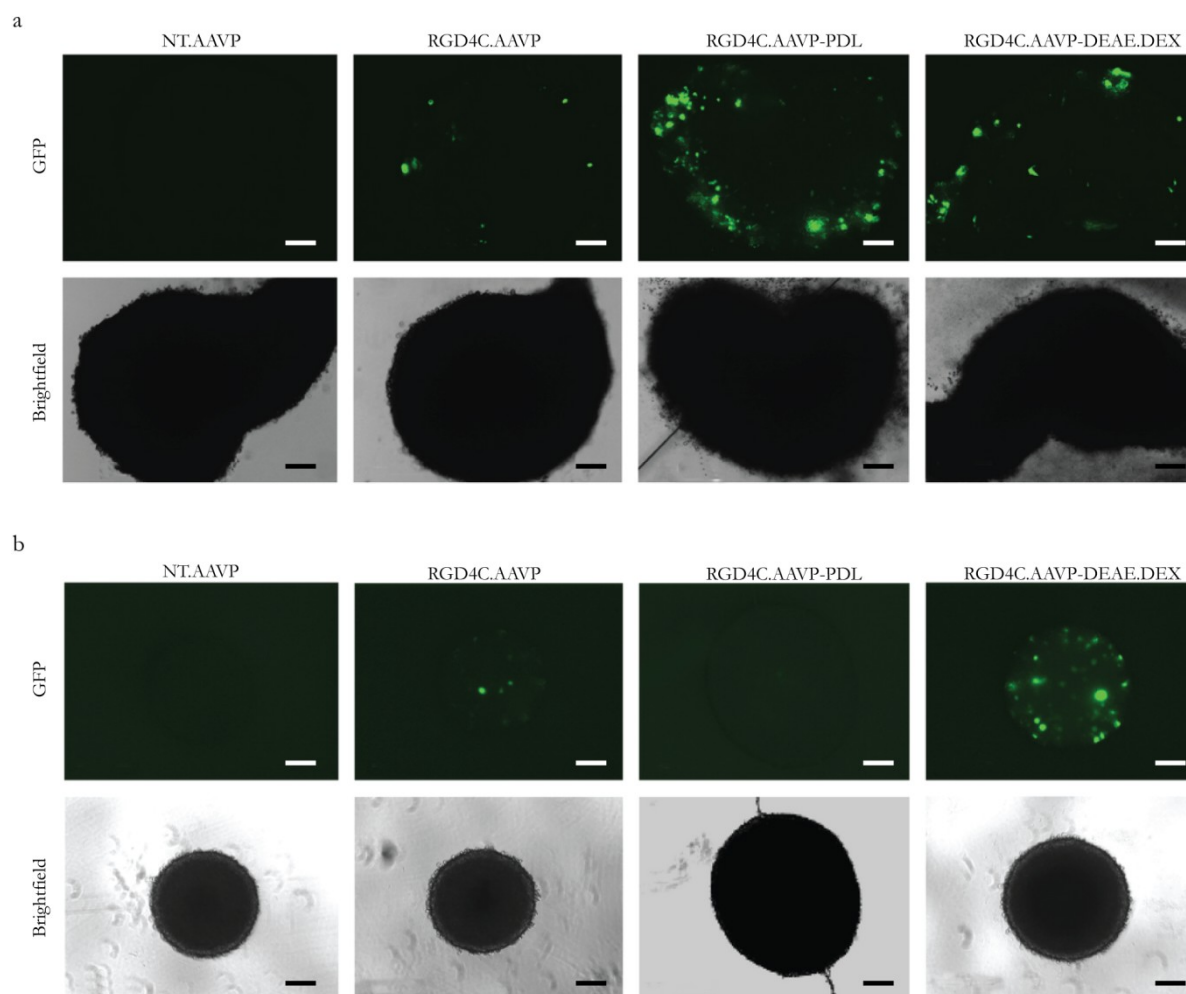
Figure 4.10: Transduction of 3D tumour spheroids by the smart bacteriophage complex.
The spheroids were treated with smart bacteriophage complexes (i.e. RGD4C.AAVP-PDL and
RGD4C.AAVP-DEAE.DEX) or uncomplexed RGD4C.AAVP and control non-targeted AAVP
carrying the *GFP* reporter gene. Representative images showing GFP expression in the spheroids
were taken at day 15 post transduction. **a**) 9L **b**) LN229 cells-derived spheroids. Scale bar = 0.5
mm.
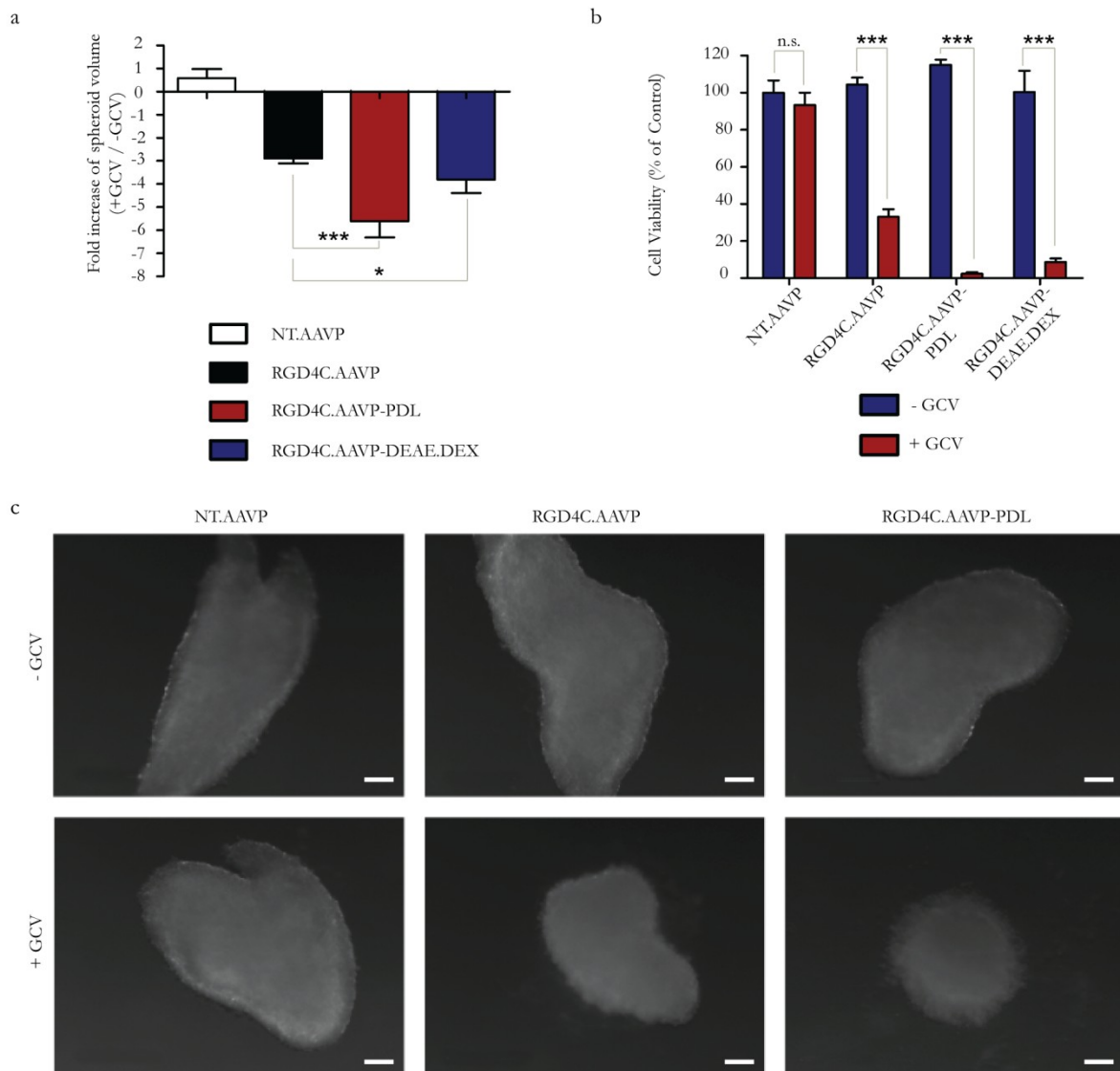
Figure 4.11: Therapeutic efficacy of the smart bacteriophage complex in 9L tumour spheroid models. a) Measurement of the spheroid volumes following transduction with non-targeted AAVP, RGD4C.AAVP or the smart bacteriophage complex carrying the HSVtk gene. GCV was added daily and images were taken at day 5 following addition of GCV. **b**) Evaluation of cell viability in the spheroids at day 7 post GCV treatment, by using the CellTiter-Glo® cell viability assay. Data represent the mean + SEM of triplicate samples from one representative experiments of three, significant difference; n.s.-not significant, * $p<0.05$, ** $p<0.01$, ***$p<0.001$ (one way or two way ANOVA with tukey's post hoc test).**c**) Phase contrast images showing the size of the spheroids. Scale bar = 0.5 mm.

4.3. Discussion

Advances in gene transfer technologies have had major impacts within the field of cancer gene therapy. In 2006, Hajitou *et al.* developed a hybrid prokaryotic-eukaryotic vector, which is a combination between the filamentous bacteriophage and AAV designated as AAVP.[244] Incorporation of ITRs from AAV in the single stranded genome of bacteriophage is associated with improved fate of delivered transgenes i.e. the conversion of single stranded DNA to double stranded DNA, better persistence of episomes and concatamers, resulting in subsequent enhanced gene delivery efficacy over conventional phage-based vectors.[244] The RGD4C.AAVP vector was originally developed for anti-cancer gene therapy. It has been assessed and showed promising results in a range of animal models of cancer, including mice, rat, and pet dogs with natural tumours.[245] Despite promising results in these studies, the transduction efficacy of RGD4C.AAVP vector is still poor. Indeed such genetic improvement is actually one last step of a series of steps involved in gene delivery processes. Therefore, the attachment, entry, and intracellular trafficking of the vector remain barriers that AAVP vector has to overcome.

In the previous chapter, we demonstrated that the low affinity between AAVP vectors and cell surfaces is a limitation of cell accessibility. Stoneham *et al.* previously identified the endosomal-lysosomal pathway as another barrier to efficient gene delivery and demonstrated that disturbing this partway is a promising strategy for improving gene transfer by AAVP.[246] In order to obtain the ideal gene

delivery vector system capable of overcoming these barriers, we combined the attributes of different types of vectors and therefore introduced the novel hybrid multi-component vector designated as the smart bacteriophage complex. Specifically, we combined the advantages of three gene delivery vectors: the filamentous M13 bacteriophage, the genome of a recombinant AAV and cationic polymers. In this novel gene delivery platform, i) the phage particle serves as a vehicle displaying targeting peptides on its capsid to maintain vector specificity, ii) the rAAV cassette allows amplification and long-term expression of the transgene, and iii) cationic polymers create positively charged AAVP particles resulting in enhanced attachment to negatively charged eukaryotic cell surfaces. Additionally we yielded evidence that endosomal escape of smart bacteriophage complexes occur via a proton sponge mechanism.

The limitations of chemotherapy in systemic glioblastoma treatment, referred to as chemoresistance, may be partially due to the presence of BBB that acts as a physical and biochemical barrier. Thus, it hinders the transport of conventional systemic drugs into the CNS.[247] One of the most widely used chemotherapeutic drugs to treat glioblastoma is TMZ. Although TMZ in combination with radiotherapy and surgery improves the overall survival in patients with glioblastoma, the prognosis of patients remains poor, with a median survival of about one year after diagnosis.[248] In addition, the presence of subpopulations of tumour cells with stem cell-like properties is another factor underlying glioblastoma chemoresistance.[249] Glioblastoma is therefore considered to be fatal

and incurable by conventional therapies[250], and has attracted considerable attention as a target for gene therapy.[251] We sought to use this novel vector system for glioblastoma gene therapy.

In contrast to cancers in other parts of the body, glioblastoma is an attractive target for local gene therapy because of its restricted anatomical location and absence of metastases outside the CNS. This allows delivery of vectors directly to the desired site with only a small risk of systemic toxicity.[233] Although these methods have yielded promising results in preclinical studies and satisfied safety profiles in phase I/II clinical trials[252], only a handful are currently being investigated in phase III clinical trials[231]. One of many barriers limiting the use of gene therapy in clinical trials includes unique anatomical barriers of the CNS that limit the spatial distribution of the therapeutic payload. Despite direct delivery, the gene transfer efficacy to glioblastoma with currently available gene delivery vectors remains poor, partly due to the low expression of cognate receptors for viral vectors that enable the efficient internalization. For example, the poor expression of the CAR receptor on primary glioblastoma limits Adenovirus5-based gene therapy.[253] Previous investigations found that αvβ3 and αvβ5 are expressed on glioma cells and vasculature.[254] The RGD motif is an essential binding motif for αv integrin receptors[255], thus making it a promising ligand for glioblastoma targeting.[256] We previously reported the therapeutic feasibility of α_v integrin-mediated glioblastoma treatment, as well as the potential of using RGD4C.AAVP as a targeted gene carrier in the treatment of glioblastoma.[237] In the present work, we designed smart

bacteriophage vectors by complexing RGD4C.AAVP with cationic polymers. This complex had high binding affinities with glioblastoma cell lines tested, facilitating highly efficacious targeted gene delivery against glioblastoma compared to the previously reported RGD4C.AAVP vector.

We examined gene delivery efficacy of smart bacteriophage complexes and used four glioblastoma cell lines to demonstrate that our findings are not specific to a particular cell line. Our results clearly indicate that the transduction efficacy of smart bacteriophage complexes were significantly higher than the uncomplexed RGD4C.AAVP vector. However, different polymers have different efficacies despite producing similar trends. For example, a higher transduction efficiency of a particular polymer in a cell line was found to be lower in a different cell line. We also noticed that DEAE.DEX retained higher specificity than PDL. It is important that optimization is required in order to maximize the therapeutic efficacy. Furthermore, we have demonstrated the efficacy of smart bacteriophage complexes in a novel *in vitro* environment that mimics *in vivo* tumour microenvironments. The 3D spheroids have gained increased attention in cancer research as an *in vitro* model to reduce the need for *in vivo* studies. Several methods have been used to produce multicellular spheroids, for example hanging drop, liquid overlay on agar, and rotary culture system.[257] Our studies, we used a 96-well ULA plate to generate single spheroids of similar size with high reproducibility across different experiments.[236] We have shown that the smart bacteriophage complex is able to transduce glioblastoma spheroids with higher efficacy than the

conventional RGD4C.AAVP. The transduction efficacy of RGD4C.AAVP vector is markedly reduced when transgene expression of 3D spheroids were compared to 2D monolayers. Tumour spheroids more closely resemble *in vivo* tumour microenvironments in terms of gene expression profiles, cell-cell interactions, concentration gradients, hypoxic regions, and extracellular matrix deposition.[236,240,258,259] A possible factor that may contribute to lower activity is that penetration into the solid structure of spheroids was a limitation to RGD4C.AAVP particles. Previous studies have highlighted major differences and outcomes of using 2D and 3D culture models, showing that 3D cultures are more resistant to drug treatments compared to conventional 2D cultures. This reflects the importance of drug screening and testing in clinically relevant *in vitro* models.[235]

The presence of a BBB would potentially limit the delivery of the smart bacteriophage complex as well as other macromolecules. In future investigations, the use of CED is suggested to be a delivery method of choice for evaluating the *in vivo* efficacy of smart bacteriophage complexes to treat glioblastoma. Previous investigations of CED have demonstrated that a wide range of therapeutic substances can be delivered and distribution to the target site. This includes conventional chemotherapeutic drugs[260-262], monoclonal antibodies[263,264], targeted toxins[265-267], proteins[268], viruses[269,270], nanocarriers[271-274], and filamentous bacteriophage.[230] However, injection protocols can be technically demanding, requiring high precision and accuracy to deliver the therapeutic compounds[231] Moreover, local administration by direct injection of vector to a diseased site can

sometimes lead to undesired, distribution to other tissues.[34] The accuracy and targeting capacity of the therapeutic payloads themselves or their delivery protocols can be significantly improved. In this study, we confirmed that transduction of glioblastoma cells by the smart bacteriophage complexes remains specific and occurs through binding of the RGD4C ligand to the α_v integrin receptors overexpressed on glioblastoma cells. In addition, localized delivery of smart bacteriophage complexes to glioblastoma cells can maintain elevated AAVP concentrations in the tumour environment through efficient binding to cells. As a result, unwanted distribution to distant tissues can be avoided.

Gene therapy for glioblastoma treatment using different gene transfer vectors combined with different strategies has been investigated as an alternative approach to conventional chemotherapy. Retroviral and adenoviral vectors have been most popular for the delivery of therapeutic genes into glioblastoma.[223] However, alternative vehicles such as stem cells, nanoparticles and liposome, have also been extensively developed, with some having reached clinical testing stages.[251] Several strategies include pro-drug activation/suicide gene therapy, anti-angiogenic gene therapy, correction of gene defects, induction of apoptosis, inhibition of tumour invasion, oncolytic virotherapy, antisense and RNAi-based approaches and gene therapy to enhance chemo- and radiotherapy.[251]

The enzyme-prodrug suicide gene therapy system is the most commonly used approach against glioblastoma in preclinical studies as well as in clinical trials.[231] In this respect, the cytotoxic suicide gene 'HSVtk' is the most extensively investigated

suicide gene therapy system against glioblastoma.[231] As proof of concept, application of the smart bacteriophage vector carrying HSVtk resulted in eradication of glioblastoma upon ganciclovir treatment, which was significantly more efficacious than the established RGD4C.AAVP vector system. HSVtk converts the inactive prodrug GCV into a toxic GCV-triphosphate that is subsequently incorporated into the DNA of actively proliferating cells, blocking DNA replication.[232] One advantage of this system is the induction of a 'bystander effect', which can be observed when there is a transfer of toxic metabolic products of GCV from the originally transduced cells to non-transduced tumour cells at nearby sites through intercellular gap junctions.[275] We also observed this phenomenon, despite a small fraction of transduced cells expressing GFP, complete tumour eradication occurred when tumour cells were transduced with the smart bacteriophage complex carrying HSVtk in combination with GCV treatment, indicating the potency of the bystander effect. The spread of cytotoxicity has been shown to be dependent on connexin-mediated intercellular communication.[276-278] Phagocytosis of dead tumour cell-derived apoptotic vesicles by live tumour cells cause them to undergo apoptosis as well.[279] In addition, the immune system also contributed to the bystander effect, resulting in significant tumour regression *in vivo*.[280-283] It has been shown that significant therapeutic efficacies have been observed in a xenograft glioma model when approximately 10% of tumour cells are transduced with HSVtk.[284,285]

Another major hurdle for successful clinical gene therapy for glioblastoma is the immune response elicited by viral vectors.[231] Host immune responses have been implicated as a major problem in clinical trials.[286,287] A number of extensively used viral vectors are based on mammalian viruses and natural exposure of mammals to parental viruses has led to pre-existing immunity against the recombinant vectors. A number of strategies currently under investigation to protect the vector from neutralizing antibodies and to potentially mitigate immune responses against the vector to allow repeated administration. A promising strategy for overcoming this hurdle is to use polymers to shield viral vectors from components of the host immune system, potentially reducing inflammatory and immune responses.[34] For example, Adenoviral vectors were chemically modified with polymers to reduce immune response. Polymer-modified Ad vectors can evade pre-existing anti-Ad antibodies, allow for repeated administration of vector.[288] Although no severe immune responses or any safety concerns have been reported when bacteriophages were administered to human for treatment of bacterial infection[17,289,290], there is the evidence for the immunogenicity of bacteriophage in animal studies. Induction of anti-phage antibody response was observed in mice after single administration of filamentous bacteriophage.[291-293] Three mouse monoclonal antibodies recognize epitopes of major coat protein pVIII of filamentous phage.[294] A polyclonal rabbit antiserum was also shown to bind to the N-terminal region of the pVIII coat protein.[295] In this study, the smart bacteriophage complex proved to be more resistant to the neutralizing antibody compared to the naked RGD4C.AAVP. This

suggests that polymer-mediated modification of the AAVP surface potentially addresses the immunogenicity problem by masking AAVP particles from immune components.

4.4. Conclusion

The novel hybrid multi-component vector termed the smart bacteriophage was generated by complexing cationic polymers with the AAVP vector displaying the RGD4C ligand and carrying an AAV ITR-flanked mammalian DNA cassette. We tested if the smart bacteriophage complex was applicable to glioblastoma gene therapy. A study of the expression of reporter genes, as well as the assessment of therapeutic efficacy using the HSVtk/GCV system clearly indicated that the smart bacteriophage complexes were superior to the established RGD4C.AAVP vector. The original RGD4C.AAVP vector was developed for cancer gene therapy and has shown promising results as assessed in a number of animal models of cancer including mice, rats and pet dogs with natural tumours. Another important attribute of the smart bacteriophage complex is its ability to resist neutralization by antibodies, which potentially should allow it to achieve efficacy with repeated vector administrations. We conclude that the innovative combination of different types of vectors into a single particle provides significant extension to the development of novel gene delivery platforms, which can be used as tool for glioblastoma gene therapy.

5. Controlled Extracellular Matrix Degradation in Cancer Improves the effectiveness of gene delivery by AAVP

5.1. Introduction

Fundamental differences existing between malignant and normal cells have encouraged the specific design of gene delivery vectors capable of efficiently targeting cancer cells to improve gene delivery efficiency.[186] The higher than normal expressions of tumour-specific markers on cancer cell membranes can be used as docking sites to concentrate therapeutic agents at tumours. Engineering bacteriophage to actively target specific receptors has improved specificity, yet it remains a challenge to increase the efficacy.[24] The RGD4C-displaying hybrid vector AAVP targeted to α_v integrins, which are overexpressed in cancer cells and cancer-associated endothelial cells, have been successfully used for delivering therapeutic/imaging genes selectively to tumours.[171-174]

An important factor to consider in cell targeting is the accessibility of the receptors that are targeted by the probe.[186] In fact, the extracellular obstacles make up the first-line bottle neck which the vector has to confront before reaching its receptor. Extracellular matrix (ECM), composed of fibrous proteins (collagen, elastin, fibronectin and laminin) and glycosaminoglycans (GAGs) such as hyaluronan, is secreted locally and assembled into a network in close association with the membrane of the cell that produced them. A complex network structure of ECM, represents a major barrier for the delivery of therapeutic agents.[296] We hypothesized that ECM molecules occupy the binding sites of the AAVPs and

create another barrier for gene delivery. We therefore propose to enhance accessibility of receptors through ECM clearance by using enzymes to degrade the hindering molecules.

In addition, unique structural properties of solid tumours compared with healthy tissues restrict transport and distribution of therapeutic compound throughout malignant tissues. Following the tumour accumulation of the therapeutic agents facilitated by the well-known enhanced permeability and retention (EPR) effect found in the abnormal tumour vasculature[297], the ability to subsequently diffuse into the individual cancer cells remains a significant challenge. In solid tumours, there is a huge increase in ECM components which creates fibrosis and often encapsulates the tumour in a shell of structural fibres consisting of a structural collagen network embedded in a gel of glycosaminoglycans.[296] The ECM composition, structure, and distribution play a crucial role in the transport properties in tumours.[298] We hypothesized that in addition to physical masking of receptors, ECM in solid tumours affects the effectiveness of AAVP-mediated gene delivery through blocking diffusion of AAVP vectors to malignant cells.

5.2. Results

5.2.1. Optimizing collagenase and hyaluronidase concentrations

We first compared the effect of collagenase and hyaluronidase on the transduction efficiency of AAVP. To rule out the possibility that these effects might be cell line or species specific, we conducted experiments on the 9L rat glioma, the human M21melanoma and the human MCF-7 breast adenocarcinoma cell lines. Transduction efficiencies as a function of collagenase or hyaluronidase concentration (**Figure 5.1a and 5.1b**, respectively) were studied by using AAVP vectors carrying the Luc reporter gene. Luciferase activity was quantified after 72 hours by using a luciferase assay kit. Results showed that pretreatment of 9L cells with 0.2 mg/ml of collagenase and 0.4 mg/ml of hyaluronidase greatly increased luciferase transgene expression, with maximal 3- and 2-fold increases, respectively (**Figure 5.1a, b**). Collagenase also increased the luciferase gene expression in M21 and MCF-7, with maximal increase (2.2- and 7.4-fold, respectively) at 0.3 mg/ml, whereas hyaluronidase had no effect (**Figure 5.1a, b**). It is also important to note that ECM depletion did not affect the cell specificity of RGD4C.AAVP as the non-targeted NT.AAVP remained unable to transduce cells despite a range of enzyme concentrations used.
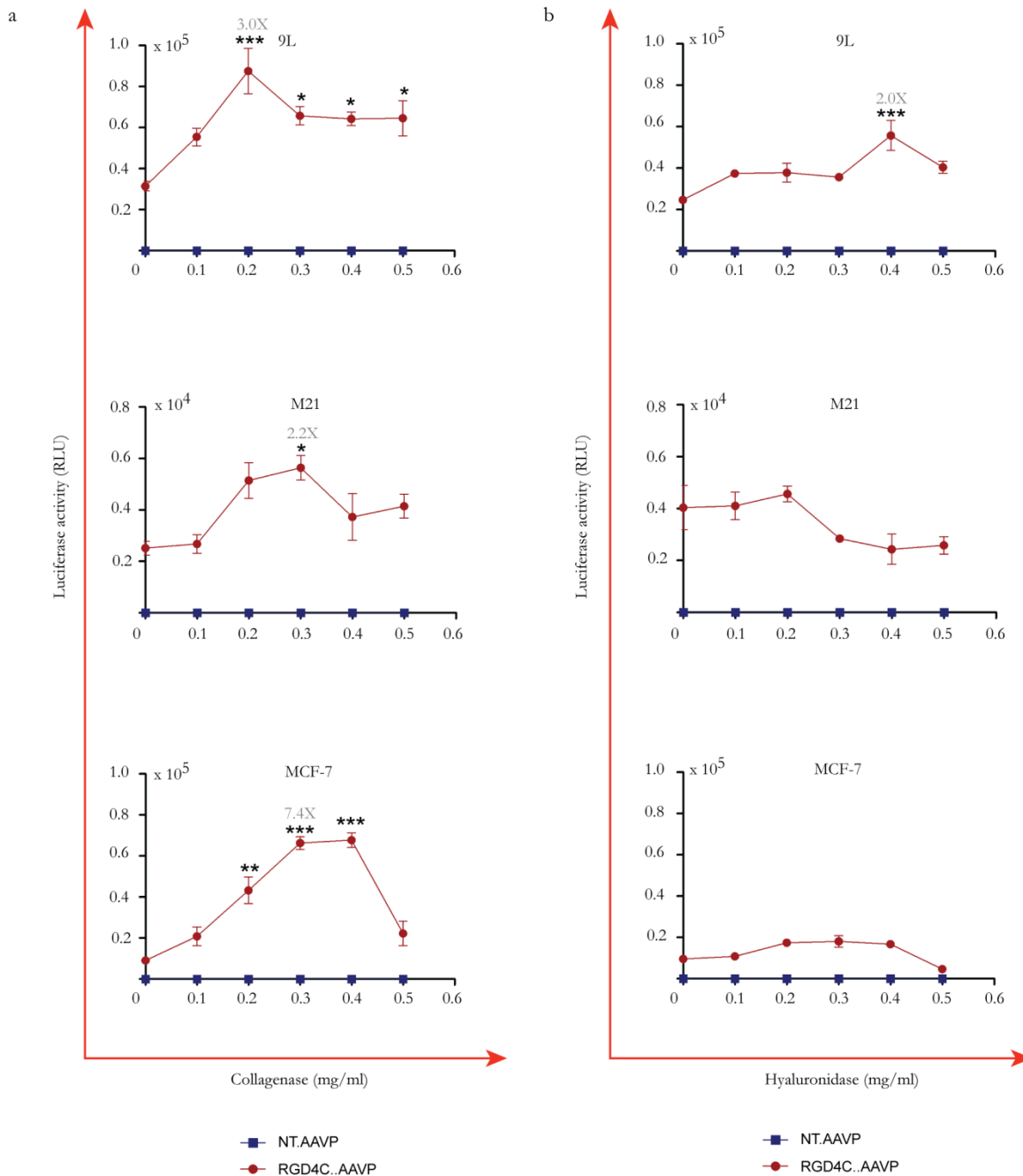
Figure 5.1: Characterization of ECM depletion effects in 9L, M21, and MCF-7 cell lines. Cells were pretreated with a range of **a**) collagenase and **b**) hyaluronidase concentrations for 1 hr followed by AAVP transduction in order to determine the maximal level of transgene expression. Luciferase activity was quantified by Steady-Glo® luciferase assay kit at 72 hr post transduction. The results show the mean relative luminescence units of triplicate wells ±SEM, from one representative of three independent experiments. Statistical analysis was performed using two way ANOVA with tukey's post hoc test, n.s.-not significant, * $p<0.05$, ** $p<0.01$, ***$p<0.001$.

5.2.2. Effect of collagenase treatment on collagen content

The above results indicate that degradation of the structural collagen network is more important than degradation of hyaluronan in order to improve the gene delivery by AAVP. Consequently, we set out to measure the collagen content in cells before and after enzymatic treatment with collagenase. A Sirius Red assay was carried out to measure the levels of collagen type I remaining on the cells before and after enzyme treatment as well as the levels of collagen I released into the media resulting from collagenase treatment. We found that the cellular collagen of 9L, M21, and MCF-7 was significantly reduced by 50-80% after application of collagenase, and subsequently released into the cell media (**Figure 5.2a-c**). These findings thus confirm that enzymatic depletion of ECM can be used to modulate the cellular microenvironment.
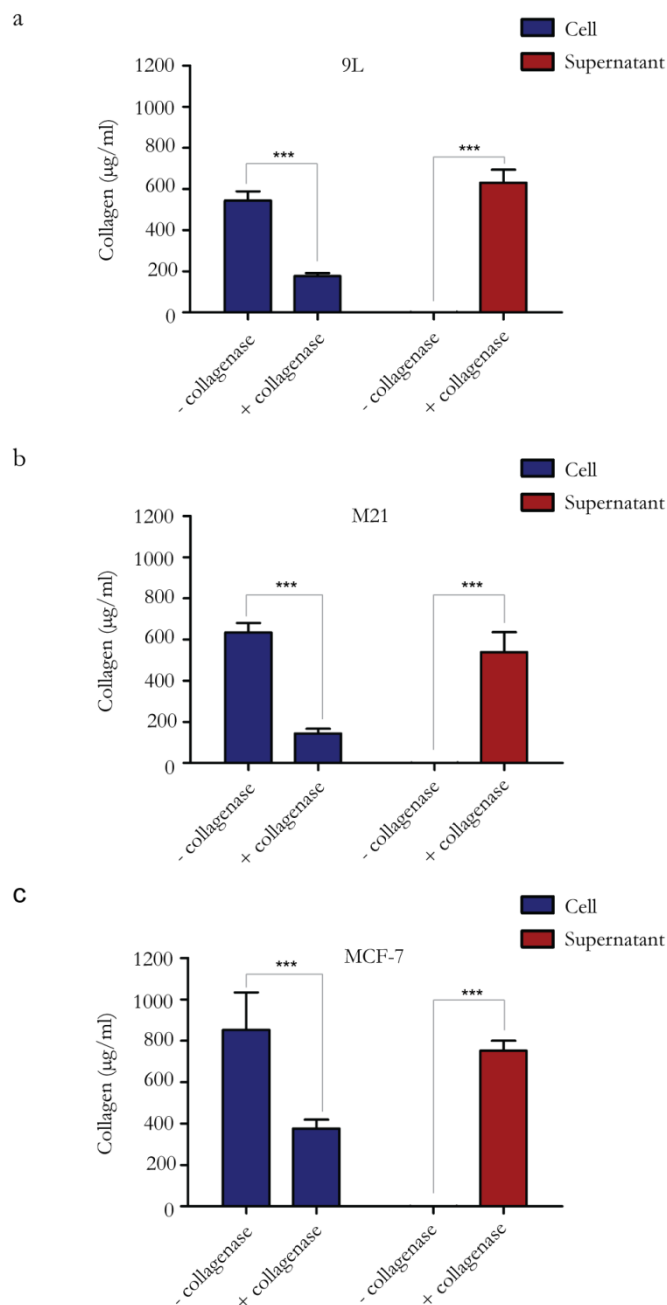
Figure 5.2: Collagen depletion assay in cancer cells using Sirius Red dye as a detector. Cells were incubated with 0.2 mg/ml collagenase for 1 hour and controls had no intervention .Collagen levels remaining on the cells or released into the supernatant fraction were quantified. Each condition was measured in triplicate and statistics were obtained by unpaired student t-test, ***, p<0.001. Data were presented as mean ± SEM. **a**) 9L **b**) M21 and **c**) MCF-7 cells.

5.2.3. Enzymatic degradation of ECM significantly increases AAVP transduction efficiency and demonstrates transgene expression in a time dependent manner

Having proven that ECM degradation is effective across multiple species and cell lines, we carried out further experiments focusing on the 9L glioblastoma model as both collagenase and hyaluronidase were effective to enhance the transduction rate. We next determined if a combination application of both enzymes would result in an even higher transduction efficiency compared to that of each enzyme alone. Using either collagenase or hyaluronidase alone resulted in luciferase expression levels of ~2.7- and 2.6-fold increase higher than without any enzymatic treatment, respectively (**Figure 5.3a**). Interestingly, combination treatment with both enzymes gave a further significant increase of up to 5-fold of RGD4C.AAVP when compared to transduction in the absence of ECM depletion (**Figure 5.3a**).

Next we monitored gene expression daily over the course of 5 days post transduction by sequential luciferase assays in order to determine whether such improvements in gene delivery by AAVP upon ECM depletion occur over time (**Figure 5.3b**). Although luciferase expression in all groups continued increasing over time, there was a significant difference in transgene expression between the control RGD4C.AAVP alone and the combination enzyme treatment (**Figure 5.3b**). These results demonstrate that ECM depletion can result in a long-lasting enhanced gene expression from RGD4C.AAVP vector.

As shown in **Figure 5.3c**, fluorescence microscopic analysis of transgene expression 72 hours post transduction using RGD4C.AAVP vector carrying the GFP reporter gene supported the results obtained from the luciferase assay. Comparing collagenase or hyaluronidase alone caused a gain in GFP expression that was higher than transduction without any enzyme treatment and the combination treatment with both enzymes further enhanced transgene expression (**Figure 5.3b**).

Taken together, these results confirm that depletion of the ECM through enzymatic degradation by collagenase or hyaluronidase enhances transgene expression from RGD4C.AAVP and combination treatment with both enzymes further increases AAVP gene delivery efficacy.
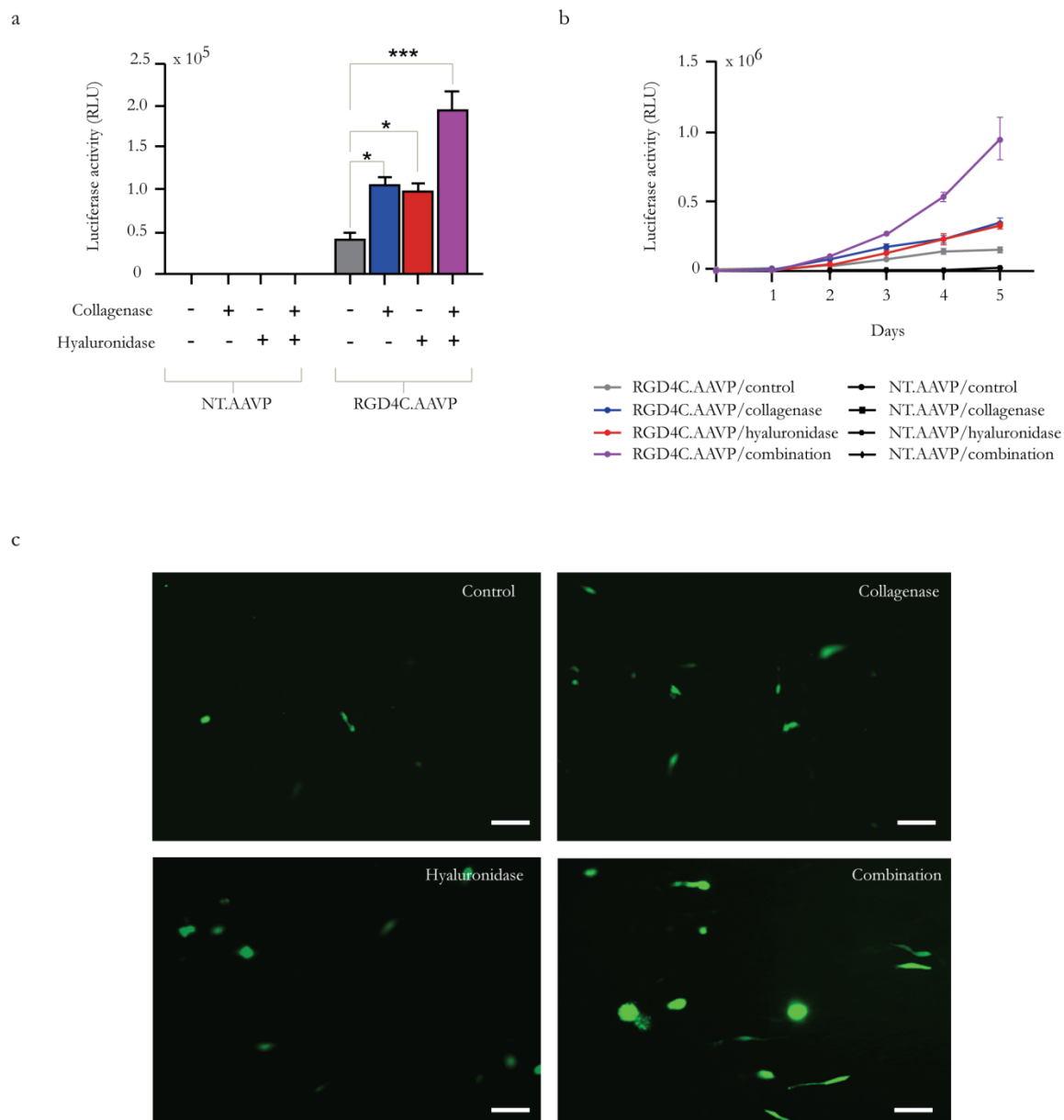
Figure 5.3: ECM depletion enhances targeted RGD4C.AAVP transduction efficacy. a) luciferase gene expression at day 3 post transduction in 9L cells after treatment with different enzymes in combination with non-targeted (NT.AAVP) or targeted AAVP (RGD4C.AAVP). The results show the mean relative luminescence units of triplicate wells +SEM, from one representative of three independent experiments, significant difference; n.s.-not significant, * p<0.05, ** p<0.01, ***p<0.001 (one way ANOVA with tukey's post hoc test). **b**) Time course luciferase gene expression over 5 days with targeted RGD4C.AAVP alone or following treatment with collagenase alone (0.2 mg/ml), with hyaluronidase alone (0.4 mg/ml) or with combination of both collagenase and hyaluronidase. Similar enzymatic treatments were included with the control non-targeted AAVP (NT.AAVP) vector. The results show the mean relative luminescence units of triplicate wells ±SEM, from one representative of three independent experiments **c**) GFP expression in 9L cells under different enzymatic regimes. Images were visualized by fluorescence microscopy 3 days post vector transduction. (0.2 mg/ml collagenase and/or 0.4 mg/ml hyaluronidase). Scale bar = 100 μm.

5.2.4. Removal of ECM promotes AAVP internalization into cells

To demonstrate the feasibility of our hypothesis that ECM molecules occupy the binding sites of the RGD4C.AAVP vectors and therefore ECM clearance could enhance accessibility of the receptors, leading to increased binding and subsequent cell uptake, we set out to determine whether there was increased cell internalization after pretreatment of 9L cell cultures with collagenase and hyaluronidase. An AAVP internalization assay was carried out by which the AAVP cellular load was determined by intracellular phage immunochemistry followed by flow cytometry quantification of the signal. The results showed that there was a considerable increase in AAVP internalization following ECM depletion over treatment with RGD4C.AAVP alone in the absence of enzyme treatment. Removal of collagen and hyaluronan allowed up to 37% increase in AAVP endocytosis (**Figure 5.4a**), manifesting as higher intracellular AAVP signal as well as enhanced AAVP signal counts/10,000 cells (**Figure 5.4b**). These results therefore cement proof of ECM as a physical barrier to efficient RGD4C.AAVP entry into mammalian cells.
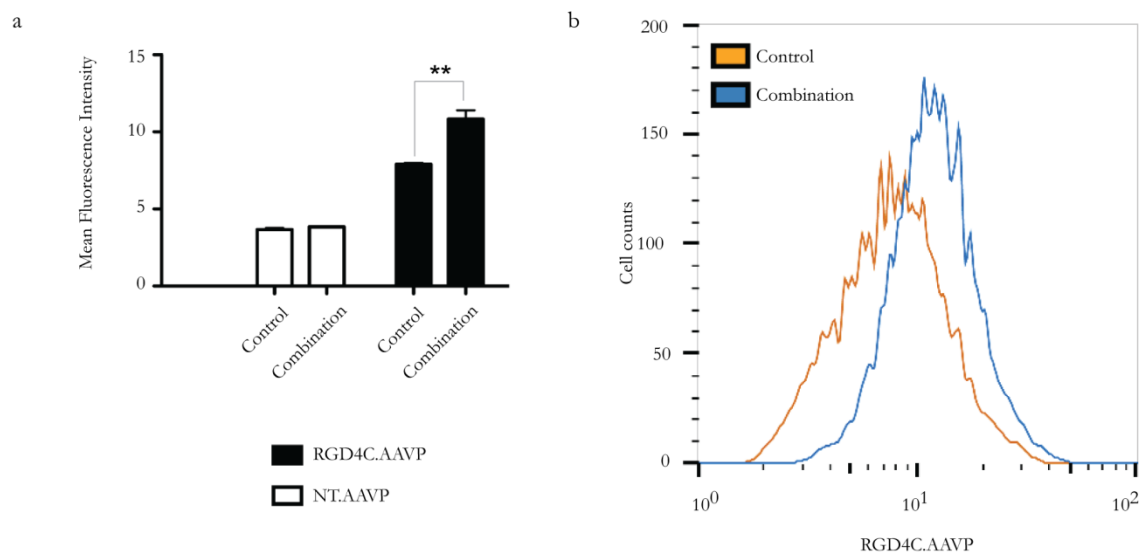
Figure 5.4: Cellular internalization of AAVP is boosted by ECM clearance. a) Flow cytometric analysis of AAVP uptake was carried out in 9L cells after ECM depletion. Cells were treated either with a combination of collagenase (0.2mg/ml) and hyaluronidase (0.4 mg/ml) without any enzyme (control) for 1 hour before transduction with either non-targeted NT.AAVP or RGD4C.AAVP. Fixation was conducted 4 hours post-transduction and immunofluorescence performed using anti-phage primary and goat anti-rabbit AlexaFluor-647 secondary antibodies. Gating threshold was set at 10,000 events of total cell population. Data represent the mean + SEM of triplicate samples from one representative experiments of three, significant difference; n.s.-not significant, * p<0.05, ** p<0.01, ***p<0.001 (two way ANOVA with tukey's post hoc test). **b**) Representative results showing the shift in mean fluorescence intensity and AAVP positive cell counts between control condition and enzyme combination treatment.

5.2.5. AAVP/HSVtk and GCV treatment in ECM depletion leads to enhanced tumour cell killing

To determine whether the enhanced gene transfer that we reported above following ECM depletion through enzymatic degradation would improve the efficacy of gene therapy, we transduced 9L cells with AAVP vectors carrying the HSVtk cytotoxic gene in combination with GCV treatment. Cell viability was assessed by quantification of ATP levels through the luminescence cell viability assay. We found that collagenase or hyaluronidase pretreatment enhanced the cell killing by RGD4C.AAVP when compared to control condition in the absence of enzymatic pretreatment, eliminating up to 80% of cancer cells after GCV treatment (**Figure 5.5a**). Interestingly, combinations of both enzymes dramatically enhanced tumour cell death by RGD4C.AAVP to 98% (**Figure 5.5a**). No cell death was detected in conditions without GCV or with application of the non-targeted NT.AAVP, suggesting that such tumour killing remains specific and targeted to cancer cells. Morphological analysis confirms the extent of the tumour cellular destruction; showing how ECM depletion causes extensive cell death when compared to vector alone (**Figure 5.5b**). Importantly, extensive destruction of tumour cells by RGD4C.AAVP can be observed in cells pretreated with both collagenase and hyaluronidase. These data demonstrate that combining ECM depletion with AAVP transduction can lead to strong anticancer efficacy.

a
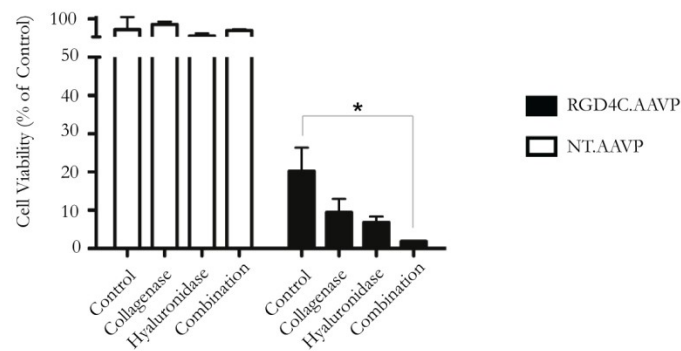
b
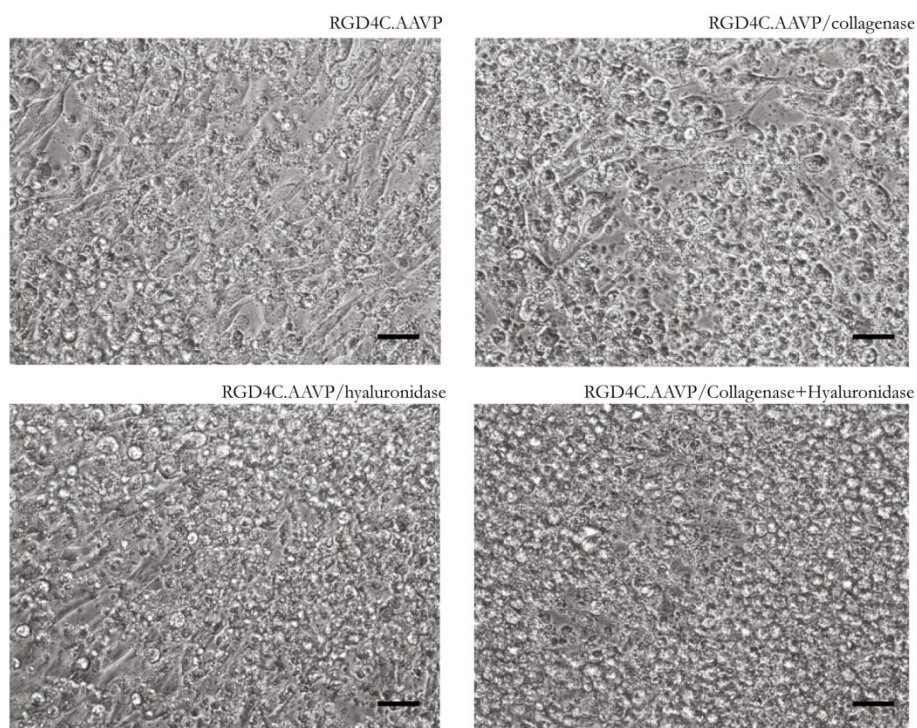
Figure 5.5: ECM degradation results in significant cell-killing effects by targeted RGD4C.AAVP mediated HSVtk/GCV gene therapy. a) 9L cell viability measured after ECM treatment in conjunction with transduction by non-targeted- and targeted RGD4C.AAVP carrying the *HSVtk* suicide gene. Media containing 20µM GCV was added and renewed daily for 5 days starting 72 hours after transduction. Cell killing was quantified by the CellTiter-Glo® cell viability assay and viability was expressed as percentage of matched experimental conditions (0.2 mg/ml of collagenase and 0.4 mg/ml of hyaluronidase) of cells in the absence of GCV. Mean cell viability was normalised to non-treated controls, with the mean of n=3 independent experiments shown (+ SEM), significant difference; n.s.-not significant, * $p < 0.05$, ** $p < 0.01$, ***$p < 0.001$ (two way ANOVA with tukey's post hoc test). **b**) Morphological characteristics of 9L cells after enzymatic treatment and RGD4C.AAVP/HSVtk transduction. Differences in cell viability are visualized by the number of dead cells seen in different treatments. Scale bar = 100 µm.

5.2.6. Multicellular tumour spheroid (MCTS) models showed increased targeted gene transfer by RGD-AAVP in combination with ECM depletion

Tumour spheroids are recognized as superior tools over monolayer cell culture systems as models for cancer investigation.[241] Spheroids closely mimic solid tumours, including parameters such as ECM composition and thus drug transport in tumours. As such, AAVP gene therapy was applied to the spheroid model to investigate whether ECM degradation would prove efficacious for situations resembling *in vivo* solid tumour environments. Tumour spheroids were pretreated with a range of collagenase or hyaluronidase concentrations followed by AAVP transduction and a liciferase assay. Maximal levels of luciferase activity were observed with 0.2 mg/ml of collagenase and 1 mg/ml of hyaluronidase; with activity dropping sharply with further increases in concentration (**Figure 5.6a, b**). The optimal concentrations were therefore used in further experiments of combination treatment on the spheroid model showing a significant 2.6-fold increase of transduction efficacy over control conditions in the absence of enzyme pretreatment (**Figure 5.6c**) These findings support that ECM effects are highly relevant in *in vivo* situations and confirm that ECM removal should be considered to improve RGD4C.AAVP diffusion and delivery especially in environments involving solid tumours.
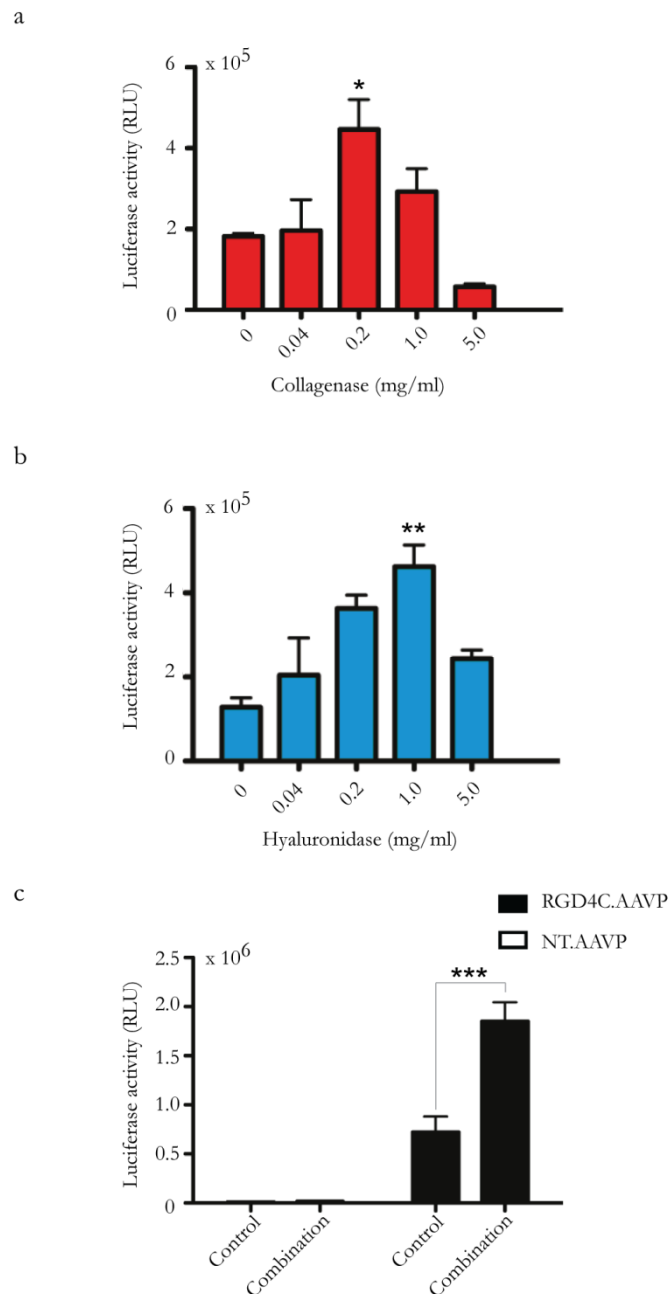
Figure 5.6: Effect of ECM depletion on RGD4C.AAVP transduction in tumour spheroid models. Concentration gradient curve of ECM degrading enzymes in 9L tumour spheroids generated by quantification of post-transduction day 3 luciferase gene expression through Steady-Glo® assay. RGD4C.AAVP carrying *Luc* gene was applied to spheroids that underwent **a**) collagenase or **b**) hyaluronidase treatment. **c**) Quantification of luciferase activity following treatment with enzymatic combination versus control treatment in tumour spheroids. The results show the mean relative luminescence units of triplicate wells +SEM, from one representative of three independent experiments, significant difference; n.s.-not significant, * $p<0.05$, ** $p<0.01$, ***$p<0.001$ (one and two way ANOVA with tukey's post hoc test).

5.2.7. The ECM represents a major obstacle to AAVP vectors and the transport is determined by the ECM concentration

Increased ECM deposition resulting from the desmoplastic reaction is a characteristic observed in solid tumours and presents a transport barrier that restricts drug penetration, thereby limiting the efficacy of delivery vehicles for cancer therapy.[299] To test our hypothesis that the lower transduction efficiency of RGD4C.AAVP prior to ECM depletion was due to limited transport of RGD4C.AAVP particles through the tumour ECM, we performed diffusion assays to investigate the impact of ECM barriers on AAVP movement by looking at different concentrations of ECM network. The tumour-derived ECM was used as a model system and diffusion of fluorescently-tagged AAVP particles in two different concentrations of ECM-gel matrix was measured using fluorescence microscopy. We observed that higher ECM concentration (5.0 mg/ml) reduced the diffusion area of AAVP compared to lower concentrations (2.5 mg/ml). Fluorescently-labeled AAVP diffused through the 2.5 mg/ml ECM 2.6 times faster and covered an area 3 times larger when compared to the 5.0 mg/ml ECM (**Figure 5.7a, b**). These findings confirm that the ECM presents a major barrier to AAVP.

a

b
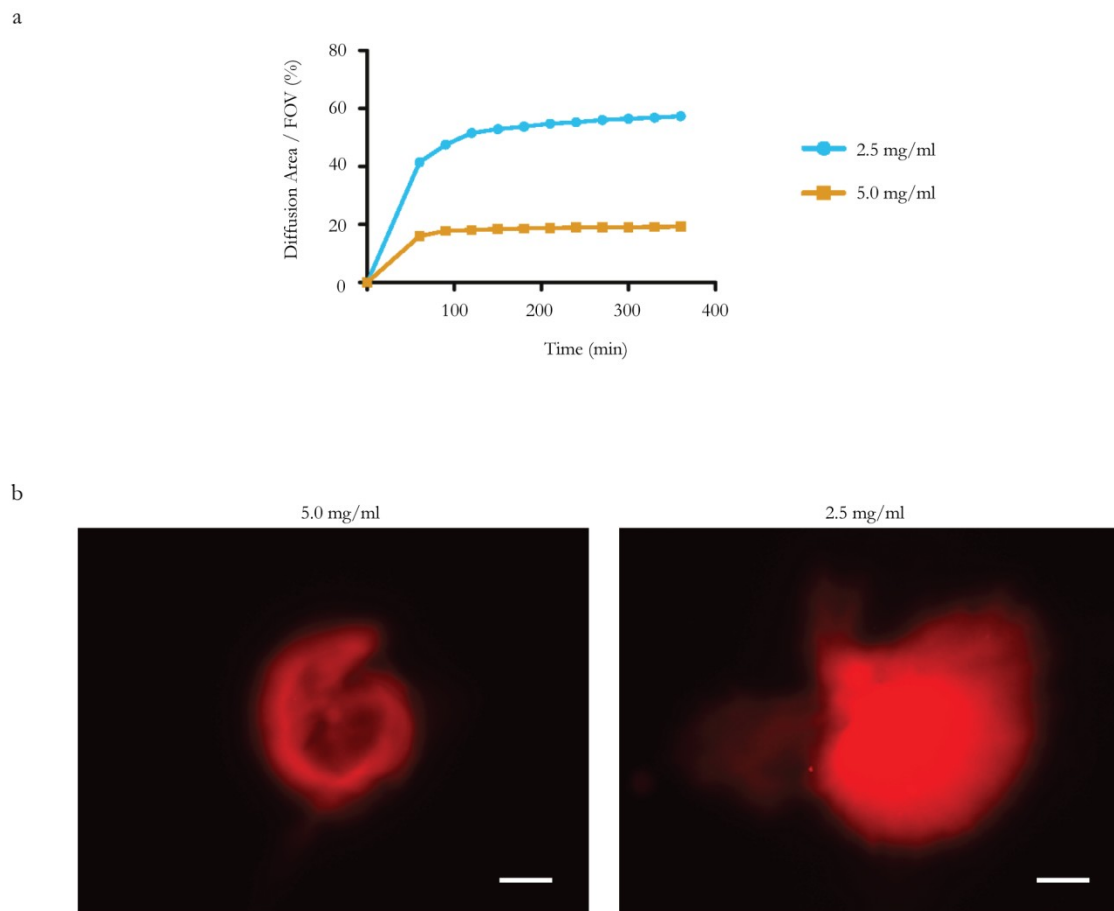
Figure 5.7: Effect of ECM on AAVP transport and diffusion. a) AAVP diffusion assay was performed using fluorescently labelled AAVP and tracked through the tumour-derived ECM gel matrix in order to investigate the impact of ECM barriers on AAVP movement. Two ECM concentrations were investigated (2.5 and 5.0 mg/ml). AAVP was tracked using fluorescent microscopy. AAVP diffusion was measured for a total time of 6h and expressed as diffusion area per field of view (FOV). **b**) Representative images demonstrating the diffusion of fluorescently labelled AAVP in different concentrations of ECM gel. Scale bar = 0.5 mm.

5.2.8. Losartan improves targeted gene transfer by RGD4C.AAVP

Systemic delivery of collagenase has been investigated and shown efficacious to enhance tumour perfusion in *in vivo* models.[300] However, we sought to use clinically approved drugs that could be used for lessening ECM in order to accelerate our findings to translational applications. Losartan is a FDA approved treatment for hypertension and has been proven to have anti-fibrotic effect by inhibition of collagen type I synthesis.[301] Luciferase assays were performed to examine if losartan could be a possible substitution for collagenase. Cells were treated with a range of losartan concentrations overnight before transduction with AAVP vectors carrying the Luc gene. A maximal gene expression increase of 2.4-fold above the baseline transduction level (in the absence of losartan) was observed in cells pretreated with losartan at a concentration of 100 μM (**Figure 5.8**). This demonstrates that losartan is a viable replacement for collagenase and can be a potentially superior ECM-modulatory procedure especially when side effects and safety issue are considered.
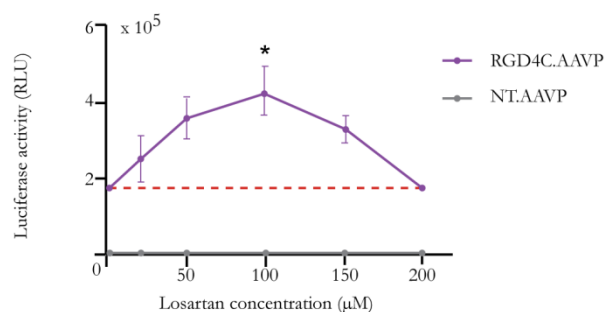
Figure 5.8: The effect of losartan on RGD4C.AAVP transduction. Gene delivery efficacy of RGD4C.AAVP was quantified, 3 days post vector transduction, by luciferase assay with Steady-Glo® assay kit after 9L pretreatment with the drug losartan. Cells were incubated overnight with increasing concentrations of losartan and transduced the following day with targeted or control non-targeted AAVP vectors carrying the Luc gene. The results show the mean relative luminescence units of triplicate wells ±SEM, from one representative of three independent experiments, significant difference; n.s.-not significant, * $p<0.05$, ** $p<0.01$, ***$p<0.001$ (one way ANOVA with tukey's post hoc test).

5.3. Discussion

Herein, we have demonstrated the potential use of ECM removal as a strategy to improve targeted gene transfer to cancer cells by a hybrid RGD4C.AAVP bacteriophage-based vector. As can be seen from increases in transduction efficacies after ECM depletion; ECM-vector interactions are important players in gene delivery to target cells and are first-line determinants in success gene delivery.

In active drug targeting, targeting ligands are attached to therapeutic agents to act as homing devices for binding to receptor structures expressed at the target site.[302] ECM molecules occupy receptors which serve as binding sites of AAVP vectors. Our experiments are the first proof of concept that ECM clearance can be used specifically in phage vector-based gene transfer to improve transduction efficacies. As we have shown, specific amounts of collagenase and hyaluronidase are able to significantly enhance gene transfer efficacy of AAVP. However, high levels of enzymes, especially collagenase, seem to be non-advantageous to transduction.

The present study indicates that degradation of the structural collagen network is more important than degradation of hyaluronan in order to improve the gene delivery by RGD4C.AAVP. A possible explanation is the shared receptor by AAVP and collagen fiber. Cell attachment to ECM is achieved through the action of cell surface receptors. Naive collagen produced by normal cells binds to their $\alpha_1\beta_1$, $\alpha_2\beta_1$, $\alpha_{10}\beta_1$, and $\alpha_2\beta_1$, and $\alpha_{11}\beta_1$ integrin receptors.[303,304] However, altered integrin expression is often observed during different stages of tumour progression.[305] For example, integrin $\alpha_v\beta_3$ is a receptor for tumour-associated ECM

including proteolyzed/denatured collagen in which cryptic RGD-sites in the relaxed collagen triple helix are exposed, and recognised by the RGD-directed $\alpha_v\beta_3$ integrins.[306,307] Incidentally, these are the same receptors that mediate RGD4C.AAVP internalization through the RGD motif. Therefore, collagen fibre is a barrier to RGD4C.AAVP through physical masking of target receptors on malignant cells.

A major obstacle is the transport and delivery of sufficient amount of gene delivery vectors to the target cells. In solid tumours, vectors have to extravasate across the capillary wall into ECM and move through the ECM to reach the individual cancer cells.[308] The high interstitial fluid pressure (IFP) in tumours hinders fluid flow into the tumour from blood capillaries of abnormal tumour vasculature. As a result, insufficient convection transport of therapeutic agents force drugs to be transported primarily by diffusion mechanism.[309-311] However, the diffusion of particles through the complex structure of ECM to reach malignant cells is a significant problem for relative large particles such as nanoparticles and viruses.[108] The fluid saturated gel-like extracellular space in solid tumours is composed of fibrous macromolecules, including collagen and glycosaminoglycans (GAGs). Here, we have demonstrated a greater degree of AAVP diffusion in lower concentrations of ECM-gel matrix compared to higher concentrations, suggesting ECM as a barrier to AAVP transport.

Collagen is the major protein component of the ECM and the collagen network is a significant barrier to the delivery of therapeutic macromolecules.[298,312,313] The

collagen content in solid tumours is significantly higher than in normal tissues, resulting in a relatively dense extracellular space.[314] Recent studies point out collagen as a likely target for modification to improve delivery of therapeutic agents.[315-318] Pretreatment of tumour spheroids with collagenase enzyme improved the penetration of nanoparticles through the cellular mass.[319]

Although collagenase is more efficient to increase gene transfer efficacy than hyaluronidase, additive effects could be achieved when both enzymes are synergistically applied. These additive effects can be explained, as collagen and hyaluronan are separate ECM entities. We have investigated the effect of the combination of enzyme treatment and gene therapy by AAVP in glioblastoma model, in this study, as this tumour type remains a challenge due to very limited therapeutic options and short survival of glioblastoma patients.[231] Several collagen types have been reported to be overproduced by glioblastoma cells and by endothelial cells during brain tumor angiogenesis, but are not significantly present in the normal brain tissue.[320] As well as collagen, hyaluronan is constitutively produced by glioma cells and its production is increased during cell proliferation promoting glioma invasion.[321-323]

We have also investigated the feasibility of ECM depletion in a spheroid tumour model which has superior properties for resembling *in vivo* environments of solid tumours.[324] Cells cultured on conventional two-dimensional plates lack the *in vivo* tumour environment. Multicellular spheroid models have been widely used to investigate many aspects of solid tumours and have proven particularly useful in

understanding the transport of anti-cancer nanomedicines.[325,326] The spheroid models is particularly compelling as a more realistic model in these experiments as they better reflect possible resistance to the AAVP's penetration and cell accessibility, by virtue of their metabolic activities (hypoxia and poor core vascularization) and possible interactions with the ECM.[241] By proving ECM modulation therapy in multicellular tumour setting, we hereby demonstrate that the strategy is relevant for *in vivo* situations.

Degradation of some ECM proteins, including collagen and hyaluronan, by the application of ECM-degrading enzymes has improved the penetration of drugs or nanoparticles through solid tumours.[108] Collagen depletion improves the intratumoural dispersion of nanomedicines, including monoclonal antibodies, liposomal doxorubicin, 10-500 kDa dextran, and herpes simplex virus, due to reduced IFP and enhanced extravasation.[315-318] A recently FDA-approved recombinant human hyaluronidase in pegylated formulation, PEGPH20 (Halozyme Therapeutics) is being investigated in an ongoing clinical trial with advanced solid tumours[327,328], suggesting that hyaluronidase can be an effective and clinically feasible anti-cancer drug. Earlier clinical trials suggest that hyaluronidase, given in combination with chemotherapy, does not pose significant toxicity to normal tissues.[329-331] However, the use of collagenase is currently not FDA-approved for cancer treatment in human as the clinical utility of enzymatic degradation is uncertain.[108] High levels of interstitial metalloproteinase especially collagenase have been found to correlate with a poor patient prognosis in a variety

of cancers.[332,333] ECM degradation may promote cancer progression, invasion, and metastasis in some cancers.[332,334] The complex ECM composition and the substantial heterogeneities in tumour microenvironment make it difficult to select the type and optimal dose of enzyme, for example the acidic microenvironment in solid tumours may diminish enzyme activity.[317,335] It may be advantageous to find a more practical method to target the ECM. Losartan provides the benefits of reducing ECM barriers and IFP while avoiding potential toxicity of direct collagenase activity. Losartan has been originally used as an angiotensin II type I receptor antagonist in clinical use for hypertention. It has also been shown to have anti-fibrotic activity mediated by knock-on effects on the transforming Growth Factor-β1 (TGF-β1) pathway through thrombospondin-1 (TSP-1) resulting in inhibition of collagen type I synthesis.[336,337] Its combination with oncolytic HSV or liposomal doxorubicin (Doxil) has proven efficacious in mouse xenograft models of cancers.[301] It has also been shown limited side effects[338], offering a better safety profile than systemic administration of collagenase.

5.4. Conclusion

ECM in solid tumours affects the effectiveness of RGD4C.AAVP-mediated gene delivery through blocking diffusion and/or physical masking of target receptors on malignant cells. In this study, the effect of ECM modulation on transduction efficiency of RGD4C.AAVP was investigated in cancer cells. We further evaluated the therapeutic effects of co-administering AAVPs carrying the HSVtk suicide gene in conjunction with ECM removal. We have also substantiated this strategy

through a more realistic cell culture model of multicellular spheroid tumour model and through the FDA- approved drug, lorsartan. The present results showed that ECM modulation could enhance transduction efficiency by AAVP vectors. These findings support the potential use of ECM depletion as a strategy to enhance gene delivery in tumours.

6. New generation of Multi-functional Filamentous Bacteriophage for peptide and gene delivery

6.1. Introduction

The concept of multifunctional vectors capable of simultaneously performing multiple functions has emerged and attracted the attention of a large and diverse number of investigations. Such functions include the delivery of therapeutic agents, biomarker-based targeting, the avoidance of extra-/intracellular barriers, and reporting of therapeutic efficacy (optical imaging).[339] The advantages of using a multifunctional system are associated with complementing or synergistic effects and less administration of adjuvants.[340]

To date, the development of a vast majority of multifunctional vehicles largely relies on synthetic conjugates using coupling chemistries to introduce functional moieties into different genetic or molecular constructs.[341] These synthetic processes are complicated and usually very system-specific, which limits cross-system application. Furthermore, many materials are not suitable for clinical application due to poor biocompatibility and potential toxicity resulting from the use of inorganic materials or surfactants.[340]

The filamentous bacteriophage contains a core comprised of circular single stranded DNA encapsulated in approximately 2700 copies of the major coat protein pVIII and minor coat proteins (3-5 copies each) pIII, pVI, pVII and pIX capped at the tips of the virion. In certain aspects, they can be regarded as efficient machines that can be developed into the potential nanomedicines.[188] A number of

characteristics make them well suited for constructing a multifunctional particle, offering novel solutions to the challenges of improving the efficacy of drug delivery to cells. In contrast to other materials, bacteriophages can be intentionally modified using routine genetic engineering techniques because their structure and function are encrypted in their genomic DNA.[342] The desired ligands (e.g., peptides, proteins, or antibodies) can be displayed on the bacteriophage capsid in a site-specific manner and carry a large payload of a cytotoxic drug. Another point of contrast to the sophisticated and poorly controlled synthesis procedures used to incorporate peptides and antibodies to targeted vehicles, the phage-based approach involves a simple yet powerful and precise mechanism of biosynthesis and self-assembly.[343] The production of phage vectors is simple and cost effective because they are easily produced with high titres in the supernatant of host *E.coli* cultures and can be purified on a large scale. Finally, bacteriophages have long been administered intranasally, topically, orally, subcutaneously and intravenously to humans; for example, they are used to treat pathogenic bacterial infections and only minor side effects have been observed in over 12 years of use.[290,344] Certain phage preparations have recently been approved by the Food and Drug Administration of USA as antibacterial food additives.[345]

We have therefore developed a novel bacteriophage, which exhibits a number of novel functions. To demonstrate the simultaneous expression of functional foreign peptides displayed on the capsid of the multifunctional bacteriophage, we used three well-characterized peptides: i) the double cyclic RGD4C peptide, ii) a

streptavidin-binding peptide (SBP), and iii) gold-binding peptide (GBP). The mammalian DNA cassette flanked by ITRs from AAV2 was incorporated into the phage genome to confirm its use for the delivery of transgenes.

Next, we used the multifunctional phage to construct an ideal bacteriophage vector capable of combining multiple strategies for overcoming the mammalian cell barriers to phage into a single particle, in addition to effective transgene expression. Therefore, we have generated multifunctional bacteriophage-based vectors as a proof-of-concept prototype; this particular phage simultaneously carries the RGD4C ligand for specific targeting *in vivo*, a tetrapeptide AKAS for the avoidance of plasma protein adsorption and a DNA cassette for transgene expression.
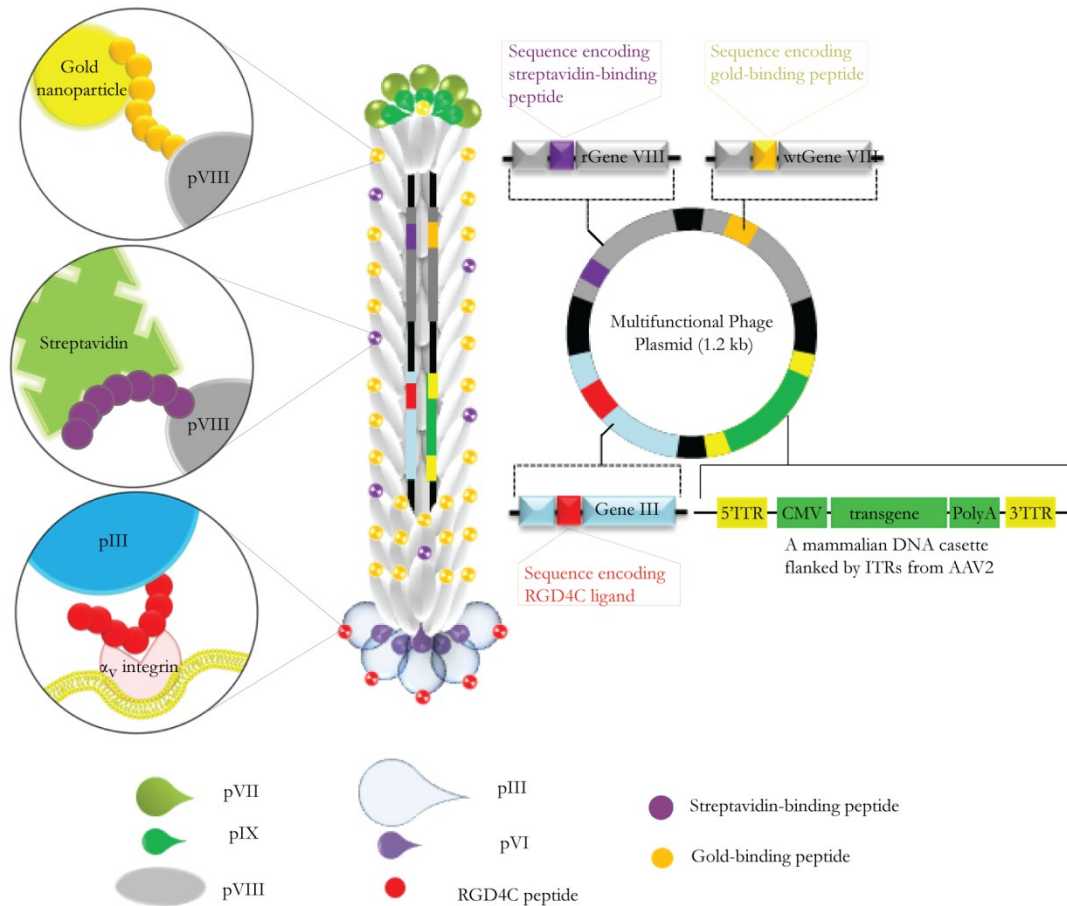
Figure 6.1: A schematic representation of a multifunctional phage particle model system. The phage is tetrafunctional, displaying a targeting RGD4C ligand on the pIII minor coat protein and multiple copies of gold binding and streptavidin-binding peptides on the surface. Additionally, a mammalian transgene cassette, driven by the CMV promoter, was also inserted in the bacteriophage genome to allow transgene expression by the multifunctional phage.

6.2. Results

6.2.1.   Construction and characterization of a multifunctional display model system

To construct the trifunctional phage, the plasmid DNA of two existing phages which share similar genetic backbones and contain unique restriction sites at similar locations were chosen to construct a multifunctional display model system. The fUSE5 (GenBank Accession number: AF218364) bears a single gene III and f88.4 (GenBank Accession number: AF218363) that contains two genes VIII, encoding two different types of pVIII molecules namely wild type and the recombinant one bearing a foreign DNA insert. A chimera between fUSE5 and f88.4 was constructed prior to introducing sequences encoding the desired peptides on different coat protein genes by using a subcloning strategy and site-directed mutagenesis. The double cyclic RGD4C ligand is displayed on the pIII minor coat protein. The coding sequences of the streptavidin binding peptide were fused in frame with the recombinant VIII gene. The coding sequence of the gold-binding peptide was inserted into the genome of the modified vector through gene fusion with the wild type major coat protein pVIII. Thus, the resulting phage particle simultaneously displayed an RGD ligand at the phage end, and multiple copies of gold binding peptide and streptavidin-binding peptide on the surface as schematically shown in **Figure 6.1**. Sequencing analysis of all recombinant plasmids was carried out to confirm the presence of the correct orientation of the

insert and to determine if any mutations occurred during cloning. Four phage

vectors were constructed in this study and are shown in **Figure 6.2**.
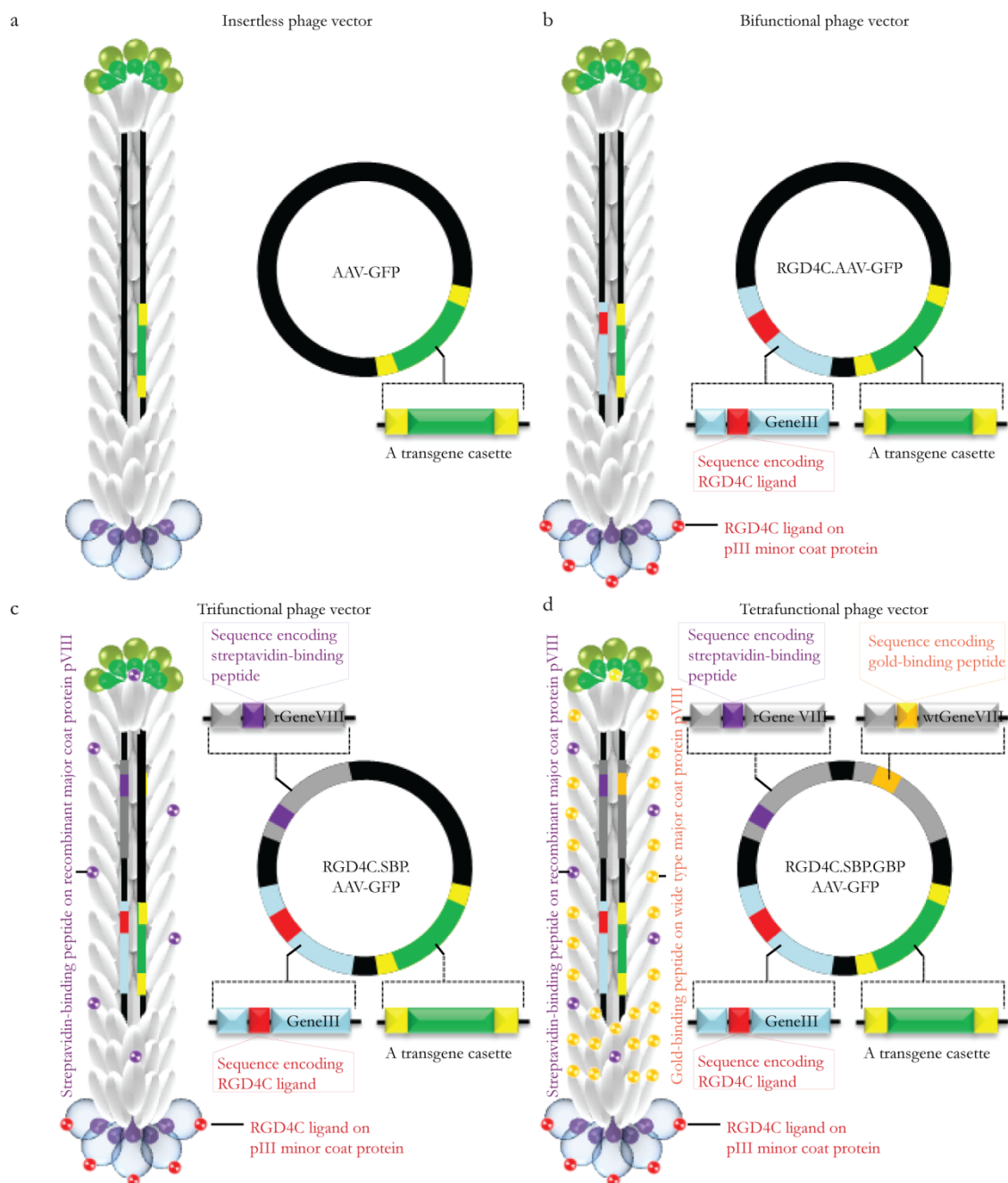
Figure 6.2: schematic representation of four phage vectors used in this study. **a**) Insertless phage carrying a mammalian transgene cassette, without any ligand on display. **b**) bifunctional phage, displaying the RGD4C ligand and carrying a mammalian transgene cassette. **c**) Trifunctional phage, simultaneously carrying RGD4C, streptavidin-binding peptide (SBP), and mammalian transgene cassettes. **d**) Tetrafunctional phage, simultaneously displaying RGD4C, streptavidin-binding peptide (SBP), gold-binding peptide (GBP) and mammalian transgene cassettes.

6.2.2. Cell surface α_v integrin receptors binding characteristics of the multifunctional phage

In order to demonstrate that all moieties displayed on the pIII and recombinant as well as on wild type pVIII proteins are functional, we performed various binding assays. Firstly, we validated the function of the RGD4C targeting ligand displayed on the pIII minor coat protein by assessing binding and internalisation to cells expressing $\alpha_v\beta_3$ integrin receptors. Immunofluorescence and confocal microscopy using antibodies against the phage capsid were performed on highly $\alpha_v\beta_3$ integrin-expressing M21 cells.[346] As shown in **Figure 6.3**, we demonstrated that targeting and internalization capabilities of the RGD4C peptide remained intact and functional in the multifunctional phage as well as in the trifunctional and bifunctional phages. The insertless phage showed background signal only.
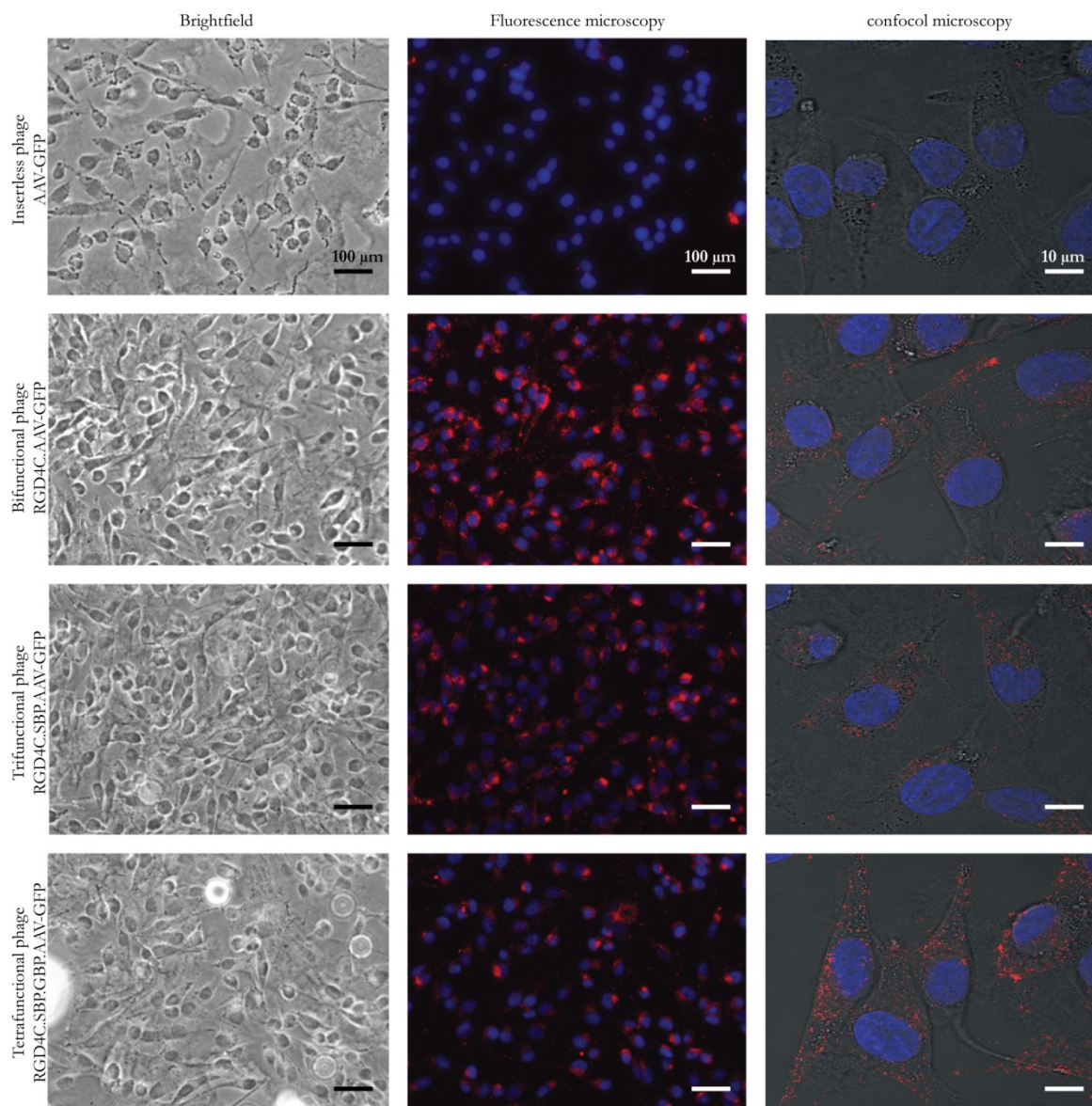
Figure 6.3: Immunofluorescence-based phage binding and internalization assay. Cultured human M21 melanoma cells were incubated with different phage preparations, all carrying a phage input of 1 mg/well. The red colour represents fluorescence from phage staining, and the blue colour shows fluorescence of DAPI-stained cell nuclei.

6.2.3. Analysis of the streptavidin binding capacity of the multifunctional phage

In vitro phage binding assays were used to assess the functionality of the strptavidin-binding peptide displayed on the surface of the multifunctional phage. Unbound phages were recovered from the streptavidin coated plate by infection of host bacteria *E.coli* K91. As shown in **Figure 6.4**, the trifunctional (RGD4C.SBP.AAV-GFP) and tetrafunctional phage (RGD4C.SBP.GBP.AAV-GFP), both of which display streptavidin-binding peptides had higher and similar levels of binding to immobilized streptavidin as determined by the greater number of bacterial transducing units. In contrast, insertless phage (AAV-GFP) and bifunctional phage (RGD4C.AAV-GFP) did not show any binding.
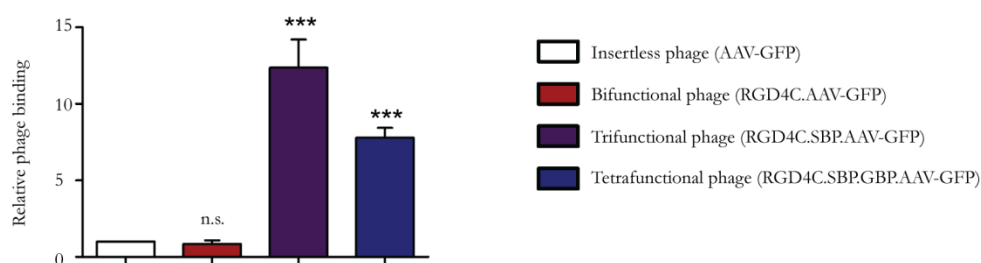
Figure 6.4: The streptavidin binding capacity of the multifunctional phage. Different phage constructs were incubated with immobilised streptavidin and washed prior to infection of *E.coli* K91. Shown are the mean from triplicate wells. Data represent the mean + SEM of triplicate samples from one representative experiments of three, significant difference; n.s.-not significant, * $p<0.05$, ** $p<0.01$, ***$p<0.001$ (one way ANOVA with tukey's post hoc test).

6.2.4. Testing the colloidal gold binding capacity of the tetrafunctional phage

Colloidal gold was used in this study to assess gold-multifunctional phage interactions. First, we carried out a dot blot-diffusion assay to evaluate the functionality of the gold binding peptide displayed on the capsid of the multifunctional phage (**Figure 6.5a**). Different phage preparations were directly added onto the nitrocellulose membrane, after which the solution of colloidal gold was added on top of phage dotted on the membrane. The ability to bind to gold was determined by the diffusion pattern formation of colloidal gold on the membrane. Significant staining was observed in the dot of tetrafunctional phage (RGD4C.SBP.GBP.AAV-GFP), suggesting its effective colloidal gold binding capacity (**Figure 6.5a**). No staining was observed in dots of insertless, bifunctional and trifunctional phage, where gold colloids tend to move from a region of high concentration of phage to the peripheral regions of lower concentration of gold colloids (**Figure 6.5a**). This indicates that insertless, bifunctional and trifunctional phages, all of which lack the gold-binding peptide on the surface, did not bind to gold.

To confirm the gold binding capacity of the multifunctional phage, we performed a precipitation test in which phage suspension solutions were mixed with a colloidal gold suspension (**Figure 6.5b**). After overnight incubation, a visible precipitate was observed in the mixture of the tetrafunctional phage (RGD4C.SBP.GBP.AAV-GFP) with the gold colloidal suspension (**Figure 6.5b**),

indicating that the gold colloids formed aggregates. The mixtures with the insertless phage remained clear as shown in **Figure 6.5b**).
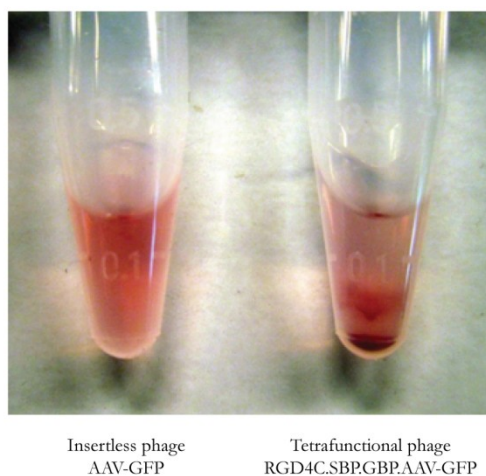
Figure 6.5: The gold binding capacity of the multifunctional phage. a) Dot blot of phage-binding gold colloids. Dots (from left to right) represent insertless, bifunctional, trifunctional, and tetrafunctional phages. **b**) Precipitation assays were carried out to visualize precipitate formation upon mixing a gold colloidal solution with the phage. Photographs of insertless and tetrafunctional phages mixed with 10-nm colloidal gold overnight are shown.

6.2.5. Evaluation of transgene expression by the multifunctional phage

To examine that the multifunctional phage can deliver transgenes into mammalian cells, we carried out cell transduction experiments on HEK293 cells. This was previously used as a standard *in vitro* model for transduction by the well-characterized RGD4C.AAVP. We used vectors carrying the GFP reporter gene, which provides a convenient way to visualize gene expression. Analysis of GFP expression showed GFP expression in cells transduced with the multifunctional phage (**Figure 6.6**). No GFP expression was observed in the insertless phage-transduced cells (**Figure 6.6**). The data prove that multifunctional phages successfully mediate transgene expression in mammalian cells.
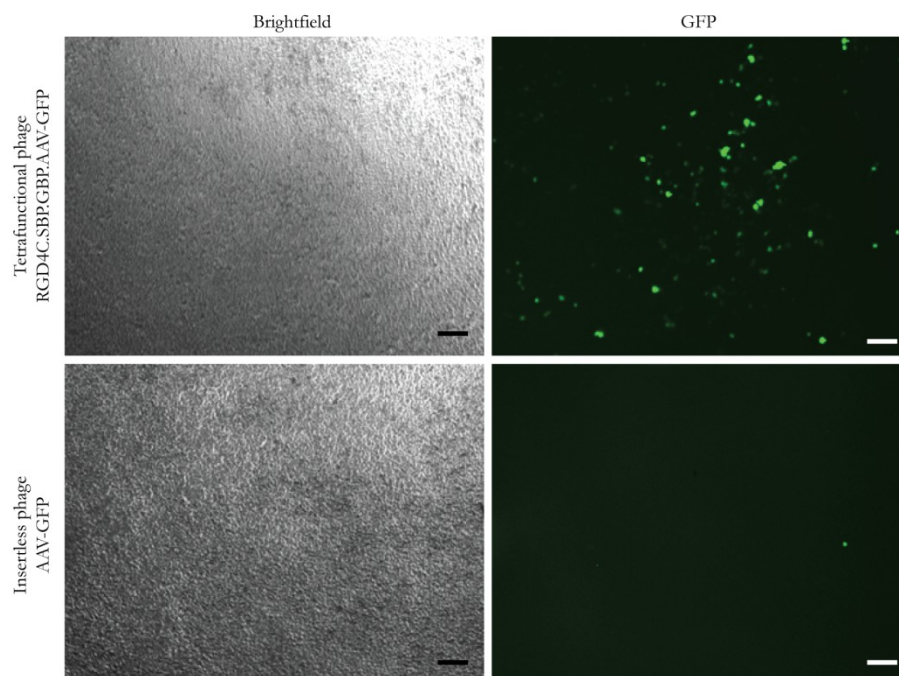
Figure 6.6: GFP expression by the multifunctional phage in HEK293 cells. GFP expression was visualized under a fluorescent microscope. Shown are representative images of cells at day 5 following transduction with insertless and multifunctional phages. Scale bar = 0.5 mm.

6.2.6. Construction and production of a multifunctional phage, carrying RGD4C, a tetrapeptide AKAS and a transgene cassette

Next, to investigate whether the multifunctional phage can be used to enhance phage-based applications in gene delivery, we assessed gene transfer efficacy. One major extracellular barrier to systemic gene delivery vectors is the formation of a "protein corona" caused by non-specific plasma protein adsorption to vectors.[347] One way to tackle this problem is to introduce zwitterionic properties, known for being resistant to plasma protein adsorption, onto the particle surface.[348,349] We generated the RGD4C.AKAS.AAV-GFP by introducing a tetrapeptide (AKAS) to the N-terminus of each copy of the major coat protein as schematically shown in **Figure 6.7**. This genetic modification resulted in an additional zwitterionic property of the surface of the bacteriophage.[350] To engineer this new phage, we used the original vector in which the sequence encoding the RGD4C ligand has already been fused in frame with gene III.[22] The first genetic engineering step was to introduce the tetrapeptide AKAS between residues Gly3 and Asp4 of the N-terminal region of the major coat protein pVIII using site-directed mutagenesis. The correct insertion of the AKAS nucleotide sequence of the resultant plasmid (RGD4C.AKAS) was confirmed by sequencing analysis. Next, the transgene cassette (GFP reporter gene) flanked by ITRs from AAV was inserted into the intergenic region of RGD4C.AKAS vector. Finally, a positive clone was used for phage production followed by phage purification (See materials and methods).

Similar to the original RGD4C.AAV-GFP phage, the new phage can be produced with high titres and within a workable range. These data show that fusion of the AKAS tetrapeptide with N-terminus of pVIII major coat protein did not affect phage production.
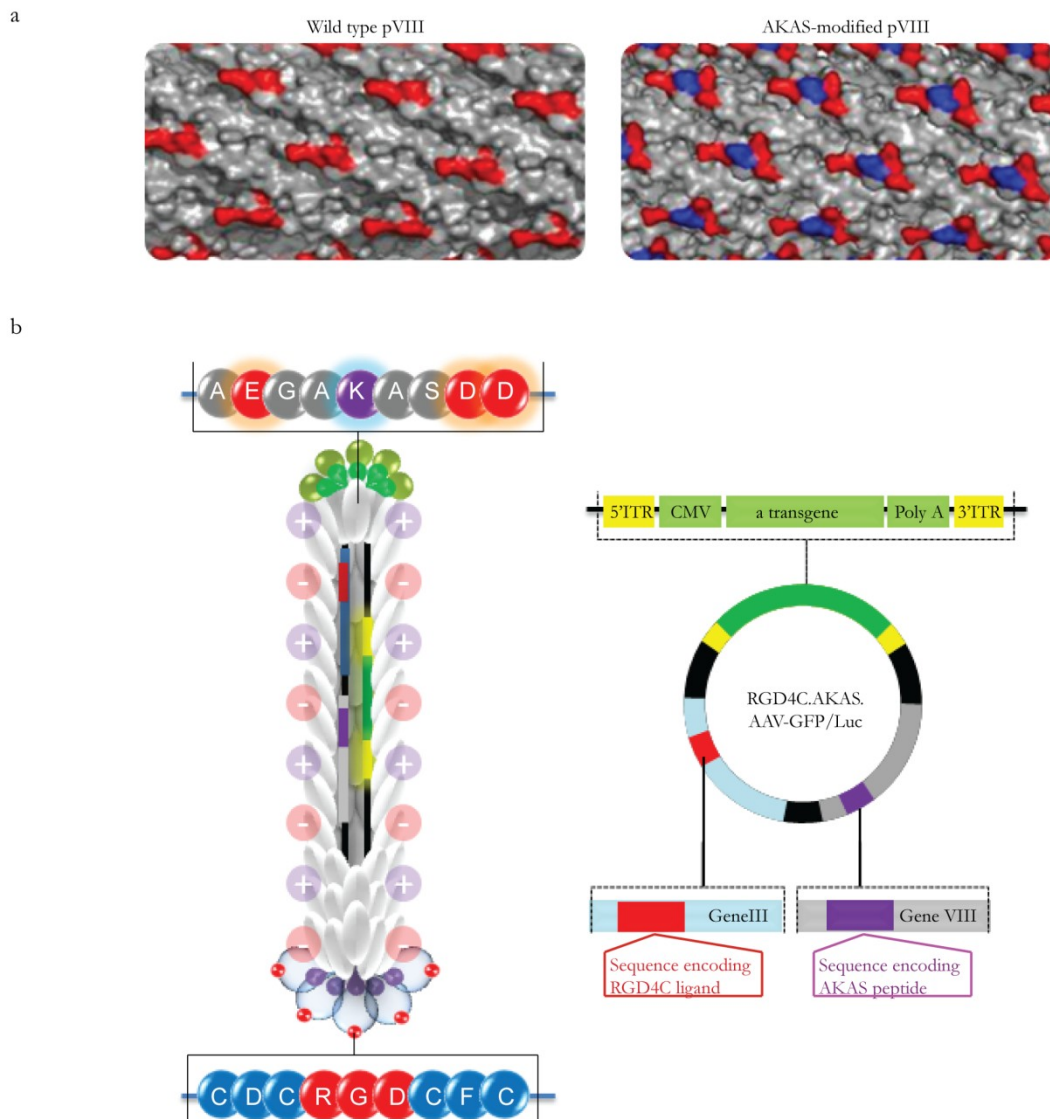
Figure 6.7: The zwitterionic surface of filamentous bacteriophage. a) The AKAS tetrapeptide insertion allows the phage surface to mimic the zwitteronic character.[350] The wild type major coat protein pVIII of phage includes 3 carboxylate groups bearing side chains at its N-terminus (left) and an insertion of a 4-mer peptide into each copy of pVIII results in a zwitterionic surface. **b**) Construction of the multifunctional phage, simultaneously carrying RGD4C, a tetrapeptide AKAS and a transgene cassette.

6.2.7. Display of the tetrapeptide AKAS alters the surface of the multifunctional RGD4C.AKAS.AAV-GFP phage

A general characteristic of zwitterionic materials is their both positive and negative charged moieties on the same side chain, maintaining total charge neutrality.[351-353] To confirm that the AKAS peptide neutralized the negatively charged phage capsid, we carried out an experiment to demonstrate that the new multifunctional phage surface has different charge properties compared to the parental one, as determined by its cationic polymer binding capacity. We incubated the phages with the positively charged DEAE.DEX polymers and expected the lower affinity of the new phage to DEAE.DEX polymer. After overnight incubation on DEAE.DEX-coated plate, the unbound phages were recovered from the supernatant by infection of K91 followed by colony counting. As shown in **Figure 6.8,** insignificant number of the RGD4C.AAV-GFP phage was recovered as compared to the RGD4C.AKAS.AAV-GFP phage, suggesting that the original vector was almost completely sequestered by the DEAE.DEX polymers. Interestingly, 30% of the RGD4C.AKAS.AAV-GFP phage was recovered (**Figure 6.8**). These results clearly demonstrate that the surface of the newly generated phage is genetically modified to reduce the binding capacity to positive charged molecules.
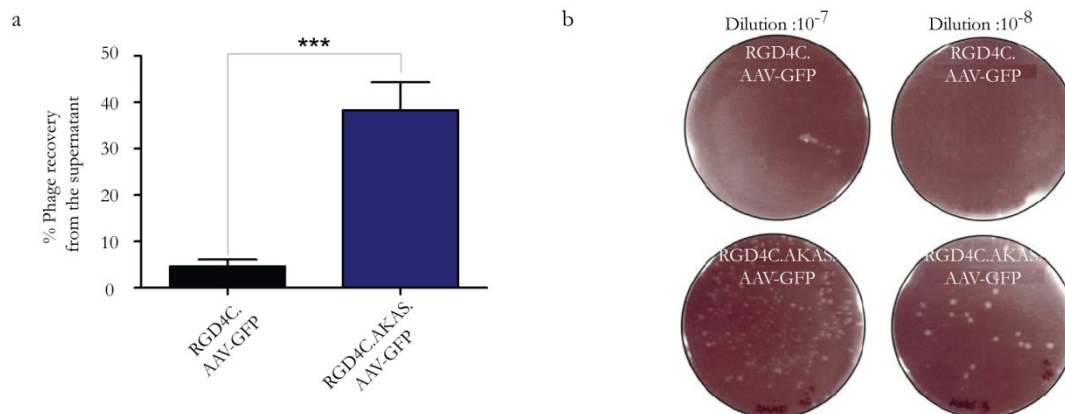
Figure 6.8: The cationic polymer binding capacity of multifunctional RGD4C.AKAS.AAV-GFP phage. a) Percentage of phage recovery from the DEAE.DEX-coated plate (phage recovery in term of percentage of input). Phages were incubated overnight on the cationic DEAE.DEX- coated plates. The supernatant containing unbound phage particles were recuperated and used to infect *E.coli* K91Kan. **b**) LB-agar plates showing the colony formation between the parental RGD4C.AAV-GFP phage and the RGD4C.AKAS.AAV-GFP phage. One representative plate of each phage and each dilution are shown. Data represent the mean + SEM of triplicate samples from one representative experiments of three, significant difference; n.s.-not significant, * $p<0.05$, ** $p<0.01$, ***$p<0.001$ (one way ANOVA with tukey's post hoc test).
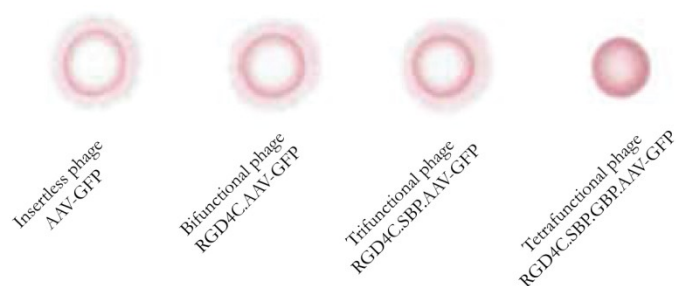
6.2.8. Phage incubation with fibrinogen decreases the transduction levels of RGD4C.AAV-GFP phage while the efficacy of the multifunctional RGD4C.AKAS.AAV-GFP remains intact

Fibrinogen is extensively used as a model protein to assess the protein adsorption resistance of biomaterials.[354] Therefore, in this study the protein-fouling resistant property of RGD4C.AKAS.AAV-GFP phage was tested by cell transduction after phage incubation with fibrinogen proteins. Thus, we transduced the 9L cells with the RGD4C.AAV-Luc and RGD4C.AKAS.AAV-Luc phages under normal conditions or following incubation with fibrinogen for 60 mins (**Figure 6.9**). No differences in Luc expression were detected in normal transduction conditions (**Figure 6.9**). Interestingly, a 2.2- fold decrease in Luciferase activity was observed in RGD4C.AAV-Luc-transduced cells compared with RGD4C.AKAS.AAV-Luc-transduced cells after incubation with fibrinogen (**Figure 6.9**). This result suggested that the multifunctional phage with the altered surface is able to avoid non-specific binding to fibrinogen.

6.2.9. Resistance of the multifunctional phage to antibody neutralization

To uncover further improvements and advantages acquired by the multifunctional RGD4C.AKAS.AAV-Luc phage, we evaluated the effect of a neutralizing antibody against bacteriophage on the transduction efficiency of the multifunctional phage. 9L cells were transduced with the RGD4C.AAV-Luc and RGD4C.AKAS.AAV-Luc phage in the presence of anti-phage antibody and the Luciferase activity was

determined 3 days post-transduction (**Figure 6.10**). The results showed a significant transduction difference in the presence of the anti-phage antibody (1:8000). We observed 2.5-fold higher transduction efficiency in RGD4C.AKAS.AAV-Luc-treated cells compared to cells transduced with RGD4C.AAV-Luc phage (**Figure 6.10**). These data indicated that the novel multifunctional phage gained potential to escape from the neutralizing antibodies against the capsid of the parental phage vector.
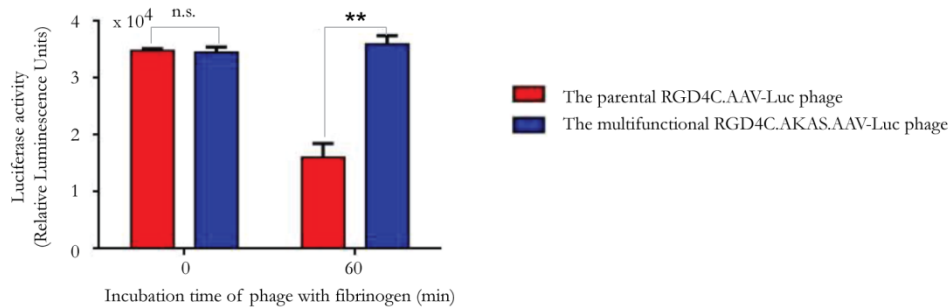
Figure 6.9: Luciferase expression following phage incubation with fibrinogen. The 9L cells (60-80% confluent in 48-well plates) were transduced with phages carrying the Luc reporter gene (25µg/well). Two conditions were assessed: cells treated directly with the phages stock solution (left bars) or cells treated with the remaining phage after 60 minutes incubation with fibrinogen (right bars). The results show the mean relative luminescence units of triplicate wells ±SEM, from one representative of three independent experiments, significant difference; n.s.-not significant, * p<0.05, ** p<0.01, ***p<0.001 (two way ANOVA with tukey's post hoc test).
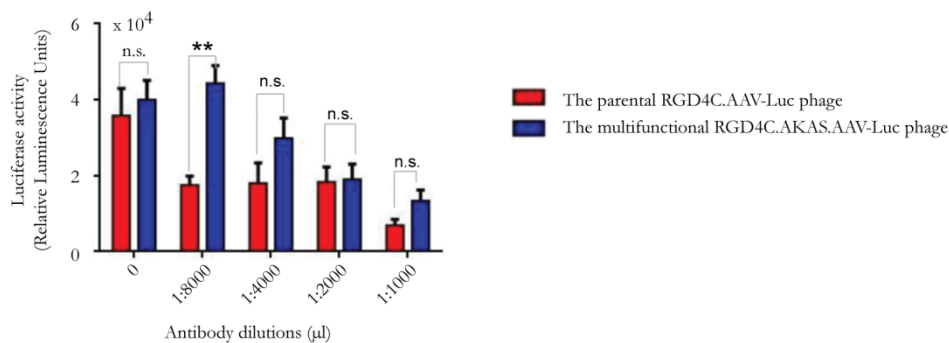
Figure 6.10: Effect of anti-phage antibody on luciferase expression in cells transduced with RGD4C.AAV-Luc or RGD4C.AKAS.AAV-Luc phage. The 9L cells (60-80% confluent in 48-well plates) were transduced with 25µg/well of phages solution containing complete media and a serial dilution of anti-phage antibody concentrations. The results show the mean relative luminescence units of triplicate wells ±SEM, from one representative of three independent experiments, significant difference; n.s.-not significant, * p<0.05, ** p<0.01, ***p<0.001 (two way ANOVA with tukey's post hoc test).

6.2.10. Mutations in the N-terminus of the major coat protein pVIII of the multifunctional phage affect infectivity

Phage concentration was measured by spectrophotometric quantification of DNA and protein. After being adjusted to an identical phage particle number, clones were assayed for infectivity by counting colonies (colony forming units; cfu) formed on LB agar plates. Although phage of all constructs tested were assembled and released, there was a difference in their ability to infect bacteria. As well as the phage without capsid modification, phages bearing either engineered pIII or recombinant pVIII alone formed similar number of colonies (**Figure 6.11**). Surprisingly, one of the selected peptides (GBP) displayed on wild type pVIII yielded lower number of colonies whereas AKAS remained intact and similar to the unmodified phage (**Figure 6.11**). This suggests that the insertion of a particular sequence on wild type pVIII can affect its ability to infect bacteria.
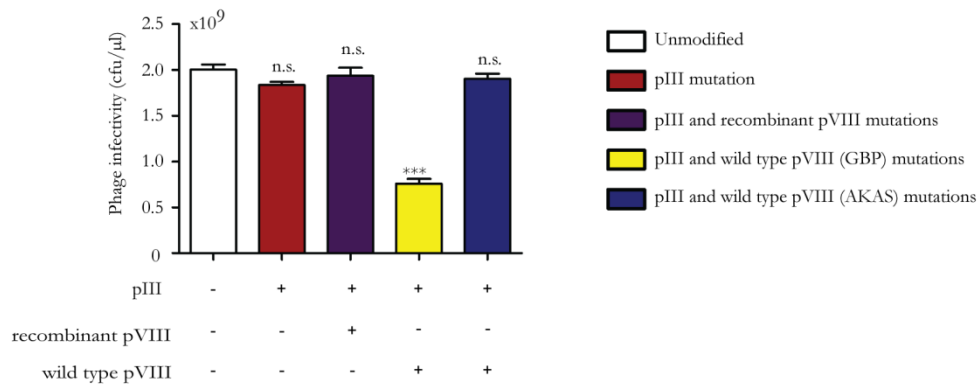
Figure 6.11: The effect of coat protein mutations on the multifunctional phage infectivity. The phage particle number was calculated from measuring protein and DNA by spectrophotometry (adapted from protocol by George P. Smith *et al.)*. An aliquot of phage stocks being previously adjusted to an identical particle number was incubated with host K91 *E.coli*. The infected cells were plated onto LB plates containing 50 μg/ml kanamycin and 40 μg/ml tetracycline. Infectivity (colony forming units/μl) was calculated from the number of colonies that grew on the plates overnight. Data represent the mean + SEM of triplicate samples from one representative experiments of three, significant difference; n.s.-not significant, * $p < 0.05$, ** $p < 0.01$, ***$p < 0.001$ (one way ANOVA with tukey's post hoc test).

6.3. Discussion

We found that the wild type, recombinant major (pVIII) and minor (pIII) coat proteins provide the ability to display a wide range of foreign peptides of differing sizes. Therefore, it is possible to design novel bacteriophage constructs depending on which foreign proteins need to be displayed on the outer capsid. In this study, we proved the possibility of constructing multifunctional phage, showing that all moieties displayed on the phage capsid remain intact and functional by displaying the RGD4C ligand, streptavidin-binding and gold-binding peptides, and carrying a mammalian DNA cassette expressing the GFP or Luc reporter gene.

The double cyclic RGD4C ligand identified by injection of phage peptide libraries into the circulation of mice bearing human breast carcinomas[355,356] are displayed on the pIII minor coat protein. This peptide contains an embedded RGD motif found in a number of extracellular matrix proteins ligands and allows targeting of tumour vasculature.

The coding sequences of streptavidin-binding peptide (ANRLCHPQFPCTSHE) were fused in frame with recombinant pVIII coding gene. This 15-mer streptavidin-binding peptide motif has previously been screened through a f88-cys5 phage display library for specific binding on immobilized streptavidin.[357] The coding sequence of gold-binding peptide (VSGSSPDS) was isolated by panning a type 8 phage display library on gold surface[358], which was then inserted into the genome of the modified vector through gene fusion with the wild-type major coat protein pVIII. This gold binding motif contains four serine residues, each of which

contains a hydroxyl group on the side chain. Hydroxyl-rich peptides have been reported to have high affinity to gold lattices.[359,360]

As a proof of concept, the resultant phage that simultaneously displays RGD4C, streptavidin binding, and gold binding peptides could be effectively internalised by $\alpha_v\beta_3$ integrin-expressing cells, and bind to gold nanoparticles and immobilised streptavidin as well. These results demonstrate that our multifunctional phage prototypes can be useful carriers for functional peptides, and for use in a number of applications such as the delivery of molecules such as therapeutic peptides. A broad spectrum of novel anticancer peptides have been reported and used for therapy or identified for potential application. This includes necrotic, apoptotic, function-blocking, antiangiogenic and immunostimulatory peptides.[361] Bacteriophages can be therefore used as a scaffold for constructing multifunctional nanocarriers, which may permit a cocktail of anti-cancer agents to be loaded onto a single carrier.

We also reported that by incorporating transgene expression cassette, our prototype vector showed transgene expression in mammalian cell lines. We utilized the mammalian gene cassette flanked by ITRs from AAV2. Our group previously showed that incorporation of ITRs is associated with improved fate of delivered transgenes, maintenance of the entire mammalian transgene cassette, better persistence of episomal DNA, and formation of concatamers of the transgene cassette, resulting in increased transduction efficiency over conventional phage-based vectors.[171] Such vector is therefore useful for a number of applications such

as gene therapy and vaccine development. Recent investigations have shown that phage particles can be applied either to deliver a vaccine expression cassette cloned into their genome (DNA vaccine technology) or to display specific antigenic peptides on their surface via a translational fusion with the capsid protein. The combination of the two strategies above may result in a promising tool to create cocktail vaccines.[362] Our prototype multifunctional phage capable of simultaneously carrying peptides and delivering transgenes may be ideally suited for this application.

One possible strategy for efficient transgene expression is the development of a multifunctional vector that integrates multiple ligands and peptides to escape a series of significant barriers to the delivery of therapeutic/imaging genes by bacteriophage into target cells.

One important extracellular barrier to systemic delivery of bacteriophage is its rapid removal from the circulation by cells of the RES and neutralizing antibododies after intravenous administration.[363] In general, it is acknowledged that non-specific protein adsorption is the first event that occurs in blood-biomaterial interactions, which may contribute to the stimulation of intrinsic cascade, leading to the immune response and therefore compromise the therapeutic efficacy. Plasma proteins play an important role in the identification of foreign bodies in the blood stream.[364] Once the gene delivery vectors are systemically administered, they are immediately coated by plasma proteins, which form a protein corona.[365] The binding of proteins that serve as opsonins are recognized to increase phagocytosis

by immune cells. These proteins include fibrinogen, immunoglobulin G, complement factors, etc.[366,367] It has been reported that the filamentous bacteriophage can non-specifically bind to a number of proteins (around 35% of proteins in the human genome)[368] Filamentous phages present three solvent-exposed acidic residues within the N-terminal five positions of the ~2700 copy, major coat protein pVIII. This acidic region contributes to a net negative charge of the phage surface, and can cause nonspecific interactions with proteins having an abundance of positively charged residues.[368]

One way to address this problem is to introduce zwitterionic properties, known for conferring resistance to plasma protein adsorption on the particle surface.[348,349] This design follows a previous study which demonstrated that the introduction of the AKAS tetrapeptide, with an additional lysine residue inserted into every copy of the pVIII phage protein, can neutralize the negative charge of the filamentous phage by generating a zwitterionic surface.[368] The AKAS peptide has been originally developed to reduce background binding for effective phage display technology[368] and to allow phage display of membrane-associated proteins.[350]

We sought to prove that the efficacy of multifunctional phages is enhanced through overcoming the obstacle of non-specific protein binding. We generated a multifunctional phage that displays the targeting RGD4C ligand on the pIII minor coat protein, carries the AKAS tetrapeptides on the pVIII major coat protein and expresses a transgene through a mammalian cassette inserted in phage genome. The protein-fouling resistant property of RGD4C.AKAS.AAV-GFP phage was

tested and the results proved the capability of genetic modification to reduce the amount of fibrinogen adhesion compared with the original RGD4C.phage. Moreover, we also showed that in addition to chemical modification as shown in the previous chapter the phage's ability to resist to antibody neutralization can be acquired by such genetic modification of the phage capsid. The altered surface of phage is believed to prevent the antibody recognition of epitopes on the major coat protein pVIII.

We further investigated whether the multifunctional phage could be modified to further improve its gene delivery efficiency. We realised that the major intracellular barriers to bacteriophage-based gene transfer are vector inactivation in the acidic lysosome[178], and transport of the bacteriophage to the nucleus of mammalian cells.[369] Our first attempt was to construct a phage which displays an endosomal escape peptide (EEP) or nuclear localization signal (NLS) on wild type major coat protein pVIII. Unfortunately, we failed to obtain these plasmid constructions and sequencing analysis revealed that they tended to mutate randomly (data not shown). This observation can be attributed to the previously reported dependence on both the size and charge of the foreign peptides expressed on the phage particle.[370] A previous investigation has shown that the display of positively charged peptides on the major coat protein pVIII was less efficient than that of neutrally charged peptides.[370] Unfortunately, most NLS sequences contain a high proportion of positively charged residues (i.e. lysine and arginine), which gives rise to the overall positive charge of NLS., for example, the classical NLS

(PKKKRKV) derived from SV40 large tumour antigen and Tat peptides (GRKKRRQRRRPQ) derived from the transactivator of transcription (TAT) of the HIV-1.[371] Indeed, the N-terminus of the major coat protein pVIII of bacteriophages can accommodate no more than 10 amino acid residues of foreign peptides as it has a tendency to affect phage assembly and production.[372] Any genetic modification of the major coat proteins pVIII must be able to accommodate their biological roles during the phage lifecycle, including transcription, translation, membrane insertion, signal peptidase cleavage, assembly and extrusion, and infection.[373,374] The genetic sequence will be more stable, and phages can be produced if the interactions between modified pVIII are biologically favourable within this context. In contrast, if the insert peptide makes pVIII interactions less favourable, it will be more likely to mutate and/or produce fewer number of phage particles.[375]

Protein translation was another process that may impose strong limitations on the allowed insert sequence. Our observation that the NLS sequence containing lysine residue repeats could not be expressed can be attributed to the previously shown dependence of protein translation accuracy in the E.coli host.[376] The repetitive use of amino acids with high copy number of pVIII proteins results in recruiting the pool of available corresponding tRNA isoacceptors and therefore slowing the translation process. As a result, the single stranded phage DNA accumulates, thus causing host cell death.[376-378] Our observation that mutations of phage vectors after attempts to engineer pVIII to display repeated lysine residue-containing NLS

peptide (data not shown) is in agreement with the previous study that this phenomenon is common in long stretches of repeated residues.[379] These explanations supported our observation that the positively charged NLS containing lysine residue repeats and the 23 amino acid long histidine-rich peptide H5WYG (GLFHAIAHFIHGGWHGLIHGWYG) cannot be displayed on the major coat protein pVIII. Among our several attempts, only certain peptides such as AKAS tetrapeptide could be constructed successfully and displayed on the produced phage particles.

One solution to overcome this limitation is to use a phage that bears two pVIII genes, producing two different types of pVIII protein. Due to increased expressional flexibility, recombinant pVIII allows the display of a variety of proteins on the virion surface while the wild type pVIII is used to support phage assembly. In our preliminary study, we constructed the phage vectors carrying NLS and H5WYG on recombinant pVIII and obtained high titres of the new phage constructs. However, viability of the resultant phage does not guarantee efficient incorporation of engineered pVIII into phage particles. Although we observed a small improvement in transduction efficacies by these newly generated vectors, the levels were not satisfying. Even though the recombinant pVIII offers greater flexibility, limitations still exist. Problems associated with the efficiency of fusions to pVIII that can be incorporated into the phage particle have been reported. Most large proteins are displayed below one copy per phage particle.[380] Inefficient display of large polypeptides on pVIII is partially limited by both the size and the

properties of the phage extrusion channel formed by pIV proteins on the outer bacterial membrane.[374,381] A phage carrying a large peptide on pVIII may be too large in diameter to pass through the 6-9 nm exit pore of pIV.[382]

A possible solution to efficiently display large peptides or proteins on most of the pVIII major coat protein is by chemical conjugation. This method gives the phage coat protein an ability to carry a large payload of molecules of interest. The molecule is linked to the phage through a chemical linker.[383] The payload capacity of phage particle can be improved further by introducing extra functional groups, which serve as a carrier for construction of chemical conjugates with a wide range of molecules of interest on every copy of the major coat protein of the phage.

For example, the filamentous bacteriophage was genetically modified to display two additional glutamate residues in the N-terminal of pVIII protein and was used for amine-terminated cadmium selenide quantum dots (QDs) via the carboxylic acid side groups on the engineered coat protein. This glutamic acid-rich phage (4E phage) exhibited increased conjugation to QDs compared with the wild type phage. This study demonstrated that genetic engineering is essential to improve the biotemplating.[384] Interestingly, the E4 phage is another example of successful display of repeating residues on pVIII that do not cause mutations that affect phage production as discussed above.[379] This was due to the large number of Glu isoacceptors in *E.coli* cells[375] and to the favourable negative charge at pVIII N-terminus region.

However, incorporation of molecules using a chemical method is often hampered by cross-reactivity or non-specific interactions with other functional groups present on the phage capsid, and requires multistep of synthesis and purification processes.[385] To overcome this limitation, sortase-mediated chemo-enzymatic reactions were used to covalently attach a variety of moieties to bacteriophage coat proteins.[386] The widely used sortase A includes $SrtA_{aureus}$ from *Staphylococcus aureus* and $SrtA_{pyogenes}$ from *Streptococcus pyogenes*. Sortase enzymes attach oligoglycine or oligoalanine-containing peptides to substrates that contain LPXTG sequence or LPXTA sequence in the case of $SrtA_{aureus}$ and $SrtA_{pyogenes}$.[387,388] The reaction is site-specific as certain motifs are required to be displayed on the coat proteins in order to serve as substrates for sortase. These motifs are small and therefore can be easily displayed on the phage coat protein.[389] Hess *et al.* demonstrated that by using this method, phage coat proteins can be functionalized with entities ranging from small molecules (e.d., fluorophores, biotin) to correctly folded proteins (e.g., GFP, antibodies, streptavidin) in a site-specific manner.[386] It is therefore possible to utilize this strategy to address problems associated with peptide properties (charge, size etc.). Consequently, this will increase the repertoire of proteins that can be expressed on pVIII, allowing newer multifunctional bacteriophages with desired multiple functions to be generated.

Another aspect of multifunctional bacteriophage is its infectivity after a series of genetic modifications of its capsid. Our findings are in agreement with a previous study showing that the display of peptides on wild type pVIII affects their ability to

infect bacteria. Interestingly, the infectivity of phages bearing both wide type and fusion pVIII remain intact because the deleterious effects of the fusion are attenuated by the presence of the wild type coat protein.[390] Indeed, pIII minor coat protein is necessary for the infection process as the N-terminal domain of pIII minor coat protein initiates translocation of the phage genome into host becteria.[390] However, previous investigations demonstrated that large peptides (up to 38 amino acids long) can be introduced into the-N-terminus of pIII without the loss of phage infectivity or particle assembly.[391,392] Thus, the display of the short RGD4C peptide on pIII protein of multifunctional phages did not affect their ability to infect bacteria.

6.4. Conclusion

We have designed a multifunctional filamentous phage (**see Figure 6.1**) that has potential to simultaneously carry multiple functions within a single virus particle. (i) It displays the targeting ligand on the pIII minor coat protein to bind a mammalian cell surface receptor, (ii) serves as a genetic carrier of foreign functional peptides to be displayed on the wild-type pVIII major coat protein, (iii) allows the display of large foreign peptides on the virion surface by the recombinant pVIII protein, and (iv) delivers a mammalian transgene cassette inserted in an intergenic region of the phage genome for expression in mammalian cells. In order to assess the function of the multifunctional phage in promoting phage-based gene delivery, we combined multiple solutions to overcome extracellular and intracellular hurdles to phage-mediated gene transfer into a single phage particle. Here, we proved the

ability of genetic modifications to reduce the amount of fibrinogen adhesion when compared to the original AAVP. In conclusion, the bacteriophage scaffold can potentially be used as a platform to generate a multifunctional gene transfer vector. The success of these strategies will present a breakthrough in gene delivery by bacteriophage and bring to fruition the promise of phage technology as a realistic and efficient systemic tissue-targeted delivery of genes.

7. General Discussion

The objective of the vectorology platform is to construct and produce gene delivery vectors to be used in various applications such as in basic research, gene therapy, cellular therapy and DNA vaccine. In order to make great progress in vectorology, it is of paramount importance to develop effective vectors capable of delivering a gene of interest to target cells to achieve sufficient and sustained transgene expression, with minimal toxicity. The design of gene delivery vectors has followed two parallel paths. One has taken advantage of animal viruses which have highly evolved their gene delivery capacity. Viral vectors have therefore received considerable attention and become powerful tools of gene transfer. However, the clinical application of viral vectors is limited because of unfavourable immunological features and mutagenic integration for some viruses. Their natural tropism is regarded as a double-edged sword. As viruses have highly evolved to infect their specific host cells, retargeting them to the desired tissue have frequently failed. Additionally, high security laboratory standards are often required. The other path has been to identify non-viral carriers capable of packaging and delivering DNA to target cell for transgene expression. The main limitation for this approach has been poor efficiency of gene delivery.

Recently, phage has been exploited as gene-delivery vectors for mammalian cells. As shown in **Table 7.1,** bacteriophage-based vectors have many of the desirable properties of both animal viral and non-viral systems without the significant drawbacks. For example, bacteriophage lacks natural tropism for mammalian cells

which is a major concern for animal viral vector targeting. The genetic or structural modification of the phage coat proteins can be easily manipulated, allowing selective targeting of mammalian cell receptors and subsequent tissue-specific transduction. Phage production is simpler and more cost effective than many existing systems.

Bacteriophage has come a long way since its first application as antibacterial and is further being engineered into new exciting phage-based therapeutics such as targeted gene delivery vectors. Bacteriophages have been used clinically to treat human bacterial infections since the early years following their first discovery by Frederick Twort and Felix d'Hérelle in 1915 and 1917, respectively.[393] Although the use of phage therapies for bacterial diseases continued in the Soviet Union and Eastern Europe, it almost disappeared due to the discovery of antibiotics.[394] More recently, the field has been reactivated as the prevalence of antibiotic-resistant bacterial strains continues to rise.[363] Bacteriophages have also been used as tools in genetic research, and the discovery of specific target-binding peptides or proteins, and vaccine development.[395] However, the greatest limitation of phage-mediated gene transfer to mammalian cells is low efficiency compared with typical viral vectors which has restricted its use.

An impressive amount of effort has been put into the improvement of bacteriophage to be used as a safe selective and efficient vector for gene delivery to mammalian cells. These improvements include 1) conferring mammalian cells tropism to bacteriophage by inserting a mammalian DNA cassette and displaying a

cell targeting ligand, 2) enhancing persistence of transgene expression by incorporating regulatory genetic elements from mammalian viruses, and 3) providing the precise control of spatial and temporal gene expression which is important in determining the safety and efficacy of gene transfer. In 1999, Larocca *et al* first described phage-mediated gene delivery to mammalian cells. Specifically, they adapted filamentous bacteriophage vectors by inserting a CMV regulated GFP reporter gene and genetically targeting cell surface receptors with either FGF2 or EGF ligands, and demonstrated that such phage undergo receptor-mediated endocytosis, resulting in the expression of transgenes in mammalian cells.[185] In 2006, Hajitou *et al* introduced a new generation of phage-based vector by incorporating genetic elements from AAV2. With the display of RGD4C targeting peptide on its surface coat as an N-terminal fusion to pIII and the incorporation of ITR from AAV into its genome, cell transduction efficiency was dramatically improved. This AAVP hybrid vector showed superior gene delivery over conventional bacteriophage vectors with long-term transgene expression *in vivo*.[171] In 2012, a double-targeted bacteriophage vector was reported by Kia *et al*. The ligand-directed targeting of AAVP vectors was combined with transcriptional targeting using the tumour specific promoter of the stress-inducible glucose-regulated protein 78 (Grp78) in one single phage vector. The double-targeted vector provides sustained and long-term transgene expression compared to the conventional phage carrying the CMV promoter. They also showed the superior tumour transduction *in vivo* after systemic delivery with tumour killing using

HSVtk/GCV suicide gene therapy.[182] In this study, we have placed an emphasis on the vectorology platform, namely chemical or genetic engineering of the bacteriophage capsid as well as their evaluation *in vitro*.

Previous studies as aforementioned have been performed to engineer phage particles, aimed at modifying the tropism by capsid manipulation mostly through genetic modification to incorporate the mammalian cell surface receptor-targeted ligand into phage capsid. We have demonstrated that in addition to genetic modification, chemical modification of the capsid proteins allows alternating the tropism of the bacteriophage, leading to the production of phage-based vectors able to transfer genes to mammalian cells. We also demonstrated that chemical modification also influences the subsequent barriers to gene delivery and the efficiency of transduction can be dramatically improved. Depending on the curtain material used, the phage vector acquires endosomal escape capability.

Despite considerable progress in the development of phage vectors for gene delivery, more advances must be made in order to increase the efficiency of the overall gene transfer process. The most interesting finding in this study was that a combined genetic and chemical modification of AAVP capsid further enhances gene transfer. We have thus introduced the novel hybrid multi-component vector termed the smart bacteriophage generated by complexing cationic polymer with the AAVP vector displaying the RGD4C ligand and carrying an AAV ITR-flanked mammalian DNA cassette (**Figure 7.1**). In addition to the transient expression, we expanded the utility of such combined chemical and genetic modified-

bacteriophage as gene transfer vectors for selection of cell lines that stably maintain expression of the reporter gene. More importantly, we showed that this novel vector provides significant extension to the development of novel therapeutic platforms, which can be used as a tool for cancer gene therapy.

Previous investigations have determined the extent of the bottleneck of each of extracellular and intracellular barriers and yielded mechanistic information useful for designing the vector to overcome these barriers.[396] To date, the design of gene delivery vectors has placed an emphasis on the development of multifunction vectors able to execute multiple tasks to simultaneously overcome delivery obstacles. In this study, we have generated multifunctional bacteriophage-based vectors as a proof-of-concept prototype. We used the multifunctional phage to construct an ideal bacteriophage vector capable of combining multiple strategies for overcoming the mammalian cell barriers to phage into a single particle.

Gene delivery approaches can be manipulated at multiple levels. In addition to the vectorology platform, we demonstrated that the manipulation of target cells could improve the delivery efficacy. Recently, there has been a renewed interest in the tumour microenvironment because of its role in a drug delivery obstacle.[296] We showed that the ECM affects the effectiveness of phage-based vectors through blocking diffusion and/or physical masking of target receptors on malignant cells and ECM modulation could therefore enhance transduction efficiency by AAVP phage vectors. These findings support the potential use of ECM depletion as a strategy to enhance phage-mediated gene delivery in tumours.

	Animal virus	Synthetic vector	Bacteriophage
Potential toxicity	High	Low	Low
Generation of competent virus	Yes	No	No
Viral protein expressed	Yes	No	No
Complexity	High	Low	Low
Cost	High	Low	Low
Gene transfer efficiency	High	Low	Low
Reproducibility	High	Low	High
Genetic targeting	Limited	Limited	Yes
Directed evolution	No	Yes	Yes

Table 7.1: A comparison of features of phage vectors with animal and synthetic vectors. Bacteriophage-based vectors offer an attractive alternative to various viral and synthetic vectors, because they can potentially overcome the drawbacks of either approach. (Larocca and Baird, 2001)
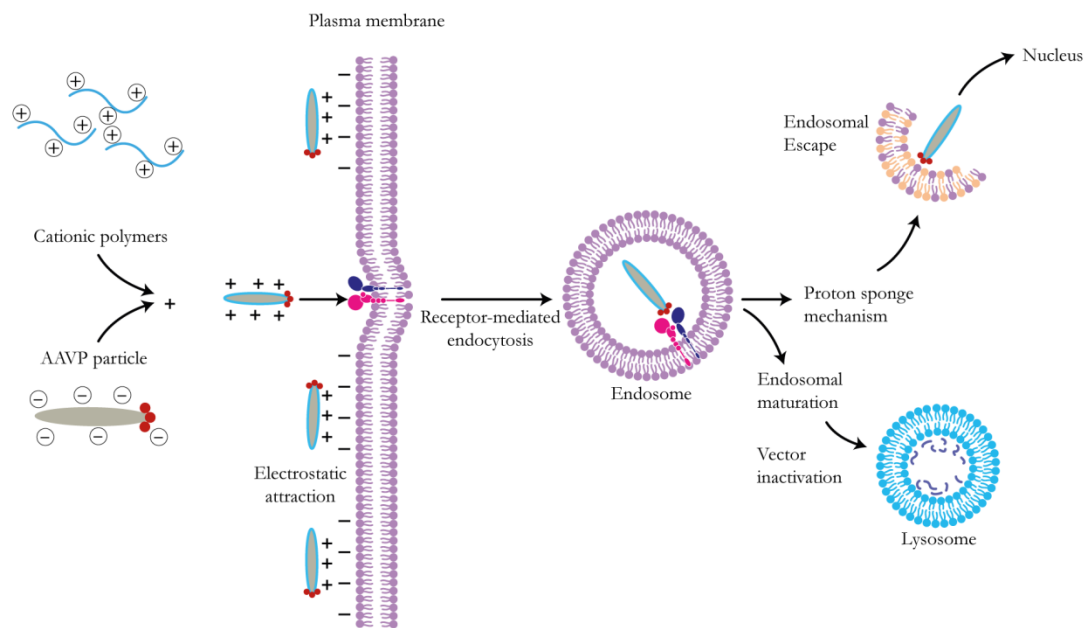
Figure 7.1: Schematic representation of the proposed pathway of the AAVP/polymer complex-mediated transduction. The polymer component of the hybrid vector mediates cell attachment via electrostatic attraction, in which the polymers generate positive charge of bacteriophage capsid. Following receptor-mediated endocytosis and entrapment in acidic endosome, the vector escape is promoted by the proton sponge mechanism mediated by cationic polymers.

Different and promising strategies have been proposed in this study. We have developed these new methodologies as promising tools that gene delivery with bacteriophage-based vector has evolved rapidly from bacteria to successful gene delivery to mammalian cells. Given that these different strategies demonstrated the promising improvement of AAVP-mediated gene expression in 2D and 3D cell culture models, these will be the likely candidates to be taken to *in vivo* studies. Furthermore, it can be hypothesized that combination of these strategies could further improve or may be significantly greater than a single strategy.

8. Biobliography

1. Cichon G, Schmidt HH, Benhidjeb T, et al. Intravenous administration of recombinant adenoviruses causes thrombocytopenia, anemia and erythroblastosis in rabbits. *J Gene Med* 1999; **1**(5): 360-71.
2. Salimzadeh L, Jaberipour M, Hosseini A, Ghaderi A. Non-viral transfection methods optimized for gene delivery to a lung cancer cell line. *Avicenna J Med Biotechnol* 2013; **5**(2): 68-77.
3. Luo D, Saltzman WM. Synthetic DNA delivery systems. *Nat Biotechnol* 2000; **18**(1): 33-7.
4. Muruve DA, Barnes MJ, Stillman IE, Libermann TA. Adenoviral gene therapy leads to rapid induction of multiple chemokines and acute neutrophil-dependent hepatic injury in vivo. *Hum Gene Ther* 1999; **10**(6): 965-76.
5. Buckley RH. Gene therapy for SCID--a complication after remarkable progress. *Lancet* 2002; **360**(9341): 1185-6.
6. Marshall E. Clinical research. Gene therapy a suspect in leukemia-like disease. *Science* 2002; **298**(5591): 34-5.
7. Romano G, Pacilio C, Giordano A. Gene transfer technology in therapy: current applications and future goals. *Stem Cells* 1999; **17**(4): 191-202.
8. Romano G, Pacilio C, Giordano A. Gene Transfer Technology in Therapy: Current Applications and Future Goals. *Oncologist* 1998; **3**(4): 225-36.
9. Yang NS, Sun WH, McCabe D. Developing particle-mediated gene-transfer technology for research into gene therapy of cancer. *Mol Med Today* 1996; **2**(11): 476-81.
10. Bouard D, Alazard-Dany D, Cosset FL. Viral vectors: from virology to transgene expression. *Br J Pharmacol* 2009; **157**(2): 153-65.
11. Mizuguchi H, Hayakawa T. Targeted adenovirus vectors. *Hum Gene Ther* 2004; **15**(11): 1034-44.
12. Muller OJ, Kaul F, Weitzman MD, et al. Random peptide libraries displayed on adeno-associated virus to select for targeted gene therapy vectors. *Nat Biotechnol* 2003; **21**(9): 1040-6.
13. Kamimura K, Suda T, Zhang G, Liu D. Advances in Gene Delivery Systems. *Pharmaceut Med* 2011; **25**(5): 293-306.
14. Barr JJ, Auro R, Furlan M, et al. Bacteriophage adhering to mucus provide a non-host-derived immunity. *Proc Natl Acad Sci U S A* 2013; **110**(26): 10771-6.
15. McCarty DM, Ni TH, Muzyczka N. Analysis of mutations in adeno-associated virus Rep protein in vivo and in vitro. *J Virol* 1992; **66**(7): 4050-7.
16. Im DS, Muzyczka N. Partial purification of adeno-associated virus Rep78, Rep52, and Rep40 and their biochemical characterization. *J Virol* 1992; **66**(2): 1119-28.
17. Muzyczka N. Use of adeno-associated virus as a general transduction vector for mammalian cells. *Curr Top Microbiol Immunol* 1992; **158**: 97-129.
18. Khan J, Wei JS, Ringner M, et al. Classification and diagnostic prediction of cancers using gene expression profiling and artificial neural networks. *Nat Med* 2001; **7**(6): 673-9.
19. Resnier P, David S, Lautram N, et al. EGFR siRNA lipid nanocapsules efficiently transfect glioma cells in vitro. *Int J Pharm* 2013; **454**(2): 748-55.
20. Li H, Chen L, Zhang A, et al. Silencing of IKKepsilon using siRNA inhibits proliferation and invasion of glioma cells in vitro and in vivo. *Int J Oncol* 2012; **41**(1): 169-78.
21. Huang S, Kamihira M. Development of hybrid viral vectors for gene therapy. *Biotechnology advances* 2013; **31**(2): 208-23.
22. Hajitou A, Rangel R, Trepel M, et al. Design and construction of targeted AAVP vectors for mammalian cell transduction. *Nature protocols* 2007; **2**(3): 523-31.
23. Larocca D, Jensen-Pergakes K, Burg MA, Baird A. Gene transfer using targeted filamentous bacteriophage. *Methods in molecular biology* 2002; **185**: 393-401.

24.   Larocca D, Witte A, Johnson W, Pierce GF, Baird A. Targeting bacteriophage to mammalian cell surface receptors for gene delivery. *Hum Gene Ther* 1998; **9**(16): 2393-9.

25.   Daya S, Berns KI. Gene therapy using adeno-associated virus vectors. *Clin Microbiol Rev* 2008; **21**(4): 583-93.

26.   Yuan B, Ran B, Wang S, Liu Z, Zheng Z, Chen H. siRNA directed against Livin inhibits tumor growth and induces apoptosis in human glioma cells. *J Neurooncol* 2012; **107**(1): 81-7.

27.   Wang J, Wang C, Meng Q, et al. siRNA targeting Notch-1 decreases glioma stem cell proliferation and tumor growth. *Mol Biol Rep* 2012; **39**(3): 2497-503.

28.   Akasaki Y, Kikuchi T, Irie M, et al. Cotransfection of Poly(I: C) and siRNA of IL-10 into fusions of dendritic and glioma cells enhances antitumor T helper type 1 induction in patients with glioma. *J Immunother* 2011; **34**(2): 121-8.

29.   Cameron BJ, Gerry AB, Dukes J, et al. Identification of a Titin-derived HLA-A1-presented peptide as a cross-reactive target for engineered MAGE A3-directed T cells. *Sci Transl Med* 2013; **5**(197): 197ra03.

30.   Levine PM, Craven TW, Bonneau R, Kirshenbaum K. Chemoselective fragment condensation between peptide and peptidomimetic oligomers. *Org Biomol Chem* 2013; **11**(25): 4142-6.

31.   Waehler R, Russell SJ, Curiel DT. Engineering targeted viral vectors for gene therapy. *Nature reviews Genetics* 2007; **8**(8): 573-87.

32.   Volpers C, Kochanek S. Adenoviral vectors for gene transfer and therapy. *J Gene Med* 2004; **6 Suppl 1**: S164-71.

33.   Wagner R, Wolff T, Herwig A, Pleschka S, Klenk HD. Interdependence of hemagglutinin glycosylation and neuraminidase as regulators of influenza virus growth: a study by reverse genetics. *J Virol* 2000; **74**(14): 6316-23.

34.   Jang JH, Schaffer DV, Shea LD. Engineering biomaterial systems to enhance viral vector gene delivery. *Mol Ther* 2011; **19**(8): 1407-15.

35.   Davidson BL, Stein CS, Heth JA, et al. Recombinant adeno-associated virus type 2, 4, and 5 vectors: transduction of variant cell types and regions in the mammalian central nervous system. *Proc Natl Acad Sci U S A* 2000; **97**(7): 3428-32.

36.   Maheshri N, Koerber JT, Kaspar BK, Schaffer DV. Directed evolution of adeno-associated virus yields enhanced gene delivery vectors. *Nature biotechnology* 2006; **24**(2): 198-204.

37.   Perabo L, Buning H, Kofler DM, et al. In vitro selection of viral vectors with modified tropism: the adeno-associated virus display. *Molecular therapy : the journal of the American Society of Gene Therapy* 2003; **8**(1): 151-7.

38.   ZengHui X, XiuMei Z, WenFang S, QiJun Q. Capsid modification of adeno-associated virus and tumor targeting gene therapy. *Chinese Science Bulletin* 2008; **53**(24): 3790-7.

39.   Barquinero J, Eixarch H, Perez-Melgosa M. Retroviral vectors: new applications for an old tool. *Gene Ther* 2004; **11 Suppl 1**: S3-9.

40.   Daniel R, Smith JA. Integration site selection by retroviral vectors: molecular mechanism and clinical consequences. *Hum Gene Ther* 2008; **19**(6): 557-68.

41.   Kay MA, Glorioso JC, Naldini L. Viral vectors for gene therapy: the art of turning infectious agents into vehicles of therapeutics. *Nat Med* 2001; **7**(1): 33-40.

42.   Sheridan C. Gene therapy finds its niche. *Nature biotechnology* 2011; **29**(2): 121-8.

43.   Schultz BR, Chamberlain JS. Recombinant adeno-associated virus transduction and integration. *Molecular therapy : the journal of the American Society of Gene Therapy* 2008; **16**(7): 1189-99.

44.   Graham FL, van der Eb AJ. Transformation of rat cells by DNA of human adenovirus 5. *Virology* 1973; **54**(2): 536-9.

45.   Felgner PL. Particulate systems and polymers for in vitro and in vivo delivery of polynucleotides. *Advanced Drug Delivery Reviews* 1990; **5**(3): 163-87.

46.   Sarbolouki M, Sadeghizadeh M, Mohammad M, Karami A, Lohrasbi T. Dendrosomes: a novel family of vehicles for transfection and therapy. *Chemical technology and biotechnology* 2000; **75**(10): 919-22.

47.   Park TG, Jeong JH, Kim SW. Current status of polymeric gene delivery systems. *Adv Drug Deliv Rev* 2006; **58**(4): 467-86.

48.   Dash PR, Read ML, Barrett LB, Wolfert MA, Seymour LW. Factors affecting blood clearance and in vivo distribution of polyelectrolyte complexes for gene delivery. *Gene Ther* 1999; **6**(4): 643-50.

49.   Liu G, Molas M, Grossmann GA, et al. Biological properties of poly-L-lysine-DNA complexes generated by cooperative binding of the polycation. *J Biol Chem* 2001; **276**(37): 34379-87.

50.   Kichler A. Gene transfer with modified polyethylenimines. *J Gene Med* 2004; **6 Suppl 1**: S3-10.

51.   Chaney WG, Howard DR, Pollard JW, Sallustio S, Stanley P. DNA transfection of Mammalian cells using polybrene. *Methods Mol Biol* 1988; **4**: 363-70.

52.   Haensler J, Szoka FC, Jr. Polyamidoamine cascade polymers mediate efficient transfection of cells in culture. *Bioconjug Chem* 1993; **4**(5): 372-9.

53.   Kukowska-Latallo JF, Bielinska AU, Johnson J, Spindler R, Tomalia DA, Baker JR, Jr. Efficient transfer of genetic material into mammalian cells using Starburst polyamidoamine dendrimers. *Proc Natl Acad Sci U S A* 1996; **93**(10): 4897-902.

54.   Rosenkranz AA, Yachmenev SV, Jans DA, et al. Receptor-mediated endocytosis and nuclear transport of a transfecting DNA construct. *Exp Cell Res* 1992; **199**(2): 323-9.

55.   Kabanov AV, Kabanov VA. DNA complexes with polycations for the delivery of genetic material into cells. *Bioconjug Chem* 1995; **6**(1): 7-20.

56.   Ogris M, Brunner S, Schuller S, Kircheis R, Wagner E. PEGylated DNA/transferrin-PEI complexes: reduced interaction with blood components, extended circulation in blood and potential for systemic gene delivery. *Gene Ther* 1999; **6**(4): 595-605.

57.   Plank C, Mechtler K, Szoka FC, Jr., Wagner E. Activation of the complement system by synthetic DNA complexes: a potential barrier for intravenous gene delivery. *Hum Gene Ther* 1996; **7**(12): 1437-46.

58.   Ward CM, Read ML, Seymour LW. Systemic circulation of poly(L-lysine)/DNA vectors is influenced by polycation molecular weight and type of DNA: differential circulation in mice and rats and the implications for human gene therapy. *Blood* 2001; **97**(8): 2221-9.

59.   Choi YH, Liu F, Kim JS, Choi YK, Park JS, Kim SW. Polyethylene glycol-grafted poly-L-lysine as polymeric gene carrier. *J Control Release* 1998; **54**(1): 39-48.

60.   Kunath K, von Harpe A, Petersen H, et al. The structure of PEG-modified poly(ethylene imines) influences biodistribution and pharmacokinetics of their complexes with NF-kappaB decoy in mice. *Pharm Res* 2002; **19**(6): 810-7.

61.   Kwoh DY, Coffin CC, Lollo CP, et al. Stabilization of poly-L-lysine/DNA polyplexes for in vivo gene delivery to the liver. *Biochim Biophys Acta* 1999; **1444**(2): 171-90.

62.   Merdan T, Callahan J, Petersen H, et al. Pegylated polyethylenimine-Fab' antibody fragment conjugates for targeted gene delivery to human ovarian carcinoma cells. *Bioconjug Chem* 2003; **14**(5): 989-96.

63.   Ogris M, Walker G, Blessing T, Kircheis R, Wolschek M, Wagner E. Tumor-targeted gene therapy: strategies for the preparation of ligand-polyethylene glycol-polyethylenimine/DNA complexes. *J Control Release* 2003; **91**(1-2): 173-81.

64.   Toncheva V, Wolfert MA, Dash PR, et al. Novel vectors for gene delivery formed by self-assembly of DNA with poly(L-lysine) grafted with hydrophilic polymers. *Biochim Biophys Acta* 1998; **1380**(3): 354-68.

65.   Erbacher P, Bettinger T, Belguise-Valladier P, et al. Transfection and physical properties of various saccharide, poly(ethylene glycol), and antibody-derivatized polyethylenimines (PEI). *J Gene Med* 1999; **1**(3): 210-22.

66.   Oupicky D, Ogris M, Howard KA, Dash PR, Ulbrich K, Seymour LW. Importance of lateral and steric stabilization of polyelectrolyte gene delivery vectors for extended systemic circulation. *Mol Ther* 2002; **5**(4): 463-72.

67.   Hashida M, Takemura S, Nishikawa M, Takakura Y. Targeted delivery of plasmid DNA complexed with galactosylated poly(L-lysine). *J Control Release* 1998; **53**(1-3): 301-10.

68.   Nishikawa M, Takemura S, Takakura Y, Hashida M. Targeted delivery of plasmid DNA to hepatocytes in vivo: optimization of the pharmacokinetics of plasmid DNA/galactosylated poly(L-lysine) complexes by controlling their physicochemical properties. *J Pharmacol Exp Ther* 1998; **287**(1): 408-15.

69.   Wagner E, Plank C, Zatloukal K, Cotten M, Birnstiel ML. Influenza virus hemagglutinin HA-2 N-terminal fusogenic peptides augment gene transfer by transferrin-polylysine-DNA complexes: toward a synthetic virus-like gene-transfer vehicle. *Proc Natl Acad Sci U S A* 1992; **89**(17): 7934-8.

70.   Suh W, Chung JK, Park SH, Kim SW. Anti-JL1 antibody-conjugated poly (L-lysine) for targeted gene delivery to leukemia T cells. *J Control Release* 2001; **72**(1-3): 171-8.

71.   Zhang L, Granick S. How to stabilize phospholipid liposomes (using nanoparticles). *Nano Lett* 2006; **6**(4): 694-8.

72.   Cortesi R, Esposito E, Gambarin S, Telloli P, Menegatti E, Nastruzzi C. Preparation of liposomes by reverse-phase evaporation using alternative organic solvents. *J Microencapsul* 1999; **16**(2): 251-6.

73.   Simberg D, Weisman S, Talmon Y, Barenholz Y. DOTAP (and other cationic lipids): chemistry, biophysics, and transfection. *Crit Rev Ther Drug Carrier Syst* 2004; **21**(4): 257-317.

74.   Masotti A, Mossa G, Cametti C, et al. Comparison of different commercially available cationic liposome-DNA lipoplexes: Parameters influencing toxicity and transfection efficiency. *Colloids Surf B Biointerfaces* 2009; **68**(2): 136-44.

75.   Zhou X, Huang L. DNA transfection mediated by cationic liposomes containing lipopolylysine: characterization and mechanism of action. *Biochim Biophys Acta* 1994; **1189**(2): 195-203.

76.   Liu D, Ren T, Gao X. Cationic transfection lipids. *Curr Med Chem* 2003; **10**(14): 1307-15.

77.   Montier T, Benvegnu T, Jaffres PA, Yaouanc JJ, Lehn P. Progress in cationic lipid-mediated gene transfection: a series of bio-inspired lipids as an example. *Curr Gene Ther* 2008; **8**(5): 296-312.

78.   Pack DW, Hoffman AS, Pun S, Stayton PS. Design and development of polymers for gene delivery. *Nature reviews Drug discovery* 2005; **4**(7): 581-93.

79.   Marjuki H, Alam MI, Ehrhardt C, et al. Membrane accumulation of influenza A virus hemagglutinin triggers nuclear export of the viral genome via protein kinase Calpha-mediated activation of ERK signaling. *J Biol Chem* 2006; **281**(24): 16707-15.

80.   Taxman DJ, Lee ES, Wojchowski DM. Receptor-targeted transfection using stable maleimido-transferrin/thio-poly-L-lysine conjugates. *Anal Biochem* 1993; **213**(1): 97-103.

81.   Klenk HD, Wagner R, Heuer D, Wolff T. Importance of hemagglutinin glycosylation for the biological functions of influenza virus. *Virus Res* 2002; **82**(1-2): 73-5.

82.   Choi HS, Liu W, Misra P, et al. Renal clearance of quantum dots. *Nat Biotechnol* 2007; **25**(10): 1165-70.

83.   Deen WM, Lazzara MJ, Myers BD. Structural determinants of glomerular permeability. *Am J Physiol Renal Physiol* 2001; **281**(4): F579-96.

84.   Mahato RI, Takakura Y, Hashida M. Nonviral vectors for in vivo gene delivery: physicochemical and pharmacokinetic considerations. *Crit Rev Ther Drug Carrier Syst* 1997; **14**(2): 133-72.

85.   Pecot CV, Calin GA, Coleman RL, Lopez-Berestein G, Sood AK. RNA interference in the clinic: challenges and future directions. *Nature reviews Cancer* 2011; **11**(1): 59-67.

86.   Kuntz E, Kuntz H-D. Hepatology: principles and practice: history, morphology, biochemistry, diagnostic, clinic, therapy. Heidelberg: Springer; 2006.

87.   Brannon-Peppas L, Blanchette JO. Nanoparticle and targeted systems for cancer therapy. *Adv Drug Deliv Rev* 2004; **56**(11): 1649-59.

88.   Li SD, Huang L. Nanoparticles evading the reticuloendothelial system: role of the supported bilayer. *Biochim Biophys Acta* 2009; **1788**(10): 2259-66.

89.   Csortos C, Kolosova I, Verin AD. Regulation of vascular endothelial cell barrier function and cytoskeleton structure by protein phosphatases of the PPP family. *Am J Physiol Lung Cell Mol Physiol* 2007; **293**(4): L843-54.

90.   Longmire M, Choyke PL, Kobayashi H. Clearance properties of nano-sized particles and molecules as imaging agents: considerations and caveats. *Nanomedicine (Lond)* 2008; **3**(5): 703-17.

91.   Sarin H. Physiologic upper limits of pore size of different blood capillary types and another perspective on the dual pore theory of microvascular permeability. *J Angiogenes Res* 2010; **2**: 14.

92.   Torchilin VP. Drug targeting. *Eur J Pharm Sci* 2000; **11 Suppl 2**: S81-91.

93.   Aird WC. Phenotypic heterogeneity of the endothelium: I. Structure, function, and mechanisms. *Circ Res* 2007; **100**(2): 158-73.

94.   Yuan F, Dellian M, Fukumura D, et al. Vascular permeability in a human tumor xenograft: molecular size dependence and cutoff size. *Cancer Res* 1995; **55**(17): 3752-6.

95.   Yuan F, Leunig M, Huang SK, Berk DA, Papahadjopoulos D, Jain RK. Microvascular permeability and interstitial penetration of sterically stabilized (stealth) liposomes in a human tumor xenograft. *Cancer Res* 1994; **54**(13): 3352-6.

96.   Hobbs SK, Monsky WL, Yuan F, et al. Regulation of transport pathways in tumor vessels: role of tumor type and microenvironment. *Proc Natl Acad Sci U S A* 1998; **95**(8): 4607-12.

97.   Cabral H, Matsumoto Y, Mizuno K, et al. Accumulation of sub-100 nm polymeric micelles in poorly permeable tumours depends on size. *Nat Nanotechnol* 2011; **6**(12): 815-23.

98.   Chauhan VP, Stylianopoulos T, Martin JD, et al. Normalization of tumour blood vessels improves the delivery of nanomedicines in a size-dependent manner. *Nat Nanotechnol* 2012; **7**(6): 383-8.

99.   Jacobetz MA, Chan DS, Neesse A, et al. Hyaluronan impairs vascular function and drug delivery in a mouse model of pancreatic cancer. *Gut* 2013; **62**(1): 112-20.

100.   Pardridge WM. Blood-brain barrier delivery. *Drug Discov Today* 2007; **12**(1-2): 54-61.

101.   Banks WA. Characteristics of compounds that cross the blood-brain barrier. *BMC Neurol* 2009; **9 Suppl 1**: S3.

102.   Abbott NJ, Ronnback L, Hansson E. Astrocyte-endothelial interactions at the blood-brain barrier. *Nature reviews Neuroscience* 2006; **7**(1): 41-53.

103.   Pardridge WM. Blood-brain barrier delivery of protein and non-viral gene therapeutics with molecular Trojan horses. *J Control Release* 2007; **122**(3): 345-8.

104.   Herve F, Ghinea N, Scherrmann JM. CNS delivery via adsorptive transcytosis. *AAPS J* 2008; **10**(3): 455-72.

105.   Whitehead KA, Langer R, Anderson DG. Knocking down barriers: advances in siRNA delivery. *Nat Rev Drug Discov* 2009; **8**(2): 129-38.

106.   Stylianopoulos T, Poh MZ, Insin N, et al. Diffusion of particles in the extracellular matrix: the effect of repulsive electrostatic interactions. *Biophys J* 2010; **99**(5): 1342-9.

107.   Jain RK. Transport of molecules in the tumor interstitium: a review. *Cancer Res* 1987; **47**(12): 3039-51.

108.   Waite CL, Roth CM. Nanoscale drug delivery systems for enhanced drug penetration into solid tumors: current progress and opportunities. *Crit Rev Biomed Eng* 2012; **40**(1): 21-41.

109.   Chauhan VP, Jain RK. Strategies for advancing cancer nanomedicine. *Nat Mater* 2013; **12**(11): 958-62.

110.   Leopold PL, Crystal RG. Intracellular trafficking of adenovirus: many means to many ends. *Adv Drug Deliv Rev* 2007; **59**(8): 810-21.

111.   Nel AE, Madler L, Velegol D, et al. Understanding biophysicochemical interactions at the nano-bio interface. *Nature materials* 2009; **8**(7): 543-57.

112.   Fleck CC, Netz RR. Electrostatic colloid-membrane binding. *Europhys Lett* 2004; **67**: 314-20.

113.   Chithrani BD, Ghazani AA, Chan WC. Determining the size and shape dependence of gold nanoparticle uptake into mammalian cells. *Nano Lett* 2006; **6**(4): 662-8.

114.   Decuzzi P, Ferrari M. The role of specific and non-specific interactions in receptor-mediated endocytosis of nanoparticles. *Biomaterials* 2007; **28**(18): 2915-22.

115.   Gao H, Shi W, Freund LB. Mechanics of receptor-mediated endocytosis. *Proc Natl Acad Sci U S A* 2005; **102**(27): 9469-74.

116.   Leroueil PR, Berry SA, Duthie K, et al. Wide varieties of cationic nanoparticles induce defects in supported lipid bilayers. *Nano Lett* 2008; **8**(2): 420-4.

117.   Daniels TR, Delgado T, Rodriguez JA, Helguera G, Penichet ML. The transferrin receptor part I: Biology and targeting with cytotoxic antibodies for the treatment of cancer. *Clinical immunology* 2006; **121**(2): 144-58.

118.   Dass CR, Choong PF. Selective gene delivery for cancer therapy using cationic liposomes: in vivo proof of applicability. *J Control Release* 2006; **113**(2): 155-63.

119.   de Bruin K, Ruthardt N, von Gersdorff K, et al. Cellular dynamics of EGF receptor-targeted synthetic viruses. *Mol Ther* 2007; **15**(7): 1297-305.

120.   Garanger E, Boturyn D, Dumy P. Tumor targeting with RGD peptide ligands-design of new molecular conjugates for imaging and therapy of cancers. *Anticancer Agents Med Chem* 2007; **7**(5): 552-8.

121.   Hilgenbrink AR, Low PS. Folate receptor-mediated drug targeting: from therapeutics to diagnostics. *J Pharm Sci* 2005; **94**(10): 2135-46.

122.   Xu L, Pirollo KF, Tang WH, Rait A, Chang EH. Transferrin-liposome-mediated systemic p53 gene therapy in combination with radiation results in regression of human head and neck cancer xenografts. *Hum Gene Ther* 1999; **10**(18): 2941-52.

123.   Luhmann T, Rimann M, Bittermann AG, Hall H. Cellular uptake and intracellular pathways of PLL-g-PEG-DNA nanoparticles. *Bioconjug Chem* 2008; **19**(9): 1907-16.

124.   Marie R, Beech JP, Voros J, Tegenfeldt JO, Hook F. Use of PLL-g-PEG in micro-fluidic devices for localizing selective and specific protein binding. *Langmuir* 2006; **22**(24): 10103-8.

125.   Katakura H, Harada A, Kataoka K, et al. Improvement of retroviral vectors by coating with poly(ethylene glycol)-poly(L-lysine) block copolymer (PEG-PLL). *J Gene Med* 2004; **6**(4): 471-7.

126.   Wang X, Li J, He J, Liu J. Synthesis, properties and biological activity of organotitanium substituted heteropolytungstates. *Met Based Drugs* 2001; **8**(4): 179-82.

127.   Petros RA, DeSimone JM. Strategies in the design of nanoparticles for therapeutic applications. *Nature reviews Drug discovery* 2010; **9**(8): 615-27.

128.   Dimitrov DS. Virus entry: molecular mechanisms and biomedical applications. *Nature reviews Microbiology* 2004; **2**(2): 109-22.

129.   Kielian M, Rey FA. Virus membrane-fusion proteins: more than one way to make a hairpin. *Nat Rev Microbiol* 2006; **4**(1): 67-76.

130.   Cho YW, Kim JD, Park K. Polycation gene delivery systems: escape from endosomes to cytosol. *J Pharm Pharmacol* 2003; **55**(6): 721-34.

131.   Sasaki K, Kogure K, Chaki S, et al. An artificial virus-like nano carrier system: enhanced endosomal escape of nanoparticles via synergistic action of pH-sensitive fusogenic peptide derivatives. *Anal Bioanal Chem* 2008; **391**(8): 2717-27.

132. Moore NM, Sheppard CL, Barbour TR, Sakiyama-Elbert SE. The effect of endosomal escape peptides on in vitro gene delivery of polyethylene glycol-based vehicles. *J Gene Med* 2008; **10**(10): 1134-49.

133. Hurdle JG, O'Neill AJ, Chopra I, Lee RE. Targeting bacterial membrane function: an underexploited mechanism for treating persistent infections. *Nature reviews Microbiology* 2011; **9**(1): 62-75.

134. Stewart M. Molecular mechanism of the nuclear protein import cycle. *Nat Rev Mol Cell Biol* 2007; **8**(3): 195-208.

135. Collas P, Husebye H, Alestrom P. The nuclear localization sequence of the SV40 T antigen promotes transgene uptake and expression in zebrafish embryo nuclei. *Transgenic Res* 1996; **5**(6): 451-8.

136. Subramanian A, Ranganathan P, Diamond SL. Nuclear targeting peptide scaffolds for lipofection of nondividing mammalian cells. *Nat Biotechnol* 1999; **17**(9): 873-7.

137. Badiga AV, Chetty C, Kesanakurti D, et al. MMP-2 siRNA inhibits radiation-enhanced invasiveness in glioma cells. *PLoS One* 2011; **6**(6): e20614.

138. Zhao ZK, Jiang ZM, Liu XZ, Chen YT, Jia WJ. [Study on reversion of malignant phenotype of glioma by siRNA targeting p75 neurotrophin receptor]. *Zhonghua Bing Li Xue Za Zhi* 2010; **39**(6): 400-4.

139. Lang FF, Yung WK, Sawaya R, Tofilon PJ. Adenovirus-mediated p53 gene therapy for human gliomas. *Neurosurgery* 1999; **45**(5): 1093-104.

140. Zhang B, Feng X, Wang J, Xu X, Lin N, Liu H. Combined antitumor effect of Ad-bFGF-siRNA and Ad-Vpr on the growth of xenograft glioma in nude mouse model. *Pathol Oncol Res* 2011; **17**(2): 237-42.

141. Pang JC, Li KK, Lau KM, et al. KIAA0495/PDAM is frequently downregulated in oligodendroglial tumors and its knockdown by siRNA induces cisplatin resistance in glioma cells. *Brain Pathol* 2010; **20**(6): 1021-32.

142. Brummelkamp TR, Bernards R, Agami R. Stable suppression of tumorigenicity by virus-mediated RNA interference. *Cancer Cell* 2002; **2**(3): 243-7.

143. Crnkovic-Mertens I, Hoppe-Seyler F, Butz K. Induction of apoptosis in tumor cells by siRNA-mediated silencing of the livin/ML-IAP/KIAP gene. *Oncogene* 2003; **22**(51): 8330-6.

144. Xu G, McLeod HL. Strategies for enzyme/prodrug cancer therapy. *Clin Cancer Res* 2001; **7**(11): 3314-24.

145. Waite CL, Roth CM. PAMAM-RGD conjugates enhance siRNA delivery through a multicellular spheroid model of malignant glioma. *Bioconjug Chem* 2009; **20**(10): 1908-16.

146. Han L, Zhang AL, Xu P, et al. Combination gene therapy with PTEN and EGFR siRNA suppresses U251 malignant glioma cell growth in vitro and in vivo. *Med Oncol* 2010; **27**(3): 843-52.

147. Tritz R, Mueller BM, Hickey MJ, et al. siRNA Down-regulation of the PATZ1 Gene in Human Glioma Cells Increases Their Sensitivity to Apoptotic Stimuli. *Cancer Ther* 2008; **6**(B): 865-76.

148. Pu P, Zhang Z, Kang C, et al. Downregulation of Wnt2 and beta-catenin by siRNA suppresses malignant glioma cell growth. *Cancer Gene Ther* 2009; **16**(4): 351-61.

149. Danhier F, Le Breton A, Preat V. RGD-based strategies to target alpha(v) beta(3) integrin in cancer therapy and diagnosis. *Molecular pharmaceutics* 2012; **9**(11): 2961-73.

150. George AJ, Lee L, Pitzalis C. Isolating ligands specific for human vasculature using in vivo phage selection. *Trends Biotechnol* 2003; **21**(5): 199-203.

151. Zhang Q, Shi Y, Niu Q. [Selection of bax siRNA sequences and its influence on aluminum induced glioma cell apoptosis]. *Wei Sheng Yan Jiu* 2008; **37**(3): 269-73.

152. Zhao P, Wang C, Fu Z, et al. Lentiviral vector mediated siRNA knock-down of hTERT results in diminished capacity in invasiveness and in vivo growth of human glioma cells in a telomere length-independent manner. *Int J Oncol* 2007; **31**(2): 361-8.

153.   Yang XY, Lai XG, Zhang Y, Pei JM, Yang AG, Zhou SS. [siRNA-mediated silencing of ClC-2 gene inhibits proliferation of human U-87 glioma cells]. *Ai Zheng* 2006; **25**(7): 805-10.

154.   Gondi CS, Lakka SS, Dinh DH, Olivero WC, Gujrati M, Rao JS. Downregulation of uPA, uPAR and MMP-9 using small, interfering, hairpin RNA (siRNA) inhibits glioma cell invasion, angiogenesis and tumor growth. *Neuron Glia Biol* 2004; **1**(2): 165-76.

155.   Pu P, Kang C, Zhang Z, Liu X, Jiang H. Downregulation of PIK3CB by siRNA suppresses malignant glioma cell growth in vitro and in vivo. *Technol Cancer Res Treat* 2006; **5**(3): 271-80.

156.   Verrax J, Defresne F, Lair F, et al. Delivery of soluble VEGF receptor 1 (sFlt1) by gene electrotransfer as a new antiangiogenic cancer therapy. *Mol Pharm* 2011; **8**(3): 701-8.

157.   Kang CS, Pu PY, Li YH, et al. An in vitro study on the suppressive effect of glioma cell growth induced by plasmid-based small interference RNA (siRNA) targeting human epidermal growth factor receptor. *J Neurooncol* 2005; **74**(3): 267-73.

158.   Thorpe PE, Chaplin DJ, Blakey DC. The first international conference on vascular targeting: meeting overview. *Cancer Res* 2003; **63**(5): 1144-7.

159.   Zitzmann S, Ehemann V, Schwab M. Arginine-glycine-aspartic acid (RGD)-peptide binds to both tumor and tumor-endothelial cells in vivo. *Cancer Res* 2002; **62**(18): 5139-43.

160.   Daniels TR, Delgado T, Helguera G, Penichet ML. The transferrin receptor part II: targeted delivery of therapeutic agents into cancer cells. *Clinical immunology* 2006; **121**(2): 159-76.

161.   Misra R, Acharya S, Sahoo SK. Cancer nanotechnology: application of nanotechnology in cancer therapy. *Drug Discov Today* 2010; **15**(19-20): 842-50.

162.   Westphal EM, Ge J, Catchpole JR, Ford M, Kenney SC. The nitroreductase/CB1954 combination in Epstein-Barr virus-positive B-cell lines: induction of bystander killing in vitro and in vivo. *Cancer Gene Ther* 2000; **7**(1): 97-106.

163.   Byrne JD, Betancourt T, Brannon-Peppas L. Active targeting schemes for nanoparticle systems in cancer therapeutics. *Adv Drug Deliv Rev* 2008; **60**(15): 1615-26.

164.   Temming K, Schiffelers RM, Molema G, Kok RJ. RGD-based strategies for selective delivery of therapeutics and imaging agents to the tumour vasculature. *Drug Resist Updat* 2005; **8**(6): 381-402.

165.   Maeda H, Sawa T, Konno T. Mechanism of tumor-targeted delivery of macromolecular drugs, including the EPR effect in solid tumor and clinical overview of the prototype polymeric drug SMANCS. *J Control Release* 2001; **74**(1-3): 47-61.

166.   Malam Y, Loizidou M, Seifalian AM. Liposomes and nanoparticles: nanosized vehicles for drug delivery in cancer. *Trends Pharmacol Sci* 2009; **30**(11): 592-9.

167.   Izawa JI, Sweeney P, Perrotte P, et al. Inhibition of tumorigenicity and metastasis of human bladder cancer growing in athymic mice by interferon-beta gene therapy results partially from various antiangiogenic effects including endothelial cell apoptosis. *Clin Cancer Res* 2002; **8**(4): 1258-70.

168.   Smith GP, Petrenko VA. Phage Display. *Chem Rev* 1997; **97**(2): 391-410.

169.   Paschke M. Phage display systems and their applications. *Appl Microbiol Biotechnol* 2006; **70**(1): 2-11.

170.   Tonikian R, Zhang Y, Boone C, Sidhu SS. Identifying specificity profiles for peptide recognition modules from phage-displayed peptide libraries. *Nat Protoc* 2007; **2**(6): 1368-86.

171.   Hajitou A, Trepel M, Lilley CE, et al. A hybrid vector for ligand-directed tumor targeting and molecular imaging. *Cell* 2006; **125**(2): 385-98.

172.   Hajitou A, Lev DC, Hannay JA, et al. A preclinical model for predicting drug response in soft-tissue sarcoma with targeted AAVP molecular imaging. *Proc Natl Acad Sci U S A* 2008; **105**(11): 4471-6.

173.   Paoloni MC, Tandle A, Mazcko C, et al. Launching a novel preclinical infrastructure: comparative oncology trials consortium directed therapeutic targeting of TNFalpha to cancer vasculature. *PLoS One* 2009; **4**(3): e4972.

174. Trepel M, Stoneham CA, Eleftherohorinou H, et al. A heterotypic bystander effect for tumor cell killing after adeno-associated virus/phage-mediated, vascular-targeted suicide gene transfer. *Mol Cancer Ther* 2009; **8**(8): 2383-91.

175. Villa-Diaz LG, Garcia-Perez JL, Krebsbach PH. Enhanced transfection efficiency of human embryonic stem cells by the incorporation of DNA liposomes in extracellular matrix. *Stem Cells Dev* 2010; **19**(12): 1949-57.

176. Baird A. Gene transfer into Mammalian cells using targeted filamentous bacteriophage. *Cold Spring Harbor protocols* 2011; **2011**(8): 950-7.

177. Weiss GA, Wells JA, Sidhu SS. Mutational analysis of the major coat protein of M13 identifies residues that control protein display. *Protein science : a publication of the Protein Society* 2000; **9**(4): 647-54.

178. Stoneham CA, Hollinshead M, Hajitou A. Clathrin-mediated endocytosis and subsequent endo-lysosomal trafficking of adeno-associated virus/phage. *The Journal of biological chemistry* 2012; **287**(43): 35849-59.

179. Longstreth WT, Jr., Kronmal RA, Thompson JL, et al. Amino terminal pro-B-type natriuretic peptide, secondary stroke prevention, and choice of antithrombotic therapy. *Stroke* 2013; **44**(3): 714-9.

180. Shoji-Kawata S, Sumpter R, Leveno M, et al. Identification of a candidate therapeutic autophagy-inducing peptide. *Nature* 2013; **494**(7436): 201-6.

181. He CX, Tabata Y, Gao JQ. Non-viral gene delivery carrier and its three-dimensional transfection system. *Int J Pharm* 2010; **386**(1-2): 232-42.

182. Kia A, Przystal JM, Nianiaris N, Mazarakis ND, Mintz PJ, Hajitou A. Dual systemic tumor targeting with ligand-directed phage and Grp78 promoter induces tumor regression. *Mol Cancer Ther* 2012; **11**(12): 2566-77.

183. Kia A, Yata T, Hajji N, Hajitou A. Inhibition of histone deacetylation and DNA methylation improves gene expression mediated by the adeno-associated virus/phage in cancer cells. *Viruses* 2013; **5**(10): 2561-72.

184. Schneider-Schaulies J. Cellular receptors for viruses: links to tropism and pathogenesis. *J Gen Virol* 2000; **81**(Pt 6): 1413-29.

185. Larocca D, Kassner PD, Witte A, Ladner RC, Pierce GF, Baird A. Gene transfer to mammalian cells using genetically targeted filamentous bacteriophage. *FASEB journal : official publication of the Federation of American Societies for Experimental Biology* 1999; **13**(6): 727-34.

186. Ruoslahti E, Bhatia SN, Sailor MJ. Targeting of drugs and nanoparticles to tumors. *J Cell Biol* 2010; **188**(6): 759-68.

187. Bella J, Humphries MJ. Calpha-H...O = C hydrogen bonds contribute to the specificity of RGD cell-adhesion interactions. *BMC Struct Biol* 2005; **5**: 4.

188. Hemminga MA, Vos WL, Nazarov PV, et al. Viruses: incredible nanomachines. New advances with filamentous phages. *Eur Biophys J* 2010; **39**(4): 541-50.

189. Chilton JM, Le Doux JM. Complexation of retroviruses with polymers significantly increases the number of genes transferred to murine embryonic stem cells, but does not raise transgene expression levels. *Biotechnol Appl Biochem* 2008; **51**(Pt 3): 141-51.

190. Fasbender A, Zabner J, Chillon M, et al. Complexes of adenovirus with polycationic polymers and cationic lipids increase the efficiency of gene transfer in vitro and in vivo. *J Biol Chem* 1997; **272**(10): 6479-89.

191. Hsu PY, Yang YW. Effect of polyethylenimine on recombinant adeno-associated virus mediated insulin gene therapy. *J Gene Med* 2005; **7**(10): 1311-21.

192. Landazuri N, Krishna D, Gupta M, Le Doux JM. Retrovirus-polymer complexes: study of the factors affecting the dose response of transduction. *Biotechnol Prog* 2007; **23**(2): 480-7.

193. Lee JH, Zabner J, Welsh MJ. Delivery of an adenovirus vector in a calcium phosphate coprecipitate enhances the therapeutic index of gene transfer to airway epithelia. *Hum Gene Ther* 1999; **10**(4): 603-13.

194.   Morling FJ, Russell SJ. Enhanced transduction efficiency of retroviral vectors coprecipitated with calcium phosphate. *Gene Ther* 1995; **2**(7): 504-8.

195.   Sakoda T, Kasahara N, Kedes L, Ohyanagi M. Calcium phosphate coprecipitation greatly enhances transduction of cardiac myocytes and vascular smooth muscle cells by lentivirus vectors. *Exp Clin Cardiol* 2007; **12**(3): 133-8.

196.   Walters RW, Duan D, Engelhardt JF, Welsh MJ. Incorporation of adeno-associated virus in a calcium phosphate coprecipitate improves gene transfer to airway epithelia in vitro and in vivo. *J Virol* 2000; **74**(1): 535-40.

197.   Yang YW, Chao CK. Incorporation of calcium phosphate enhances recombinant adeno-associated virus-mediated gene therapy in diabetic mice. *J Gene Med* 2003; **5**(5): 417-24.

198.   Fleck C, Netz R. Electrostatic colloid-membrane binding *Europhys Lett* 2004; **67**: 314.

199.   Alberts B, Johnson A, Lewis J, Raff M, Roberts K, Walter P. Molecular Biology of the Cell. 4 ed. New York: Garland Science; 2002.

200.   Hong S, Leroueil PR, Janus EK, et al. Interaction of polycationic polymers with supported lipid bilayers and cells: nanoscale hole formation and enhanced membrane permeability. *Bioconjug Chem* 2006; **17**(3): 728-34.

201.   Parimi S, Barnes TJ, Prestidge CA. PAMAM dendrimer interactions with supported lipid bilayers: a kinetic and mechanistic investigation. *Langmuir* 2008; **24**(23): 13532-9.

202.   Zhang ZY, Smith BD. High-generation polycationic dendrimers are unusually effective at disrupting anionic vesicles: membrane bending model. *Bioconjug Chem* 2000; **11**(6): 805-14.

203.   Fernandez CA, Rice KG. Engineered nanoscaled polyplex gene delivery systems. *Mol Pharm* 2009; **6**(5): 1277-89.

204.   Nichols BJ, Lippincott-Schwartz J. Endocytosis without clathrin coats. *Trends Cell Biol* 2001; **11**(10): 406-12.

205.   Swanson JA, Watts C. Macropinocytosis. *Trends Cell Biol* 1995; **5**(11): 424-8.

206.   Varga CM, Wickham TJ, Lauffenburger DA. Receptor-mediated targeting of gene delivery vectors: insights from molecular mechanisms for improved vehicle design. *Biotechnol Bioeng* 2000; **70**(6): 593-605.

207.   Ziello JE, Huang Y, Jovin IS. Cellular endocytosis and gene delivery. *Mol Med* 2010; **16**(5-6): 222-9.

208.   Liu J, Bauer H, Callahan J, Kopeckova P, Pan H, Kopecek J. Endocytic uptake of a large array of HPMA copolymers: Elucidation into the dependence on the physicochemical characteristics. *J Control Release* 2010; **143**(1): 71-9.

209.   Ding W, Zhang L, Yan Z, Engelhardt JF. Intracellular trafficking of adeno-associated viral vectors. *Gene therapy* 2005; **12**(11): 873-80.

210.   Mayor S. Finding better ways to deliver taxanes to cancer cells. *Lancet Oncol* 2007; **8**(2): 100.

211.   Mullock BM, Bright NA, Fearon CW, Gray SR, Luzio JP. Fusion of lysosomes with late endosomes produces a hybrid organelle of intermediate density and is NSF dependent. *J Cell Biol* 1998; **140**(3): 591-601.

212.   Lee D, Upadhye K, Kumta P. Nano-Sized Calcium Phosphate (CaP) Carriers for Non-Viral Gene/Drug Delivery. *Materials Science and Engineering B* 2013; **177**: 289-302.

213.   Huang Z, Teng W, Liu L, Wang L, Wang Q, Dong Y. Efficient cytosolic delivery mediated by polymersomes facilely prepared from a degradable, amphiphilic, and amphoteric copolymer. *Nanotechnology* 2013; **24**(26): 265104.

214.   Boussif O, Lezoualc'h F, Zanta MA, et al. A versatile vector for gene and oligonucleotide transfer into cells in culture and in vivo: polyethylenimine. *Proc Natl Acad Sci U S A* 1995; **92**(16): 7297-301.

215.   Sonawane ND, Szoka FC, Jr., Verkman AS. Chloride accumulation and swelling in endosomes enhances DNA transfer by polyamine-DNA polyplexes. *J Biol Chem* 2003; **278**(45): 44826-31.

216. Xia T, Kovochich M, Liong M, et al. Comparison of the mechanism of toxicity of zinc oxide and cerium oxide nanoparticles based on dissolution and oxidative stress properties. *ACS Nano* 2008; **2**(10): 2121-34.

217. Parton RG, Lindsay M. Exploitation of major histocompatibility complex class I molecules and caveolae by simian virus 40. *Immunol Rev* 1999; **168**: 23-31.

218. Grimm S. The art and design of genetic screens: mammalian culture cells. *Nat Rev Genet* 2004; **5**(3): 179-89.

219. Wurm FM. Production of recombinant protein therapeutics in cultivated mammalian cells. *Nature biotechnology* 2004; **22**(11): 1393-8.

220. Nakai H, Yant SR, Storm TA, Fuess S, Meuse L, Kay MA. Extrachromosomal recombinant adeno-associated virus vector genomes are primarily responsible for stable liver transduction in vivo. *J Virol* 2001; **75**(15): 6969-76.

221. Ostrom QT, Gittleman H, Farah P, et al. CBTRUS Statistical Report: Primary Brain and Central Nervous System Tumors Diagnosed in the United States in 2006-2010. *Neuro-oncology* 2013; **15 Suppl 2**: ii1-ii56.

222. UK CR. UK Cancer Incidence (2010) by Country Summary2013. (accessed.

223. Pulkkanen KJ, Yla-Herttuala S. Gene therapy for malignant glioma: current clinical status. *Mol Ther* 2005; **12**(4): 585-98.

224. Norden AD, Drappatz J, Wen PY. Antiangiogenic therapies for high-grade glioma. *Nature reviews Neurology* 2009; **5**(11): 610-20.

225. Krex D, Klink B, Hartmann C, et al. Long-term survival with glioblastoma multiforme. *Brain : a journal of neurology* 2007; **130**(Pt 10): 2596-606.

226. Claes A, Idema AJ, Wesseling P. Diffuse glioma growth: a guerilla war. *Acta neuropathologica* 2007; **114**(5): 443-58.

227. Neuwelt EA. Reversible osmotic blood-brain barrier disruption in humans: implications for the chemotherapy of malignant brain tumors. *Neurosurgery* 1980; **7**(2): 204.

228. Bobo RH, Laske DW, Akbasak A, Morrison PF, Dedrick RL, Oldfield EH. Convection-enhanced delivery of macromolecules in the brain. *Proc Natl Acad Sci U S A* 1994; **91**(6): 2076-80.

229. Ferguson S, Lesniak MS. Convection enhanced drug delivery of novel therapeutic agents to malignant brain tumors. *Curr Drug Deliv* 2007; **4**(2): 169-80.

230. Ksendzovsky A, Walbridge S, Saunders RC, Asthagiri AR, Heiss JD, Lonser RR. Convection-enhanced delivery of M13 bacteriophage to the brain. *J Neurosurg* 2012; **117**(2): 197-203.

231. Tobias A, Ahmed A, Moon KS, Lesniak MS. The art of gene therapy for glioma: a review of the challenging road to the bedside. *J Neurol Neurosurg Psychiatry* 2013; **84**(2): 213-22.

232. Natsume A, Yoshida J. Gene therapy for high-grade glioma: current approaches and future directions. *Cell Adh Migr* 2008; **2**(3): 186-91.

233. Immonen A, Vapalahti M, Tyynela K, et al. AdvHSV-tk gene therapy with intravenous ganciclovir improves survival in human malignant glioma: a randomised, controlled study. *Mol Ther* 2004; **10**(5): 967-72.

234. Bansal K, Engelhard HH. Gene therapy for brain tumors. *Current oncology reports* 2000; **2**(5): 463-72.

235. Mikhail AS, Eetezadi S, Allen C. Multicellular tumor spheroids for evaluation of cytotoxicity and tumor growth inhibitory effects of nanomedicines in vitro: a comparison of docetaxel-loaded block copolymer micelles and Taxotere(R). *PLoS One* 2013; **8**(4): e62630.

236. Vinci M, Gowan S, Boxall F, et al. Advances in establishment and analysis of three-dimensional tumor spheroid-based functional assays for target validation and drug evaluation. *BMC Biol* 2012; **10**: 29.

237. Li C, Diprimio N, Bowles DE, et al. Single amino acid modification of adeno-associated virus capsid changes transduction and humoral immune profiles. *J Virol* 2012; **86**(15): 7752-9.

238.   Malek-Hedayat S, Rome LH. Expression of multiple integrins and extracellular matrix components by C6 glioma cells. *J Neurosci Res* 1992; **31**(3): 470-8.

239.   Tchaicha JH, Reyes SB, Shin J, Hossain MG, Lang FF, McCarty JH. Glioblastoma angiogenesis and tumor cell invasiveness are differentially regulated by beta8 integrin. *Cancer Res* 2011; **71**(20): 6371-81.

240.   Friedrich J, Ebner R, Kunz-Schughart LA. Experimental anti-tumor therapy in 3-D: spheroids--old hat or new challenge? *Int J Radiat Biol* 2007; **83**(11-12): 849-71.

241.   Kunz-Schughart LA, Freyer JP, Hofstaedter F, Ebner R. The use of 3-D cultures for high-throughput screening: the multicellular spheroid model. *J Biomol Screen* 2004; **9**(4): 273-85.

242.   Al-Abd AM, Lee SH, Kim SH, et al. Penetration and efficacy of VEGF siRNA using polyelectrolyte complex micelles in a human solid tumor model in-vitro. *J Control Release* 2009; **137**(2): 130-5.

243.   Al-Jamal WT, Al-Jamal KT, Bomans PH, Frederik PM, Kostarelos K. Functionalized-quantum-dot-liposome hybrids as multimodal nanoparticles for cancer. *Small* 2008; **4**(9): 1406-15.

244.   Nawata H, Maeda Y, Sumimoto Y, Miyatake J, Kanamaru A. A mechanism of apoptosis induced by all-trans retinoic acid on adult T-cell leukemia cells: a possible involvement of the Tax/NF-kappaB signaling pathway. *Leuk Res* 2001; **25**(4): 323-31.

245.   Dincer S, Turk M, Karagoz A, Uzunalan G. Potential c-myc antisense oligonucleotide carriers: PCl/PEG/PEI and PLL/PEG/PEI. *Artif Cells Blood Substit Immobil Biotechnol* 2011; **39**(3): 143-54.

246.   Desgrosellier JS, Cheresh DA. Integrins in cancer: biological implications and therapeutic opportunities. *Nat Rev Cancer* 2010; **10**(1): 9-22.

247.   Castro MG, Cowen R, Williamson IK, et al. Current and future strategies for the treatment of malignant brain tumors. *Pharmacology & therapeutics* 2003; **98**(1): 71-108.

248.   Tran B, Rosenthal MA. Survival comparison between glioblastoma multiforme and other incurable cancers. *Journal of Clinical Neuroscience* 2010; **17**(4): 417-21.

249.   Nduom EK, Hadjipanayis CG, Van Meir EG. Glioblastoma cancer stem-like cells: implications for pathogenesis and treatment. *Cancer journal* 2012; **18**(1): 100-6.

250.   Louis DN. Molecular pathology of malignant gliomas. *Annual review of pathology* 2006; **1**: 97-117.

251.   Kwiatkowska A, Nandhu MS, Behera P, Chiocca EA, Viapiano MS. Strategies in gene therapy for glioblastoma. *Cancers (Basel)* 2013; **5**(4): 1271-305.

252.   Kroeger KM, Muhammad AK, Baker GJ, et al. Gene therapy and virotherapy: novel therapeutic approaches for brain tumors. *Discov Med* 2010; **10**(53): 293-304.

253.   Miller CR, Buchsbaum DJ, Reynolds PN, et al. Differential susceptibility of primary and established human glioma cells to adenovirus infection: targeting via the epidermal growth factor receptor achieves fiber receptor-independent gene transfer. *Cancer Res* 1998; **58**(24): 5738-48.

254.   Bello L, Francolini M, Marthyn P, et al. Alpha(v)beta3 and alpha(v)beta5 integrin expression in glioma periphery. *Neurosurgery* 2001; **49**(2): 380-9; discussion 90.

255.   Schottelius M, Laufer B, Kessler H, Wester HJ. Ligands for mapping alphavbeta3-integrin expression in vivo. *Acc Chem Res* 2009; **42**(7): 969-80.

256.   Chen X, Park R, Shahinian AH, Bading JR, Conti PS. Pharmacokinetics and tumor retention of 125I-labeled RGD peptide are improved by PEGylation. *Nucl Med Biol* 2004; **31**(1): 11-9.

257.   Achilli TM, Meyer J, Morgan JR. Advances in the formation, use and understanding of multi-cellular spheroids. *Expert Opin Biol Ther* 2012; **12**(10): 1347-60.

258.   De Witt Hamer PC, Van Tilborg AA, Eijk PP, et al. The genomic profile of human malignant glioma is altered early in primary cell culture and preserved in spheroids. *Oncogene* 2008; **27**(14): 2091-6.

259.   Ghosh S, Spagnoli GC, Martin I, et al. Three-dimensional culture of melanoma cells profoundly affects gene expression profile: a high density oligonucleotide array study. *J Cell Physiol* 2005; **204**(2): 522-31.

260.   Degen JW, Walbridge S, Vortmeyer AO, Oldfield EH, Lonser RR. Safety and efficacy of convection-enhanced delivery of gemcitabine or carboplatin in a malignant glioma model in rats. *J Neurosurg* 2003; **99**(5): 893-8.

261.   Lidar Z, Mardor Y, Jonas T, et al. Convection-enhanced delivery of paclitaxel for the treatment of recurrent malignant glioma: a phase I/II clinical study. *J Neurosurg* 2004; **100**(3): 472-9.

262.   Rousseau J, Boudou C, Barth RF, Balosso J, Esteve F, Elleaume H. Enhanced survival and cure of F98 glioma-bearing rats following intracerebral delivery of carboplatin in combination with photon irradiation. *Clin Cancer Res* 2007; **13**(17): 5195-201.

263.   Patel SJ, Shapiro WR, Laske DW, et al. Safety and feasibility of convection-enhanced delivery of Cotara for the treatment of malignant glioma: initial experience in 51 patients. *Neurosurgery* 2005; **56**(6): 1243-52; discussion 52-3.

264.   Vandergrift WA, Patel SJ, Nicholas JS, Varma AK. Convection-enhanced delivery of immunotoxins and radioisotopes for treatment of malignant gliomas. *Neurosurg Focus* 2006; **20**(4): E13.

265.   Muro K, Das S, Raizer JJ. Convection-enhanced and local delivery of targeted cytotoxins in the treatment of malignant gliomas. *Technol Cancer Res Treat* 2006; **5**(3): 201-13.

266.   Rainov NG, Soling A. Clinical studies with targeted toxins in malignant glioma. *Rev Recent Clin Trials* 2006; **1**(2): 119-31.

267.   Weber FW, Floeth F, Asher A, et al. Local convection enhanced delivery of IL4-Pseudomonas exotoxin (NBI-3001) for treatment of patients with recurrent malignant glioma. *Acta Neurochir Suppl* 2003; **88**: 93-103.

268.   Saito R, Bringas JR, Panner A, et al. Convection-enhanced delivery of tumor necrosis factor-related apoptosis-inducing ligand with systemic administration of temozolomide prolongs survival in an intracranial glioblastoma xenograft model. *Cancer Res* 2004; **64**(19): 6858-62.

269.   Cunningham J, Oiwa Y, Nagy D, Podsakoff G, Colosi P, Bankiewicz KS. Distribution of AAV-TK following intracranial convection-enhanced delivery into rats. *Cell Transplant* 2000; **9**(5): 585-94.

270.   Nguyen JB, Sanchez-Pernaute R, Cunningham J, Bankiewicz KS. Convection-enhanced delivery of AAV-2 combined with heparin increases TK gene transfer in the rat brain. *Neuroreport* 2001; **12**(9): 1961-4.

271.   Corem-Salkmon E, Ram Z, Daniels D, et al. Convection-enhanced delivery of methotrexate-loaded maghemite nanoparticles. *Int J Nanomedicine* 2011; **6**: 1595-602.

272.   Noble CO, Krauze MT, Drummond DC, et al. Novel nanoliposomal CPT-11 infused by convection-enhanced delivery in intracranial tumors: pharmacology and efficacy. *Cancer Res* 2006; **66**(5): 2801-6.

273.   Perlstein B, Ram Z, Daniels D, et al. Convection-enhanced delivery of maghemite nanoparticles: Increased efficacy and MRI monitoring. *Neuro Oncol* 2008; **10**(2): 153-61.

274.   Wu G, Barth RF, Yang W, Kawabata S, Zhang L, Green-Church K. Targeted delivery of methotrexate to epidermal growth factor receptor-positive brain tumors by means of cetuximab (IMC-C225) dendrimer bioconjugates. *Mol Cancer Ther* 2006; **5**(1): 52-9.

275.   Touraine RL, Ishii-Morita H, Ramsey WJ, Blaese RM. The bystander effect in the HSVtk/ganciclovir system and its relationship to gap junctional communication. *Gene therapy* 1998; **5**(12): 1705-11.

276.   Duflot-Dancer A, Piccoli C, Rolland A, Yamasaki H, Mesnil M. Long-term connexin-mediated bystander effect in highly tumorigenic human cells in vivo in herpes simplex virus thymidine kinase/ganciclovir gene therapy. *Gene therapy* 1998; **5**(10): 1372-8.

277. Estin D, Li M, Spray D, Wu JK. Connexins are expressed in primary brain tumors and enhance the bystander effect in gene therapy. *Neurosurgery* 1999; **44**(2): 361-8; discussion 8-9.

278. McMasters RA, Saylors RL, Jones KE, Hendrix ME, Moyer MP, Drake RR. Lack of bystander killing in herpes simplex virus thymidine kinase-transduced colon cell lines due to deficient connexin43 gap junction formation. *Human gene therapy* 1998; **9**(15): 2253-61.

279. Colombo BM, Benedetti S, Ottolenghi S, et al. The "bystander effect": association of U-87 cell death with ganciclovir-mediated apoptosis of nearby cells and lack of effect in athymic mice. *Human gene therapy* 1995; **6**(6): 763-72.

280. Barba D, Hardin J, Sadelain M, Gage FH. Development of anti-tumor immunity following thymidine kinase-mediated killing of experimental brain tumors. *Proc Natl Acad Sci U S A* 1994; **91**(10): 4348-52.

281. Caruso M, Panis Y, Gagandeep S, Houssin D, Salzmann JL, Klatzmann D. Regression of established macroscopic liver metastases after in situ transduction of a suicide gene. *Proc Natl Acad Sci U S A* 1993; **90**(15): 7024-8.

282. Ramesh R, Munshi A, Abboud CN, Marrogi AJ, Freeman SM. Expression of costimulatory molecules: B7 and ICAM up-regulation after treatment with a suicide gene. *Cancer gene therapy* 1996; **3**(6): 373-84.

283. Vile RG, Nelson JA, Castleden S, Chong H, Hart IR. Systemic gene therapy of murine melanoma using tissue specific expression of the HSVtk gene involves an immune component. *Cancer research* 1994; **54**(23): 6228-34.

284. Chen CY, Chang YN, Ryan P, Linscott M, McGarrity GJ, Chiang YL. Effect of herpes simplex virus thymidine kinase expression levels on ganciclovir-mediated cytotoxicity and the "bystander effect". *Human gene therapy* 1995; **6**(11): 1467-76.

285. Sandmair AM, Loimas S, Puranen P, et al. Thymidine kinase gene therapy for human malignant glioma, using replication-deficient retroviruses or adenoviruses. *Human gene therapy* 2000; **11**(16): 2197-205.

286. Manno CS, Pierce GF, Arruda VR, et al. Successful transduction of liver in hemophilia by AAV-Factor IX and limitations imposed by the host immune response. *Nat Med* 2006; **12**(3): 342-7.

287. Mingozzi F, Hasbrouck NC, Basner-Tschakarjan E, et al. Modulation of tolerance to the transgene product in a nonhuman primate model of AAV-mediated gene transfer to liver. *Blood* 2007; **110**(7): 2334-41.

288. Kreppel F, Kochanek S. Modification of adenovirus gene transfer vectors with synthetic polymers: a scientific review and technical guide. *Mol Ther* 2008; **16**(1): 16-29.

289. Bruttin A, Brussow H. Human volunteers receiving Escherichia coli phage T4 orally: a safety test of phage therapy. *Antimicrob Agents Chemother* 2005; **49**(7): 2874-8.

290. Sulakvelidze A. Phage therapy: an attractive option for dealing with antibiotic-resistant bacterial infections. *Drug Discov Today* 2005; **10**(12): 807-9.

291. Esposito M, Luccarini I, Cicatiello V, et al. Immunogenicity and therapeutic efficacy of phage-displayed beta-amyloid epitopes. *Mol Immunol* 2008; **45**(4): 1056-62.

292. van Houten NE, Henry KA, Smith GP, Scott JK. Engineering filamentous phage carriers to improve focusing of antibody responses against peptides. *Vaccine* 2010; **28**(10): 2174-85.

293. van Houten NE, Zwick MB, Menendez A, Scott JK. Filamentous phage as an immunogenic carrier to elicit focused antibody responses against a synthetic peptide. *Vaccine* 2006; **24**(19): 4188-200.

294. Micheel B, Heymann S, Scharte G, et al. Production of monoclonal antibodies against epitopes of the main coat protein of filamentous fd phages. *J Immunol Methods* 1994; **171**(1): 103-9.

295. Kneissel S, Queitsch I, Petersen G, Behrsing O, Micheel B, Dubel S. Epitope structures recognised by antibodies against the major coat protein (g8p) of filamentous bacteriophage fd (Inoviridae). *J Mol Biol* 1999; **288**(1): 21-8.

296.   Wiig H, Tenstad O, Iversen PO, Kalluri R, Bjerkvig R. Interstitial fluid: the overlooked component of the tumor microenvironment? *Fibrogenesis Tissue Repair* 2010; **3**: 12.

297.   Greish K. Enhanced permeability and retention of macromolecular drugs in solid tumors: a royal gate for targeted anticancer nanomedicines. *J Drug Target* 2007; **15**(7-8): 457-64.

298.   Pluen A, Boucher Y, Ramanujan S, et al. Role of tumor-host interactions in interstitial diffusion of macromolecules: cranial vs. subcutaneous tumors. *Proc Natl Acad Sci U S A* 2001; **98**(8): 4628-33.

299.   Whatcott CJ, Han H, Posner RG, Hostetter G, Von Hoff DD. Targeting the tumor microenvironment in cancer: why hyaluronidase deserves a second look. *Cancer Discov* 2011; **1**(4): 291-6.

300.   Kato M, Hattori Y, Kubo M, Maitani Y. Collagenase-1 injection improved tumor distribution and gene expression of cationic lipoplex. *Int J Pharm* 2012; **423**(2): 428-34.

301.   Diop-Frimpong B, Chauhan VP, Krane S, Boucher Y, Jain RK. Losartan inhibits collagen I synthesis and improves the distribution and efficacy of nanotherapeutics in tumors. *Proc Natl Acad Sci U S A* 2011; **108**(7): 2909-14.

302.   Allen TM. Ligand-targeted therapeutics in anticancer therapy. *Nat Rev Cancer* 2002; **2**(10): 750-63.

303.   Gullberg DE, Lundgren-Akerlund E. Collagen-binding I domain integrins--what do they do? *Prog Histochem Cytochem* 2002; **37**(1): 3-54.

304.   Hynes RO. Integrins: bidirectional, allosteric signaling machines. *Cell* 2002; **110**(6): 673-87.

305.   Havaki S, Kouloukoussa M, Amawi K, et al. Altered expression pattern of integrin alphavbeta3 correlates with actin cytoskeleton in primary cultures of human breast cancer. *Cancer Cell Int* 2007; **7**: 16.

306.   Davis GE. Affinity of integrins for damaged extracellular matrix: alpha v beta 3 binds to denatured collagen type I through RGD sites. *Biochem Biophys Res Commun* 1992; **182**(3): 1025-31.

307.   Stringa E, Knauper V, Murphy G, Gavrilovic J. Collagen degradation and platelet-derived growth factor stimulate the migration of vascular smooth muscle cells. *J Cell Sci* 2000; **113 (Pt 11)**: 2055-64.

308.   Jain RK. Delivery of molecular and cellular medicine to solid tumors. *Adv Drug Deliv Rev* 2001; **46**(1-3): 149-68.

309.   Boucher Y, Baxter LT, Jain RK. Interstitial pressure gradients in tissue-isolated and subcutaneous tumors: implications for therapy. *Cancer Res* 1990; **50**(15): 4478-84.

310.   Boucher Y, Jain RK. Microvascular pressure is the principal driving force for interstitial hypertension in solid tumors: implications for vascular collapse. *Cancer Res* 1992; **52**(18): 5110-4.

311.   Brekken C, Bruland OS, de Lange Davies C. Interstitial fluid pressure in human osteosarcoma xenografts: significance of implantation site and the response to intratumoral injection of hyaluronidase. *Anticancer Res* 2000; **20**(5B): 3503-12.

312.   Davies MM, Mathur P, Carnochan P, Saini S, Allen-Mersh TG. Effect of manipulation of primary tumour vascularity on metastasis in an adenocarcinoma model. *Br J Cancer* 2002; **86**(1): 123-9.

313.   Netti PA, Berk DA, Swartz MA, Grodzinsky AJ, Jain RK. Role of extracellular matrix assembly in interstitial transport in solid tumors. *Cancer Res* 2000; **60**(9): 2497-503.

314.   Holback H, Yeo Y. Intratumoral drug delivery with nanoparticulate carriers. *Pharm Res* 2011; **28**(8): 1819-30.

315.   Brown E, McKee T, diTomaso E, et al. Dynamic imaging of collagen and its modulation in tumors in vivo using second-harmonic generation. *Nat Med* 2003; **9**(6): 796-800.

316.   Eikenes L, Bruland OS, Brekken C, Davies Cde L. Collagenase increases the transcapillary pressure gradient and improves the uptake and distribution of monoclonal antibodies in human osteosarcoma xenografts. *Cancer Res* 2004; **64**(14): 4768-73.

317.   Magzoub M, Jin S, Verkman AS. Enhanced macromolecule diffusion deep in tumors after enzymatic digestion of extracellular matrix collagen and its associated proteoglycan decorin. *FASEB J* 2008; **22**(1): 276-84.

318.   McKee TD, Grandi P, Mok W, et al. Degradation of fibrillar collagen in a human melanoma xenograft improves the efficacy of an oncolytic herpes simplex virus vector. *Cancer Res* 2006; **66**(5): 2509-13.

319.   Goodman TT, Olive PL, Pun SH. Increased nanoparticle penetration in collagenase-treated multicellular spheroids. *Int J Nanomedicine* 2007; **2**(2): 265-74.

320.   Noreen R, Moenner M, Hwu Y, Petibois C. FTIR spectro-imaging of collagens for characterization and grading of gliomas. *Biotechnol Adv* 2012; **30**(6): 1432-46.

321.   Park JB, Kwak HJ, Lee SH. Role of hyaluronan in glioma invasion. *Cell Adh Migr* 2008; **2**(3): 202-7.

322.   Wiranowska M, Ladd S, Moscinski LC, et al. Modulation of hyaluronan production by CD44 positive glioma cells. *Int J Cancer* 2010; **127**(3): 532-42.

323.   Wiranowska M, Naidu AK. Interferon effect on glycosaminoglycans in mouse glioma in vitro. *J Neurooncol* 1994; **18**(1): 9-17.

324.   Hirschhaeuser F, Menne H, Dittfeld C, West J, Mueller-Klieser W, Kunz-Schughart LA. Multicellular tumor spheroids: an underestimated tool is catching up again. *J Biotechnol* 2010; **148**(1): 3-15.

325.   Fracasso G, Colombatti M. Effect of therapeutic macromolecules in spheroids. *Crit Rev Oncol Hematol* 2000; **36**(2-3): 159-78.

326.   Goodman TT, Chen J, Matveev K, Pun SH. Spatio-temporal modeling of nanoparticle delivery to multicellular tumor spheroids. *Biotechnol Bioeng* 2008; **101**(2): 388-99.

327.   Bookbinder LH, Hofer A, Haller MF, et al. A recombinant human enzyme for enhanced interstitial transport of therapeutics. *J Control Release* 2006; **114**(2): 230-41.

328.   Yocum RC, Kennard D, Heiner LS. Assessment and implication of the allergic sensitivity to a single dose of recombinant human hyaluronidase injection: a double-blind, placebo-controlled clinical trial. *J Infus Nurs* 2007; **30**(5): 293-9.

329.   Albanell J, Baselga J. Systemic therapy emergencies. *Semin Oncol* 2000; **27**(3): 347-61.

330.   Maier U, Baumgartner G. Metaphylactic effect of mitomycin C with and without hyaluronidase after transurethral resection of bladder cancer: randomized trial. *J Urol* 1989; **141**(3): 529-30.

331.   Smith KJ, Skelton HG, Turiansky G, Wagner KF. Hyaluronidase enhances the therapeutic effect of vinblastine in intralesional treatment of Kaposi's sarcoma. Military Medical Consortium for the Advancement of Retroviral Research (MMCARR). *J Am Acad Dermatol* 1997; **36**(2 Pt 1): 239-42.

332.   Brinckerhoff CE, Rutter JL, Benbow U. Interstitial collagenases as markers of tumor progression. *Clin Cancer Res* 2000; **6**(12): 4823-30.

333.   Roy R, Yang J, Moses MA. Matrix metalloproteinases as novel biomarkers and potential therapeutic targets in human cancer. *J Clin Oncol* 2009; **27**(31): 5287-97.

334.   Kovar JL, Johnson MA, Volcheck WM, Chen J, Simpson MA. Hyaluronidase expression induces prostate tumor metastasis in an orthotopic mouse model. *Am J Pathol* 2006; **169**(4): 1415-26.

335.   Tannock IF, Rotin D. Acid pH in tumors and its potential for therapeutic exploitation. *Cancer Res* 1989; **49**(16): 4373-84.

336.   Cohn RD, van Erp C, Habashi JP, et al. Angiotensin II type 1 receptor blockade attenuates TGF-beta-induced failure of muscle regeneration in multiple myopathic states. *Nat Med* 2007; **13**(2): 204-10.

337.   Habashi JP, Judge DP, Holm TM, et al. Losartan, an AT1 antagonist, prevents aortic aneurysm in a mouse model of Marfan syndrome. *Science* 2006; **312**(5770): 117-21.

338.   Johnston CI. Angiotensin receptor antagonists: focus on losartan. *Lancet* 1995; **346**(8987): 1403-7.

339.   Ferrari M. Cancer nanotechnology: opportunities and challenges. *Nat Rev Cancer* 2005; **5**(3): 161-71.

340.   Guo R, Zhang L, Qian H, Li R, Jiang X, Liu B. Multifunctional nanocarriers for cell imaging, drug delivery, and near-IR photothermal therapy. *Langmuir* 2010; **26**(8): 5428-34.

341.   Gariepy J, Kawamura K. Vectorial delivery of macromolecules into cells using peptide-based vehicles. *Trends Biotechnol* 2001; **19**(1): 21-8.

342.   Valery Petrenko GPS. Phage Nanobiotechnology. 1 ed: Royal Society of Chemistry; 2011.

343.   Petrenko V. Evolution of phage display: from bioactive peptides to bioselective nanomaterials. *Expert opinion on drug delivery* 2008; **5**(8): 825-36.

344.   Monk AB, Rees CD, Barrow P, Hagens S, Harper DR. Bacteriophage applications: where are we now? *Letters in applied microbiology* 2010; **51**(4): 363-9.

345.   Lang LH. FDA approves use of bacteriophages to be added to meat and poultry products. *Gastroenterology* 2006; **131**(5): 1370.

346.   Albelda SM, Mette SA, Elder DE, et al. Integrin distribution in malignant melanoma: association of the beta 3 subunit with tumor progression. *Cancer Res* 1990; **50**(20): 6757-64.

347.   Caracciolo G, Callipo L, De Sanctis SC, Cavaliere C, Pozzi D, Lagana A. Surface adsorption of protein corona controls the cell internalization mechanism of DC-Chol-DOPE/DNA lipoplexes in serum. *Biochim Biophys Acta* 2010; **1798**(3): 536-43.

348.   Kirk JT, Brault ND, Baehr-Jones T, Hochberg M, Jiang S, Ratner DM. Zwitterionic polymer-modified silicon microring resonators for label-free biosensing in undiluted human plasma. *Biosens Bioelectron* 2013; **42**: 100-5.

349.   Xiao W, Lin J, Li M, et al. Prolonged in vivo circulation time by zwitterionic modification of magnetite nanoparticles for blood pool contrast agents. *Contrast Media Mol Imaging* 2012; **7**(3): 320-7.

350.   Vithayathil R, Hooy RM, Cocco MJ, Weiss GA. The scope of phage display for membrane proteins. *J Mol Biol* 2011; **414**(4): 499-510.

351.   Chang Y, Higuchi A, Shih YJ, et al. Bioadhesive control of plasma proteins and blood cells from umbilical cord blood onto the interface grafted with zwitterionic polymer brushes. *Langmuir* 2012; **28**(9): 4309-17.

352.   Chang Y, Shu SH, Shih YJ, Chu CW, Ruaan RC, Chen WY. Hemocompatible mixed-charge copolymer brushes of pseudozwitterionic surfaces resistant to nonspecific plasma protein fouling. *Langmuir* 2010; **26**(5): 3522-30.

353.   Lowe AB, McCormick CL. Synthesis and solution properties of zwitterionic polymers. *Chem Rev* 2002; **102**(11): 4177-89.

354.   Gorbet MB, Sefton MV. Biomaterial-associated thrombosis: roles of coagulation factors, complement, platelets and leukocytes. *Biomaterials* 2004; **25**(26): 5681-703.

355.   Arap W, Pasqualini R, Ruoslahti E. Cancer treatment by targeted drug delivery to tumor vasculature in a mouse model. *Science* 1998; **279**(5349): 377-80.

356.   Koivunen E, Wang B, Ruoslahti E. Phage libraries displaying cyclic peptides with different ring sizes: ligand specificities of the RGD-directed integrins. *Biotechnology (N Y)* 1995; **13**(3): 265-70.

357.   Chen L, Zurita AJ, Ardelt PU, Giordano RJ, Arap W, Pasqualini R. Design and validation of a bifunctional ligand display system for receptor targeting. *Chem Biol* 2004; **11**(8): 1081-91.

358.   Huang Y, Chiang CY, Lee SK, et al. Programmable assembly of nanoarchitectures using genetically engineered viruses. *Nano Lett* 2005; **5**(7): 1429-34.

359.   Brown S. Metal-recognition by repeating polypeptides. *Nat Biotechnol* 1997; **15**(3): 269-72.

360.   Sarikaya M, Tamerler C, Jen AK, Schulten K, Baneyx F. Molecular biomimetics: nanotechnology through biology. *Nat Mater* 2003; **2**(9): 577-85.

361.   Bhutia SK, Maiti TK. Targeting tumors with peptides from natural sources. *Trends Biotechnol* 2008; **26**(4): 210-7.

362.   Clark JR, March JB. Bacteriophages and biotechnology: vaccines, gene therapy and antibacterials. *Trends Biotechnol* 2006; **24**(5): 212-8.

363.   Merril CR, Biswas B, Carlton R, et al. Long-circulating bacteriophage as antibacterial agents. *Proc Natl Acad Sci U S A* 1996; **93**(8): 3188-92.

364.   Gref R, Minamitake Y, Peracchia MT, Trubetskoy V, Torchilin V, Langer R. Biodegradable long-circulating polymeric nanospheres. *Science* 1994; **263**(5153): 1600-3.

365.   Cedervall T, Lynch I, Lindman S, et al. Understanding the nanoparticle-protein corona using methods to quantify exchange rates and affinities of proteins for nanoparticles. *Proc Natl Acad Sci U S A* 2007; **104**(7): 2050-5.

366.   Camner P, Lundborg M, Lastbom L, Gerde P, Gross N, Jarstrand C. Experimental and calculated parameters on particle phagocytosis by alveolar macrophages. *J Appl Physiol (1985)* 2002; **92**(6): 2608-16.

367.   Ishida T, Harashima H, Kiwada H. Interactions of liposomes with cells in vitro and in vivo: opsonins and receptors. *Curr Drug Metab* 2001; **2**(4): 397-409.

368.   Lamboy JA, Tam PY, Lee LS, et al. Chemical and genetic wrappers for improved phage and RNA display. *Chembiochem* 2008; **9**(17): 2846-52.

369.   Wagstaff KM, Jans DA. Nucleocytoplasmic transport of DNA: enhancing non-viral gene transfer. *Biochem J* 2007; **406**(2): 185-202.

370.   Imai S, Mukai Y, Takeda T, et al. Effect of protein properties on display efficiency using the M13 phage display system. *Pharmazie* 2008; **63**(10): 760-4.

371.   Bousarghin L, Touze A, Combita-Rojas AL, Coursaget P. Positively charged sequences of human papillomavirus type 16 capsid proteins are sufficient to mediate gene transfer into target cells via the heparan sulfate receptor. *The Journal of general virology* 2003; **84**(Pt 1): 157-64.

372.   Li Z, Koch H, Dubel S. Mutations in the N-terminus of the major coat protein (pVIII, gp8) of filamentous bacteriophage affect infectivity. *Journal of molecular microbiology and biotechnology* 2003; **6**(1): 57-66.

373.   Stopar D, Spruijt RB, Wolfs CJ, Hemminga MA. Protein-lipid interactions of bacteriophage M13 major coat protein. *Biochim Biophys Acta* 2003; **1611**(1-2): 5-15.

374.   Rodi DJ, Mandova S, Makowski L. Phage display in biotechnology and drug discovery. Boca Raton, FL: CRC Press Taylor & Francis Group; 2005.

375.   Merzlyak A, Lee SW. Engineering phage materials with desired peptide display: rational design sustained through natural selection. *Bioconjug Chem* 2009; **20**(12): 2300-10.

376.   Elf J, Nilsson D, Tenson T, Ehrenberg M. Selective charging of tRNA isoacceptors explains patterns of codon usage. *Science* 2003; **300**(5626): 1718-22.

377.   Hohn B, von Schutz H, Marvin DA. Filamentous bacterial viruses. II. Killing of bacteria by abortive infection with fd. *J Mol Biol* 1971; **56**(1): 155-65.

378.   Pratt D, Tzagoloff H, Erdahl WS. Conditional lethal mutants of the small filamentous coliphage M13. I. Isolation, complementation, cell killing, time of cistron action. *Virology* 1966; **30**(3): 397-410.

379.   Vilette D, Ehrlich SD, Michel B. Transcription-induced deletions in Escherichia coli plasmids. *Mol Microbiol* 1995; **17**(3): 493-504.

380.   Sidhu SS, Weiss GA, Wells JA. High copy display of large proteins on phage for functional selections. *J Mol Biol* 2000; **296**(2): 487-95.

381.   Makowski L. Structural constraints on the display of foreign peptides on filamentous bacteriophages. *Gene* 1993; **128**(1): 5-11.

382.   Opalka N, Beckmann R, Boisset N, Simon MN, Russel M, Darst SA. Structure of the filamentous phage pIV multimer by cryo-electron microscopy. *J Mol Biol* 2003; **325**(3): 461-70.

383. Zhao W, Jin L, Yuan H, et al. Targeting human embryonic stem cells with quantum dot-conjugated phages. *Sci Rep* 2013; **3**: 3134.

384. Chiang C, Mello CM, Gu J, Silva ECCM, Vliet KJV, Belcher AM. Weaving Genetically Engineered Functionality into Mechanically Robust Virus Fibers. *Advanced materials* 2007; **19**: 826–32.

385. Nwe K, Brechbiel MW. Growing applications of "click chemistry" for bioconjugation in contemporary biomedical research. *Cancer biotherapy & radiopharmaceuticals* 2009; **24**(3): 289-302.

386. Hess GT, Cragnolini JJ, Popp MW, et al. M13 bacteriophage display framework that allows sortase-mediated modification of surface-accessible phage proteins. *Bioconjugate chemistry* 2012; **23**(7): 1478-87.

387. Race PR, Bentley ML, Melvin JA, et al. Crystal structure of Streptococcus pyogenes sortase A: implications for sortase mechanism. *J Biol Chem* 2009; **284**(11): 6924-33.

388. Ton-That H, Liu G, Mazmanian SK, Faull KF, Schneewind O. Purification and characterization of sortase, the transpeptidase that cleaves surface proteins of Staphylococcus aureus at the LPXTG motif. *Proc Natl Acad Sci U S A* 1999; **96**(22): 12424-9.

389. Antos JM, Chew GL, Guimaraes CP, et al. Site-specific N- and C-terminal labeling of a single polypeptide using sortases of different specificity. *Journal of the American Chemical Society* 2009; **131**(31): 10800-1.

390. Sidhu SS. Engineering M13 for phage display. *Biomol Eng* 2001; **18**(2): 57-63.

391. Arap MA. Phage display technology - Applications and innovations. *Genetics and Molecular Biology* 2005; **28**(1): 1-9.

392. Kay BK, Adey NB, He YS, Manfredi JP, Mataragnon AH, Fowlkes DM. An M13 phage library displaying random 38-amino-acid peptides as a source of novel sequences with affinity to selected targets. *Gene* 1993; **128**(1): 59-65.

393. Haq IU, Chaudhry WN, Akhtar MN, Andleeb S, Qadri I. Bacteriophages and their implications on future biotechnology: a review. *Virol J* 2012; **9**: 9.

394. Sulalvelidze A, Alavidze Z, Morris JG. Bacteriophage therapy. *Antimicrob Agents Chemother* 2001; **45**: 649–59.

395. Kaur T, Nafissi N, Wasfi O, Sheldon K, Wettig S, Slavcev R. Immunocompatibility of Bacteriophages as Nanomedicines. *Journal of Nanotechnology* 2012; **2012**.

396. Wang T, Upponi JR, Torchilin VP. Design of multifunctional non-viral gene vectors to overcome physiological barriers: dilemmas and strategies. *Int J Pharm* 2012; **427**(1): 3-20.
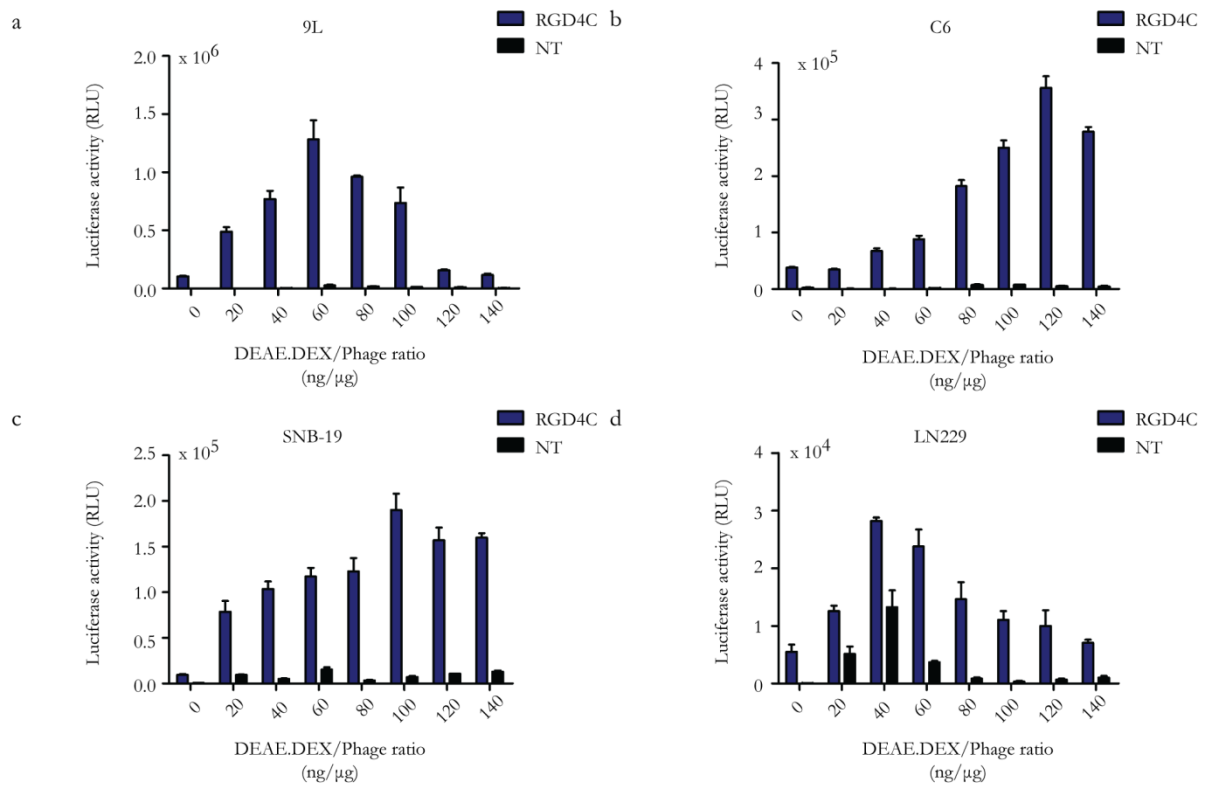
Appendix A

Optimisation of AAVP/cationic lipids. HEK293 cells were cultured in 48-well plates and treated with NT.AAVP or RGD4C.AAVP carrying the Luc gene, premixed with increasing ratios of cationic polymer per AAVP. Luciferase activity was analysed at day 3 post transduction. **a**) Fugene. **b**) Lipofectamine. **c**) DOTAB. The results show the mean relative luminescence units of triplicate wells +SEM, from one representative of three independent experiments.
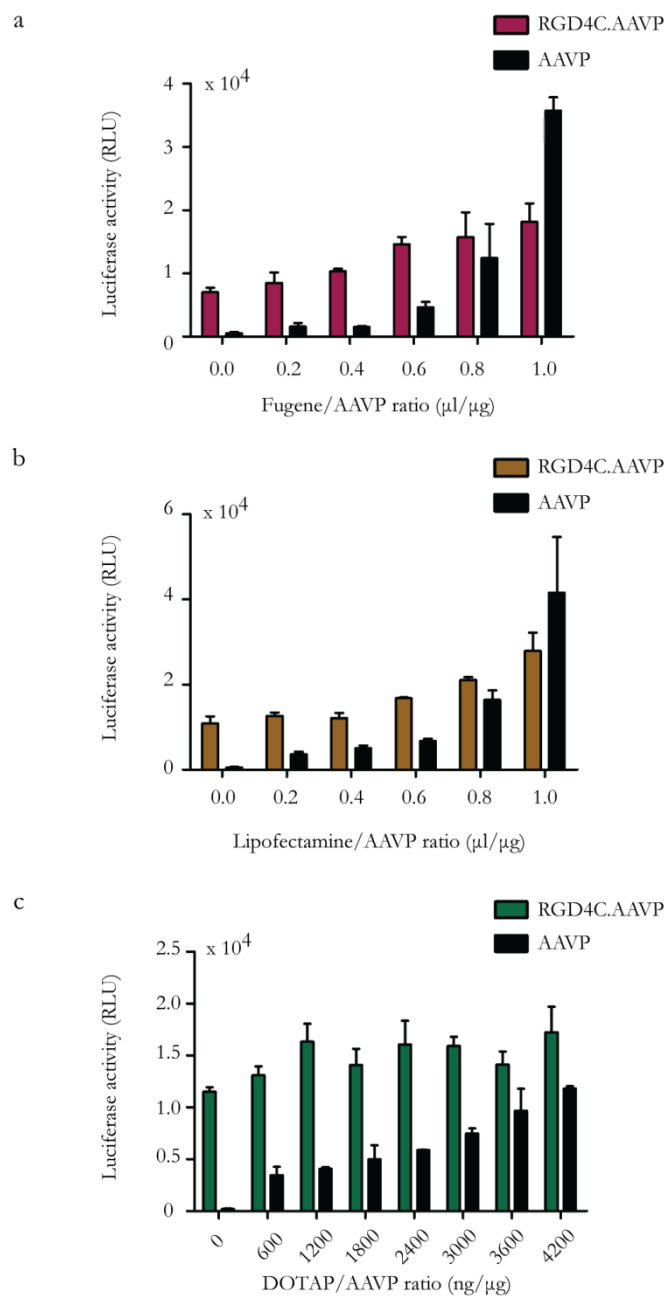
Optimisation of AAVP pretreated with chemical reagents. HEK293 cells were cultured in 48-well plates and treated with AAVP carrying the Luc gene, premixed with increasing ratios of chemical reagents per AAVP as indicated in the figure. Luciferase activity was analysed at day 3 post transduction. The results show the mean relative luminescence units of triplicate wells ±SEM, from one representative of three independent experiments.
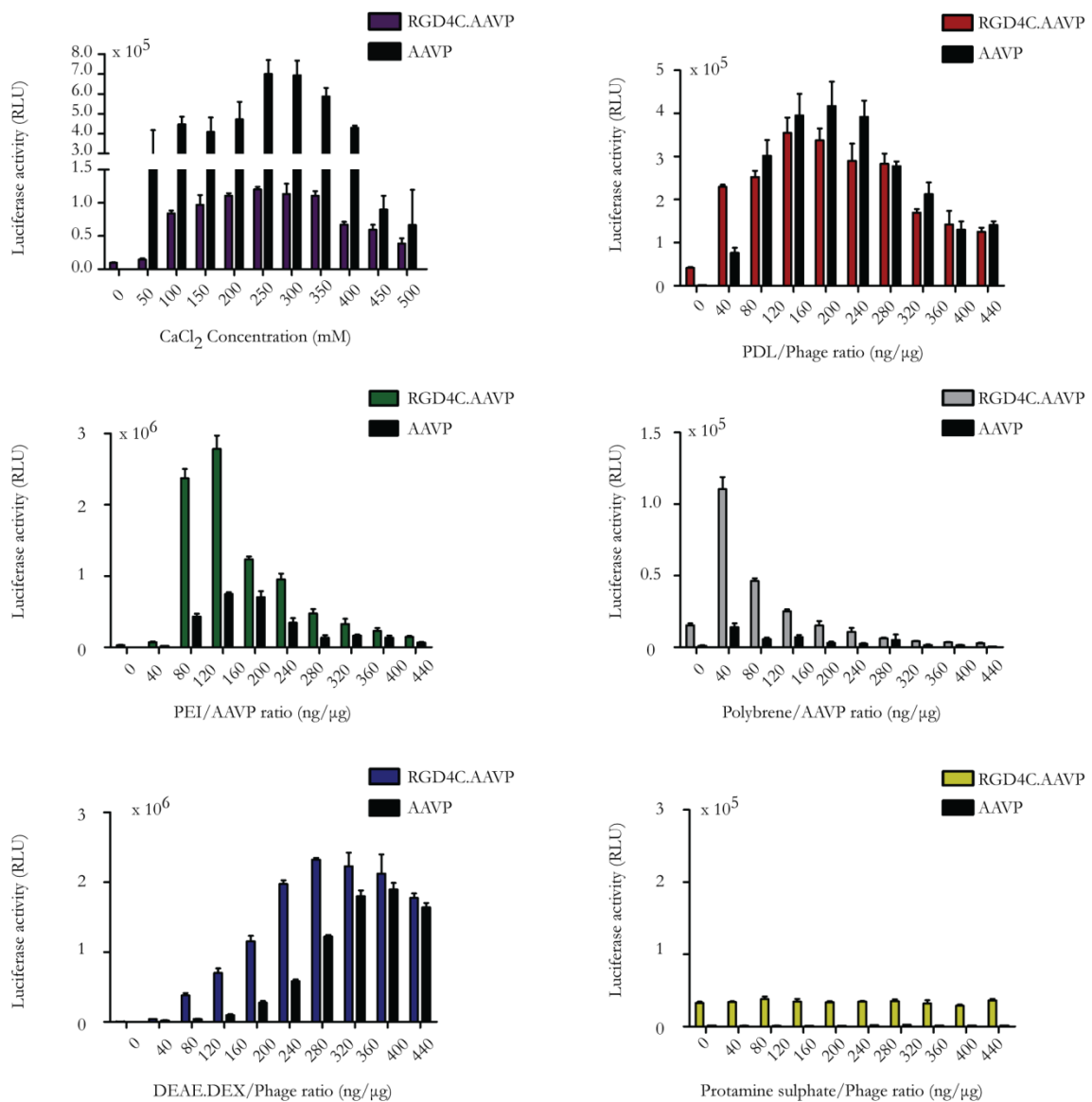
Optimisation of AAVP/cationic polymer complexes in glioblastomas. Cells were cultured in 48-well plates and treated with AAVP carrying the Luc gene, premixed with increasing ratios of cationic polymer per AAVP. Luciferase activity was analysed at day 3 post transduction. The results show the mean relative luminescence units of triplicate wells ±SEM, from one representative of three independent experiments.
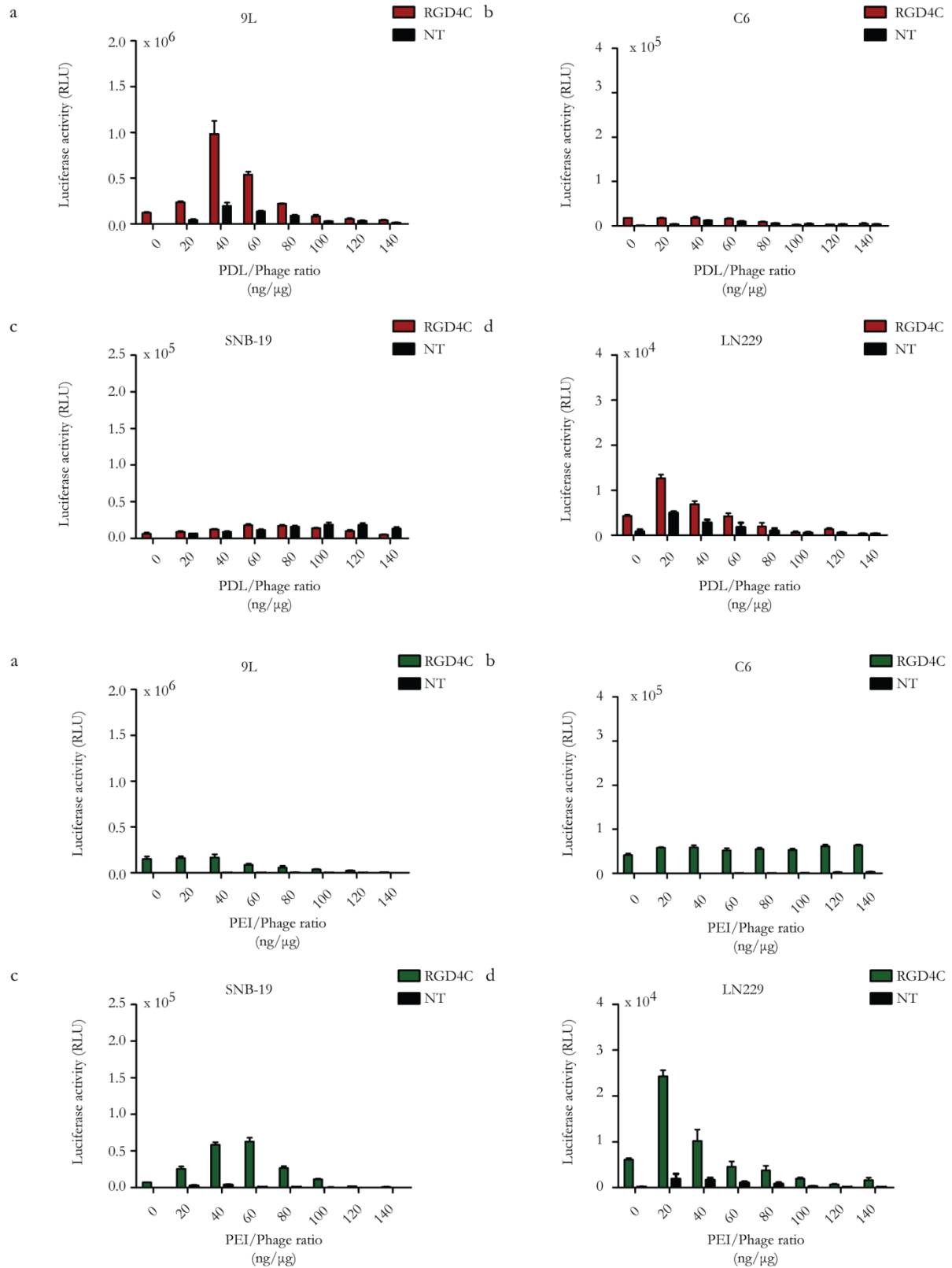
Appendix B
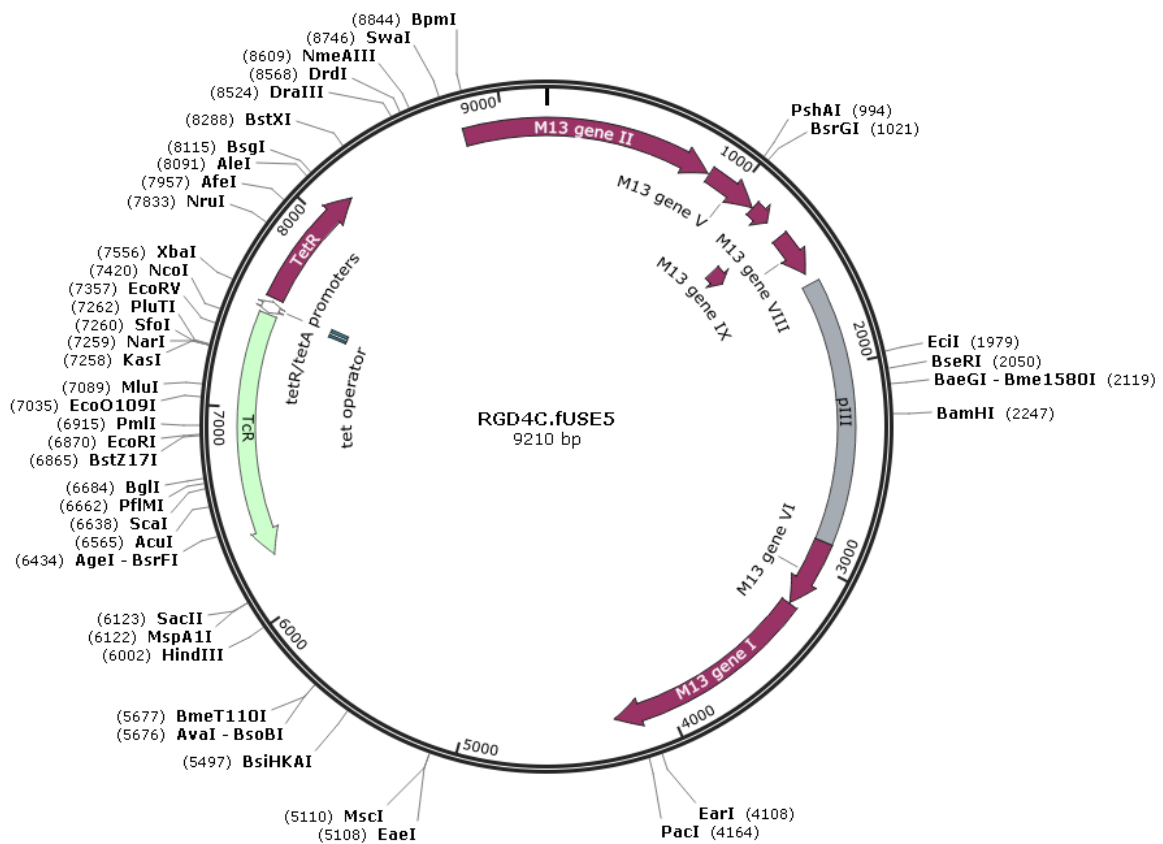

```
gtgaaaaaattattattcgcaattcctttagttgttcctttctattctcactccgtctgt
 V  K  K  L  L  F  A  I  P  L  V  V  P  F  Y  S  H  S  V  C
gattgtagggggggattgttttttgtgaaactgttgaaagttgtttagcaaaacctcataca
 D  C  R  G  D  C  F  C  E  T  V  E  S  C  L  A  K  P  H  T
gaaaattcatttactaacgtctggaaagacgacaaaactttagatcgttacgctaactat
 E  N  S  F  T  N  V  W  K  D  D  K  T  L  D  R  Y  A  N  Y
gagggctgtctgtggaatgctacaggcgttgtggtttgtactggtgacgaaactcagtgt
 E  G  C  L  W  N  A  T  G  V  V  V  C  T  G  D  E  T  Q  C
tacggtacatggggttcctattgggcttgctatccctgaaaatgagggtggtggctctgag
 Y  G  T  W  V  P  I  G  L  A  I  P  E  N  E  G  G  G  S  E
ggtggcggttctgagggtggcggttctgagggtggcggtactaaacctcctgagtacggt
 G  G  G  S  E  G  G  G  S  E  G  G  G  T  K  P  P  E  Y  G
gatacacctattccgggctatacttatatcaaccctctcgacggcacttatccgcctggt
 D  T  P  I  P  G  Y  T  Y  I  N  P  L  D  G  T  Y  P  P  G
actgagcaaaaccccgctaatcctaatccttctcttgaggagtctcagcctcttaatact
 T  E  Q  N  P  A  N  P  N  P  S  L  E  E  S  Q  P  L  N  T
ttcatgtttcagaataataggttccgaaataggcagggtgcattaactgtttatacgggc
 F  M  F  Q  N  N  R  F  R  N  R  Q  G  A  L  T  V  Y  T  G
```
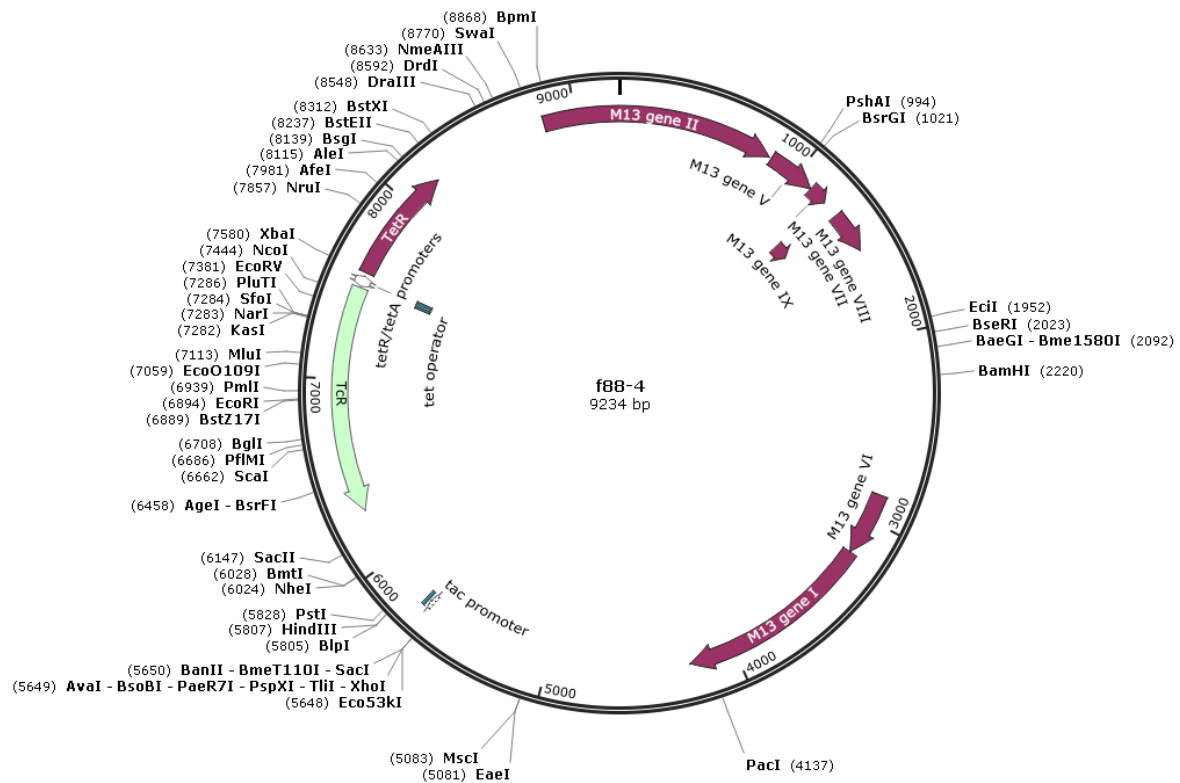
```
5647 in fd-tet
↓      XhoI
AGCTCGAGCTTACTCCCCA
tac promoter
TCCCCCTGTTGACAATTAATCATCGGCTCGTATAATGTGTGGAATTGTGAGCGGATAACAATTTC
gene VIII translation initiation region
TTAATGGAAACTTCCTC ATG AAA AAG TCT TTA
                    M   K   K   S   L


GTT CTT AAA GCA TCT GTT GCT GTT GCG ACT CTT GTT
 V   L   K   A   S   V   A   V   A   T   L   V
                  HindIII
PstI
           ↓                   stuffer              ↓
CCT ATG CTA^AGC TTT GCC AAC GTC CCT GCA^GAA GGT GAT GAC CCG GCT AAA
 P   M   L   S   F   A ^ N   V   P   A   E   G   D   D   P   A   K
             Signal Peptidase
GCT GCT TTT GAC TCT CTT CAG GCT TCT GCT ACT GAA TAC ATC GGC TAC GCT
 A   A   F   D   S   L   Q   A   S   A   T   E   Y   I   G   Y   A
TGG GCT ATG GTG GTT GTT ATC GTT GGT GCT ACT ATT GGC ATC AAA CTT TTC
 W   A   M   V   V   V   I   V   G   A   T   I   G   I   K   L   F
AAA AAA TTC ACT TCT AAA GCG TCT
 K   K   F   T   S   K   A   S
             trpA terminator
NheI
TAATG  AACTCAGATACCCAGCCCGCCTAATGAGCGGGCTTTTTTTT  AAGCTAGCTT
```
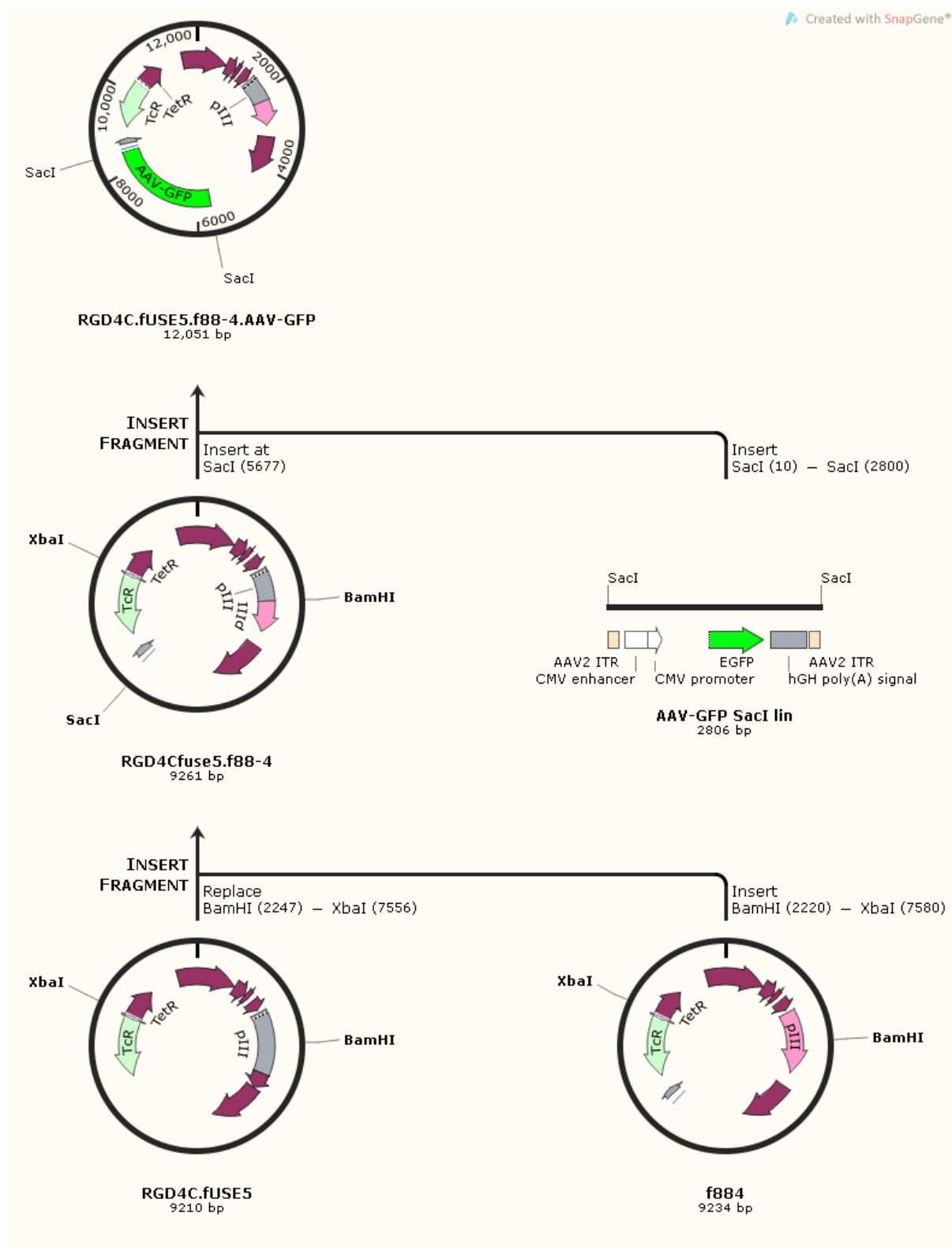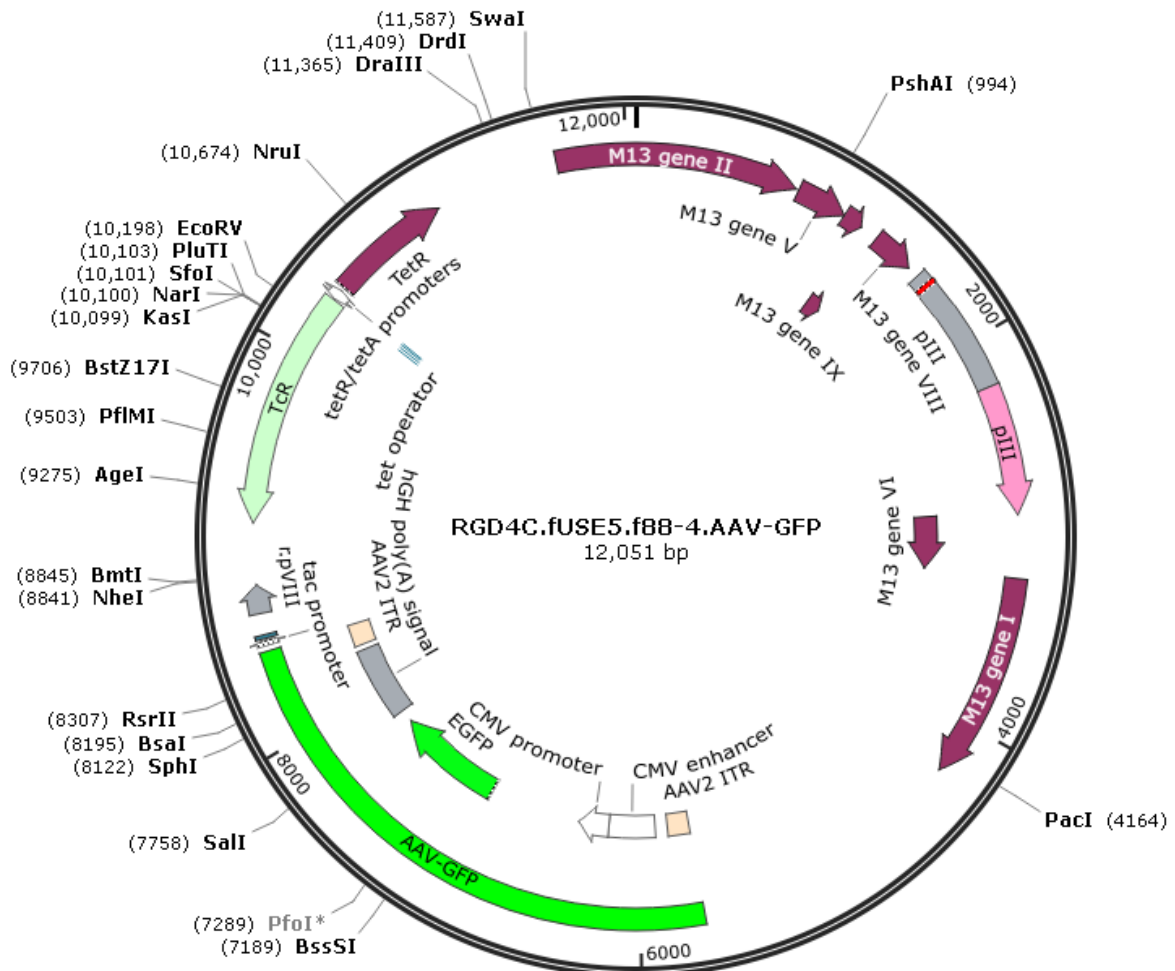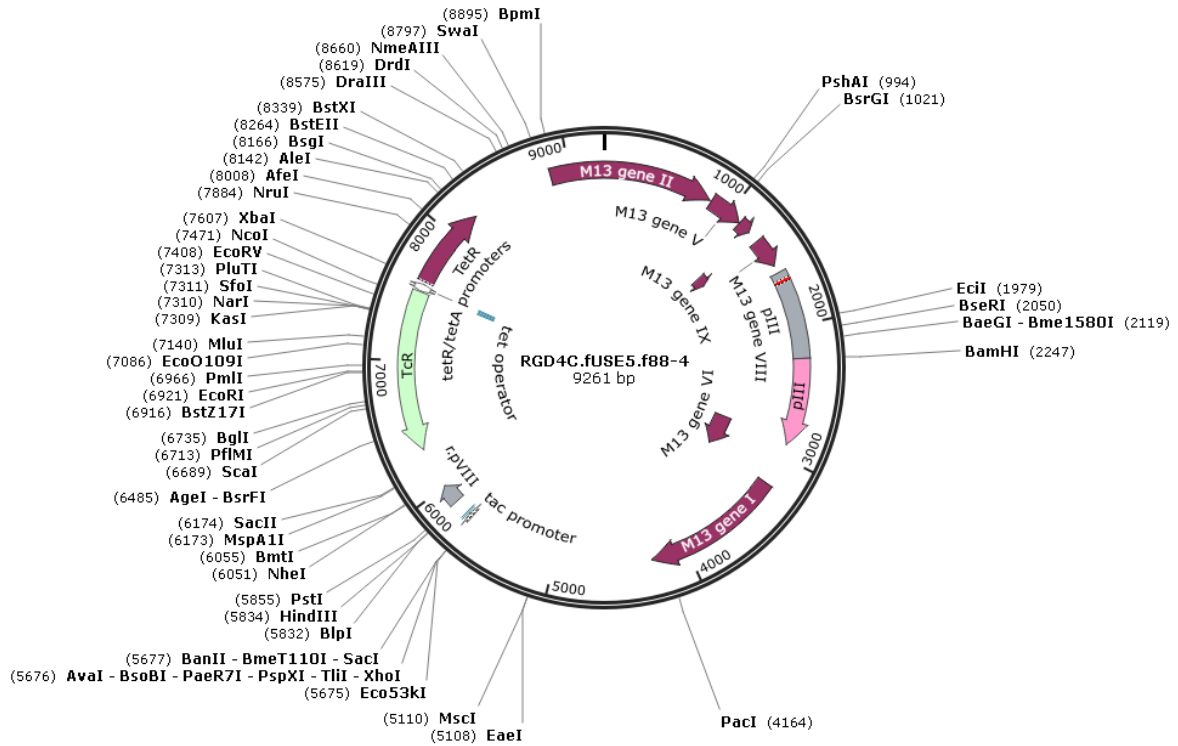
Construction of RGD4C.fUSE5.f88.AAV-GFP plasmid

RGD4C.fUSE5.f88-4.AAV-GFP
12,051 bp

INSERT FRAGMENT

Insert at
SacI (5677)

Insert
SacI (10) — SacI (2800)

XbaI

BamHI

SacI

RGD4Cfuse5.f88-4
9261 bp

SacI

SacI

AAV2 ITR
CMV enhancer

EGFP

CMV promoter

AAV2 ITR
hGH poly(A) signal

AAV-GFP SacI lin
2806 bp

INSERT FRAGMENT

Replace
BamHI (2247) — XbaI (7556)

Insert
BamHI (2220) — XbaI (7580)

XbaI

BamHI

RGD4C.fUSE5
9210 bp

XbaI

BamHI

f884
9234 bp

Appendix C

Reagents set up

PEG/NaCl	500 g of PEG (Sigma) and 584.5 g of NaCl (Sigma) in 2,380 ml H_2O (double-distilled) and store at 4°C
50x TAE buffer	242g of Tris, 100mL of 0.5M EDTA pH 8.0 and 57.1mL of Glacial Acetic Acid (Ficher). Add enough H_2O to dissolve solids, then bring up to final volume of 1000mL. autoclaved and stored RT.
0.5M EDTA pH 8.0	186.1g of EDTA (Ficher) in 900ml of H_2O and stir until completely dissolved. Adjusted the pH with NaOH, then bring up to 1000 ml, autoclaved and stored RT.
LB broth	18 g of LB powder (Sigma) in 1000 ml of H_2O, sterilise by autoclaving.
LB agar	9 g of LB powder and 9 g of agar in 450 ml of H_2O, sterilise by autoclaving, Let agar cool to ~55°C, then add antibiotics before pour plates
TB medium	9.6 g of tryptone (Sigma), 19.2 g of yeast extract (Sigma) and 3.2 ml of glycerol in 1 liter of H_2O. Autoclave, add 100 ml of TB supplements and 50 mg of kanamycin (Sigma).
TB supplement	23.1 g of KH_2PO_4 (Sigma) and 125.4 g of K_2HPO_4 (Sigma) in 1 liter of H_2O (double-distilled). Filter through 0.22 μm filter units and store at 4°C